Driven lattice gases: models for intracellular transport

Paolo Pierobon

München 2006

Driven lattice gases: models for intracellular transport

Paolo Pierobon

Dissertation
der Fakultät für Physik
der Ludwig–Maximilians–Universität
München

vorgelegt von
Paolo Pierobon
aus Montebelluna (Italy)

München, 27. Februar 2006

Contents

Abstract

This thesis has been motivated by intracellular transport phenomena, such as kinesins and myosins moving along cytoskeletal filaments or ribosomes along messenger RNA. In both cases molecular motors move uni-directionally along a one-dimensional track. This motion is driven by the free energy released in the chemical hydrolysis reaction of ATP (adenosine-triphosphate). It drives conformational changes of the protein and at the same time switches the affinity to the cytoskeletal filaments. The detailed mechanisms are still a matter of debate and intensive research. They do not concern us here, since we are not interested in the principles governing the chemo-mechanics of individual enzymes, but in the possible cooperativity in the intracellular transport resulting from the interplay between externally driving the system and the interaction between the motors. We are interested in the emergent properties of the system, such as the density and current profiles along the track in the ensuing non-equilibrium steady state.

We idealize the dynamics in terms of driven lattice gases, which model the motors as particles occupying one or more lattice sites whose dynamics is given by a simple Poisson process. The track is represented by a one-dimensional periodic lattice with open boundaries, where particles may enter or leave the system stochastically. Interaction between the particles is restricted to hard core repulsion such that each lattice site can at most be occupied by one particle. As such the system is known as the Totally Asymmetric Simple Exclusion Process (TASEP), which shows a non-trivial phase diagram as a function of the entrance and exit rates. Though describing some key features of intracellular transport this simple model misses several important aspects such as the exchange of particles between molecular track and the cytoplasm, the extended molecular structure of each motor, and the interaction of motors with microtubule associated proteins which may act as road blocks for intracellular traffic.

The goal of this thesis is to account for some of these additional features and explore their possible relevance for the nature of the non-equilibrium steady state and correlations in the single particle and collective dynamics. To achieve this goal we use both analytical approaches (mean field theories, Langevin equations) and numerical methods (kinetic Monte Carlo simulations).

In the first part of the thesis we build on recent advances in the field, which have been achieved by taking into account particle exchange between the track and bulk solution (Langmuir kinetics). It was found that this violation of current conservation along the track leads to phase coexistence regions in the phase diagram not present in the TASEP. We

have extended these studies in two ways. First, motivated by the fact that many molecular motors are dimers, we study how the stationary properties of the system (density profile and phase behavior) change upon replacing monomers with extended particles. Analytical refined and generalized mean field theory, supported by numerical Monte Carlo simulations, give a detailed description of the phase diagram. As a consequence of the on-off kinetics, a new phase coexistence region arises intervening between low and high density phases such that the discontinuous transition lines of the TASEP splits into two continuous transition lines. This proves that the extension gives quantitative but not qualitative changes in the phase diagram, showing that the picture obtained in the case of monomers is robust upon considering extended particles. Second, motivated by the presence of structural imperfections of the track that act as road blocks, we study the influence of an isolated defect characterized by a reduced hopping rate on the non-equilibrium steady state. Again, upon combining mean-field studies with MC simulations we explore the phase behavior in the full parameter range and find the following results. The phase diagram changes qualitatively as compared to the case without defects, showing new phase coexistence regions. This can be determined upon studying the *carrying capacity*, i.e. maximal current that can flow through a given site, which now depends on the defect parameters (i.e. its position and strength). For a weak defect its presence is irrelevant for the density profile, and the behavior without defect is recovered. Above a certain threshold strength of the defect, its presence induces a macroscopic change in the density profile. The regions where the defect is relevant (called *bottleneck phases*) are identified and studied.

In the second part of the thesis we investigate the dynamical features of these models. First we concentrate on the dynamics of the simple TASEP, for which a complete analysis was missing. We use a technique borrowed from solid state physics, the Boltzmann-Langevin method, to give a full description of the correlation function in the whole parameter space. It turns out that most of the dynamics can be nicely explained in terms of the combined effect of local density fluctuations and collective domain wall motion. Finally we study the dynamics of a tracer particle in a TASEP with on-off kinetics. We observe that it is possible to reconstruct the density profile from the velocity of the tracer particle. Interestingly, the reconstruction of the profile is possible already with quite low statistics, i.e. with less than one hundred tracer particles. On the basis of these observations we propose to perform single molecule experiments with fluorescently labelled molecular motors to explore the density profile and ultimately test the phase behavior predicted in this thesis.

Zusammenfassung

Die vorliegende Doktorarbeit behandelt Phänomene intrazellulärer Transportprozesse. Kinesin und Myosin bewegen sich entlang der Filamente des Zytoskeletts, Ribosome entlang von Messenger RNA. In beiden Fällen handelt es sich um molekulare Motoren, die gerichtet auf einem eindimensionalen Strang wandern. Angetrieben wird diese Bewegung durch freie Energie, die von der chemischen Hydrolyse von ATP (Adenosintriphosphat) freigesetzt wird. Sie bewirkt Konformationsänderungen des Proteins und gleichzeitige Änderungen in der Stärke der Bindung an das Filament des Zytoskeletts. Die genauen Mechanismen sind Gegenstand des derzeitigen Diskurses, intensive Forschungen sind hier im Gang. Sie sollen uns in dieser Arbeit jedoch nicht näher beschäftigen, da wir uns anstelle des detaillierten chemo-mechanischen Verhaltens des einzelnen Enzyms kollektiven Eigenschaften zuwenden wollen. Diese entstehen durch das Zusammenspiel von externem Antrieb und der Wechselwirkung zwischen den Motoren. Wir interessieren uns also für emergente Eigenschaften des Systems, wie beispielsweise den Dichte- und Teilchenstromprofilen entlang der Schiene im stationären Zustand, der sich im Nichtgleichgewicht bildet.

Die Dynamik der Motoren wird idealisiert durch getriebene Gittergase beschrieben. Motoren werden als Teilchen, ein oder mehrere Gitterplätze besetzend, dargestellt, ihre Dynamik ist die des Poisson Prozesses. Ein eindimensionales Gitter bildet die Schiene, an den offenen Enden, den Rändern, können Teilchen stochastisch in das System eintreten oder es verlassen. Die Wechselwirkung zwischen den Teilchen beschränkt sich auf Ausschließung, jeder Gitterplatz kann von höchstens einem Teilchen besetzt sein. Dieses System ist als vollständig asymmetrischer einfacher Ausschließungsprozeß (Totally Asymmetric Simple Exclusion Process, TASEP) bekannt, und zeigt in Abhängigkeit der Eintritts- und Austrittsraten ein nichttriviales Phasendiagramm. Obwohl dieses Modell wichtige Aspekte von intrazellulärem Transport beschreibt, sind andere grundlegende Eigenschaften, wie der Austausch von Teilchen zwischen molekularen Schienen und dem umgebenden Zytoplasma, die ausgedehnte molekulare Struktur des einzelnen Motors oder die Wechselwirkung der Motoren mit Proteinen des Mikrotubuli, welche als Hindernis für den Transport wirken können, nicht berücksichtigt.

Das Ziel dieser Arbeit ist es, einige der letztgenannten Aspekte in die theoretische Beschreibung mit einzubeziehen. Ihre Bedeutung für die Natur des stationären Zustands im Nichtgleichgewicht, Korrelationen und kollektive Dynamik sollen untersucht werden. Dazu verwenden wir zum einen analytische Zugänge, wie Mean-field-Theorien oder Langevin-Gleichungen, zum anderen stützen wir uns auf numerische Methoden in Form von kineti-

schen Monte-Carlo Simulationen.

Im ersten Teil der vorliegenden Arbeit diskutieren wir Fortschritte der letzten Jahre auf diesem Gebiet, die durch Betrachtung des Teilchenaustauschs zwischen Schiene und Umgebung mittels Langmuir Kinetik erreicht wurden. Der nicht länger räumlich erhaltene Teilchenstrom entlang der Schiene führt hier zu Phasenkoexistenz mit einer lokalisierten Domänenwand, wie sie im TASEP nicht auftritt. Wir haben diese Studien in zwei Richtungen erweitert. Motiviert durch die Dimerstruktur vieler molekularer Motoren haben wir zum einen untersucht, wie sich das stationäre Verhalten des Systems, Dichteprofile und Phasen, verändern, wenn statt Monomeren ausgedehnte Teilchen angenommen werden. Eine analytische, angepaßte Mean-field-Theorie ergibt das detaillierte Phasendiagramm, welches durch numerische Monte-Carlo Simulationen bestätigt wird. Als Konsequenz des Teilchenaustauschs zwischen Schiene und Umgebung entsteht Phasenkoexistenz in einer Region im Parameterraum, die sich zwischen die Niedrig- und die Hochdichtephase schiebt. Der diskontinuierliche Phasenübergang des TASEP teilt sich so in zwei kontinuierliche Phasenübergänge auf. Die Veränderung von Monomeren zu Dimeren bringt quantitative, aber keine qualitativen Veränderungen mit sich, so daß das Modell, welches auf Monomeren basiert, robust unter Erweiterung auf ausgedehnte Teilchen ist. Zum anderen betrachten wir das Vorhandensein von strukturellen Ungleichheiten auf der Schiene, die als Hindernis wirken können. Den Einfluss von einzelnen solchen Defekten charakterisieren wir hierbei durch eine reduzierte Rate der Vorwärtsbewegung. Die Kombination von Mean-field-Theorie und Monte-Carlo Simulationen erlaubt es auch hier, das Phasenverhalten im gesamten Parameterraum zu studieren. Wir erhalten die folgenden Resultate. Das Phasendiagramm verändert sich qualitativ gegenüber dem Modell ohne Defekte, neue Phasenkoexistenzregionen erscheinen. Die Betrachtung der *Tragekapazität*, also des maximalen Teilchenstroms, der durch einen bestimmten Gitterplatz fließen kann und der nun von den Defektparametern wie Position und Stärke abhängt, macht es der analytischen Beschreibung zugänglich. Schwache Defekte stellen sich als irrelevant für das Dichteprofil heraus, das Verhalten des Systems ist das gleiche wie im Modell ohne Defekte. Überschreitet die Stärke des Defekts eine gewisse Schwelle, induziert er makroskopische Änderungen im Dichteprofil. Wir studieren und identifizieren die Regionen, in denen der Defekt relevant ist, die *Engpaßphasen*.

Der zweite Teil dieser Arbeit behandelt das dynamische Verhalten des Systems. Zum einen betrachten wir TASEP, wofür eine vollständige Beschreibung bisher fehlte. Der Boltzmann-Langevin Ansatz, aus der Festkörperphysik kommend, erlaubt uns die vollständige Analyse der Korrelationen im gesamten Parameterraum. Es stellt sich heraus, daß der überwiegende Teil der Dynamik sehr schön durch Kombination lokaler Dichtefluktuationen und kollektiver Bewegungen der Domänenwand erklärt werden kann. Schließlich untersuchen wir die Dynamik von Indikatorteilchen in TASEP unter Einbeziehung der Langmuir Kinetik. Wir zeigen, daß die Rekonstruktion des Dichteprofils aus der Geschwindigkeit des Indikatorteilchens möglich ist. Interessanterweise ist dies schon mit niedriger Statistik, tatsächlich weniger als hundert Indikatorteilchen, möglich. Aufgrung dieser Resultate schlagen wir Einzelmolekülexperimente vor, in denen mit Fluoreszenz markierte molekulare Motoren benutzt werden, um Rückschlüsse auf das Dichteprofil zu ziehen und so das Phasenverhalten, das in dieser Arbeit theoretisch vorhergesagt wird, zu überprüfen.

Chapter 1

Introduction and biological motivations

> Science is at its most creative when it can see a world in a grain of sand and a heaven in a wild flower.
>
> Freeman Dyson

If we approach a city by air we cannot help being impressed by the similarities in the way human structures and cells appear to be organized. As the urban arteries come into view (streets, highways, tracks) one can observe traffic in its diverse forms and an amazing level of organization developed to manage million of people moving around efficiently. A closer look, though, especially when those people are trapped in a traffic jam[1], reveals that this organization is still far from perfection. This picture is not too far from the one of a living cell.

Like cities, cells have developed diverse transport systems to ensure that the right components are delivered to, or manufactured at, the right locations at the right time. The evolution have provided cells with a central production plant (the nucleus) where proteins and enzymes are produced, several sparse power plants (the mitocondria) and many compartments where the several chemical reaction occurs in order to maintain the cell alive and allow it to reproduce. To transfer molecules from one part to another of the cell, many strategies have been developed, since diffusion is simply too inefficient. Apart from some small molecules that can simply diffuse through the cytoplasm on short scales, most of the components of the cell need special proteins to get pumped through the membranes that compartmentalize the cell or to be transported from one part to the other of the cell (e.g. along axons in neurons). In fact, cell contains a network of "motorway" on which specialized molecules move and transport objects with them. What are these

---

[1]Only in the USA largest urban area an average traveller wastes 62 hours per year just because of traffic jam [66]. According to a study of the European Commission [21], the impact of traffic congestion amounts to 0.5% of the gross domestic product and will increase up to 1% (i.e. 80 billion euros per year) by the year 2010.

transport systems? What are the intracellular roads or tracks? What are the engines and motors, and how do they operate? How are the various types of cargo shipped, and how is such transport tailored to demand? These are just some of the questions addressed by the current research in *molecular motors*. Medical applications further motivate this research: despite the work of the evolution, the cell traffic system sometimes shares the same problems with the cities one. Just as disruption of commercial traffic impairs the welfare of a city, defective molecular motors or tracks can result in developmental defects, cardiovascular problems, neuronal diseases (Alzheimer, sclerosis, retinitis pigmentosa...see e.g. [37, 5, 55, 99]).

So far the human and intracellular traffics seem exactly the same. Actually motion at the molecular scale presents many differences with the macroscopic one due to the fluctuations that characterize systems at nano-scale. In this thesis we address the problem of traffic of particles at this scale (e.g. molecular motors) through the study of a non-equilibrium statistical mechanics model.

This chapter is structured as follows. We consider in Sec. 1.1 the components of the picture we aim to describe, namely the biomolecule responsible for intracellular transport along microtubules. Next, in Sec. 1.2 we introduce some of the techniques used to monitor these molecules. In Sec. 1.3 we consider some classical models of single molecular motors. In Sec. 1.4 we consider the traffic problem and successively, in Sec. 1.5, the main theoretical challenges posed by the problem and the goal of this thesis. We conclude presenting the outline of the thesis.

1.1 Molecular traffic

1.1.1 The fuel: ATP

Motors are devices that convert energy into work. In the cell energy is transferred through a molecule, the ATP, that can be hydrolyzed to produce energy, according to the reaction

$$ATP + H_2O \rightarrow ADP + P_i + \text{energy} \,, \tag{1.1}$$

where P_i stands for inorganic phosphate. This chemical reaction releases an energy $\Delta G \sim 50 pN \cdot nm$: this collocates the force exerted by this object on the range of the pN and on the scale of nm. In the molecular motors the release of this energy gives rise to a conformational change of the protein resulting in a mechanical work. Molecules are usually active at room temperature: since in this case $1k_B T \sim 4 pN \cdot nm$ all the molecules are subject to fluctuations that can be studied using statistical mechanics techniques.

1.1.2 The tracks: filaments

In analogy with the urban traffic, the filaments are the roads where motors move. Network of filaments constitute the cytoskeleton, a rigid structure that not only gives the the cell

its structural properties but, undergoing constant rearrangements, is actively involved in its mobility.

Filaments are classified by their size and structure: *microfilaments* have a cable-like structure of ∼6nm in diameter; *intermediate filaments* have a rope-like structure and are ∼10nm in diameter; *microtubules* have a pipe-like structure of ∼25nm of external diameter (and $\sim 18nm$ of internal diameter). Only microfilaments and microtubules are involved in mobility.

Microfilaments (or *F-actin*) are formed by polymerization of a single monomer (G-actin). F-actin is a long, flexible filament that appears as a twisted string of beads. They can be closely packed in parallel arrays (bundles), as in muscle cells, or loosely packed in actin networks, that gives mechanical properties of the cell.

The microtubules are composed of 13 protofilaments arranged in a hollow cylindrical structure. The subunits of each protofilament is a tubulin heterodimers made of *α-tubulin* and *β-tubulin* monomers. Each tubulin monomer is a globular protein 4nm in diameter (each subunit is therefore 8nm long).

Microtubules and F-actin, in addition to constitute a support for motors, play a key role in cell motility and mechanics. In fact they have the capability of polymerize faster at one end (treadmilling) and of change their size rapidly as response to chemical or mechanical signals (dynamic instability). All subunits have the same polarity, i.e. they all point toward the same filament end. This means that at one end the binding cleft of a subunit is exposed to the surrounding solution, while on the other end it is tight to the neighboring subunit. This structural difference is reflected in the treadmilling mechanism: one end of the filament (called the (+) end) grows 5 times faster than the other one.

1.1.3 The motors: kinesin, myosin, dynein...

Already in the 3rd century B.C. the physician Erasistratos of Ceos associated muscle motion with the *spiritus animalis*, a sort of fluid ("pneuma") that, after being produced in the brain, is pumped through the body along hollow nerves as pipelines and makes muscles swell and shorten. The idea of "pneuma" survived until the works of Hermann von Helmholtz, who in 1847 introduced the idea that the muscle is an isothermal machine. Thanks to single molecule imaging and manipulation techniques, in the last decades we have assisted to a tremendous advancement in understanding the origin of motion in biological systems. The primary cause of motion in the cell are specialized enzymes called molecular motors or motor proteins. In addition to the contraction of muscle cells, they power smaller-scale (microscopic) intracellular movements: they help in forming mitotic spindles and moving chromosomes to the opposite sides of the cell during mitosis, enzymes along DNA strand during synthesis, and enzymes organelles along molecular tracks. These highly efficient machineries produce mechanical work by hydrolysing ATP.

Exactly as in the human-engineered devices, there are rotary and linear motors. *Rotary motors* are situated on mitocondria membrane to pomp ions through the membrane (e.g. F0/F1 ATPase) or are involved in the propulsion of cell through the motion of flagella. *Linear motors* are associated to the filaments of the cytoskeleton (microtubules or the

F-actin): they work, in a stepwise way, attached to these tracks. Within this category one find three main families: myosins, kinesins and dyneins.

The first motor protein identified was skeletal muscle **myosins** (precisely myosin II) [40]. This myosin is an elongated molecules composed of two chains that form a long coiled-coil tail and two globular domain that contains the force-generating mechanism. The long tail bundles itself with the tails of other myosins in the formation of a large bipolar thick filaments. The muscle contraction is the effect of the motion of billions of myosins sliding actin filaments parallel to the bundles.
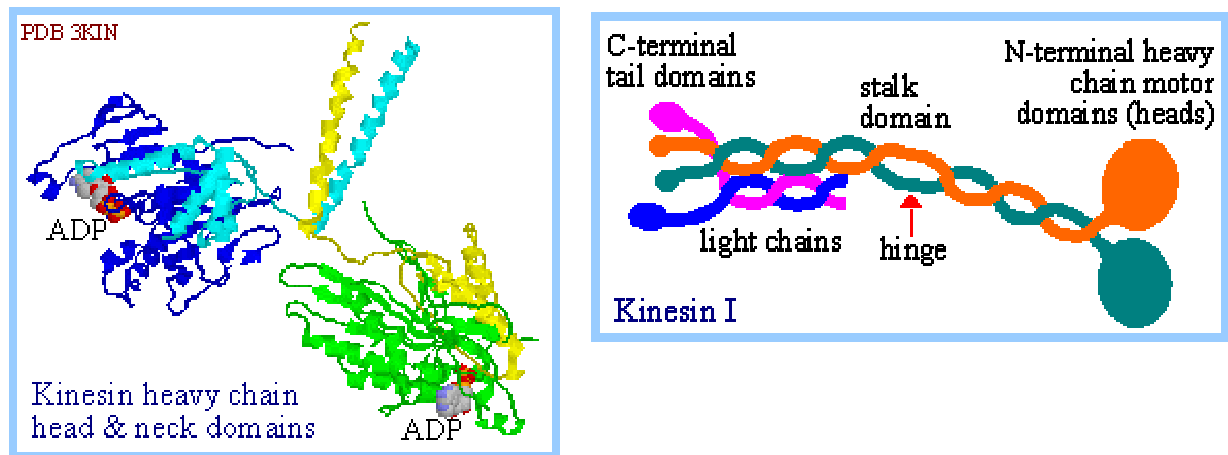
Figure 1.1: Kinesin secondary structure (left) and cartoon of the motor protein (right). (Adapted from Ref. [153])

Microtubule associated motors, the **kinesins** and the **dyneins**, move along microtubules to actuate the directional motility of membranous vesicles, organelles, chromosomes, protein rafts and RNA. Kinesins are a large family of proteins with diverse structure. Mammalian cells count at least 40 different kinesins genes, but since the first to be discovered was Kinesin I (KinI) we refer to it in the following. KinI is made of a motor domain (usually composed of two heads), a stalk domain and a tail domain. The motor domain is globular ATP binding site. Again ATP is hydrolyzed in the motor domain producing a conformational change responsible for the motion of the motor. Observations have shown that the motion can occur only in one direction, from the $(-)$ to the $(+)$ end (*anterograde*); this is due to the *stereospecifical* interaction between the two globular domains and the microtubule, i.e. they bind at a unique location on the filament and with a specific orientation. Moreover, since the motion requires a chemical reaction, it occurs with a rate which depends on the availability of the fuel (i.e. the ATP concentration). Kinesins are usually highly processive motors, i.e they can perform a long walk on the microtubules before detach from it. The physical properties are measured with high accuracy: a single motor perform a biased stochastic motion with almost no back-step probability, average speed of $1800nm/s$ in vivo ($840nm/s$ in vitro), steps of $8nm$ (compatible with the struc-

ture of the microtubules) and force $\sim 6pn$. These motors play a key role in organizing the endoplasmic reticulum and the Golgi apparatus, while in the case of axons in neural cells they move from the nucleus to the periphery of the cell. The great diversity of kinesin family motors used in axonal transport suggests that they are involved in specific targeting: the tail is in fact chemically functionalised to attach molecules wrapped in vesicles and organelles.

Dyneins are larger than kinesins, can be much faster, less processive and require a large number of accessory proteins to associate with membrane-enclosed organelles. Moreover their motion is *retrograde* i.e. from the (+) end to the (-) end of the microtubule and are involved in bringing back the old components from the axon to the nucleus for the degradation and recycling.

The different functions of the motors led to a distinction between *rowers* and *porters* [94]. The rowers are characterized by working always collectively in large arrays (some families as myosin II up to 10^9 molecules) spending little of their time in the strongly bound state. Porters are often called *processive motors*, they work mostly in low concentration and do not cooperate since they usually transport cargos by moving on a molecular track. Most of myosins are rowers, kinesins and dyneins are usually porter. However such a division is not clear: e.g. myosin V works as a dimeric porter with a speed up to $60\mu m/s$, although its processivity is rather low; kinesins are involved in the formation of mitotic spindles for which cooperative effects are required and ciliary dyneins power the beating of cilia bending the microtubules.

Clearly processive motors (like kinesins and dyneins "walking" on the microtubules or myosin V on F-actin) are the most suitable candidates to create the amazing and complex traffic picture mentioned in the first paragraph.

1.1.4 Motors on nucleic acids

A paradigmatic process in cell biology, where a molecular motor moves on a one-dimensional track, is the translation process, in which a ribosome binds to mRNA at the ribosome-binding site in an initiation step (Fig. 1.2). Next, it proceeds as in a series of elongation steps, at each of which it recruits an aminoacyl-tRNA (aa-tRNA) that is appropriate for the codon being read, and hydrolyzes two molecules of GTP (guanosine-triphosphate, the equivalent of the ATP for these motors). The aminoacid from aa-tRNA is added to the growing protein and the ribosome can advance to the next codon. Many ribosomes can work at the same time on the same substrate.

This system (actually a more general one, made just of an enzyme proceeding on a nucleic acid) suggested the first statistical model [97, 96] where traffic effects emerge. The model considers a one-dimensional lattice where extended particles, that occupy L sites, move always in one direction with certain rate and cannot overtake. We will consider this basic example in the next chapter.
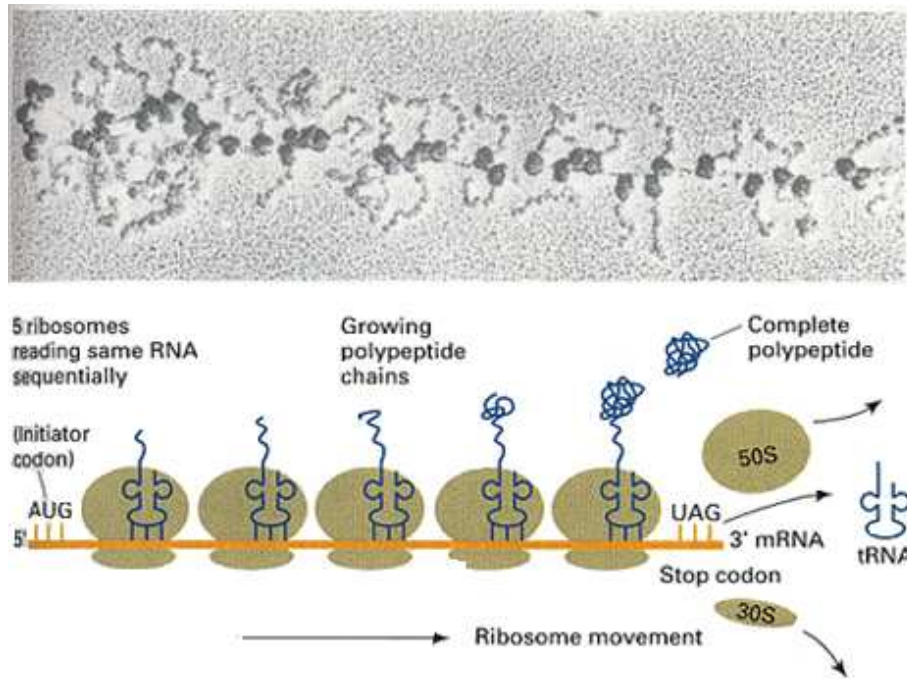
Figure 1.2: Ribosome on mRNA. (Adapted from Ref. [155])

1.2   Experimental techniques

1.2.1   Imaging techniques

The size of biomolecules are in the order of nanometers and therefore too small to be observed by conventional optical microscopy. To overcome this problem biomolecules can be fluorescently labeled and visualized using fluorescence microscopy. There are several techniques, the most important of which are maybe the Total Internal Reflection Fluorescence Microscopy (TIRFM) and the Confocal Microscopy (CFM). The first is used to increase the contrast: a laser light is incident on the interface between a glass surface (high refractive index) and the solution (low reflective index); above the critical angle the light is totally reflected and only the evanescent field penetrates shortly beyond the interface (decaying exponentially on a scale of $150nm$). The signal over noise is improved 2000 times with respect to conventional fluorescence microscopy.

The Confocal Microscopy is often used to track bigger and moving structures in three dimensions: a laser is used to illuminate a small pinhole whose image is focused at a single point at the specimen. Emitted fluorescence from this focal point is focused at a second (confocal) pinhole, while emitted light from everywhere else in the specimen is not focused and does not contribute to the final image.

The problem is to label the molecules with the proper fluorophore. Kinesin can be genetically engineered so that a part of it consists of Green Fluorescence Protein (GFP) a

natural fluorophore emitting in the green. The experiments using GFP can easily bleach the motor (i.e. the fluorophore can denature, in a sense "burn", the motor domain). This experimental difficulty has been recently tackled by using quantum dots attached to the biomolecules; they are semiconductor particles that can be excited to different energy levels and used to obtain different signals with high spatial and spectral resolution [8, 152, 134, 22]. This technique is only at its early stages but looks extremely promising.

1.2.2   Single molecule manipulation

In the last fifteen years techniques of single molecule manipulation have been increasingly developing, for example now single biomolecules can be captured by micro-needles or attached to beads through chemical functionalization of a part of the molecule. Optical tweezers are used to trap and manipulate these beads of $25nm$ to $25\mu m$ in diameter by the force of laser radiation trapper. A typical experiment consists in attaching a fluorescent beads (usually an appropriate colloidal particle) to the tail domain, and observing the fluctuations in the position of the trap caused by the movement of the motor[2]. The trap is necessary to keep the tail stretched but the fluctuations can be rather strong. Nevertheless this was the method employed to measure the stall force, i.e. the force necessary to make the motor step back (giving therefore an estimation of the maximal force a kinesin motor can exert), the length of a step and the rate limiting step in the process (see e.g. [143, 142, 151]).

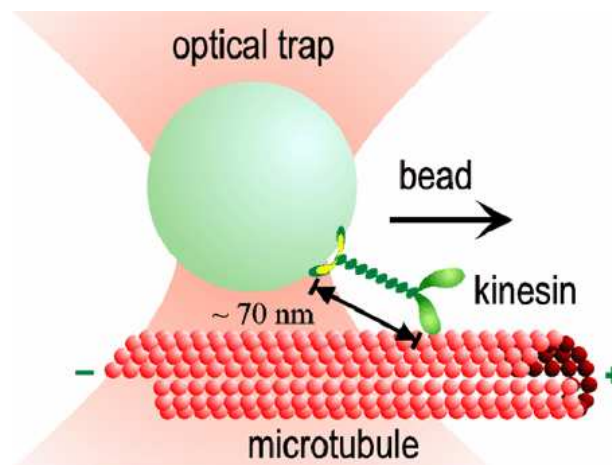Figure 1.3: Schematic representation of a single molecule manipulation experiment: a bead is attached to the functionalised tail domain of the kinesin and is manipulated using optical tweezers. (Adapted from Ref. [154])

---

[2]As some experimentalists occur to say, this is equivalent to "observe the motion of a walking man by observing a huge balloon (~ 100 times bigger) that he is carrying hundred meters below"!

1.3   Stochastic models of molecular motors

The pioneering work in modelling muscle contraction has been done by A.F. Huxley[3]. He proposed [67] an explanation for muscle contraction. It idealizes the myosin heads imbedded in the myosin filaments of a sarcomer as harmonic springs with two states. In the bound state the motor head forms a *crossbridge* between neighboring myosin and actin filaments. In the unbound state the heads are freely fluctuating around their equilibrium positions. Directed motion is explained by the ad hoc assumption that binding preferentially happens when the spring is loaded in forward direction and unbinding after finishing the work, i.e. when the spring is relaxed or loaded in backward direction. Huxley's model can also be reinterpreted as a power-stroke model, if one assumes symmetric binding and unbinding rates followed by some structural changes in the myosin heads. Binding/unbinding of the spring is then followed by a backward/forward shift of the equilibrium position. These conformational changes in the spring then generate a force in the forward direction ("power stroke").

Later on, other stochastic models have been proposed to capture the main features of the motion of the molecules. The easiest model one can think for a *single* processive motor moving on a track (e.g. kinesin on a microtubule) consists of a particle that steps *stochastically* a given number of times (α) per unit time. Such a model corresponds to a well known stochastic birth process with constant birth rate α: it is a random variable $N(t)$ which advances by one with constant rate α. In Appendix 1.A we show that this is indeed a Poisson process and that the average and variance of the motor position are therefore identical and equal to the rate:

$$\langle x \rangle = \text{Var}(x) = \alpha t \,. \tag{1.2}$$

In the last years there have been many attempts to model the proteins, taking into account the internal cycle that the motor performs.

A more sophisticated theoretical concept that helped in modelling systems with more than one time scale, is the one of *thermal ratchets* (for a comprehensive review see [124]). The word "ratchet" was used in the contest of non-equilibrium thermodynamic by Smoluchowsky back in 1912 and made famous by Feynman in one of his lecture [46]. The idea is to rectify the unbiased random motion of particles hitting a paddle by connecting it to a ratchet with an axle. The ratchet are controlled by a pawl that allows the saw-teeth to proceed in one direction but excludes a rotation in the opposite direction. The role of the pawl is controversial and closely resembles the one of Maxwell's demon: in fact the whole system is a perpetuum mobile of the second kind, that violates the second law of thermodynamics. The fact is that the device does not work since the pawl itself is subject to thermal fluctuations and eventually the ratchet can step back. To extract work two different temperatures (one for the ratchet, one for the pawl) need to be inserted in the

---

[3]A.F. Huxley (1917-), Nobel prize for medicine in 1963 for his "discoveries concerning the ionic mechanisms involved in excitation and inhibition in the peripheral and central portions of the nerve cell membrane".

system. Exploiting this concept, several ratchet models have been introduced to describe nano-devices and molecular motors: all the systems are supposed to "rectify" Brownian motion. The spatially asymmetric binding and unbinding rates in Huxley's model rectify the thermal fluctuations of the motor heads. In this sense Huxley's model is a prototypical example for a thermal ratchet model. The idea is to parameterize the motor by means of a few parameters describing the motion of a particle diffusing in an asymmetric, periodic, saw-tooth potential. A motor can escape from a minimum of the potential because of ATP hydrolysis, which is modelled by a fluctuating force or a fluctuating kinetic barrier of the chemical reaction [98, 7]. As an a-side research line, devices where fluctuations are comparable with the force exerted pose challenging questions on the laws of thermodynamics at the microscopic level (see for example [125]).

Almost all later crossbridge models are in some sense variations or refinements of the above mentioned Huxley's two-state model. Starting from these ideas many other models have been proposed, in order to describe the behavior of the motors using few experimentally accessible parameters. In particular the prediction of internal timescales, corresponding to different steps of the motor, and efficiencies have been, in the last decade, a challenge for theoretical physicists [94, 6, 71, 47, 91, 113, 110, 90].

One of the most studied processive molecular motors, where all these techniques have been applied, is kinesin[4]. It has been found, by optical and electron microscopy, NMR and molecular dynamic simulations compared with high resolution data, that kinesin is a processive motor that undergoes the following cycle (see Fig. 1.4): (1) one head of a two-headed kinesin molecule, initially with both heads in the ADP form, binds to a microtubule; (2) release of ADP and binding of ATP results in a conformational change that locks the head to the microtubule and pulls the neck linker to the head domain, throwing the second domain toward the plus end of the microtubule; (3) ATP hydrolysis occurs while the second head interacts with the microtubule; (4) the exchange of ATP for ADP in the second head pulls the first head off the microtubule, releasing phosphate and moving the first domain along the microtubule; (5) the cycle repeats, moving the kinesin dimer $8nm$ farther down the microtubule. For each of these steps a timescale is associated. More microscopic models, concerned with coarse grained or even ab initio molecular dynamics simulations, aim to measure the small conformational changes resulting from the hydrolysis of ATP. These methods have the drawback of requiring a huge amount of CPU time and to be extremely specific to the model investigated.

Parallel to the single molecule models, attempts to describe the collective motion of motors have led to considerable results, mainly in the field of rowers [72]. Not too much has been done concerning the porters, where the collective motion gives rise to traffic effects. This thesis finds its motivation in this field, hence the problems related to single molecule kinetics mentioned above, will not be touched in the following because we will consider only Poisson motors and therefore with a single time scale. The reason we can do that is because the shortest timescales are not really relevant. Indeed one can absorb the time scales in a single one just by a redefinition (and actually the slowest time scale dominates

---

[4]For an overview see the website:`http://www.proweb.org/kinesin`
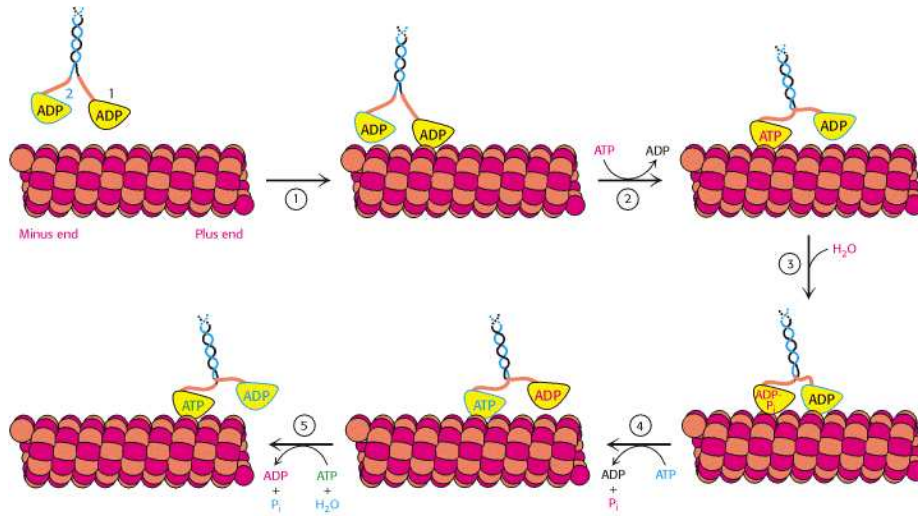
Figure 1.4: Mechanochemical cycle of Kin1. See text for explanation. (Adapted from Ref. [9])

the process). For the purpose of studying traffic behavior of many motors, one time scale is sufficient to catch all the required features. It has been shown [127] that the autocorrelation function of a single motor is not affected, for the accuracy visible in the experiments, by the presence of many time scales in the dynamics of the motor. This suggests that just by considering new microscopic internal time scales, one should not expect a collection of motors to exhibit new features; of course if a new interaction enters the system, it must be taken into account.

1.4   Traffic in biology

In the next chapter we will see how the traffic of molecular motors can be suitable described by a system of particles hopping on a discrete lattice. This kind of models has been applied in various related problems. In a recent review by Chowdhury and coworkers [20] not only the molecular motors that inspire the work done in this thesis, but also other kind of traffic are mentioned.

For example social insects like ants and termites move on pheromones tracks: each individual moves in a one-dimensional track interacting with another insect by dropping a chemical (pheromone). Both uni-directional and bi-directional motion have been considered investigating the fluxes and average speeds.

Another related example is the traffic of pedestrians on trails: pedestrians are modeled as particles moving in a two dimensional system according to their desire, the interaction with other particles and with the infrastructure. These models have application in designing anti-panic exits.

Beyond the analogies between the usual traffic and the one of many (processive) motors

on microtubules there are some major differences, the main of which is that cars move in a continuum and more or less in a parallel way. The dynamics on a single track is generally boring. In modelling real traffic of cars some other properties must be taken into account: the motion occurs in a deterministic way, but there is a stochasticity depending on the psychology of the drivers (tendency to run faster, aggressively, abruptly brake...); moreover the motion occurs often on a network or on a complicate geometry where several flows compete.

The study of these model is motivated by the diverse collective phenomena that can arise in the system such as

Jamming: the flow is limited by a bottleneck situation or by opposite current of particles (molecules, animals, people...).

Pattern formation: especially when two or more species of particle move with different properties one can see segregation, separation of the flow, pattern that form at intersection etc...

Oscillation: in counterflow at bottleneck (imagine a door) an oscillatory behavior can be observed where people enter only at regular interval.

Panic: in this case one can have the rather counterintuitive phenomena like the freezing-by-heating (or faster-is-slower) effect, when an enhancement of the individual velocity results in a global slow down.

In the following we will see some models that account for the formation of jams (and pattern) in a system intended to mimic the traffic of molecular motors on microtubules.

1.5 Theoretical challenges

In this thesis we will focus on the modelling of a system formed by a single microtubule immersed in a solution of ATP and kinesins. To the eye of a physicist there are several ingredients that a minimal model must encode in order to catch the interesting aspects of this system:

1. Motors bind specifically to the microtubule and transport occurs unidirectionally. Although some of the tracks are actually quasi-one dimensional (the microtubule is formed by 13 microfilaments, each of which constitute a track for the motors), we will consider the track-exchange event irrelevant and therefore the motion occurring in purely one dimensional fashion. These features are guaranteed by the chemical interaction between the motors and the microtubules.

2. Each particle hydrolyzes an ATP molecule (i.e. it performs a jump) every $\tau \sim 10ms$; this process occurs stochastically since each motor can be idealized as a Poisson stepper with a typical timescale given by τ.

3. A site occupied by a motor cannot be occupied by another one at the same time: motor mutually exclude each other.

4. Motors can attach and detach at each site stochastically.

5. The motors are extended particles: a single motor can occupy more than one site. In the case of a special kind of kinesin (Kif1A) the site occupied is just one, but conventional kinesin is a dimer; dyneins and myosins V are dimers; ribosomes cover 12 codons on mRNA; in the general case of real cargo one can consider a distribution of lengths; in the following we will focus only on the monomer and dimer cases.

6. In the track there could be structural defects or microtubule associated proteins interacting with the motors (the Tau proteins, for example, that seem to be relevant in Alzheimer disease). Such defects may slow down the motion of the motor and may reduce its affinity with the track (and hence its processivity) [37, 99].

The standard model that encodes the first three features exposed above is the Totally Asymmetric Simple Exclusion Process (TASEP). In this thesis we extend the TASEP, including the fourth and the fifth properties, i.e. focusing on a system of dimers without conservation of particles. We have also studied, separately, the influence of a single defect in these systems. The last part of the work is devoted to collective dynamical effects of the TASEP, and of a single tracer particle in the TASEP without conservation of particles.

The driven lattice gases in one dimension are *per se* a fascinating problem of statistical mechanics that involves non-equilibrium thermodynamics, stochastic models and diffusion processes. In addition to that, since investigating collective phenomena at the molecular scale involves experiments extremely hard to control, there is an increasing demand of quantities to be quest that are accessible with the actual technology. The aim of this work is therefore twofold: we hope to stimulate the investigation of such systems by suggesting the proper quantities to measure; moreover we aim to test the robustness of the physical picture upon the introduction of several ingredients (such as attachment and detachment, presence of extended non point-like particle, presence of a disorder, interaction between particles) and therefore understand which of these features are essential to construct a minimal model able to catch the interesting physics underlying the biological system.

1.6   Outline

The outline of the thesis is the following:

Chapter 2: In the next chapter we will review some general concepts of non-equilibrium physics, which will be used in the following. We present the known results of the Totally Asymmetric Simple Exclusion Process (TASEP) and its mean field solution. Finally we review the many TASEP-like model with peculiar attention to the results presented mainly in [111, 112] where the TASEP is couple to Langmuir kinetics, i.e. the attachment and detachment in the bulk.

Chapter 3: We present a generalization of TASEP with extended particles coupled to a reservoir. We interpret the result of MC simulations by mean of a (non-trivial) MF equation specifically derived for this problem. Interestingly the picture found in the case of monomers is confirmed since the phase diagram is distorted but topologically unchanged. We comment on the robustness of the system.

Chapter 4: We analyze the role of a bottleneck, i.e. one site on which the hopping rate is smaller than one, on the stationary profile of TASEP with on/off kinetics both in the monomer and dimer case. By mean of a simple argument based on minimization of the current we extract the whole phase diagram, checked against numerical simulations.

Chapter 5: We present the problem of the dynamics of the TASEP. We study the dynamic correlation function of the process and describe the evolution of such a function using a phenomenological approach (the Boltzmann Langevin method). This method works in some regime even at a quantitative level.

Chapter 6: We try to answer the question: what kind of quantities related to the whole system could be measured from a single molecule experiment? We show how the different phases of the phase diagram, and hence the related traffic effects, could be tracked by analyzing the average and the variance of the position of a single tracer particle.

Chapter 7: We conclude revisiting the main results of the thesis and commenting on possible outlooks.

Appendix 1.A   The Poisson stepper

In this appendix we analyze the Poisson stepper, the easiest stochastic model of molecular motor without internal dynamics. Let $p_n(t)$ be the probability for the particle to be at position n after a time t. We can write down the master equation, i.e. the equation for the time evolution of the probability, (see also next chapter), as:

$$\frac{d}{dt}p_n(t) = \alpha\left(p_{n-1}(t) - p_n(t)\right) \tag{1.3}$$

with initial condition $p_0(0) = 0$ and normalization condition $\sum_{n=0}^{\infty} p_n = 1$. Typical quantities one would like to evaluate are the average velocity, the variance and therefore the randomness parameter. This master equation describes what is known as *birth process*.

The velocity can be found easily by multiplying both sides of the master equation by n and then computing the sum over all the states:

$$\begin{aligned}
\frac{d}{dt}\langle n(t)\rangle = \frac{d}{dt}\sum_{n=0}^{\infty} np_n(t) &= \alpha\left[\sum_{n=1}^{\infty} np_{n-1}(t) - \sum_{n=0}^{\infty} np_n(t)\right] \\
&= \alpha\left[\sum_{m=0}^{\infty}(m+1)p_m(t) - \sum_{n=0}^{\infty} np_n(t)\right] \\
&= \alpha\sum_{n=0}^{\infty} p_n(t) = \alpha\,,
\end{aligned} \tag{1.4}$$

with the solution

$$\langle n(t)\rangle = \alpha t + n_0 \tag{1.5}$$

where n_0 is the initial condition (the position at time $t = 0$), which could be set to zero. The variance can be obtained in the same way and results in

$$\left\langle (n(t) - \langle n(t)\rangle)^2 \right\rangle = \alpha t \tag{1.6}$$

Another important quantity is the ratio of the variance and average of the position, the randomness parameter, which is clearly equal to one if $n_0 = 0$. Intuitively speaking, it is related to the number of stochastic processes underlying a certain phenomenon (note that the Poisson process has randomness one).

The full probability can be computed by considering that Eq. (1.3) can be rewritten as

$$\frac{d}{dt}p_n(t) + \alpha p_n(t) = \alpha p_{n-1}(t)\,, \tag{1.7}$$

which can be rephrased as a first order differential equation

$$\frac{d}{dt}\left(e^{\alpha t}p_n(t)\right) = \alpha\left(e^{\alpha t}p_{n-1}(t)\right) \tag{1.8}$$

Starting from $p_0(t)$ one can determine recursively p_n but needs to start from $p_0(t)$, i.e. the probability that no step occurs in the interval $[0, t]$. Let us divide such an interval in small intervals size Δt. If we choose the interval to be small enough only one step can occur within Δt and therefore

$$p_0(\Delta t) = 1 - \alpha \Delta t \tag{1.9}$$

Since $p_0(t)$ is just the product of the disjoint probabilities that nothing happens at each time step and since we want the interval to be as small as possible we can write:

$$p_0(t) = \lim_{\Delta t \to 0} (p_0(\Delta t))^{t/\Delta t} = \lim_{\Delta t \to 0} \left(1 - \alpha t \frac{\Delta t}{t}\right)^{t/\Delta t} = e^{-\alpha t}, \tag{1.10}$$

where we used the common definition of exponential function. By defining now $f_n \equiv e^{\alpha t} p_n(t)$ with $f_0 = 1$ the recursion relation becomes

$$\frac{df_n(t)}{dt} = \alpha f_{n-1}(t) \tag{1.11}$$

which yields then to $f_1(t) = \alpha t$, $f_2 = \frac{1}{2}\alpha^2 t^2$ and in general

$$f_n(t) = \frac{\alpha^n}{n!} t^n \tag{1.12}$$

Finally the process is characterized by the so called Poisson distribution[5]:

$$p_n(t) = e^{-\alpha t} \frac{(\alpha t)^n}{n!} = e^{\langle n(t) \rangle} \frac{(\langle n(t) \rangle)^n}{n!} \,. \tag{1.13}$$

---

[5]Note that the process is not different from the beta decay of a radioactive nucleus, where we are indeed interested in the death process.

Chapter 2

Review of driven lattice gas models

Πάντα ρει καί ούδέν πέλει
Everything flows and nothing stays
fixed

Heraclitus

In this chapter we review the main features of the driven lattice gas models used in the rest of the thesis to describe collective phenomena of self propelling particles in one dimension. After an overview of the some general concepts of non-equilibrium models we will present some standard techniques used in the rest of the work and we introduce the Totally Asymmetric Simple Exclusion Process (TASEP) together with the results obtained both from exact methods and from mean field techniques.

Intracellular transport powered by motor proteins, such as kinesins and dyneins on microtubules, constitutes a biological application related to TASEP. A substantial difference to the directed motion of ribosomes on mRNA is the exchange of molecular motors with the surrounding cytosol acting as a particle reservoir. This observation has motivated a recently proposed extension of TASEP, by supplementing the unidirectional hopping with Langmuir (on-off) kinetics in bulk [95, 111]. The study of this system has shown an unexpectedly rich and new phase diagram with phase coexistence regions. Surprisingly the in the large system size limit the density profiles show a sharp discontinuity (shock separating low form high density phase) or cusp in a large portion of the phase diagram.

2.1   Non-equilibrium physics

The aim of statistical mechanics is to deduce the macroscopic quantities (well-known from classical thermodynamics) from the microscopic components of the particle that constitute a system. Equilibrium statistical mechanics is based on Boltzmann-Gibbs ensembles theory: in the canonical ensemble, the average energy and the number of particles are constrained, the probability of finding a system in a configuration $\mathcal{C}$ with energy $H[\mathcal{C}]$ in

the phase space is given by $\exp -\beta H[\mathcal{C}]$ (with $\beta = 1/k_B T$). A crucial role is played by the partition function which is the sum over all possible configurations a system can assume in a given ensemble: $Z_N = \sum_{\{\mathcal{C}\}} \exp(-\beta H[\mathcal{C}])$. Every thermodynamic quantity can be derived from this function. If the number of particles is not fixed it is more convenient to use the grand canonical ensemble, where number fluctuations are connected to an energy fluctuation of $\beta\mu$ per particle, where μ is called chemical potential; in this case the grand canonical partition sum is used: $\mathcal{Z} = \sum_{N=0}^{\infty} \exp(\beta\mu N) Z_N$.

On the other side no general theory of non-equilibrium processes has yet been establish. A system out of equilibrium does usually have a stationary state, the so called *the non-equilibrium steady state* (NESS), but its probability in the phase space is not given by the usual Boltzmann-Gibbs distribution. In order to keep the system out of equilibrium a flux of energy is usually required, hence these systems are said to be *driven out of equilibrium*. In many systems the particles are self-propelled and the energy consumption is actually hidden in this hypothesis (e.g. molecules, swimming animals and bacteria, vehicles in traffic...). Most of the systems in nature, especially in chemistry and biology, are indeed of this kind: as a general statement one could say that the life is indeed a driven process which require a constant flux of energy to lead the system in a state which would be extremely unlikely to reach in equilibrium [2, 65, 108] (and this is probably why biology does not cease to surprise the physicists!). Small system like molecular motors operate constantly out of equilibrium, using the energy of ATP hydrolysis, moreover the fluctuations are important since comparable with the scale of energy involved in the process (see e.g.: [125]).

The NESS is characterized by means of a variable, the order parameter. Usually it is a smooth function of time and space. Although the term *phase* has well defined meaning only for equilibrium systems, it is commonly used to identify all NESSs for which the order parameters share the same analytical properties in space. In some other communities these are called patterns or structures. Consequently a system can present transition from one structure to another and hence *non-equilibrium phase transitions* (or pattern formation), where divergences of characteristic length scales (e.g. correlation lengths) arise for specific values of the parameters. The definition is rather blurry and need an ad hoc formulation for each model (especially where no exact solution is known). For some models (e.g. the totally asymmetric simple exclusion process) a partition function has been computed and the analogous of Yang-Lee theory has been constructed [14], but this is a rather exceptional case.

Since we will consider only one dimensional systems, is in order at this point to make a comment: from an equilibrium statistical mechanics perspective, the existence of phase transitions in one dimension may look surprising, since it violates the so called van Hove theorem (that states that one dimensional, homogeneous, non-driven systems of hard particle with short range introduction do not exhibit phase transition [63]) [1]. Any many-particle

---

[1]Van Hove actually proved that the free energy of a one dimensional system of particles with short range attractive interaction and hard core repulsion, does not exhibit any non-analyticity. Landau argued, more precisely, that a bistable system with finite interface energy (e.g. the energy of a kink in a spin chain) will gain entropy by breaking up into macroscopic number of domains, making macroscopic phase coexistence at any finite temperature impossible.

interacting system with site restriction and out of equilibrium has a correspondent coupled spin system with a stochastic dynamics (later we will see how to pass from a description to the another). The time takes the role of an additional dimension. Hence, the non-equilibrium system can be mapped on a $1+1$ dimensional spin system at equilibrium for which phase transitions are not surprising. Usually the problem can be written in a fermion formulation and in the lucky case transformed into a boson field theory (bosonization) usually solvable. The propagators and relevant diagrams, though, are not the same usually found in ordinary quantum field theory and therefore sometimes the system requires a study on itself (for reviews on the applicability of these methods see e.g. [146, 145, 17]).

Master equation and detailed balance In the case of systems without memory, i.e. Markovian, it is possible to describe the evolution of the probability where the transition rates depend exclusively on the configuration. The equation describing the evolution of the probability is the master equation:

$$\partial_t P(\mathcal{C}) = \sum_{\mathcal{C}' \neq \mathcal{C}} [W_{\mathcal{C}' \to \mathcal{C}} P(\mathcal{C}', t) - W_{\mathcal{C} \to \mathcal{C}'} P(\mathcal{C}, t)] \tag{2.1}$$

As can be seen, such an equation is the sum of a gain and a loss term where the transition rates $W_{\mathcal{C}' \to \mathcal{C}}$ can be inferred from the dynamical rules. It is expected that the system evolves towards a stationary ensemble $P^{st}(\mathcal{C})$ for long times.

One solution of Eq. (2.1) is available, namely the probability that satisfies:

$$\frac{W_{\mathcal{C}' \to \mathcal{C}}}{W_{\mathcal{C} \to \mathcal{C}'}} = \frac{P(\mathcal{C})}{P(\mathcal{C}')} . \tag{2.2}$$

This expression is called the *detailed balance condition*. It is satisfied only by system that are in equilibrium. In this case it is possible to associate an energy function $E(\mathcal{C})$ to each configuration and the steady state distribution $P^{st}(\mathcal{C})$ is proportional to $e^{E(\mathcal{C})/k_B T}$, i.e. is the Boltzmann distribution.

The lack of detailed balance can therefore be taken as alternative definition for a system out of equilibrium for which the existence of a stationary state is not granted and usually have to be postulated. Generally, the steady state distribution cannot be calculated and the condition (2.2) cannot be directly used. Nevertheless it is possible to give an easy condition: given the set of microscopic configurations $\mathcal{C}_1, \mathcal{C}_2 \ldots \mathcal{C}_k$, the detailed balance requires reversibility (i.e. any cycle in the configuration space must occur with the same probability independently on the way the system go through it):

$$W_{\mathcal{C}_1 \to \mathcal{C}_2} W_{\mathcal{C}_2 \to \mathcal{C}_3} \ldots W_{\mathcal{C}_k \to \mathcal{C}_1} = W_{\mathcal{C}_1 \to \mathcal{C}_k} W_{\mathcal{C}_k \to \mathcal{C}_{k-1}} \ldots W_{\mathcal{C}_2 \to \mathcal{C}_1} \tag{2.3}$$

for each cycle in configuration space $\mathcal{C}_1, \mathcal{C}_2 \ldots \mathcal{C}_k$. This condition is called *Kolmogorov criteria* and is equivalent to Eq. (2.2) (for a short proof see [104]), therefore to prove that a system is not in thermal equilibrium it is enough to find a single path in configuration where Eq. (2.3) is not satisfied.

2.2 Methods

In this section we present some of the methods used to study driven lattice gases. After having introduced the quantum Hamiltonian formalism we connect it to the typical quantities one is interested in. This approach allows to map classical stochastic processes on quantum problem. Unfortunately the quantum problems usually treat other quantities and the formalism is often interesting only as a recipe to get the equation of motion for a specific observable, but not to solve it. In many cases one requires approximated treatment, the easiest of which is the conventional "mean field", which will be described in the following. Most of the research on non-equilibrium systems relies therefore on Monte Carlo simulations, which will be presented later on.

2.2.1 Quantum Hamiltonian

The master equation (2.1) describing a non-equilibrium lattice gas of N sites, can be conveniently rewritten as a Schrödinger-like equation in imaginary time. The idea is to rewrite the configuration $\mathcal{C}$, which is completely specified by the set of occupation numbers $\underline{n} = (n_1 \ldots \underline{n}_N)$ (with $\underline{n}_i = 0, 1$ particle occupation number at site i). One can introduce the basis of orthonormal vectors $|\underline{n}\rangle$ and $\langle\underline{n}|$ defined as

$$
\begin{aligned}
|\underline{n}\rangle &= |n_1\rangle \otimes \cdots \otimes |n_L\rangle \\
\langle\underline{n}| &= \langle n_1| \otimes \cdots \otimes \langle n_L|
\end{aligned}
\tag{2.4}
$$

where the vectors $|n_i\rangle$ belong to the two dimensional space at each site, which account for the two possible states at that site. The representation in such Hilbert space is

$$
\begin{pmatrix} 0 \\ 1 \end{pmatrix}_i \qquad \text{if site } i \text{ is occupied}, \tag{2.5}
$$

$$
\begin{pmatrix} 1 \\ 0 \end{pmatrix}_i \qquad \text{if site } i \text{ is empty}. \tag{2.6}
$$

These vectors span an Hilbert space of dimension 2^N, where one defines the vector probability as the state:

$$
|P(t)\rangle \equiv \sum_{\underline{n}} P(\underline{n}, t)|\underline{n}\rangle \tag{2.7}
$$

where $P(\underline{n}, t)$ is the probability for the system to be in configuration $\underline{n}$. Consistently one can also define the operator $\hat{H}$ as

$$
\hat{H} = \sum_{\underline{n}' \neq \underline{n}} |\underline{n}\rangle W(\underline{n}', \underline{n})\langle\underline{n}| - |\underline{n}\rangle W(\underline{n}, \underline{n}')\langle\underline{n}'| \tag{2.8}
$$

which will be called *stochastic Hamiltonian*. The reason for the name comes from the analogy between the Schrödinger equation and the master equation (2.1), which can be rewritten as

$$
\partial_t|P(t)\rangle = -\hat{H}|P(t)\rangle. \tag{2.9}
$$

The Hamiltonian obeys the condition

$$\sum_{\underline{n}} \langle \underline{n}|\hat{H}|\underline{n}'\rangle = 0\,, \tag{2.10}$$

which encodes the probability conservation and it is not necessarily hermitian (actually, in general, it is not). This tells that there must be at a least an eigenvalue equal to zero with the eigenstate correspondent to the steady state and that the left and right eigenstate might not be equal. Note that, although the formalism looks similar (after the usual Wick rotation $i\tau \to t$) there is a fundamental difference with quantum mechanics i.e. the ket states are already probabilities and not probability amplitudes: one has to construct a state $\langle s|$ on which $|P(t)\rangle$ can be projected in order to get $P(\underline{n}, t)$ (an therefore the expectation values of the operators). Since condition (2.10) is valid for arbitrary $\langle \underline{n}'|$, the steady state $\langle s|$ turns out to be the superposition of all the possible configurations:

$$\langle s| = \sum_{\underline{n}} \langle \underline{n}| = \begin{pmatrix} 1 \\ 1 \end{pmatrix}^{\otimes N}. \tag{2.11}$$

Defining the left steady state like this implies automatically the conservation of total probability:

$$\langle s|\hat{H} = 0\,. \tag{2.12}$$

With the notation the equation of motion of any operator $\hat{A}$ is given by the Heisenberg equation:

$$\partial_t \hat{A} = [\hat{H}, \hat{A}]\,. \tag{2.13}$$

Contrary to the usual quantum mechanics formalism the expectation value of an arbitrary operator $\hat{A}$ are

$$\left\langle \hat{A} \right\rangle = \langle s|\hat{A}|P\rangle\,. \tag{2.14}$$

In the case of a so called *local process*, i.e. a process involving only a finite number of neighboring sites $a_1 \ldots a_m$, the operator is constructed using the diagonal ($\hat{P}(\underline{n}_i) = |\underline{n}_i\rangle\langle n_i|$) and the off-diagonal ($\hat{Q}(n_i', n_i) = |n_i'\rangle\langle n_i|$) projectors and assumes an easy form:

$$\hat{H} = \sum_{a_1 \ldots a_m} \sum_{n_{a_1} \ldots n_{a_m}} \sum_{n'_{a_1} \ldots n'_{a_m}} W(\{n'_{a_1} \ldots n'_{a_N}\}, \{n_{a_1} \ldots n_{a_N}\})$$
$$\times \left[\hat{P}(n_{a_1}) \otimes \cdots \otimes \hat{P}(n_{a_m}) - \hat{Q}(n'_{a_1}, n_{a_1}) \otimes \cdots \otimes \hat{Q}(n'_{a_m}, n_{a_n}) \right]\,. \tag{2.15}$$

This means that for a process involving only two neighboring sites $i, i+1$ (such a diffusion with simple hard core repulsion), The Hamiltonian can be simply rewritten as

$$\hat{H} = \sum_{i,i+1} \sum_{n_i, n_{i+1}} \sum_{n'_i, n'_{i+1}} W(\{n'_i, n'_{i+1}\}, \{n_i, n_{i+1}\})$$
$$\times \left[\hat{P}(n_i) \otimes \hat{P}(n_{i+1}) - \hat{Q}(n'_i, n'_{i+1}) \otimes \hat{Q}(n'_i, n_{i+1}) \right]\,. \tag{2.16}$$

Since we are working with a two state system (full and empty sites) we can conveniently take as a vector basis the Pauli matrices σ_i^z, assigning a spin up state to an empty site and a spin down state to an occupied state. With this choice one has:

$$\hat{P}(n_i = 1) = \hat{n}_i = \frac{1}{2}(1 - \hat{\sigma}_i^z) \tag{2.17}$$

$$\hat{P}(n_i = 0) = 1 - \hat{n}_i = \frac{1}{2}(1 + \hat{\sigma}_i^z) \tag{2.18}$$

$$\hat{Q}(n_i' = 1, n_i = 0) = \hat{s}_i^- \tag{2.19}$$

$$\hat{Q}(n_i' = 0, n_i = 1) = \hat{s}_i^+ \tag{2.20}$$

where $\hat{s}_i^\pm \equiv \frac{1}{2}(\hat{\sigma}_i^x \pm i\sigma_i^y)$. With these definitions the exclusion is automatically encoded by the spin algebra of the operators acting on site i (s_i^+ and s_i^-):

$$\left\{ \hat{s}_i^+, \hat{s}_j^- \right\} = \delta_{ij} \tag{2.21}$$

$$\left[\hat{s}_i^+, \hat{s}_j^+ \right] = \left[\hat{s}_i^-, \hat{s}_j^- \right] = 0 \tag{2.22}$$

which automatically implies $[\hat{s}_i^+, \hat{n}_i] = \hat{s}_i^+$ and $[\hat{s}_i^-, \hat{n}_i] = -\hat{s}_i^-$. Consistently the creation of a particle at site i is encoded by s_i^-, the annihilation by s_i^+, a hopping to the right (from site i to site $i+1$) by $s_i^+ s_{i+1}^-$ and the hopping to the left by $s_{i-1}^- s_i^+$; by means of these rules one can write down the Hamiltonian of any system with diffusion, interaction and reaction of particles with site restriction (reaction-diffusion systems, or RDS). For example the part of the Hamiltonian that make a particle hopping to the right with rate ω_R reads:

$$\hat{H}_i = \omega_R \left[\hat{n}_i(1 - \hat{n}_{i+1}) - \hat{s}_i^+ \hat{s}_{i+1}^- \right] , \tag{2.23}$$

while the term of the Hamiltonian creating a particle at site i with rate ω_A reads

$$\hat{H}_i = \omega_A(1 - \hat{n}_i - \hat{s}_i^-) . \tag{2.24}$$

One of the main achievement of the method is the computation of the slowest relaxation time of the system, defined as the timescale on which the correlation function decays. The $2-$point density dynamic correlation function evaluated at time t on the sites i and j of a driven diffusive system is defined as

$$C(n_i, n_j, t) \equiv \langle s | \hat{n}_i \hat{n}_j e^{-Ht} | P_0 \rangle = \langle s | \hat{s}_i^+ \hat{s}_j^+ e^{-Ht} | P(t) \rangle \tag{2.25}$$

where $|P_0\rangle$ is an arbitrary initial state. The eigenstates of $\hat{H}$ are not states with a definite number of particles but the Hamiltonian can always been decomposed in term of them (in this case two particle states); the eigenstates of $\hat{H}$ with two particles are the only one that give non-zero contribution to the correlation function. Therefore the state with minimum energy which can contribute to the $2-$point correlator is the state with the lowest eigenvalue among the one that depend on two particles, which will be called E_{min} (the spectral gap of the Hamiltonian). In the long time limit the contribution of this state

(i.e. the slowest one) will decay as $C \sim e^{-E_{min}t}$. Clearly its inverse $\tau = 1/E_{min}$ identify the time scale at which the slowest mode relax.

Although for systems that are not exactly solvable it is impossible to extract all these informations from the Hamiltonian, one can write down consistent equations of motion and than use proper approximations to study the problem.

2.2.2 Mean field

The problem of a one dimensional non-equilibrium system is completely solved if one can compute the correlation function (static and dynamic) at every order. The density profile is the most natural (and the easiest) quantity to be described (and corresponds to the static one-point correlation function). In the formalism described above its equation of motion is simply:

$$\partial_t \langle \hat{n}_i \rangle = \left\langle [\hat{H}, \hat{n}_i] \right\rangle = \langle F(\{\hat{n}_i\}) \rangle \tag{2.26}$$

This can of course be written from the beginning as a rate equation. The function $\langle F(\{\hat{n}_i\}) \rangle$ can be expressed in terms of k-point correlation functions. The problem is that usually the equation of motion of the k-point correlation function depends at least on the $k + 1$-point correlation function (in some cases even on higher order correlation functions): one needs a way to truncate the hierarchy in a reasonable way. Mean field neglects all the spatial fluctuations and thus any correlations among observables: many body quantities are viewed as products of one-body observable (i.e. $\rho_i = \langle n_i \rangle$):

$$\partial_x \rho_i = \tilde{F}(\rho_1, \ldots, \rho_N). \tag{2.27}$$

The usual mean field approximation consists in replacing correlations with simple averages, e.g.: $\langle n_i n_j \rangle = \langle n_i \rangle \langle n_j \rangle$. It is by no mean trivial that this method work. Especially in one dimension MF approach gives usually bad results in reaction diffusion systems, since correlations play a crucial role. The typical example of failure is the RDS $A + A \rightarrow \emptyset$ (annihilation of particles) where the trivial mean field predicts [2] an approach to the stationary state with the power law t^{-1} instead of the exact one $t^{-1/2}$. Examples where it works relatively well are the random adsorption of point-like particles. A refined mean field will be treated in Ch. 3 and proved to give good results. In the following sections we will see the advantage of such an approximation in a system like driven systems with adsorption and desorption kinetics. More complicate traffic systems, population dynamics, reaction problems described by rate equations and extensively used in mathematical biology, are treated by mean field approach and proved to catch, at least in first approximation, the very physics of the systems [105]. The failure of mean field methods are seen by the physicist as an exciting indication of criticality that requires often more sophisticated techniques allowing for less results.

---

[2]The mean field result is obvious if one write the the rate equation as $\partial t n_i = -n_i^2$, i.e. in the continuum limit $\partial \rho = -\rho^2$, hence $\rho = 1/t$. The exact result can be obtained by Renormalization Group technique.

2.2.3   Kinetic MC: BKL method

To test the range of validity of the theories we consider in this thesis, we have performed extensive Monte-Carlo (MC) simulations. The usual MC method used to simulate driven systems generates random number to choose the move according to the transition probability (which can be determined by the energy of a state or in the case of a lattice gas by the transition rates , update the sites if possible and if not consider the wasted time as a "dead time" when nothing happen. The time scale is always the same. It is clear that such an algorithm is not optimized and on short timescales it is not appropriate to measure dynamics quantities.

In order to simulate efficiently our systems we have chosen the random sequential updating algorithm by Bortz, Kalos and Lebowitz (BKL- or n-fold method) [15, 89]. This method was first used in simple spin systems at low temperature, when the flip of a spin is very unlikely to happen. In its original version it consists of collecting the spins of an Ising like model into lists, in which each member has identical energetic local environment (i.e. same flipping probability). It is deeply connected to the Gillespie algorithm [53] used in simulations of chemical reactions.

Calling p_f the probability of flipping (usually dependent on the transition energy ΔE_l of the class l that the spin belongs to: $p_f = \exp(-\Delta E_l/k_B T)))$, the total flipping probability of any of the n_l spins of class l at a given step is $p_l = n_l p_f$. The integrated probability of some event occurring in a given step for the first M classes is therefore

$$Q_M = \sum_{l \leq M} p_l \,. \tag{2.28}$$

Clearly the total probability for all N classes is Q_N. The procedure consists is generating a random number in the interval $(0, Q_N)$ to determine the class from which the spin that will be flipped is going to be chosen; a second random number is then generated to pick up the spin in the M class (in principle this can be done with the first random number by a proper partition of the interval, speeding up the algorithm); a third random number will be generated to determine the life time of the state just changed. Each time a spin flips it changes its class: it must be removed from the list l and added to a new list according to its new energy class. In addition also its neighbors change their classes: this is the key of the efficiency of the method, which reduces to an effective way of maintaining the lists.

In order to determine the life time of a state, i.e. the time interval associated with the flipping of the spin just selected, one considers the probability that a system is in a state $\mathcal{C}$ at time t and undergoes a transition between time t and $t + \Delta t$:

$$\Delta P(t) = -P(t)\frac{Q_l}{\tau}\Delta t \tag{2.29}$$

where τ is the time needed to execute the flip (i.e. the physical time scale of the problem). The probability of a flip of a spin in any class is therefore

$$P(\Delta) = \exp\left(-\frac{Q_l}{\tau}\Delta t\right) \tag{2.30}$$

Treating this as a stochastic process we generate a random number R in $(0, 1]$ and finally inverting Eq. (2.30), the life time of the state before flipping reads

$$\Delta t = -\frac{\tau}{Q_N} \ln R \, . \tag{2.31}$$

Any statistical property of the system can be computed using ensemble averages or, once in the stationary state, using time moving average where each configuration in weighted with its life time.

Since it keeps a list of all sites which are possible candidates for a successful update, this method is (in many cases) considerably faster than conventional ones. Moreover it constitutes a reliable way to simulate *real time* dynamics of many particles (spin, cellular automata, electrons) lattice systems and achieves an excellent quality in terms of data and computational efficiency in both short and long time regimes [1]. This is due to the fact that the time (being continuous) can be recorded with the desired accuracy.

The adaptation to the case of a lattice gas is a bit subtle, because we talk of probabilities of moves. Anyway, the general idea is to classify in lists only the sites where something can happen so that if, for example, a particle cannot jump because the neighbors are occupied, it is not counted and the time that would be lost in taking into account is automatically consider in the generation of the waiting time interval. We will specify the details of the simulations, which depend on the chosen model and on the quantities we aim to measure, in the following chapters.

2.3 The TASEP

The driven lattice gases are a paradigm of non-equilibrium thermodynamics. As the name says, these models generally consist of point-like particles moving on the sites of a lattice and interacting through a potential to be chosen. These systems (so far a lattice model) can be driven by a field (usually called $\vec{E}$ but not necessarily an electric field) or by thermal gradient (e.g. a bar connecting two reservoirs) i.e. one preferential direction is usually chosen. The constant flux of particles is maintained either by imposing ad hoc boundary condition (that therefore assume a crucial role) or connecting the two boundaries in a periodic structure (note that this implies the application of a field which cannot be written as gradient of any potential!) [128].

In finite systems non-trivial (i.e. not either totally filled nor totally empty lattice) stationary states arise when the the flux of particles is maintained by injection-extraction at the two ends. This class of systems will be the object of this work.

Properties of driven diffusive systems have provided an important tool to study biological systems (such as motion of molecular motors in 1D, ribosomes on DNA track), traffic phenomena (of pedestrians, vehicles, ants) and transport (electrophoresis, thermophoresis, transport properties of (semi)conductors, diffusion in porous materials) [19, 20].

Clearly a lattice containing particles that move according to some internal rules (also called cellular automata) can be described by a driven lattice gas. Fluctuation are simply

encoded in the microscopic dynamics of the particles. In the following we will concentrate on a specific class of one-dimensional driven lattice gas: the *Totally Asymmetric Simple Exclusion Process (TASEP)*. The interest in this system arises not only from its non-trivial properties, despite its simplicity, but also because it has an exact solution (and is thus often considered the "Ising model of non-equilibrium statistical mechanics"). Such exact solutions, far from been available in many systems based on the TASEP, will not be used in the following, but give at least hints on what standard (mean field) approximations cannot catch [120].

2.3.1   The model

In the TASEP one considers a system of identical particles moving uni-directionally with a constant rate along a finite one-dimensional lattice with sites labeled $i = 1, \ldots, N$, of unit length $L = 1$; consequently the lattice spacing reads $a = L/N$ (see Fig. 2.1). The microscopic state of the system $\mathcal{C}$ is characterized by occupation numbers n_i which are binary variables with only two possible values $n_i \in \{0, 1\}$, i.e. we impose a hard-core repulsion between the particles. The system can be constrained to different boundary conditions: the system on a ring is regulated by the number of particles. Of particular interest are systems with open boundaries, where particles enter the system at the left end with a rate α and leave at the right end with a rate β. In summary we specify the dynamical evolution by the following set of updating rules:

- If the particle occupies a site $i = 2 \ldots, N-1$ and the site $i+1$ is empty, it advances one step with unit rate.

- At site $i = 1$ a particle enters the lattice with rate α provided that the first site is empty.

- A particle on site $i = N$ leaves the lattice with rate β.

Moreover we use sequential dynamics, appropriate for biological systems, where each particle moves according to an "internal clock"; this is suitable to describe a system of Poisson motors. There are other possibilities, such as parallel update, which would be more realistic for vehicular traffic (see [19]).

The TASEP is a special case of the more general (partial) asymmetric simple exclusion process (ASEP or PASEP), where the hopping can occur to the left with rate $D_L = 1$ and to right with rate $D_R = q$ (in some papers the alternative notation $D_{R,L} = (1 \pm q)/2$ is used). Clearly in the $q = 0$ limit one recovers the TASEP, while in the $q = 1$ limit one obtains the symmetric exclusion process (SEP) which identify a symmetric diffusive gas. The boundaries can be generalized as follows: at the left boundary particles enter the system with rate α (like in the TASEP) and exit the lattice with rate γ; at the right boundary particles exit the system with rate β (like in the TASEP) but also enter the system with rate δ.

Let us show that all these systems are typically out of equilibrium since they do not obey the Kolmogorov criterion Eq. (2.3). In the case of ASEP, a simple loop made of an
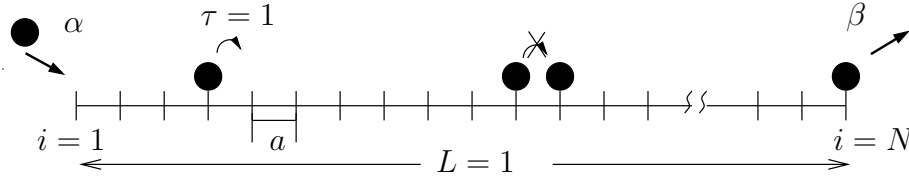
Figure 2.1: Schematic representation of the TASEP and allowed moves: forward jump (with rate $\tau = 1$), entrance at the left boundary (with rate α) and exit at the right boundary (with rate β).

empty system where a single particle enters and finally exits the system leaving it empty, cannot be inverted obtaining the same rate (in one case one gets $\alpha\beta$, and for the reverse loop $\gamma\delta q^N$). It is clear that the totally asymmetric case (TASEP), as an particular case of ASEP (with $q = 0$) does not obey the detailed balance condition. Note that even a SEP ($q = 1$) requires on the boundaries specific condition for the detailed balance $\alpha = \gamma$ and $\beta = \delta$. This stresses the fact that boundaries can add non-trivial features to the system even when many of the configurations (transition in the bulk, due simply to transport of particles) at a first sight look perfectly reversible.

According to the rules above the quantum Hamiltonian of the model reads:

$$\hat{H}_{TASEP} = \sum_{i=1}^{N-1} \left[\hat{n}_i(1 - \hat{n}_{i+1}) - \hat{s}_i^+ \hat{s}_{i+1}^- \right] + \alpha(1 - \hat{n}_i - \hat{s}_1^-) + \beta(\hat{n}_N + \hat{s}_N^+). \tag{2.32}$$

We can now compute the equation of motion for the particle number operator $\hat{n}_i$ and take the average:

$$\partial_t \langle \hat{n}_i(t) \rangle = \langle \hat{n}_{i-1}(t)[1 - \hat{n}_i(t)] - \hat{n}_i(t)[1 - \hat{n}_{i+1}(t)] \rangle \tag{2.33}$$

while at the boundaries one considers the availability of particles fixed by the left reservoir ($n_0 = \alpha$) and the possibility of having a hole fixed by the right one ($n_{N+1} = 1 - \beta$):

$$\partial_t \langle \hat{n}_1(t) \rangle = \langle \alpha[1 - \hat{n}_1(t)] - \hat{n}_1(t)[1 - \hat{n}_2(t)] \rangle \tag{2.34}$$

$$\partial_t \langle \hat{n}_N(t) \rangle = \langle \hat{n}_{N-1}(t)[1 - \hat{n}_N(t)] - \beta\hat{n}_N(t) \rangle . \tag{2.35}$$

Equation (2.33) gives what one expects for the simple rate equation: in the bulk the variation of particles at site i is the difference between a gain and a loss term (incoming and outgoing current) constructed knowing that for a particle to enter site i one needs a particle at site $i-1$ and a hole at site i. One could conveniently introduce the local current operator $\hat{j}_i(t) = \hat{n}_i(t)[1 - \hat{n}_{i+1}(t)]$ and rewrite the r.h.s. of Eq. (2.33) as the the discretized form of the discrete divergence $\nabla j_i = j_i - j_{i+1}$ and, therefore, the whole equation (2.33) as the continuity equation

$$\partial_t \langle n_i \rangle + \langle \nabla j_i \rangle = 0 . \tag{2.36}$$

which simply states the conservation of current in the steady state.

2.3.2 A word on exact solutions

The TASEP with close or open boundaries has been regarded as the Ising model for non-equilibrium systems. Indeed it is one the few exactly solvable model and quite sophisticated techniques have been developed to compute its static and even dynamical properties:

Recursive relations: the first exact solution for the steady state, proposed by Derrida, Domany and Mukamel [26] and extended by Schütz and Domany [131], consists of a recursion relation for the stationary probability of each configuration $P^s(\mathcal{C})$. The same technique could be generalized to compute the correlation function at any order [28].

Matrix ansatz: this method consists in rewriting the steady state probability in terms of matrices D and E which obeys the following ansatz: $D + E = DE$ [30, 32]. This method allows for the computation of static quantities and of the property of a tracer particle (velocity and diffusion constant). It will be presented more extensively in the next section.

Bethe ansatz: this method, which applies very well on periodic systems, consists in assuming that the eigenstates are superposition of plane waves with a non-trivial dispersion relation to be computed. Once plugged the ansatz in the master equation the dispersion relation is found and therefore the spectrum of the Hamiltonian. The main achievement of this method applied to driven diffusive systems is the computation of the gap between the two highest eigenstates of the Hamiltonian, which correspond to the longest relaxation time of the system τ; knowing how this quantity depends on the lattice size ($\tau \sim L^z$) one can extract the exact dynamical critical exponent $z = 3/2$, which means that the system relaxes super-diffusively. In principle one could find the exponents in any region of the phase diagram as it has been recently presented in Ref. [24].

Mapping to other models The mapping of TASEP to other problems allow to use results which have been derived in other contexts. The most important mapping is the one to interface growth in $1 + 1$ dimensions, by associating to each configuration of particles $\underline{n}$ a configuration (i.e. the profile) of an interface:

$$h_{i+1} - h_i = 1 - 2n_i \,. \tag{2.37}$$

With this mapping the TASEP dynamics, in which particle at site $i - 1$ hops to site i if empty, correspond to growth at site i which is a local minimum of the interface height i.e. if $h_i = h_{i-1} - 1 = h_{i+1} - 1$. Obviously the interface growth models does not consider boundaries and the mapping makes sense only for TASEP on a ring or along the line $\alpha + \beta = 1$ of the phase diagram, where the probability factorizes (i.e. the system does not present correlations since the profile is flat). The hydrodynamic limit, which corresponds to a mean field treatment of the TASEP, represents the Burgers equation without noise [57], a well known non-linear partial

differential equation appearing in turbulence [49]. It is important because it is related, through the transformation $\rho \to \partial_x h$, to the Kardar Parisi Zhang (KPZ) equation [74], which is a paradigm of surface growth. Such equation (as well as the Burgers' one) presents dynamical critical properties which will be found later studying the dynamical correlation function of the TASEP (see Ch. 5).

The matrix ansatz solution

We present here the main ideas underlying the exact solution via matrix ansatz. For the original papers we refer to [30, 32], while for exhaustive reviews we suggest Refs. [27, 25, 132]. The matrix ansatz consists in writing the stationary distribution function $|P^s(\mathcal{C})\rangle$ of each configuration as a proper combination of some matrices D and E projected on two auxiliary vectors $\langle W|$ and $|V\rangle$:

$$|P^s(\mathcal{C})\rangle = Z^{-1}\langle W| \prod_{i=1}^{N}[\hat{n}_i D + (1 - \hat{n}_i)E]|V\rangle|\mathcal{C}\rangle \tag{2.38}$$

The normalization Z (which could be seen as the canonical partition function) reads

$$Z = \sum_{n_1=0,1} \cdots \sum_{n_N=0,1} \langle W| \prod_{i=1}^{N}[n_i D + (1 - n_i)E]|V\rangle = \langle W|(D + E)^N|V\rangle . \tag{2.39}$$

Basically, in the product in Eq. (2.38) a matrix D appears whenever a site is occupied ($n_i = 1$) and a matrix E whenever a site is empty ($1 - n_i = 1$). Since D and E do not commute, in general the weights $P^s(\mathcal{C})$ are complicated functions of the occupation numbers n_i. The requirement of stationarity, $\hat{H}|P\rangle = 0$, with the Hamiltonian of Eq. (2.32) and supplemented with the self-consistence of the ansatz, leads to the following algebra for D and E:

$$DE = D + E \tag{2.40}$$

$$\langle W|E = \frac{1}{\alpha}\langle W| \tag{2.41}$$

$$D|V\rangle = \frac{1}{\beta}|V\rangle \tag{2.42}$$

(for a proof see the seminal paper [30]). Once the stationary probability is known, the stationary density profile (once we have introduced the matrix $C \equiv D+E$) can be computed with Eqs. (2.40,2.41,2.42) simply as:

$$\langle n_i \rangle = \sum_{n_1=0,1} \cdots \sum_{n_N=0,1} n_i P^s(\mathcal{C}) = \frac{\langle W|C^{i-1}DC^{N-1}|V\rangle}{\langle W|C^N|V\rangle} \tag{2.43}$$

while the current reads:

$$j = \langle n_i(1 - n_{i+1})\rangle = \frac{\langle W|C^{N-1}|V\rangle}{\langle W|C^N|V\rangle} . \tag{2.44}$$

What can one learn out of the exact solution of the TASEP? In addition to the quantities for a finite system it is possible to compute the asymptotic forms of the average quantities and of the stationary correlation function. Above all one can deduce the phase diagram (Fig. 2.2) in the case of large systems $N \to \infty$, by simply looking at the current:

- $\alpha > \beta$ and $\beta < 1/2$, the current is $j = \beta(1 - \beta)$; this is the high density phase, where the bulk density is determined by the right boundary ($\rho = 1 - \beta$); intuitively, in this phase the particle enter much more frequently than they exit and slower site (the last) determines the density.

- $\alpha < \beta$ and $\alpha < 1/2$, the current is $j = \alpha(1 - \alpha)$; this is the low density phase, where the bulk density is determined by the left boundary ($\rho = \alpha$); intuitively, in this phase the particle exit sufficiently fast and the density in the system is determined by the slowest site (i.e. the first).

- $\alpha, \beta > \frac{1}{2}$, the current is constant $j = 1/4$; this is the maximal current phase, where the bulk density is $\rho = \frac{1}{2}$.

The asymptotic behavior of the "partition function" Z changes at the phase transition, i.e. along the lines $\alpha = 1/2$, $\beta > 1/2$, $\beta = 1/2$, $\alpha > 1/2$ and $\alpha = \beta < 1/2$. Moreover there are different behavior at the lines $\alpha = 1/2$ and $\beta = 1/2$. This suggests to look at two sub-phases HDI and HDII in the HD and LDI and LDII in the LD phases. This has been done with the help of recursive solution in Ref. [131]. Moreover a more precise characterization of the phase transition has been given. In equilibrium systems phase transitions are classified according to the order of the derivative of the free energy in term of the order parameter where a discontinuity appears and it is often associated with the divergence of some length scale in the system. In non-equilibrium physics the identification of a diverging length scale might be impossible. In the case of TASEP, nevertheless, it has been proved [81] that the a "localization length", defined as $\xi^{-1} \equiv \xi_\alpha^{-1} - \xi_\beta^{-1}$ (where $\xi_\rho^{-1} \equiv \ln(4\rho(1 - \rho))$) diverges at the transitions. Such a length can diverge because because $\alpha = \beta < 1/2$ or because one of the two boundaries are equal to $1/2$. The first criterion marks the transition LD/HD, while the second identifies not only the transition LD/MC and HD/MC but divides the LD and the HD in the two sub-phases mentioned above. The boundary layers behave as follows:

- high density phase: for $\alpha < 1/2$ the profile approaches the bulk with as $x^{-\frac{1}{2}} e^{-x/\xi_\beta}$ while for $\alpha > 1/2$ the boundary layers fall like $x^{-\frac{3}{2}} e^{-x/\xi_\beta}$.

- low density phase: for $\beta < 1/2$ the profile approaches the bulk with as $x^{-\frac{1}{2}} e^{-x/\xi_\alpha}$ while for $\beta > 1/2$ the boundary layers fall like $x^{-\frac{3}{2}} e^{-x/\xi_\alpha}$.

- maximal current phase, the boundary layers approach the bulk value as power law $x^{-\frac{1}{2}}$.

From the mathematical point of view the most interesting treatment of a phase transition in equilibrium is the Yang Lee zeros theory which states that a transition occurs when, in the thermodynamics limit, the partition function written as a function of a (generalized) complex fugacity, develops real zeros [156, 93]. Depending on the way these zeros approach the real axes the transition can be continuous or discontinuous. An application to the TASEP (for which a partition function can be actually written) predicts that transitions LD/MC and HD/MC are second order phase transitions while the LD/HD is a first order phase transition [14].

Although all these techniques can give (in some regimes) all the details of the model, they are seldom applicable and can be related to the integrability of the system, i.e. on the existence of an infinite number of conserved quantities, i.e. operator which commute with the Hamiltonian (see [132]). Unfortunately in many problems these quantities cannot be found and one has to rely on numerical simulations and approximate techniques (such as MF or perturbations around it). A technical discussion on integrability of infinite quantum chains would involve mathematical concepts way beyond the purpose of this thesis.

2.3.3 The MF treatment

In this section we see how the mean field approximation, though rather crude (especially in 1D), is able to captures anyway the essential physics of the system. In the case of the TASEP, therefore, the MF treatment has just a pedagogic purpose, but in the absence of exact solutions (as it is the case for the models we are going to study in the next chapters), it constitutes a simple method to construct the phase diagram.

As said in Sec. 2.2.2, in averaging Eq. (2.33) one considers for example the correlations $\langle n_i n_{i+1} \rangle$ which would require another similar equation containing three points terms as $\langle n_{i-1} n_i n_{i+1} \rangle$. In order to avoid this hierarchic problem, one can use the mean field ansatz

$$\langle n_i(t) n_j(t) \rangle \approx \langle n_i(t) \rangle \langle n_j(t) \rangle \tag{2.45}$$

which is obviously a crude and uncontrolled approximation, but it becomes intuitively reasonable in case of low dense system, where particles are unlikely to interact. Also, because of particle-hole symmetry we can argue that MF is valid also for very dense systems, where holes are unlikely to interact. Since we are interested in the stationary state we look for the solution of the system:

$$\begin{cases} 0 = \rho_{i-1}(1 - \rho_i) - \rho_i(1 - \rho_{i+1}) & i = 1 \dots N \\ 0 = \alpha(1 - \rho_1) - \rho_1(1 - \rho_2) \\ 0 = \rho_{N-1}(1 - \rho_N) - \rho_N \beta \end{cases} \tag{2.46}$$

Such a system could in principle be solved numerically, however it is possible to reduce the set of equations to give an explicit solution. The continuity of the current in the bulk, Eq. (2.36) allows us to reduce the system to a single equation. Moreover we can use the continuum approximation: this is achieved for large number of sites N on a lattice of normalized length $L = 1$. The lattice constant is $a = L/N$ and therefore tends to zero. The

position of the particle, which was indicated by i, becomes a continuum variable $x = i/N$ rescaled in the interval $0 \leq x \leq 1$. An expansion of the density ρ in power of a leads to:

$$\rho(i \pm 1) \to \rho(x \pm a) = \rho(x) \pm a\partial_x\rho(x) + \frac{1}{2}a^2\partial_x^2\rho(x) + O(a^3) \qquad (2.47)$$

which let us approximate Eq. (2.33) as:

$$\partial_t\rho = (2\rho - 1)\partial_x\rho\,, \qquad (2.48)$$

with boundary conditions $\rho(0) = \alpha$ and $\rho(1) = 1 - \beta$. The stationary state is obtained by setting to zero the l.h.s. of this equation:

$$(1 - 2\rho)\partial_x\rho = 0\,. \qquad (2.49)$$

Since this is a first order equation and we have two boundaries to match, we are dealing with an over-determined boundary problem. The two possible solutions of the equation without boundary are $\rho^*(x) = 1/2$ and $\rho = C$. The first solution does not match any boundary while in the second one C can be chosen to match the left ($\rho_\alpha(x) = \alpha$) or the right ($\rho_\beta(x) = 1 - \beta$) boundary.

According to the mean field equation the three solutions already identify the three phases of the TASEP phase diagram, nevertheless the behavior of the boundary layers that allow to distinguish between the two sub-phases in the LD and HD regimes cannot be exactly predicted, because it involves spatial correlations (that have been actually neglected).

In order to understand how to match the two boundaries we turn to the a domain wall (DW) description of the system. This is a phenomenological interpretation of the TASEP that pictures the system as composed of two densities, the left one ρ_α and the right one ρ_β, separated by a mobile interface behaving as a *random walker* (for a rigorous proof see Ref. [4]). The dynamics of such a domain wall determines the different phases.

To compute the jump rates of the DW we can write a non-stationary state as composition of left and right stationary solutions and the relation $\partial_x j = 0$ is fulfilled everywhere except at the DW position (this captures the slowest relaxation motion and will be discussed more in detail in Ch.5). We can introduce the travelling wave ansatz i.e. the density can be written as $\rho(x - Vt)$ (where V is the collective velocity) in Eq. (2.48) and obtain $\partial_x(j - V\rho) = 0$. Integration in the interval $[x_w - \delta, x_w]$ and $[x_w, x_w + \delta]$ centered in the DW leads to $(j_\alpha - V\rho_\alpha) = (j_\beta - V\rho_\beta)$ which implies for the DW a velocity

$$V = \frac{j_\beta - j_\alpha}{\rho_\beta - \rho_\alpha} = \beta - \alpha\,. \qquad (2.50)$$

Since the DW is by hypothesis a Brownian walker, this could be interpreted as the resulting velocity between the rate of jump to the left and to the right. These rates can be defined as

$$w_L = \frac{j_\alpha}{\rho_\beta - \rho_\alpha} \quad \text{and} \quad w_R = \frac{j_\beta}{\rho_\beta - \rho_\alpha}\,. \qquad (2.51)$$
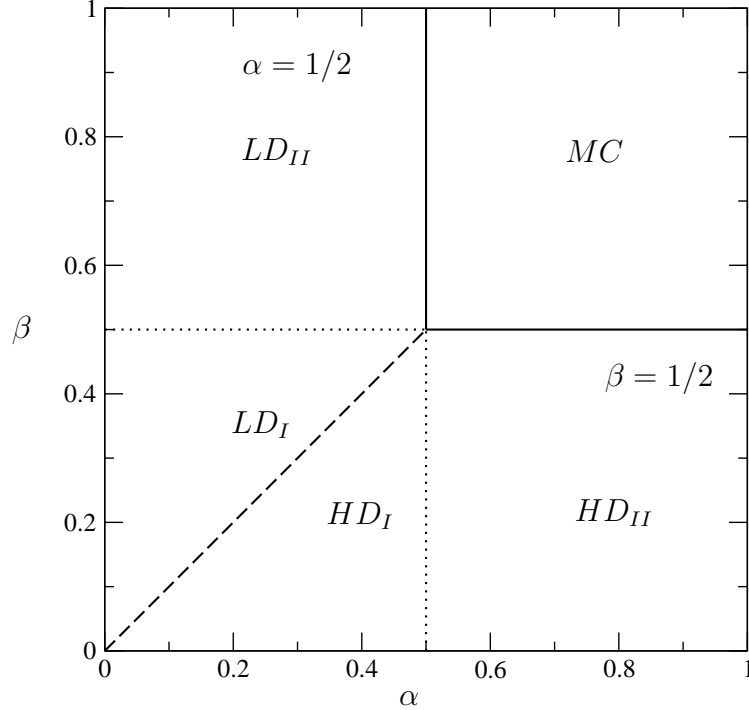
Figure 2.2: TASEP phase diagram. There are three main phases: a low density (LD) controlled by the left solution, a high density (HD) controlled by the right solution and a maximal current (MC) where the density in the bulk is constant. The four sub-phases LD_I, LD_{II}, HD_I and HD_{II} in which LD and HD split, are identified through the boundary layers studied with exact methods.

Note that the two currents can be read as the rate of entrance rate of a particle in the low density phase, i.e.

$$j_\alpha = \underbrace{\text{entry rate}}_{\alpha} \times \underbrace{\text{Probability that the first site is empty}}_{(1-\alpha)}$$

and similarly for j_β. It is easy to understand that if $V \neq 0$ the DW is pushed to one of the two boundaries and one of the two solution dominates.

In the coexistence line $\alpha = \beta < 1/2$ exact results (corroborated by simulations) show a linear profile which is not caught by mean field:

$$\rho(x) = \alpha + (1 - \alpha - \beta)x . \tag{2.52}$$

Indeed in this case the average velocity of the DW is zero, but this does not mean that it cannot diffuse: the Brownian dynamics is indeed responsible for the linear profile.

In term of current the phase diagram is rather intuitive: starting from a low entrance rate (HD) and increasing the entrance rate, results in increasing the current. At the critical value $\alpha = 1/2$ an increasing in the entrance rate cannot increase the current further, since it is already at its maximum ($j = \rho(1 - \rho)$ has a single maximum at $\rho = 1/2$), and indeed the current decreases. As a result the bulk will keep its current maximum ($j = 1/4$, $\rho = 1/2$) but a boundary layer will form to match the boundary condition. The presence of a maximal current is a mark of exclusion: for example in systems where the particles move in parallel or do not interact, exclusion does not play a role and the phase diagram does not exhibit the MC phase. Another argument derived by DW properties [81] and further applied to other methods [132, 119] is the rather general *extremal current argument*: the system tends to minimize the current if the left density is higher than the right one and to maximize the current if the left density is smaller. In the case of TASEP this means

$$j = \begin{cases} \max\{\alpha(1 - \alpha), \beta(1 - \beta)\} & \text{for} \quad \alpha < 1 - \beta \\ \min\{\alpha(1 - \alpha), \beta(1 - \beta)\} & \text{for} \quad \alpha > 1 - \beta \end{cases} . \tag{2.53}$$

2.4   Variation on the theme: TASEP-like models

In the last years a considerable effort has been devoted to the study of extension and modification of the TASEP. The system could be complicated in an amazing number of ways, along the line of including couplings to other systems, disorder and alternative updating rules (or even of including several). The effective applicability of these (often oversimplified) systems remains the real challenge and reduces considerably the possible models one can "cook up". Hereafter, some of the most interesting generalizations are briefly reviewed.

2.4.1   Different updating procedures

The original TASEP has been implemented with a random sequential updating rule in continuous time. A possible modification of the model in the updating rules is the use parallel dynamics. In this case the lattice is divided in two sub-lattice that are alternatively updated in parallel (e.g. all even sites at the same time, then all the odd sites). The injection and extraction of particle remains non-deterministic. The problem is again exactly solvable [130]. Interestingly enough there is no maximal current phase, only high density and low density separate by the diagonal $\alpha = \beta$. An alternative to the parallel and the random sequential updating is the ordered (e.g. forward) sequential, where particles are updated from the most to the right to the most to the right. This has been proved to have the same (thermodynamic) properties of the system with parallel rules [41]. These models have some relevance because the usual traffic is supposed to obey a parallel update [19].

In the same spirit sequential update with different interactions has been introduced (like the Katz-Lebowitz-Spohn or KLS model) where the current-density relation shows

multiples extrema [59, 118].

2.4.2 TASEP with disorder

Along the line of describing more realistic systems, the effects of disorder on the TASEP have been extensively studied. The most simple modification is the introduction of a *bottleneck*, i.e. a single site where the particles hop with a different rate $q < 1$. The system has been described quite successfully dividing the system in two sub-lattice (left and right) and using the mean field solution on the two sub-lattices. The resulting phase diagram is topologically the same as in usual TASEP with the difference that the critical current is now imposed by the defect and corresponds to $j_c = q/(1 + q)^2$. Consequently critical entrance and exit rates are reduced to $\alpha^* = \beta^* = q/(1 + q)$. The critical point is therefore shifted. This model will be accurately considered in Ch. 4.

Extension to disorder over the whole system both in the particle hopping (particle based) and in the lattice (quenched) have been considered and solved by simulations and (to some extent) with analytical calculations [149, 82, 60]. Studies on the current density relation show a flatten of the parabola-shaped $j = \rho(1 - \rho)$ and the whole system carry therefore the maximal current allowed by the total degree of disorder. The phase diagram is consequently modified only in the maximal current phase but not in the topological properties, where the defect is not relevant.

2.4.3 TASEP with extended particles (ℓ-TASEP)

Originally the TASEP has been motivated by the kinetics of biopolymerisation on nucleic acid template (ribosomes on mRNA, polymerases on DNA and RNA) [97]. This suggested immediately that an interesting feature of the model would be the study of extended objects [96]. Recently the problem has received much attention, above all for its interesting connection to the Tonks gas [88, 138]. The system has been solved exactly exploiting the mapping to zero range processes (directed particle transport without interaction) and through Bethe ansatz [3] and proved to belong to the same universality class as the simple TASEP. Implications of the hydrodynamic limit have been investigated [129]. In addition to these models disordered TASEP with extended particle has been studied [136, 137], to predict realistic motion of ribosome on mRNA.

2.4.4 Coupled TASEP

A simple TASEP can be coupled to different other systems, for example to other lanes. Particles can detach from the TASEP lane and diffuse in a confined (quasi 1D) geometry. In 3D the effect of exclusion in the reservoir can be neglected but interesting effects have been found, due to the conservation of particles in the whole system and to the on-off kinetics in the bulk: for some specific value of parameters the system shows a stable coexistence of low density and high density profile [95]. The coupling to one dimensional diffusive lane has been studied: in this case the exclusion plays a significant role and the phase diagram

can be studied in terms of the diffusion coefficient and the detachment rate; significant deviations from mean field have been highlighted [61]. Another system is composed by two TASEP-like lanes coupled via Langmuir kinetics: investigations on this system have showed interesting multi-criticality phenomena [123]. Other kind of coupling have been tested, for example TASEP lane coupled by a junction to a two lane TASEP system (or vice versa) [122].

2.4.5   TASEP with Langmuir kinetics

A special case of "coupled TASEP" is the one introduced in Ref.[111]. So far the processes we have considered have always been subject to particle conservation in the whole system: the only sites where particles could enter and leave the system where the first and last site respectively. There is no reason why this should be the case for realistic models and to test actually the role of on-off kinetics it is necessary to extend the TASEP to a grand canonical version. For example (see Ch.1) the molecular motors have been shown to attach on the filament, walk for some steps (about a hundred) and then detach. This suggests to couple the TASEP to a reservoir and introduce an attachment/detachment (or on/off, or Langmuir) kinetics in the bulk (see Fig. 2.3), where particle attach with rate ω_A and detach with rate ω_D (the binding constant $K = \omega_A/\omega_D$ is introduced for simplicity) [95, 111].
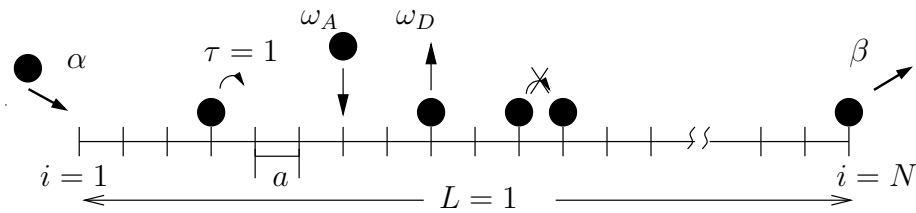

Figure 2.3: Schematic representation of the TASEP/LK and allowed moves: forward jump (with rate $\tau = 1$), entrance at the left boundary (with rate α) and exit at the right boundary (with rate β), attachment (with rate ω_A), and detachment (with rate ω_D) in the bulk.

The combination of a driven process with an equilibrium one is extremely interesting from a statistical mechanics point of view and it exhibits new unexpected behaviors, due to the competition of timescales. Single motor experiments suggest that both processes compete on the scale of the microtubule, i.e. a motor explores a significant fraction of the track before detaching [65]. To capture such an interplay mathematically, a *mesoscopic limit* has been suggested, where local adsorption-desorption rates have been rescaled in the limit of large but finite systems, such that the gross rates are comparable to the injection-extraction rates at the boundaries [111]. The term "mesoscopic" stresses the fact that the system is sufficiently coarse-grained to exhibit collective phenomena (and allow a continuum description), but not enough large to neglect the boundary effects (thermodynamic limit). The study of this system has shown an unexpectedly rich and new

phase diagram with phase coexistence regions. Surprisingly, in the mesoscopic limit the density profiles show a sharp discontinuity (shock separating low from high density phase) or cusp in a large portion of the phase diagram (see Fig. 2.4).

The main difference between the simple TASEP and the TASEP/LK is the presence of a coexistence phase where a localized domain-wall appears. The position of the domain-wall depends on the boundary parameters. Note that such a domain-wall, emerging as a crossover in finite systems, is actually a shock in infinite system, i.e. a discontinuity that the solution develops even if it starts from smooth initial condition; this behavior is typical of non-linear equations like, for example, the Burgers equation (see Ch. 5) in the inviscid limit, which happens to appear in hydrodynamics as a paradigm of turbulence. The phenomenology can be explained as follows: accumulation of particles from the bulk gives a non constant current, which, in the continuum limit, presents cusp and kinks; correspondingly, in a relevant portion of the phase diagram, the low and high density phases coexist, separated by a *stable* domain wall. Coexistence of other phases appear in other regions, such as LD-MC, MC-HD and LD-MC-HD. The rich phenomenology is presented in Fig. 2.5, where the case of equal attachment/detachment rate is considered.

PSfrag replacements
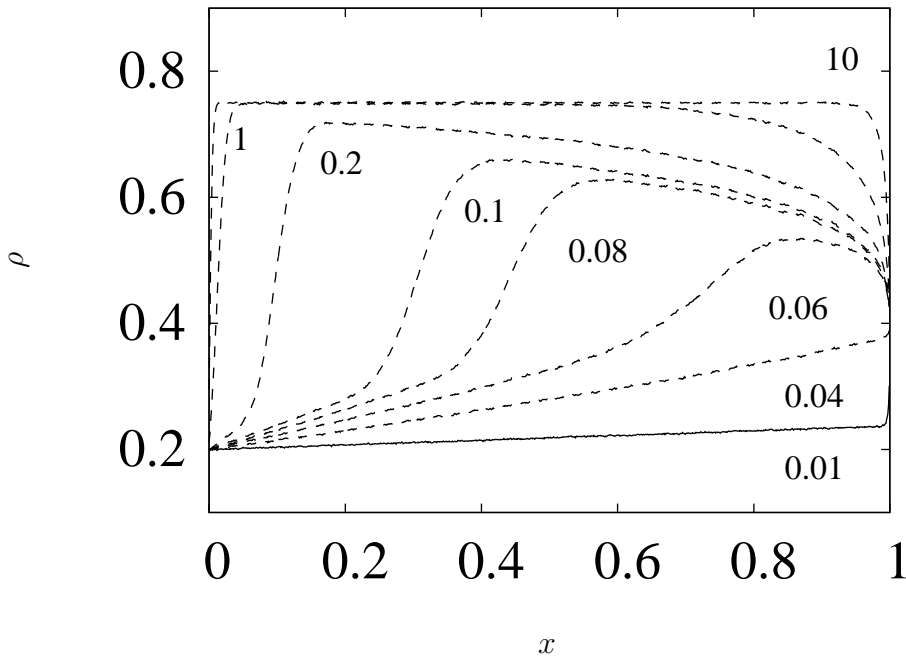
Figure 2.4: MC simulations of the density profile for the TASEP/LK for entrance and exit rates $\alpha = 0.2$, $\beta = 0.6$, system size $N = 1024$, ratio between the attachment and detachment rates $K = 3$, and the values of the detachment rate Ω_D indicated in the graph. The density profile exhibit a domain-wall separating a low and high density phase. See the text for a discussion.
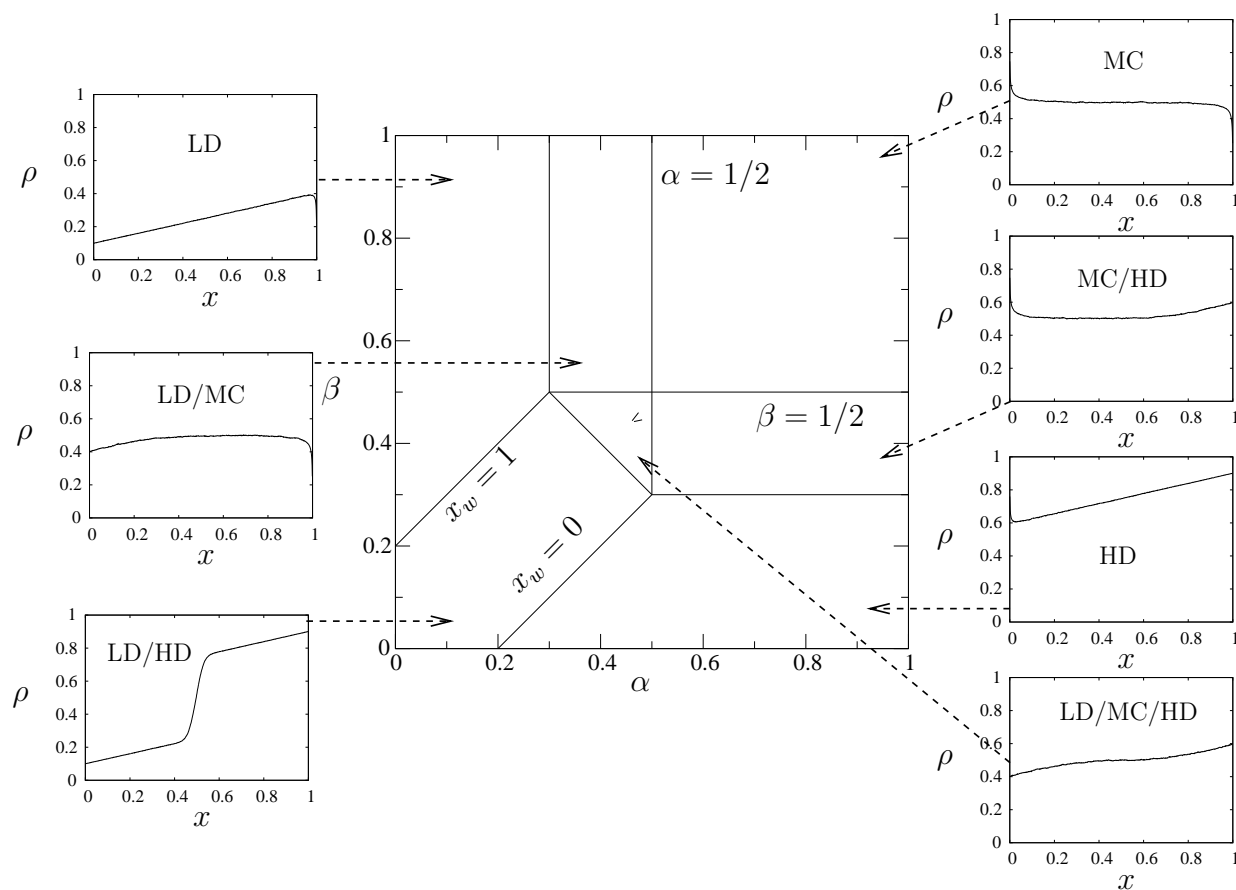
Figure 2.5: Phase diagram of TASEP/LK for $K = 1$. There are seven phases: besides the usual pure three of the TASEP, four more coexistence regions show up in this model: LD/HD, LD/MC, MC/HD and $LD/MC/HD$.

2.5   Experimental relevance

Let us speculate on the applicability of these models to describe real systems. What can be controlled in an experiment are the concentrations of motors and of ATP. The first determines the attachment rate, while the second the processivity and therefore the detachment rate. Of course the left and right boundaries are a mathematical trick to solve the system: since there is no particular reason for which motors should preferentially enter at the left end, one can set $\alpha \approx \omega_A$. For the right end one can consider the free case, $\beta = 1$, or the blocked end case, $\beta = 0$ (a blocked last site could model the effect of a strong defect on the micro-filament or a microtubules associated protein preventing the motor to advance).

Let us consider as a typical situation a system of a microtubules of length $L = 5\mu m$ ($N = 500$) sites, with a concentration of ATP of order of $[ATP] \sim 1mM$: this implies for the motor a processivity comparable with the whole filament, $\omega_D^{-1} \sim 500$ steps, which means that the detachment rates over the whole system is $\Omega_D = N\omega_D \sim 1$. One can then vary the concentration of kinesins between pM and nM investigating in principle any range of K, from a completely dilute system to the saturate regime [3]. In this way we are moving through a line of the phase diagram where a stable domain wall enters the system (see Fig.2.7). Recent experiments have qualitatively shown the possibility of stable traffic jams in a system of single head kinesins KIF1A [109]. The outcome of these experiments are shown in Fig. 2.6: one can observe the formation of "comet-like accumulation" of kinesin at the end of a microtubule. As the concentration fo KIF1A is increased the formation of shock is observed.

It is clear that the TASEP/LK model describes a situation with an infinite system coupled to reservoir. In order to consider the bulk as a reservoir its internal energy should not change too much upon addition of a motor and the fluctuations should smoothen out faster than the ones on the filament. This is guaranteed if the diffusion constant is high enough. The diffusion constant can be computed from the Stokes Einstein relation, considering a motor of radius $r \sim 1nm$, the viscosity of water $\eta \sim 1Pa \cdot s$ and the system at room temperature:

$$D = \frac{k_b T}{6\pi\eta r} \sim 10\mu m^2/s \, . \tag{2.54}$$

This suggests that the diffusion time over a hundred steps (1μ) is of the order of $\tau_D \sim 10^{-2}s$, comparable to the time scale of the directed motion on one step $\tau_M \sim 10^{-2}s \gg \tau_D$. This tells that in the solution the concentration of motor equilibrates very fast and basically it acts as a reservoir. In the extremely constrained environment of the axon, or the overcrowded picture of the cell, this might not be the case and other authors have considered the problem of motors interaction even in the bulk [95]. Although the field is extremely interesting from the biological perspective, we aim to observe the general features of the system.

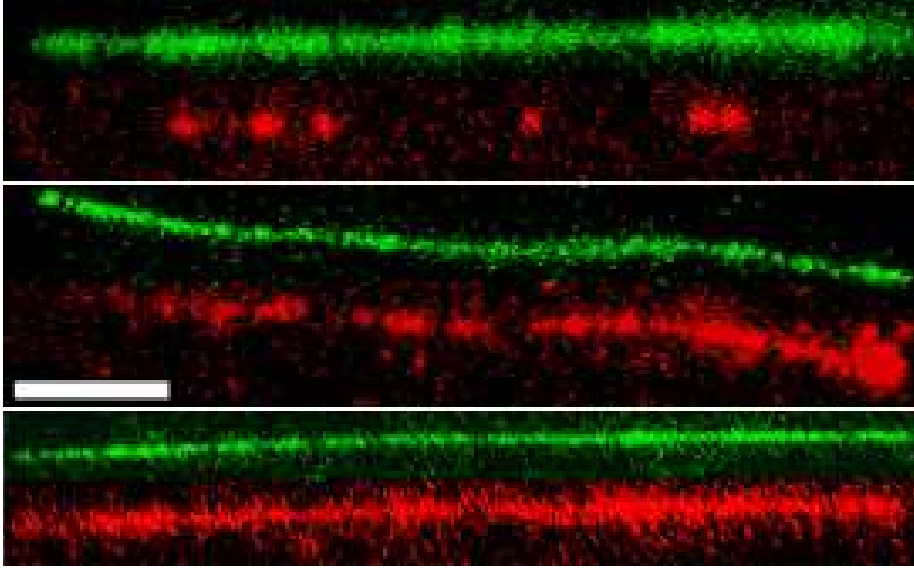[3] G. Cappello, private communication

Figure 2.6: Formation of comet-like accumulation of kinesin at the end of a microtubule. Fluorescently labeled KIF1A (red, lower lane of each figure) was introduced to microtubule (green, upper lane of each figure) at 10pM (top), 100pM (middle), and 1000pM (bottom) concentration along with 2nM ATP. The length of the white bar is 2μm. Source [109].

Anyway more realistic models have been introduced to approach the experimental frame. Initially the model did not consider motors but ribosomes and was proposed more as a mathematical curiosity than as a testable system [97, 96]; later site-based disorder and approximate description help to deduce the behavior of a ribosome on mRNA [138, 137, 135]. The first model on motors consisted of a filament in a closed system with diffusion in the bulk [95] or special ad hoc geometry for the reservoir [77, 75]. Models with two species moving in opposite direction have proved to self organize in order to optimize the process [76]. In models where the filament is not coupled to a reservoir but to a diffusive lane with exclusion [61], the system does not need to be neither infinite, neither coupled to an ideal reservoir. In the above cited Ref.[109], the authors considered the case of KIF1A, a special kinesins which is actually a monomer and apply a ratchet model to it: the particle can detach, diffuse on a short time scale, and re-attach; his is the first attempt to include internal feature of the motors and to match the model (at least on a qualitative level) with experimental data.

All the models mentioned above (but the list could be certainly enlarged) exhibit more or less the same qualitative behavior, with the formation, for specific range of the parameters, of a stable domain wall. The questions of which features are relevant to capture the most important aspects of such systems remains.

In the next chapter we will test the influence of a new detail added to the model: the fact that they can occupy more than a site. We will investigate in which aspects the methods introduced above need to be extended and how the phase diagram is changed.
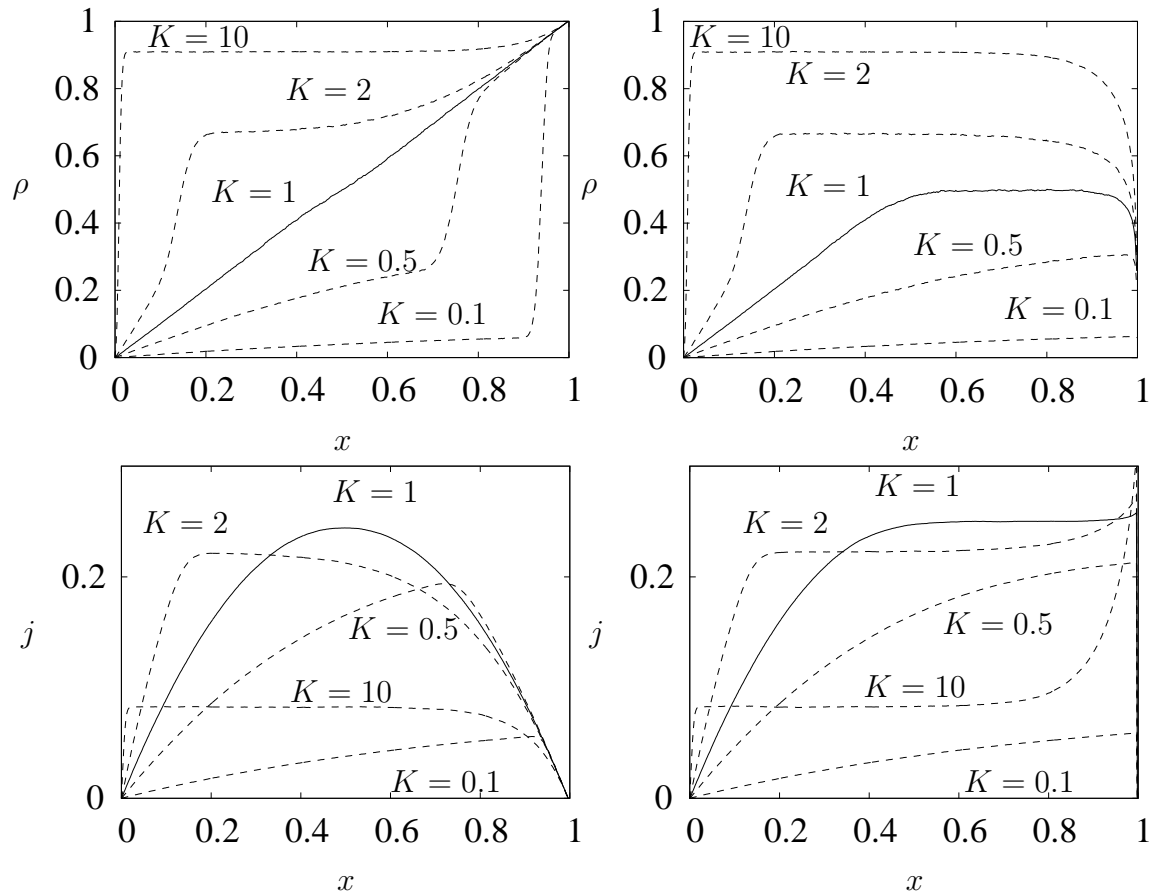
Figure 2.7: Density profile and current for possible experimental regime: $\Omega_D = 1$ and different values of K indicated in the graphs. Left column: blocked end, $\alpha = 0$, $\beta = 1$. Right column: free end $\alpha = \beta = 0$, same values of parameters Ω_D and K.

Let us repeat, anyway, that the physics of the system is remarkably interesting in itself, independently of the possible experimental applications that initially motivated the study.

Chapter 3

Dimeric lattice gas: a minimal model for collective molecular transport

> Every move you make
> Every bond you break
> Every step you take
> I'll be watching you.
>
> The Police
> *Every breath you take*

Molecular motors like kinesin and dyneins are dimeric proteins with two heads which attach specifically to neighboring binding sites on a protofilament of a microtubule. In this chapter we have extended previous work in this field to account for the dimeric nature of the motors and asked what quantitative and qualitative changes occurs in the phase behavior. To this end we have analyzed the properties of a one-dimensional driven lattice gas composed of dimers, without particle conservation in the bulk. The equations of motion for the density of particles are obtained through a refined mean field approximation that captures consistently the main features of on-off and the driven kinetics. We discuss in detail the complete phase diagram of the driven dimers lattice gas through extensive Monte Carlo (MC) simulations interpreted with the mean field theory. We prove in this way that the picture found for the monomer lattice gas is robust.

This chapter is organized as follows: in Sec. 3.1 we review the main motivations, both biological and physical, behind the work and the main results already known. In Sec. 3.2 we specify the model under consideration and introduce the used formalism. Section 3.3 exemplifies results of the MC simulations and puts extracted features into proper perspective. In Sec. 3.4 we construct a suitable set of mean field equations relying on results for ℓ-TASEP and on-off kinetics. In Sec. 3.5, with the help of these equations, we rationalize the MC data and study the complete phase diagram. In the Conclusion, Sec. 3.6, we discuss the robustness of the model and give a possible generalization to ℓ-mers.[1]

---

[1]This chapter is almost entirely covered by reference [115].

3.1   Introduction

Driven lattice gas models have recently received much attention due to their possible application to intracellular transport. The connection of non-equilibrium transport to biology has been recognized almost 40 years ago by modelling ribosome motion on mRNA [97, 96]. The problem later received much attention of non-equilibrium statistical mechanics, where it became known as Totally Asymmetric Simple Exclusion Process (TASEP). We have given a review of the main features of this model in Ch. 2.

Previous work has concentrated almost exclusively on the mathematical properties and statistical physics perspectives. Only recently, the application to biology reentered the focus of attention in the context of systems of extended particles. In particular, ribosomes bind to mRNA occupying twelve codons and progressively advance by a single codon through two cycle of GTP hydrolysis (elongation step). The implications of mutual steric hindrance of ℓ-mers (monomers, dimers, 12-mers) have been studied by Monte Carlo simulations and 'refined mean field theory' for ℓ-TASEP [88, 138]. The picture already found for monomers has been corroborated also by exact methods (Bethe ansatz [3] and mapping to zero range process [129]).

A substantial difference to the directed motion of ribosomes on mRNA is the exchange of molecular motors with the surrounding cytosol acting as a particle reservoir. This observation has motivated a recently proposed extension of TASEP (see Ch. 2), by supplementing the unidirectional hopping with Langmuir (on-off) kinetics in bulk [95, 111]. Single motor experiments suggest that both processes compete on the scale of the microtubule, i.e. a motor explores a significant fraction of the track before detaching [64]. To capture such an interplay mathematically, a *mesoscopic limit* has been suggested, where local adsorption-desorption rates have been rescaled in the limit of large but finite systems, such that the gross rates are comparable to the injection-extraction rates at the boundaries [111]. The study of this system has shown an unexpectedly rich and new phase diagram with phase coexistence regions. Surprisingly in the mesoscopic limit the density profiles show a sharp discontinuity (shock separating low from high density phase) or cusp in a large portion of the phase diagram.

Here we propose a model for intracellular transport incorporating both coupling to a reservoir as well as the finite extension of particles in a unifying picture. The model is motivated by the fact that many processive molecular motors (e.g. kinesins, dyneins and myosin V) are composed of two heads (trail and lead) that bind specifically each to a subunit of the molecular track (α- and β-tubulin in case of microtubules). Hence, we concentrate on particles which occupy two sites, i.e. dimers, and advance by a single site per hopping event.

The theoretical challenge arises from finding an appropriate and quantitative description that captures both the on-off kinetics as well as the ℓ-TASEP features on an equal footing. Whereas for monomers a straightforward decoupling of correlations yields a consistent mean field theory, such an approach fails even to describe the chemical equilibrium of a pure on-off kinetics [88]. In the following paragraphs we review some aspects of our model where the geometric constraints usually play an important role introducing non-

trivial static and dynamic correlations.

At the *static* level the geometrical frustration emerges already in the equilibrium thermodynamics of the one-dimensional *Tonks gas*. Identical extended particles are distributed according to the grand canonical ensemble on a one dimensional lattice. A hard core repulsion reduces the task to a combinatorial problem [148, 147]. It turns out that the single site occupation densities do not determine the configurational probabilities, contrary to the monomer case. There the *Langmuir kinetics* specified in terms of attachment and detachment rates ω_A and ω_D, or equivalently the binding constant $K = \omega_A/\omega_D$. The coverage density is simply determined by a single site consideration, resulting in the *Langmuir isotherm*: $\rho_I = K/(K+1) = \omega_A/(\omega_A + \omega_D)$. This is to be contrasted with the dimer case where a full evaluation of the grand canonical partition function is required leading to an equilibrium coverage density [102]:

$$\rho_I = 1 - \frac{1}{\sqrt{1+4K}} \,. \tag{3.1}$$

At a *dynamical* level a non-trivial approach to the steady state is found in the on-off kinetics in the fast attachment limit: at short time scales only deposition processes are frequent, while detachment processes are still unlikely. The kinetics belong to the class of problems referred to as *random sequential adsorption (RSA)* and the so-called "Flory plateau" [48] is reached exponentially fast. After this transient the particles can detach (on longer time scales) freeing new gaps; this process results in a long tail relaxation where the isotherm is approached with a power law $t^{-1/2}$. Such behavior has been explained using the mapping of the gap dynamics to a 1D reaction diffusion system $A + A \to \emptyset$ (for a review see [41, 101, 120] and references therein) for which this anomalous power law dynamics is known. This two step relaxation has been found also in other models like in irreversible deposition of dimers (i.e. RSA) with diffusion [121] and is intrinsically related to the extended nature of the particles.

Driving a system of extended particles far from equilibrium, e.g. introducing the ℓ-TASEP dynamics, suggests a variety of competing time scales and ordering phenomena, i.e. non-equilibrium phase transitions. The purpose of this chapter is to shed light on density and current profiles in the stationary state for a model incorporating such aspects, as well as to provide a complete analytical theory supported by Monte-Carlo data.

3.2   Model and notation

We consider a finite one dimensional lattice with sites labeled $i = 1, \ldots, N$, of unit length $L = 1$; consequently the lattice spacing reads $a = L/N$. The first two sites ($i = 1, 2$) and the last two sites, ($i = N-1, N$) represent, respectively, the left and right boundary. The lattice is partially covered by dimers, i.e. composite objects consisting of two monomers rigidly tied together. A dimer occupies two lattice sites, see Fig. 3.1; we refer to the monomer to the right of the dimer as the *lead head* and correspondingly to the left monomer as the *trail head*.

A microscopic state $\mathcal{C}$ of the system consists of a configuration of non-overlapping indistinguishable dimers on the lattice. Non-overlapping requires that no two heads (trail or lead) occupy the same lattice site. We specify the dynamical evolution by the following set of updating rules:

- If the lead head of a dimer occupies a site $i = 2, \ldots, N - 1$ and the following site is empty, the dimer advances one step with unit rate.

- At site $i = 1$ a dimer enters the lattice with its trail head with rate α provided that the first two sites are empty.

- A dimer with its lead head on site $i = N$ leaves the lattice with rate β emptying the last two sites.

- Everywhere in the bulk (i.e. trail head on a site $i = 2, \ldots, N - 2$) a dimer leaves the lattice emptying two sites with a site independent detachment rate ω_D.

- Everywhere in the bulk ($i = 2, \ldots, N - 2$) a dimer enters the lattice with its trail head, provided that the considered site as well as its right neighbor is empty, with a site-independent attachment rate ω_A.

The first three rules encode the usual Totally Asymmetric Simple Exclusion Process (TASEP) of extended objects, while the last two implement the coupling of the lattice to a reservoir of dimers with fixed chemical potential[2].

The rules entail that a complete description of the underlying stochastic Markov process is given in terms of the time-dependent probability $P(\mathcal{C}, t)$. The time evolution is governed by the associated master equation

$$\partial_t P(\mathcal{C}) = \sum_{\mathcal{C}' \neq \mathcal{C}} \left[W_{\mathcal{C}' \to \mathcal{C}} P(\mathcal{C}', t) - W_{\mathcal{C} \to \mathcal{C}'} P(\mathcal{C}, t) \right], \tag{3.2}$$

where the transition rates $W_{\mathcal{C}' \to \mathcal{C}}$ can be inferred form the dynamical rules.

It is expected that the system evolves towards a stationary ensemble $P^{st}(\mathcal{C})$ for long times. Due to the lack of detailed balance this macroscopically stationary state does not correspond to an equilibrium ensemble, i.e. there is no Gibbs-Boltzmann measure to be inferred from thermodynamics arguments. The macroscopic quantities we aim to compute are understood as averages over this distribution.

To exploit probabilistic methods we label sites according to: empty (state $s = 0$), occupied with the trail head (state $s = 1$) or with the lead head (state $s = 2$). The configuration $\mathcal{C}$ can be represented as a string of occupation number $\mathcal{C} = \{n_1, \ldots, n_N\}$, with $n_i = \{0, 1, 2\}$. The quantity of fundamental interest in the following is the average site-dependent dimer density in the stationary state, In particular we shall derive equations

---

[2]A slight modification of the dynamical rules at the boundaries, e.g. allowing particles to enter (leave) the system gradually, has been shown not to introduce new features (see [88, 138] for discussion).

for the density of the lead head ($n_i = 2$) at site i, $\rho_i \equiv \langle \delta_{n_i,2} \rangle$. Since the dimers are rigidly connected, the corresponding density for the trail head at site i simply reads ρ_{i+1}.

The probability of having site i in state s will be denoted by $p(i, s) \equiv P(n_i = s)$. Since the states mutually exclude, the probability $p(i, 2)$ immediately yields the average lead head density: $\rho_i = p(i, 2)$. The coverage density ρ_i^c is sum of the lead head density and the trail head density, i.e. $\rho_i^c = p(i, 2) + p(i + 1, 2)$. Consistently with the notation the joint probability will read $p(i, s; j, s')$. We also shall need the conditional probability $p(i + 1, s|i, s')$, i.e. the probability for site $i + 1$ to be in state s provided site i is in state s'.

In the simulations we will concentrate on the average coverage density ρ_i^c, and the spatially resolved current j_i, defined as the flux of particle through site i per unit time. Only averages on the stationary state will be considered: a comparison between ensemble and time-moving averages corroborates the hypothesis that the system is ergodic.
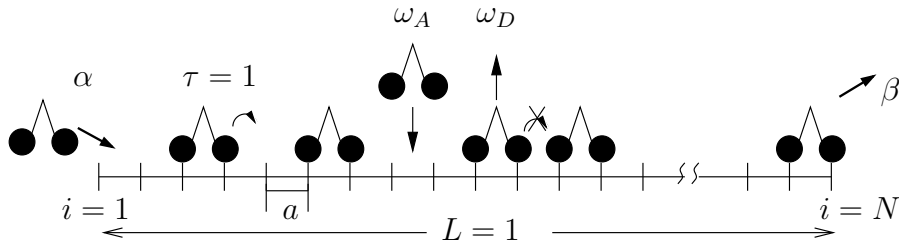
Figure 3.1: Schematic representation of the model and allowed moves: forward jump (with rate $\tau = 1$), entrance at the left boundary (with rate α), exit at the right boundary (with rate β), attachment (with rate ω_A), and detachment (with rate ω_D) in the bulk.

As indicated in the Introduction, a non-trivial competition between boundary induced phenomena and bulk dynamics arises in the *mesoscopic limit*, i.e. the gross on/off rates, Ω_A and Ω_D, should be of the same order of magnitude as the boundary entry/exit rates α and β. This requires that the single site on/off rates, ω_A, ω_D, scale with the system size N as:

$$\omega_A = \frac{\Omega_A}{N}, \qquad \omega_D = \frac{\Omega_D}{N} \tag{3.3}$$

with Ω_A and Ω_D fixed.

3.3 MC results and description of the phase diagram in general

In this section we present the method used to perform numerical simulations and the results obtained from them. Density profiles much different from the TASEP motivate our interest in the model.

3.3.1 Method

We have simulate the stochastic equation through a kinetic Monte Carlo algorithm, to determine the average density profile in the stationary state with high accuracy. The results have been obtained using a random sequential updating algorithm by Bortz, Kalos and Lebowitz (BKL-method or n-fold way) [15, 89]: a list of all sites which are possible candidates for a successful move is stored and dynamically updated. The method is (for the present case) faster than the conventional kinetic Monte Carlo algorithms and constitutes a reliable way to simulate *real time* dynamics, although here we focus on equal-time averages in the stationary state (note that the algorithm is equivalent to the Gillespie's one, commonly used in chemical reactions [53]).

Explicitly, we keep three lists of sites for the respective allowed moves: there are N_J sites where particles can perform a jump forward, N_A sites that may accept a particle from the reservoir, and N_D sites from which a particle can detach. Furthermore we keep track of the occupation of the boundaries (n_0 and n_N). One of these moves is selected randomly with the appropriate weights: $1 \times N_J, \omega_A \times N_A, \omega_D \times N_D, \alpha \times (1 - n_1), \beta \times n_{N-1}$. Then we increment time by an interval drawn from an exponential distribution with timescale $T = (\alpha(1-n_0)+\beta n_N + N_J + \omega_A N_A + \omega_D N_D)^{-1}$. The lists are updated correspondingly and the procedure is iterated for many events. We have started the algorithm from an empty configuration and after the stationary state has been reached, the coverage density and the current have been measured. Moving time averages typically cover a window of $O(10^6)$ time units. We have investigated finite-size effects by considering lattices varying from 128 up to 4096 sites. Furthermore, we have checked the ergodicity by comparing time-moving and ensemble averages. The longest simulations have been performed approximately a day on a 1GHz processor.

3.3.2 Results

We exemplify our results by fixing the binding constant to $K = 3$ and the entrance/exit rates to $\alpha = 0.1$ and $\beta = 0.6$. We measured the stationary density profiles as well as the current for different values of the detachment rate Ω_D. For very low Ω_D we find almost flat profiles for both ρ and j, in accordance with the picture of simple dimer TASEP. On the other hand, for very large detachment rates the on/off kinetics dominates the bulk of the density profile. However, contrary to equilibrium thermodynamics of on/off kinetics, a large directed current is simultaneously present.

For intermediate values of the detachment rate, neither the density profile nor the current is constant anymore. There appear rather narrow regions where the density steeply rises from an almost linear profile to one that approaches the isotherm value. Such findings are similar to the ones of monomeric TASEP coupled to Langmuir kinetics [111, 112]. In these works it has been shown that the steep increase corresponds to a domain wall of a coexistence phase in the mesoscopic limit.
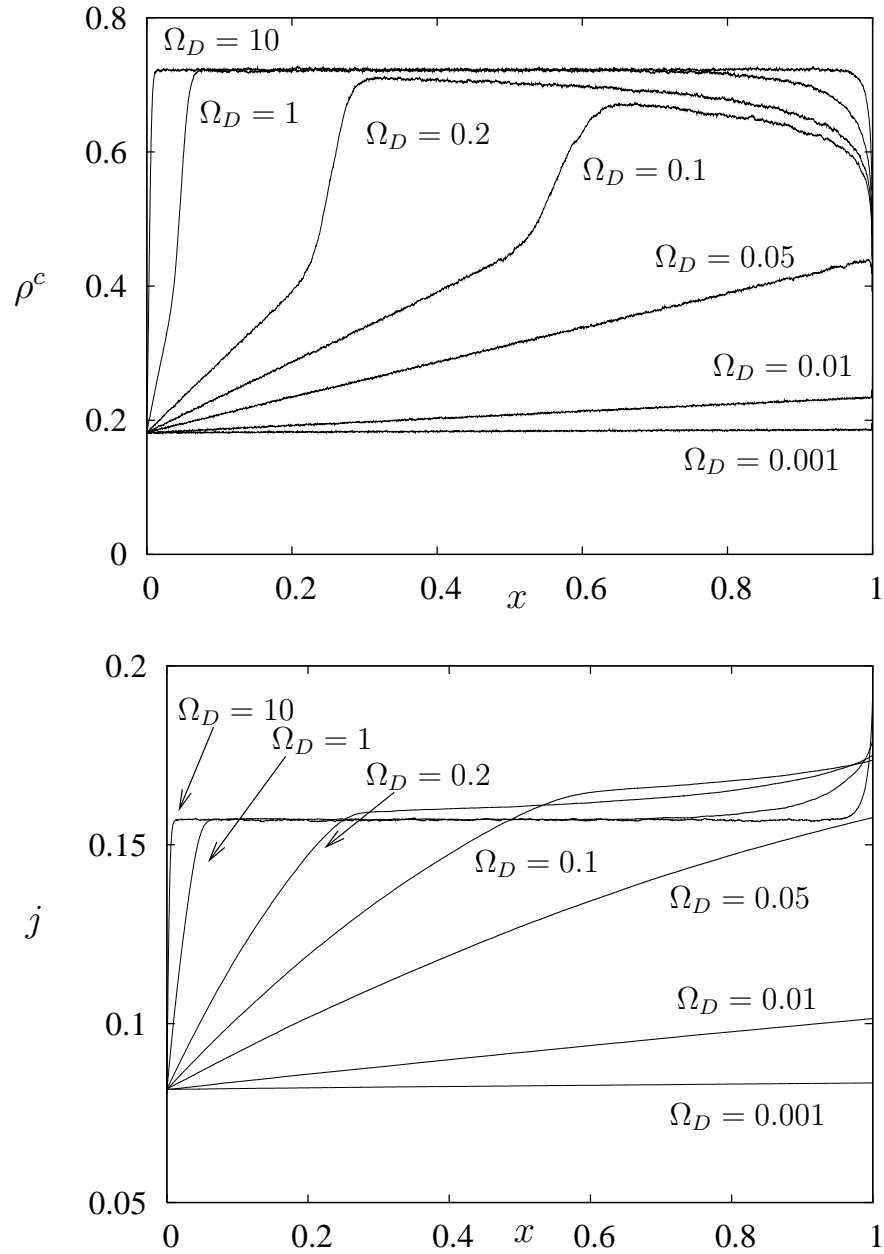
Figure 3.2: Monte Carlo results for stationary density profiles and corresponding currents for a system of $N = 4096$ lattice sites. Parameters have been fixed to $\alpha = 0.1$, $\beta = 0.6$, $K = 3$, and Ω_D are varied as indicated in the figures.

3.4 Construction of the MF equation

Since the stationary density profiles for TASEP of monomers coupled to Langmuir kinetics have been successfully described in terms of mean field theory, it appears promising to look for an analytical description for dimers also. However, it turns out that in the case of dimers the conventional mean field approach, i.e. a decoupling of correlations at lowest order starting from the quantum Hamiltonian formulation, see e.g.[112], is inappropriate: the non-trivial correlations, arising from the fact that the particles are extended, manifest themselves already at the level of pure TASEP of dimers [88].

The failure of conventional mean field approach requires the introduction of phenomenological methods. The aim of this section is to identify useful strategies that are capable to deal first with the simple on/off kinetics of extended objects without directed motion and second with pure TASEP for dimers. We will then combine the two cases to obtain a formulation for the complete problem, and we will provide arguments that the aspects of correlations are captured on a reliable level for both processes.

The density profile in the mesoscopic limit will be described in terms of a balance equation. The evolution of the course-grained dimer density is determined by: (a) a flux j of dimers within the lattice that encodes the asymmetric diffusion, (b) two source terms that represent the on-off kinetics of dimers:

$$\partial_t \rho = -\partial_x j + F_A - F_D \tag{3.4}$$

The non-trivial task is to provide reasonable expressions for the current and the sources in terms of the local density. In Sec. 3.5 we shall compare the analytical results to Monte-Carlo simulations and demonstrate the validity of this approach.

3.4.1 ON-OFF kinetics of dimers

Probabilistic approach

The dynamics of the on-off kinetics in a rate equation approach is described by the difference between a gain term F_i^A and a loss term F_i^D:

$$\partial_t \rho_i = F_i^A - F_i^D \tag{3.5}$$

These two terms are proportional to the attachment and detachment rates, ω_A and ω_D. Clearly the detachment flux is exactly given by $F_i^D = \omega_D \rho_i$. Note that for a linear death process the corresponding flux follows immediately from the master equation [73, 52].

An attachment event at site i (lead head) requires both sites i and $i-1$ to be empty (i.e. in state (0)). The corresponding attachment flux then reads $F_i^A = \omega_A p(i-1,0;i,0)$, and knowledge of the joint probability is needed. In order to obtain closed equations for the lead head density we break the hierarchy of joint probabilities resulting from the master equation. Here, we rely on an *ad hoc* approximation[3] for the conditional probabilities:

---

[3]This approximation has been introduced first in the context of pure TASEP of extended objects [97, 96].

$p(i, 0 | i - 1, 0) \simeq p(i, 0 | (i - 1, 0) \vee (i - 1, 2))$. The idea is that the probability of having site i empty is independent of having a lead head or a hole in the site $i - 1$: note that this is precisely what usually the mean field approximation does in monomeric lattice gases, where correlations are broken factorizing the density: $\langle n_i n_{i+1} \rangle = \langle \rho_i \rangle \langle n_{i+i} \rangle$. In Appendix 3.A we show that this assumption yields a closed expression for the joint probability:

$$p(i, 0; i - 1, 0) = \frac{p(i - 1, 0)p(i, 0)}{1 - p(i, 2)} . \tag{3.6}$$

Eliminating the probabilities for single empty sites and collecting results, the rate equation for the lead head density reads:

$$\partial_t \rho_i = \omega_A \frac{(1 - \rho_{i-1} - \rho_i)(1 - \rho_i - \rho_{i+1})}{1 - \rho_i} - \omega_D \rho_i . \tag{3.7}$$

As a next step we perform a continuum limit. Relabelling position as fraction of the system size, $x \equiv i/N$, the density ρ_i becomes a function $\rho(x)$ in the mesoscopic limit $N \to \infty$. The average density at the neighboring sites are obtained by expansion in powers of the lattice constant $a = 1/N$:

$$\rho(x \pm a) = \rho(x) \pm a\partial_x \rho(x) + \frac{1}{2}a^2 \partial_x^2 \rho(x) + O(a^3) . \tag{3.8}$$

Introducing a new rescaled time $\tau = at$ and eliminating the single site on/off rates ω_A and ω_D in favor of the gross kinetic rates Ω_A and Ω_D we obtain the rate equation in the mesoscopic limit:

$$\partial_\tau \rho = \Omega_A \frac{(1 - 2\rho)^2}{1 - \rho} - \Omega_D \rho + O(a^2) . \tag{3.9}$$

It is natural to expect a density limited to the range $[0, 1/2]$, because there cannot be more than one lead head per site. In the stationary regime the physical solution corresponds to the constant density ρ_I, Eq. 3.1, determined solely by the binding constant $K = \Omega_A / \Omega_D$. This value of the *isotherm* is consistent with the one obtained by McGhee and Von Hippel [102] for the general case of ℓ-mers.

Tonks gas approach

To corroborate the results presented above, we compare the isotherm of the rate equation with the one computed from the grand canonical partition function of the Tonks gas. In particular, we shall identify the fugacity z with the binding constant K.

The statistical mechanics of the Tonks gas on an open lattice consists of distributing extended objects on the N sites, respecting the excluded volume constraint. In the case of the canonical ensemble this reduces to the combinatorial problem of counting the number of ways to distribute n dimers on N lattice sites. Using the standard trick to represent the

two occupied sites of each dimer by a "stick" and the $N - 2n$ empty sites by "balls" [147], one immediately concludes

$$Z(n, N) = \binom{N - n}{n}. \tag{3.10}$$

The corresponding grand canonical partition function is readily evaluated using the previous result

$$\begin{aligned} \mathcal{Z}_N &= \sum_{n=0}^{N} z^n Z(n, N) \\ &= \frac{\left(1 + \sqrt{1 + 4z}\right)^{N+1} + \left(-1 + \sqrt{1 + 4z}\right)^{N+1}}{2^{N+1}\sqrt{1 + 4z}} \end{aligned} \tag{3.11}$$

where z denotes the fugacity[4]. The average density is then obtained in the thermodynamic limit by

$$\rho = \lim_{N \to \infty} \frac{1}{N} z \frac{\partial}{\partial z} \ln \mathcal{Z}_N = \frac{1}{2}\left(1 - \frac{1}{\sqrt{4z + 1}}\right). \tag{3.12}$$

Since the master equation of pure on/off kinetics fulfills detailed balance, the stationary state is given in terms of the grand canonical ensemble. By a single detachment event a configuration $\mathcal{C}$ of n dimers connects to some new configurations $\mathcal{C}'$ of $n - 1$ dimers. For such configurations the detailed balance condition implies $P(\mathcal{C})/P(\mathcal{C}') = \omega_A/\omega_D = K$. Conversely, the ratio can be determined also from the grand canonical Boltzmann factors. Since, apart from the total exclusion, energy does not enter the problem, the probabilities are determined by the number of dimers only: $P(\mathcal{C}) = z^n/\mathcal{Z}_N$ and $P(\mathcal{C}') = z^{n-1}/\mathcal{Z}_N$. Combining both expressions, we conclude $z = K$ as in the case of monomers.

The last result shows that the "isotherm" obtained using *ad hoc* approximations (sub-Section 3.4.1) is at least consistent with thermodynamics. Let us mention that in equilibrium the situation is probably better than in the general case, since correlations are quickly washed out by the coupling to the reservoir. The relaxation towards equilibrium can be rather different from the naive picture of rate equations, see e.g. [51].

3.4.2   TASEP of dimers

In pure TASEP particles cannot leave or enter the track except at the boundaries. Correspondingly in the bulk a conservation law holds

$$\partial_t \rho_i = j_{i-1} - j_i. \tag{3.13}$$

---

[4]The grand canonical partition function could be express in term of Chebyshev polynomial of the second kind $\mathcal{Z}_N = (-x)^{N/2} U_N\left(\frac{1}{2\sqrt{-x}}\right)$; equation 3.11 is merely a different representation.

The currents j_i can be determined by probabilistic arguments. A hopping event of a dimer at site i requires first that site i is occupied by a lead head and second that site $i + 1$ is empty. Since we fixed the hopping rate to unity this yields

$$j_i = p(i, 2; i + 1, 0). \tag{3.14}$$

Hence, also in the case of pure TASEP the master equation induces a whole hierarchy of joint probabilities. To close the equation we rely on the same *ad hoc* approximation for the conditional probabilities as for the on/off kinetics. In the appendix we show that this implies for the current a closed expression

$$j_i = \frac{\rho_i(1 - \rho_{i+1} - \rho_{i+2})}{1 - \rho_{i+1}}. \tag{3.15}$$

Performing the continuum limit as in Eq. (3.9) one obtains

$$\partial_\tau \rho = -\partial_x \left[\frac{\rho(1 - 2\rho)}{1 - \rho} + \frac{1 - 2\rho^2}{(1 - \rho)^2} \frac{a}{2} \partial_x \rho + O(a^2) \right]. \tag{3.16}$$

Since, at the very end, we consider large but finite systems we have kept the leading correction in a, which will turn out to be relevant for the formation of shocks and boundary layers.

The equation of continuity in the bulk has to be supplemented with appropriate boundary conditions. Relying again on the same *ad hoc* assumption for the conditional probability, and performing the continuum limit, one finds

$$\rho(0) = \frac{\alpha}{1 + \alpha}, \tag{3.17a}$$

$$\rho(1) = \frac{1 - \beta}{2}. \tag{3.17b}$$

The details are presented in Appendix 3.B. The properties of these equations have been studied in details in Ref. [138]. The resulting phase diagram is topologically equivalent to the one of TASEP of monomers. The continuum analogue for the current-density relation, Eq. (3.15), reads

$$j = \frac{\rho(1 - 2\rho)}{1 - \rho} \tag{3.18}$$

and exhibits a maximum at a distinguished density $\rho^* = 1/(2 + \sqrt{2})$. This value will play an important role in the more general case of TASEP coupled to on/off kinetics.

3.4.3 Combining TASEP and on/off kinetics

As anticipated at the beginning of this section, we identify the current and the source terms of Eq. (3.4) and we expressed everything in term of the density. The current is described

by Eq. (3.18) and the on/off kinetics by Eq. (3.9). By taking the mesoscopic limit we have introduced the gross attachment and detachment rates and rescaled the time consistently in both processes. The balance equation to order a can be easily rewritten as

$$\partial_\tau \rho \;=\; -\partial_x \left[-\frac{a}{2} \frac{\partial_x \rho}{(1-\rho)^2} + \frac{\rho(1-2\rho)}{1-\rho} \right] + \Omega_A \frac{(1-2\rho)^2}{(1-\rho)} - \Omega_D \rho \qquad (3.19)$$

with the boundary conditions, Eq. (3.17). These equations constitute the mean field description to be discussed in the following section.

Equation 3.19 can be recast in the same form of a Fokker-Planck-like equation with a source-drift term [73]:

$$\partial_\tau \rho = -\partial_x \left[A(\rho)\rho - B(\rho)\rho\partial_x\rho \right] + C(\rho) \qquad (3.20)$$

where the coefficients A, B and C depends on ρ (that means that the analogy is merely formal). The second coefficient will prove not to be relevant (since it scales with the size of the system). The analytical properties of the solution, which determines the phase diagram, will strictly depend on the properties of $A\rho$, in particular of the maximum of $\rho A(\rho)$ (i.e. the critical density of pure TASEP) and of $B(\rho)$, in particular its zero (i.e. the isotherm of the on-off process ρ_I). A constant flat profile is expected for the critical values of the parameter when the $A(\rho)$ reach an extremal point and $B(\rho)$ a zero. Plots of $A(\rho)$ and $C(\rho)$ are presented in Figs. 3.3.
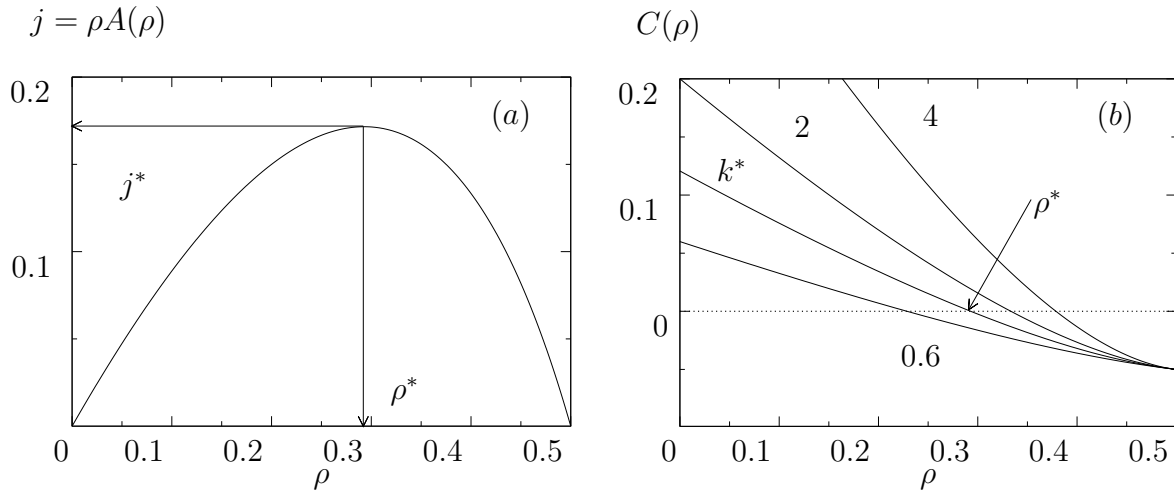

Figure 3.3: (a) Graph of the current density relation $\rho A(\rho)$ in Eq. 3.20. (b) Graph of the source-drain $C(\rho)$ term in the Fokker-Plank equation 3.20 for different values of K and $\Omega_D = 0.1$.

3.5 Solution of the mean field equation and phase diagram

This section is devoted to a discussion of the phase diagram emerging from combining TASEP of dimers with on/off kinetics. We shall derive density profiles within a mean field approach, identify different phases and phase boundaries as the kinetic rates are varied. In particular, we demonstrate the role of the binding constant in the topological changes of the phase diagram as a certain critical value is reached.

3.5.1 Emergence of shocks and boundary layers

The mean field equation for the stationary density profile, Eq. (3.19) supplemented with $\partial_\tau \rho \equiv 0$, is a second order differential equation as long as the lattice constant a is small but finite. In the limit $a \searrow 0$ the differential equation degenerates into a first order one. However, the density profile has to match the two boundaries, and it appears that the problem is overdetermined. Indeed one can construct separately a density profile fulfilling either the left or right boundary condition. The two branches will be referred to as ρ_α and ρ_β, respectively. In general, the two branches do not join smoothly together. One expects the solution of the second order differential equation to be well approximated by the two branches ρ_α and ρ_β except for a region where the solution rapidly crosses over from one branch to the other. Upon decreasing the lattice constant a the crossover region shrinks leading eventually to a discontinuity of the density profile for $a = 0$. Depending on the position of such a discontinuity x_w we refer to it as a *shock* $(0 < x_w < 1)$ or a *boundary layer* $(x_w = 0$ or $x_w = 1)$.

To locate the position of the shock or boundary layer we rely on a very general argument already used in [111, 112]. The second order differential equation for the stationary density profile can be written in the form of a balance equation $\partial_x j = F_A - F_D$, where the current along the track reads

$$j = -\frac{a}{2}\frac{\partial_x \rho}{(1-\rho)^2} + \frac{\rho(1-2\rho)}{1-\rho} \,. \tag{3.21}$$

Integrating over a small region of width $2\delta x$ around the shock one obtains

$$j(x_w + \delta x) - j(x_w - \delta x) = \int_{x_w - \delta x}^{x_w + \delta x} (F_A - F_D)dx \,. \tag{3.22}$$

In the limit $a \searrow 0$ the l.h.s. reduces to $j_\alpha(x_w + \delta x) - j_\beta(x_w - \delta x)$ (where we have defined $j_\alpha = \rho_\alpha(1 - 2\rho_\alpha)/(1 - \rho_\alpha)$ the current set by the left boundary and similarly for the right one j_β). Performing the limit $\delta x \searrow 0$ the r.h.s. of Eq. (3.22) vanishes and yields the matching rule in terms of the currents

$$j_\alpha(x_w) = j_\beta(x_w) \,. \tag{3.23}$$

Equivalently the rule implies for the densities at the matching point

$$\rho_\alpha(x_w) = \frac{1}{2} \frac{1 - 2\rho_\beta(x_w)}{1 - \rho_\beta(x_w)} \, . \tag{3.24}$$

Let us make a comment. The fact that the in-track current is continuous at the shock is consistent with the idea of the mesoscopic limit. The fluxes due to attachment and detachment are important only on the length scale of the system size. Locally, i.e. on the scale of the lattice constant, the balance equation is dominated entirely by the unidirectional hopping process (TASEP).

3.5.2 Analytical solution

The left and right branches of the stationary density profile are determined by solving Eq. (3.19), once we set the l.h.s. to zero and discard the second order derivative, i.e.

$$\frac{1}{\Omega_D} \partial_x \left[\frac{\rho(1 - 2\rho)}{1 - \rho} \right] = K \frac{(1 - 2\rho)^2}{(1 - \rho)} - \rho \, , \tag{3.25}$$

(where the binding constant $K = \Omega_A/\Omega_D$ has been introduced) which has to be supplemented by the appropriate boundary conditions Eq. (3.17). By separation of variables the general solution $G(\rho) = x + const$ is obtained after a straightforward integration (see App. 3.C) with

$$G(\rho) = \frac{1}{\Omega_D K} \Big[\ln(1 - \rho) + A_+ \ln(\rho_+ - \rho) + A_- \ln|\rho_- - \rho| \Big] \tag{3.26}$$

where we introduced the zeros of the source term

$$\rho_\pm \equiv \frac{1}{2} \left(1 \pm \frac{1}{\sqrt{1 + 4K}} \right) \tag{3.27a}$$

and the amplitudes

$$A_\pm \equiv \frac{K}{1 + 4K} \frac{1 - 4\rho_\pm + 2\rho_\pm^2}{(1 - \rho_\pm)(\rho_\pm - \rho_\mp)} \, . \tag{3.27b}$$

The function $G(\rho)$ exhibits a singularity in the physical regime $0 \le \rho \le 1/2$ at the isotherm of the on/off kinetics $\rho_I = \rho_-$. One easily checks that $G(\rho)$ exhibits an extremum when the corresponding current, Eq. (3.18), is maximal, i.e. at $\rho = \rho^*$. For $\rho_I > \rho^*$ ($\rho_I < \rho^*$) the extremum of $G(\rho)$ corresponds to a maximum (minimum). A change of topology of the graph of the solution occurs once both distinguished densities coincide $\rho_I = \rho^*$, which happens at a *critical* value of the binding constant $K^* = (1 + \sqrt{2})/2$. At this special value the amplitude A_- vanishes and the function $G(\rho)$ becomes smooth and monotonic in the physical regime $0 < \rho < 1/2$.

After matching the boundary conditions, the left and right solutions are obtained up to inversion of a function

$$L_\alpha(\rho_\alpha) \equiv G(\rho) - G(\alpha/(1 + \alpha)) = x \tag{3.28a}$$

$$R_\beta(\rho_\beta) \equiv G(\rho) - G((1-\beta)/2) + 1 = x \,. \qquad (3.28b)$$

Upon inverting, the singularity of $G(\rho)$ transforms into a horizontal asymptote, whereas the extremum manifests itself as a branch point, see Fig.(3.4). The functions are multivalued with three branches, to be referred as W_0^+, W_0^- and W_{-1}.
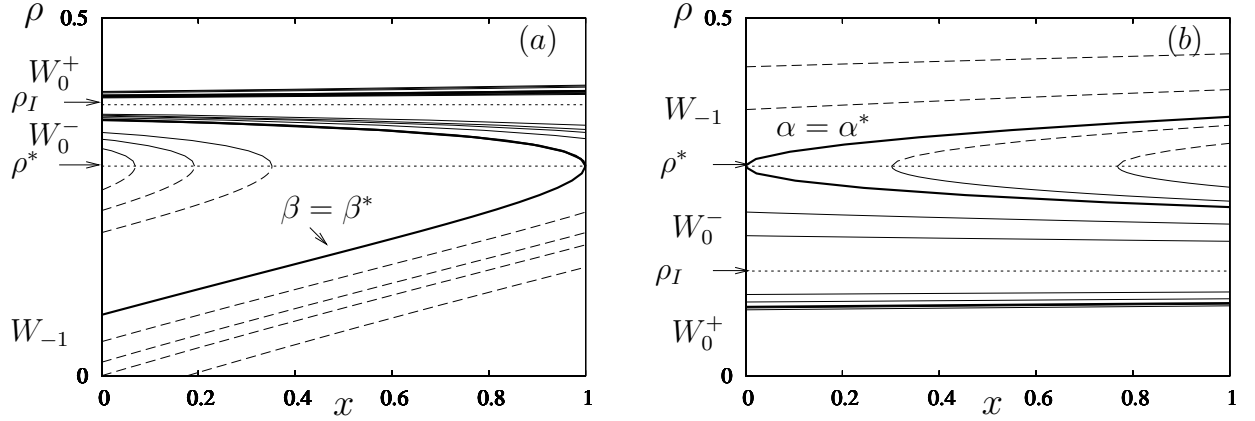

Figure 3.4: The functions W_{-1} (dashed lines), W_0^- (full lines), W_0^+ (full lines) for (a) $K = 4$, $\Omega_D = 0.05$ (high binding affinity) and (b) $K = 0.25$, $\Omega_D = 0.05$ (low binding affinity). The branches W_0^+ and W_0^- are separated by the isotherm density ρ_I. Varying α or β results in a simple shift parallel to the $x-$axis. In Fig.(a/b) the thick lines represent the solutions where the branch point hits the right/left end of the system. The dotted lines indicate the critical density value ρ^* (where branch point occurs) and the isotherm ρ_I.

3.5.3   High binding affinity: $K > K^*$

For large binding constants, $K > K^*$, the equilibrium density of the on-off isotherm is larger than critical density at which the current of pure TASEP is maximal, $\rho_I > \rho^*$, see Fig.3.4.

For densities smaller than ρ_I, the track accumulates particles from the reservoir, since

$$F_A - F_D = \Omega_D \frac{1 + 4K}{1 - \rho} \left[(\rho - \rho_-)(\rho - \rho_+)\right] \,. \qquad (3.29)$$

Hence the isotherm acts as an attractor. This property has to be reflected in the left and right solution solving the balance equation for the current, $\partial_x j = (\partial_\rho j)(\partial_x \rho) = F_A - F_D$. For $\rho(0) = \alpha/(1 + \alpha) > \rho^*$, the branches $W_0^\pm$ are unstable. For densities $\rho > \rho_I$ the coupling to reservoir induces a decrease in density, whereas W_0^+ is increasing. Similarly for $\rho^* < \rho < \rho_I$ the net gain due to the on/off kinetics is not reflected by the decreasing function W_0^-. One concludes that for the left solution the only physical branch is W_{-1}. For $\alpha > \alpha^* = \rho^*/(1 - \rho^*) = 1/(1 + \sqrt{2})$, i.e. the critical entrance rate of dimer TASEP, a left boundary layer necessarily appears.

For the right solution the argument is just reversed, i.e. the physical branches are $W_0^{\pm}$. The critical exit rate β^* of dimer TASEP is determined by $\rho(1) = (1 - \beta^*)/2 = \rho^*$ and equals $\beta^* = 1/(1 + \sqrt{2})$. For exit rates larger than the critical one a right boundary layer emerges. The complete phase diagram is obtained by identifying different scenarios to match left and right solutions. The boundary conditions, Eq. (3.17) can be satisfied by the stable branches of the left and right solution only for $\alpha < \alpha^*, \beta < \beta^*$ respectively. The merging of the two solutions by Eq. (3.24) is achieved at some position x_w. Depending on whether the (i) $0 < x_w < 1$, (ii) $x_w < 0$ and (iii) $x_w > 1$, a domain wall in the bulk emerges (i), a boundary layer at the left (ii) or right (iii) appears. For $\beta > \beta^*$ an additional boundary enters the system. The result of such an analysis is presented in Fig. 3.5, and the chain of arguments follows the one of Ref. [112].

For example, for large entrance rate α and low exit rates β the density profile is in a high density phase (HD), i.e. the solution $\rho(x)$ exceeds ρ^*, and is given by the stable right solution $\rho_{\beta}(x)$. At the left end $x = 0$ a boundary layer appears. Similarly a region of a low density phase (LD) and low density-high density phase coexistence (LD/HD) with appropriate boundary layer and domain wall is inferred from the figure.

For $\beta > \beta^*$ the right solution is replaced by the critical right solution $\rho_{\beta=\beta^*}$, which constitutes the analogue to the maximal current phase in TASEP: the system indeed cannot transport more than the current j_{β^*} imposed by the critical exit rate β^*.

Changing the exit rate beyond β^* does not affect the density profile except in a small boundary layer. This phenomenon is similar to a superconductor where an external magnetic field does not enter the sample except for a short penetration depth. This analogy suggests to denote this region in the phase diagram by M (Meissner) phase. The coexistence of low-density and Meissner phase (LD/M) extends the coexistence phase (LD/HD) for $\beta > \beta^*$.

The phase boundaries can be computed analytically up to inversion of a function. For example, the HD - LD/HD phase boundary is obtained by requiring the domain wall to fall on the left end of the system $x_w = 0$. Thus the continuity condition, Eq. (3.24) translates the boundary condition $\rho(0) = \alpha/(1 + \alpha)$ to $\rho(x + 0) = (1 - \alpha)/2$. In terms of the implicit solution, Eq. (3.28b), this implies

$$R_{\beta}\left(\frac{1 - \alpha}{2}\right) = 0\,. \tag{3.30}$$

Similarly the LD- LD/HD phase boundary is determined by placing the domain wall at $x_w = 1$, which yields

$$L_{\alpha}\left(\frac{\beta}{1 + \beta}\right) = 1\,. \tag{3.31}$$

For $\beta > \beta^*$ the preceding equations still hold provided β is replaced by the critical exit rate β^*.[5] Correspondingly, phase boundaries degenerate to straight vertical lines.

---

[5]For Eq. (3.31) the replacement is obvious in the condition, whereas for Eq. (3.30) notice that $R_{\beta}(\rho_{\beta})$ depends on β according to Eq. (3.28b)
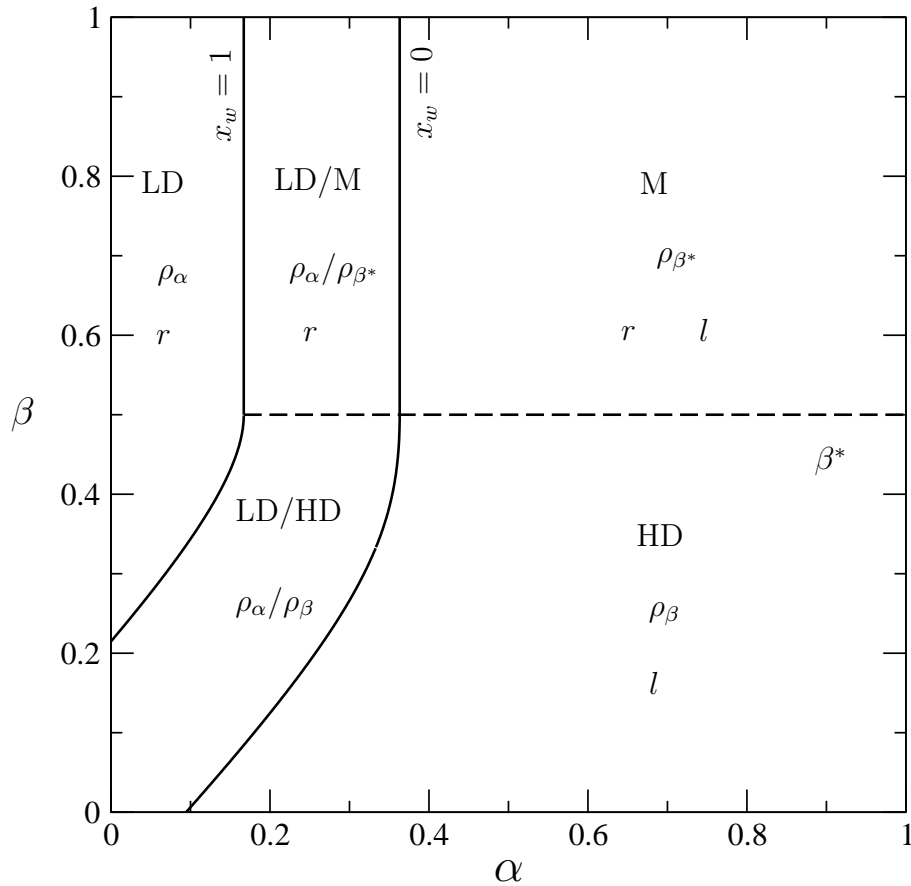
Figure 3.5: High binding affinity; phase diagram for $K = 2$, $\Omega_D = 0.1$. In the low-density (LD) phase the profile is given by the left solution ρ_α and a boundary layer appears at the right (r). The position of boundary layers (r, l), as well as the relevant bulk solution (ρ_α, ρ_β, and $\rho_{\beta*}$) are indicated for all phases (HD: high density phase, LD/HD: low density-high density coexistence phase, M: Meissner phase, LD/M: low density-Meissner coexistence phase, see text).

Density profiles exemplifying different regions of the phase diagram are showed in Figs. 3.6 and compare nicely to the corresponding Monte Carlo data.

The low density phase disappears from the phase diagram upon increasing Ω_D at fixed K. Such a topological change occurs, once the phase boundary of the LD/M coexistence phase hits the β-axis of the phase diagram (i.e. $\alpha = 0$). The condition is inferred from Eq. (3.31) and reads:

$$L_{\alpha=0}\left(\frac{\beta^*}{1+\beta^*}\right) = 1\,. \tag{3.32}$$

A numerical solution of the preceding equation for Ω_D^* as a function of K, is presented in Fig. 3.7.

In the limit $\Omega_D \to 0^+$ the LD/HD coexistence phase shrinks continuously to the line $\alpha = \beta$ and one recovers the dimer TASEP phase diagram. For $\Omega_D \gg \Omega_D^*$, the coexistence phases constitute only a marginal region in the $\alpha - -\beta$ plane, located close to the β-axis. The phase diagram is dominated by the HD and M phases, however the density profile approaches the constant value ρ_I in the bulk, as expected from pure on-off kinetics.[6]

3.5.4   Low binding affinity: $K < K^*$

If $K < K^*$ the functional form of the solutions is still given by Eqs. (3.26,3.28a,3.28b). However, now the isotherm $\rho = \rho_I$ lies below the critical density, $\rho_I < \rho^*$. By the same reasoning as above, see Eq. (3.29), the left stable branches are the one which approach the isotherm, $W_0^\pm$ in Fig. (3.4b), while the only stable solution for the right side is W_{-1}, i.e. reversed to $K > K^*$.

Using the same methods as for the high binding constant, phases and phase boundaries are identified by matching the appropriate left and right solutions. A cut of the parameter space at fixed Ω_D and K is presented in Fig. 3.8. The high density phase disappears from the phase diagram for detachment rates exceeding a critical value $\Omega_D^*(K)$, see Fig. 3.7.[7]

Let us stress that there is an important difference with respect to the monomeric analogue, namely the particle-hole symmetry is no longer present. Correspondingly, a symmetry transformation does not yield the phase diagram of the "low affinity" from the one of the "high affinity". Yet, the exchange of high densities and low densities, left and right, exit by entrance rates yields the correct topology of the phase diagram as well, as qualitatively the density profile.

---

[6] All the phase boundaries between LD-HD and HD phase intersect at a fix *nodal* point N. In this point the solution must be independent of Ω_D but must depends on the binding constant and on the boundaries: this is the point where the bulk density imposed by the right boundary becomes equal to the isotherm, moreover since it is valid also in the limit of small Ω_D one expects $\alpha = \beta$. The coordinates of such a point (α_N, β_N) can be computed from $\rho_\beta(1) = (1 - \beta)/2 = \rho_I$ and are equal to $\alpha = \beta = 1/\sqrt{4K + 1}$.

[7] In this case too there is a nodal point N where all the phase boundaries between coexistence an HD (or M) phase (that indicate the domain wall at the left boundary) intersect: it can be computed from the condition $\rho_\alpha(0) = \alpha/(1 + \alpha) = \rho_I$ and corresponds to the point $\alpha = \beta = (\sqrt{4K + 1} - 1)/(\sqrt{4K + 1} + 1)$.
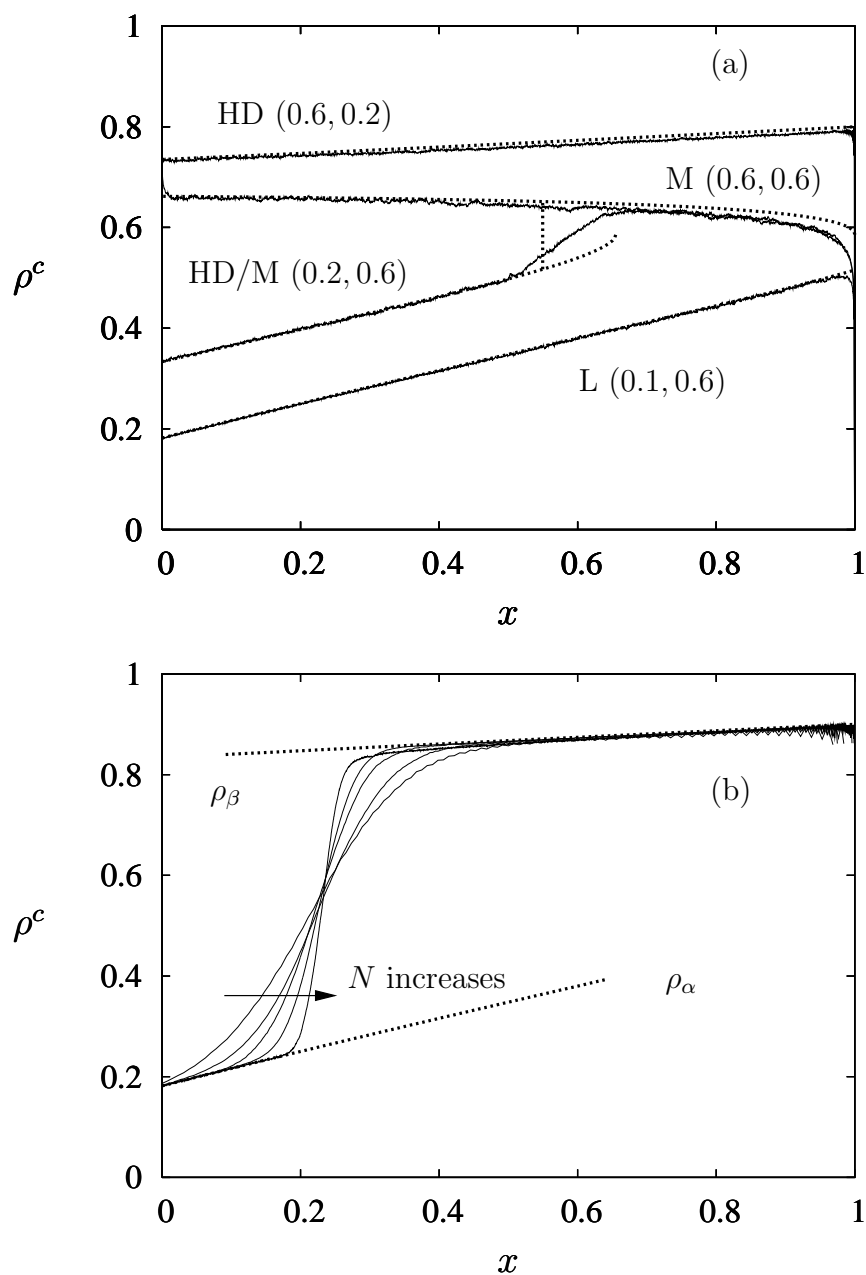
Figure 3.6: (a) Density profiles for $K = 2$ and $\Omega_D = 0.1$ in systems of $N = 4096$ lattice sites; parameters $(\alpha, \beta) = (0.1, 0.6), (0.2, 0.6), (0.6, 0.6), (0.6, 0.2)$. (b) Approach of the mesoscopic limit of the density profile for $\alpha = \beta = 0.1$, $\Omega_D = 0.1$, $K = 2$ and different system sizes ($N = 128, 256, 512, 1024, 4096$); the domain wall becomes steeper with the increasing of N. Wiggly lines represent Monte Carlo data, while dotted lines indicate analytic solutions.
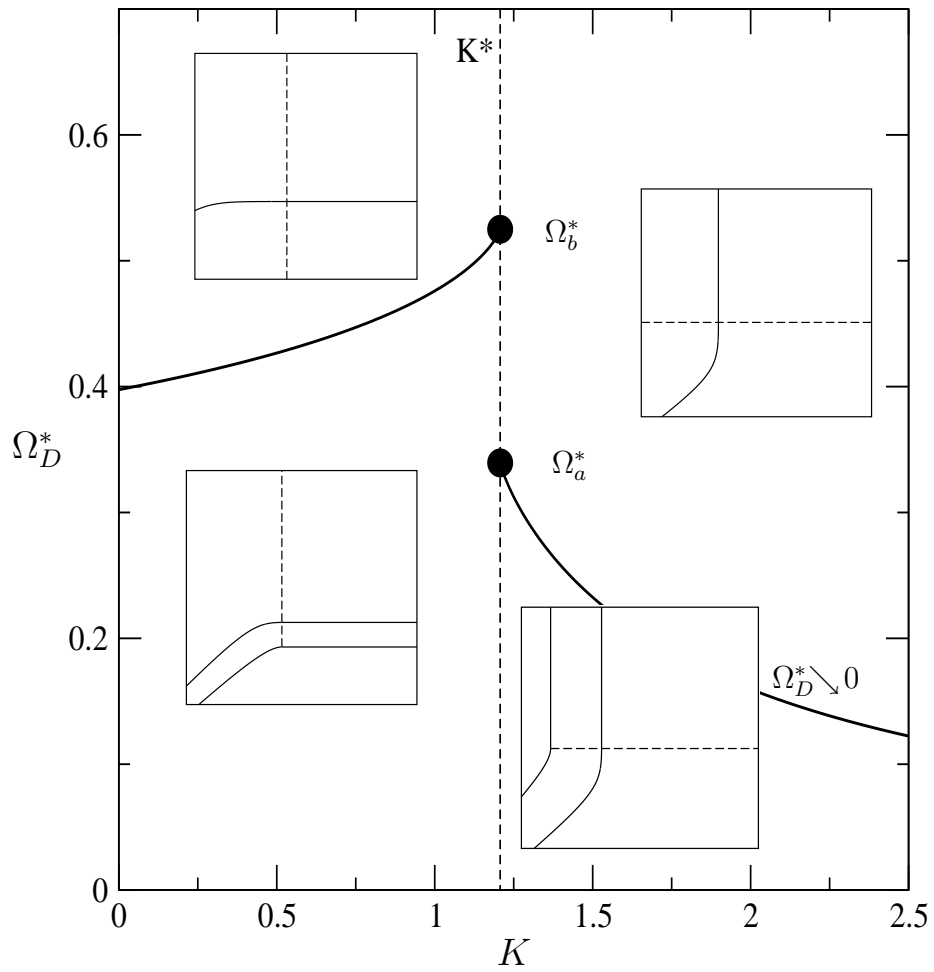
Figure 3.7: Critical detachment rate Ω_D^* as a function of the binding constant K. The dotted line K^* separates the cases of "high" form the "low" binding affinity. For large K the critical detachment rate approaches zero. Insets represent the different topologies of the $\alpha - \beta$ section of the phase diagram.
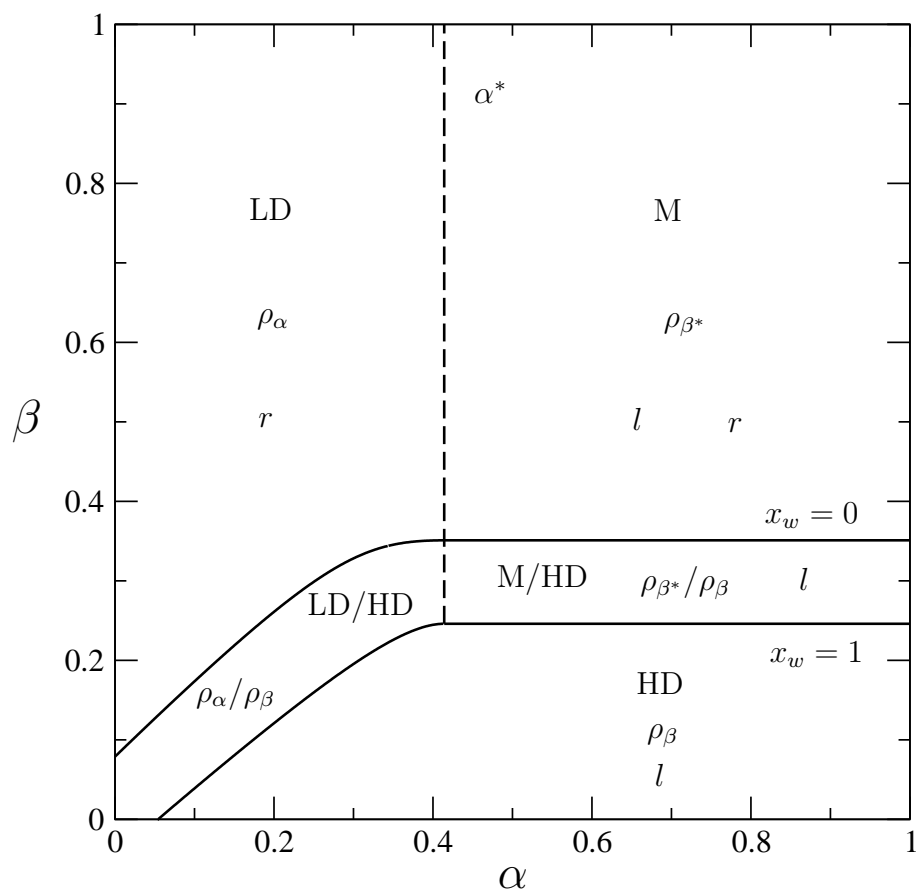
PSfrag replacements

Figure 3.8: Low binding affinity; phase diagram for $K = 0.8$, $\Omega_D = 0.1$. Legend as in Fig. (3.5).

3.5.5   The critical case $K = K^*$

The limiting case when the binding constant equals the critical one, $K = K^*$, requires a separate analysis, since the amplitude A_- vanishes, cancelling exactly the logarithmic divergence at $\rho = \rho_-$ (*nota bene* $\rho_- = \rho^* = \rho_I$). This signals that $\rho = \rho^* = const$ is a spurious solution of the balance equation for the stationary density profile. It corresponds to the maximal current (MC) phase of pure dimer TASEP. Indeed for $K = K^*$ Eq. (3.25) simplifies to

$$(\rho - \rho^*) \left[\frac{2\rho - (2 + \sqrt{2})}{(1 - \rho)} \partial_x \rho - \Omega_D \left(\rho - \frac{1}{\sqrt{2}} \right) \right] = 0 \tag{3.33}$$

The non-trivial solution Eq. (3.26) specializes to

$$G(\rho) = \frac{2\sqrt{2} - 2}{\Omega_D} \left(\ln(1 - \rho) - \sqrt{2} \ln(\frac{1}{\sqrt{2}} - \rho) \right) , \tag{3.34}$$

which is a monotonic function in the physical regime. Correspondingly, the inverse function is single valued.

The properties of the phase diagram for $K = K^*$ are obtained by assembling the resulting left and right branches, as well as the constant critical density ρ^*, for different boundary conditions. We have determined numerically the line where the domain wall hits the left and right end, $x_w = 0$ and $x_w = 1$, respectively by solving Eqs. (3.30,3.31). Moreover both left and right solutions now can approach the critical one (i.e. $\rho = \rho_I$) in the bulk and therefore a triple phase coexistence LD-MC-HD is possible. This phase is bounded by the lines $\beta = \beta^*$ above and $\alpha = \alpha^*$ on the right. Furthermore the curve $g(\alpha, \beta)$, where the left and right currents match additionally the critical one, separates the triple phase coexistence from the LD-HD phase. Implicitly $g(\alpha, \beta)$ is given by the condition $L_\alpha \left(\beta^*/(1 + \beta^*) \right) = R_\beta \left((1 - \alpha^*)/2 \right)$.

Depending on the value of the kinetic rate Ω_D, different topologies for the phase diagram arise. For example, for low Ω_D seven phases are present in the $\alpha - \beta$ diagram (see Fig. (3.9)). Upon increasing Ω_D, a first topological change, analogous to the case of high binding affinity, occurs, i.e. the LD phase exits the phase diagram. By solving Eq. (3.32), one obtains the critical value $\Omega_a^* \approx 0.33945$, see Fig. (3.7). At another critical value $\Omega_b^* \approx 0.52496$ the HD phase disappears, and at still higher detachment rates $\Omega_D > \Omega_c^* = 0.86441$ the LD-HD coexistence phase is no more present and the phase diagram (but not the density profiles) is independent of Ω_D. Representative graphs of these topologies are exhibited in Figs. (3.7) and (3.10).

3.6   Conclusions

In the following we compare our results with the ones obtained for the analogous problem of simple TASEP of monomers coupled to Langmuir kinetics (see Ch. 2). The balance
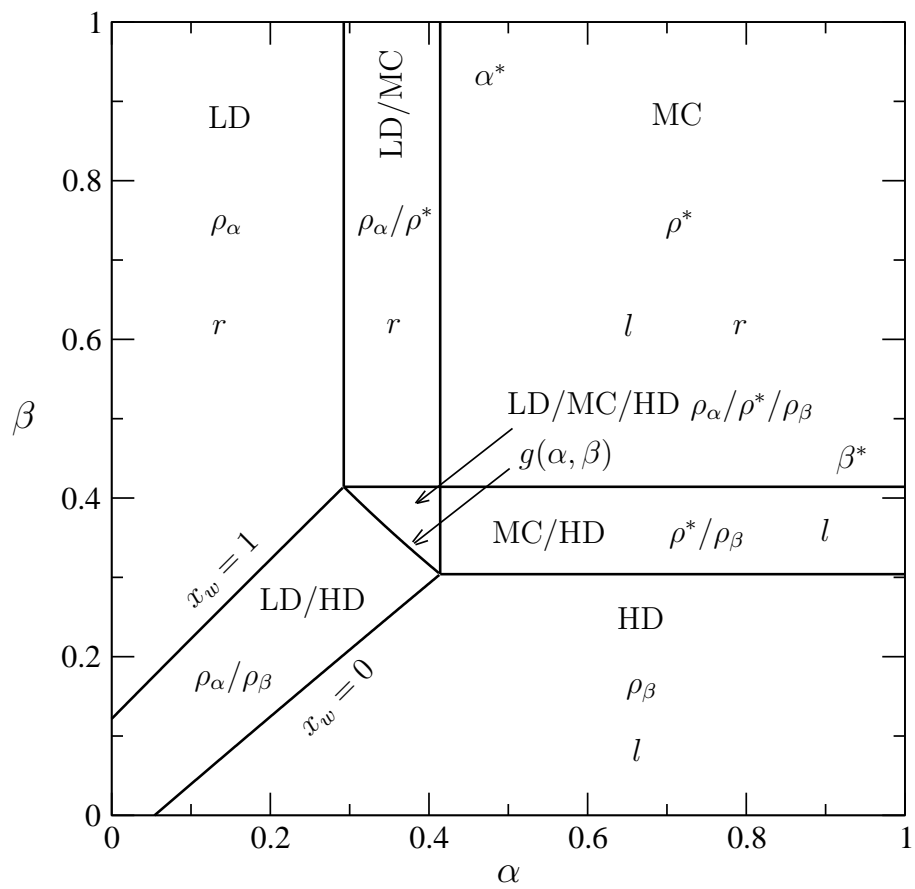
PSfrag replacements

Figure 3.9: Critical case; phase diagram for the case $K = K^*$, $\Omega_D = 0.1$. Seven phases appear: LD, MC, HD and all the possible coexistence: LD/MC, MC/HD, LD/HD, LD/MC/HD. Legend as in 3.5.
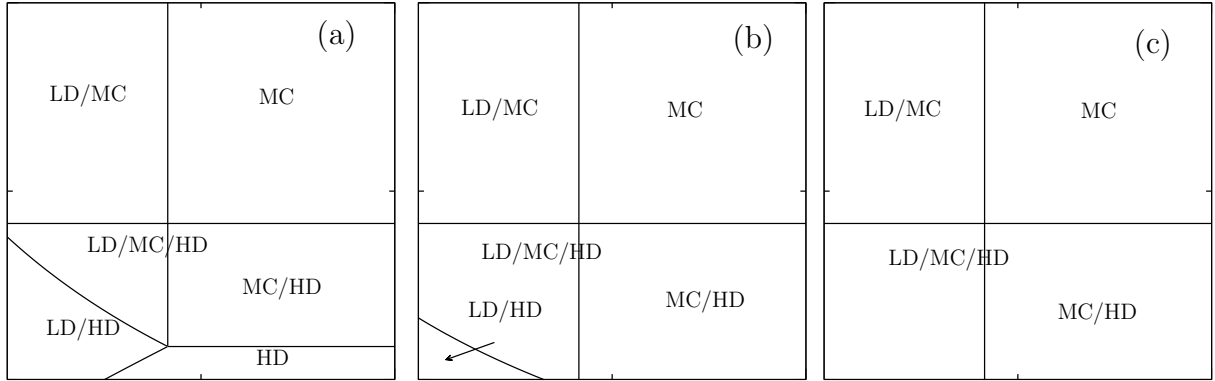
Figure 3.10: Different topologies of the phase diagram for $K = K^*$ and (a) $\Omega_a^* < \Omega_D < \Omega_b$, (b) $\Omega_b^* < \Omega_D < \Omega_c^*$ and (c) $\Omega_D > \Omega_c^*$. Phases are indicated in the graphs.

equation in the stationary state that constitutes the equivalent of Eq. (3.19) has been derived in [111, 112]:

$$\frac{1}{\Omega_D} \partial_x \left[\rho(1 - \rho)\right] = K(1 - \rho) - \rho \tag{3.35}$$

Although the structure of the equation is the same, $\partial_x j = F_A - F_D$, the current and the source terms obey a rather different functional dependence. In particular, the equation exhibits a particle-hole symmetry, i.e. density profiles and the complete phase diagram is symmetric with respect to the following transformation rule $\rho(x) \leftrightarrow 1 - \rho(1-x)$, $\Omega_D \leftrightarrow \Omega_A$, $\alpha \leftrightarrow \beta$. It was therefore sufficient to investigate one of the cases, say $K > K^* = 1$, and obtain the other by flipping the phase diagram. For dimers such an argument does not hold anymore. Although simple dimer TASEP can be cast in a particle-hole symmetric form, introducing an effective hole density $\overline{\rho}$ by the requirement $j(\rho) = j(\overline{\rho})$) and interchanging α with β; this explain why the phase diagram is symmetric along the diagonal. Similarly a pure on/off kinetics is invariant with respect to the transform $\Omega_A \leftrightarrow \Omega_D$ and an effective hole density $\overline{\rho} = (1 - 2\rho)^2/(1 - \rho)$. One easily shows that the two symmetries of simple dimer TASEP and on/off kinetics never coincide for any $K > 0$, implying that the coupling of both processes breaks the particle-hole symmetry.

It is remarkable that the topology of the resulting phase diagram is almost unaffected by the symmetry breaking. In fact, the single qualitative change of topology occurs at $K = K^*$ for intermediate Ω_D, see Fig. (3.10b). The origin of the *robustness* of the picture can be traced back to the following observations: (i) in a mean field approach the balance equation for the stationary density profile is an autonomous first order ordinary differential equation; (ii) the current density relation exhibits a single extremum for both cases[8]; (iii) the solution $\rho(x)$ is obtained by quadrature and inversion of a function resulting in a

---

[8]This is not always the case: systems where interactions between particles are taken into account, as in [59, 118] showed current-density relation with multiple maxima.

multivalued function with a simple branch point (due to the maximum in the current density relation) and a horizontal asymptote (due to the on/off isotherm). Although the shape of the explicit solution depends on the details of the density current relation and the functional form of the on/off kinetics, the overall topological features remain unchanged. This reasoning explains that particle hole symmetry is relevant for the topology of the phase diagram only if the branching point is canceled by a zero of the on/off kinetics, i.e. precisely at $K = K^*$. We conclude that the scenario for $K = K^*$ presented in Fig 3.10 generalizes the monomer TASEP coupled to Langmuir kinetics. Nevertheless there are many differences in the numerical values of several quantities, which are summarized in Table 3.1.

It is possible to generalize the continuous equation to the case of a system containing ℓ-mers, using directly the continuous results presented in [102, 138]:

$$\frac{1}{\Omega_D} \partial_x \left[\frac{\rho(1 - \ell\rho)}{1 - (\ell - 1)\rho} \right] = K \frac{(1 - \ell\rho)^\ell}{(1 - (\ell - 1)\rho)^{\ell-1}} - \rho$$

(3.36)

The qualitative picture is contained already in the case of dimers; although the functional form of the solution depends on the size of the ℓ-mers, the scenario of three branches, characterized by the maximum of the current density relation ρ^* and the horizontal asymptote ρ_I, is robust.

In conclusion we have studied a driven one dimensional lattice gas of dimers where the dynamics of the totally asymmetric exclusion process has been coupled to the on-off kinetics in the bulk. We used the ad-hoc "refined" mean field for the TASEP part introduced in previous works [96, 88, 138] and proved that it is consistent with the assumptions made for the on-off part. The main effect of extended nature of dimers on the phase behavior of the system is related to the breaking of a symmetry in the problem (particle-hole). This does have quantitative but not qualitative consequences on the density profile and on the phase diagram. The origin of the *robustness* of the picture found for monomers can be traced back to the form of the stationary density profile which depends exclusively on the form of the current-density relation and of the isotherm of the on-off kinetics. This suggests that the TASEP dynamics washes out the interesting two-step relaxation dynamics that characterizes the on-off kinetics of dimers. The non-trivial outcome is that, in these systems, the diffusion (yet asymmetric) always dominates the large time-scale relaxation.

Further studies on the dynamical correlation functions could point out more subtle differences between the dynamics of dimers and monomers. We conjecture that quite interesting phenomena would arise upon taking into account other interactions between the particles, which suggest to consider alternative current-density relations (with more maxima) or non-trivial on-off isotherm (cooperative on-off kinetics).

Quantity	Monomers	Dimers
Particle dens.	ρ	ρ
Coverage dens.	ρ	2ρ
j	$\rho(1-\rho)$	$\frac{\rho(1-2\rho)}{1-\rho}$
F_A	$\Omega_A(1-\rho)$	$\Omega_A\frac{(1-2\rho)^2}{1-\rho}$
F_D	$\Omega_D\rho$	$\Omega_D\rho$
$\rho(0)$	α	$\frac{\alpha}{1+\alpha}$
$\rho(1)$	$1-\beta$	$\frac{1-\beta}{2}$
ρ^*	$\frac{1}{2}$	$\frac{1}{\sqrt{2}(1+\sqrt{2})}$
$\alpha^*=\beta^*$	$\frac{1}{2}$	$\frac{1}{1+\sqrt{2}}$
j^*	$\frac{1}{4}$	$\frac{1}{(1+\sqrt{2})^2}$
j_α	$\alpha(1-\alpha)$	$\frac{\alpha(1-\alpha)}{1+\alpha}$
j_β	$\beta(1-\beta)$	$\frac{\beta(1-\beta)}{1+\beta}$
ρ_I	$\frac{K}{1+K}$	$\frac{1}{2}\left(1-\frac{1}{\sqrt{1+4K}}\right)$
K^*	1	$\frac{1}{2}(1+\sqrt{2})$

Table 3.1: Differences and analogies between the model with monomers and dimers: the current-density relation present in both cases a maximum at ρ^* which appears at different values, but the particle-hole symmetry which is trivial in the monomers is actually effective in the dimers; the boundary conditions, as well as the current, need to be set differently in the dimers in order to keep track of their geometry; as a consequence of this the critical values of the boundary rates are different from the critical density in the case of dimers; the the isotherm is related to the binding constant in a non trivial way in the case of dimers; the particle-hole symmetry is preserved by the sources only in the monomers case. See the text for more details.

Appendix 3.A   The conditional probability

In this appendix we derive an approximate expression for the joint probability $p((i,0) \wedge (i-1,0))$ and $p((i,2) \wedge (i+1,0))$ starting from the mean field assumption

$$p(i,0|i-1,0) \simeq p(i,0|(i-1,0) \vee (i-1,2)). \qquad (3.37)$$

Since the event $(i,0) \wedge (i-1,1)$ is excluded by the dimer geometry, the mean field approximation assumes the occupancy of site i to be independent of the state of the previous site. Using Bayes theorem, the r.h.s. of Eq. (3.37) can be expressed as

$$p((i,0)|(i-1,2) \vee (i-1,0)) = \\ \frac{p((i-1,0) \vee (i-1,2)|(i,0))p((i,0))}{p((i-1,0) \vee (i-1,2))} . \qquad (3.38)$$

The conditional probability in the numerator is unity, $p((i-1,0) \vee (i-1,2)|(i,0)) = 1$, since a trail head cannot occupy site $i-1$ if site i is empty. Moreover the events $(i,0)$ and $(i,2)$ in the denominator are mutually exclusive $p((i-1,0) \vee (i-1,2)) = p(i-1,0) + p(i-1,2)$. Collecting results and using Eq. (3.37)

$$p(i,0|i-1,0) = \frac{p(i,0)}{p(i-1,0) + p(i-1,2)} . \qquad (3.39)$$

The normalization condition compatible with the geometry of the dimers allows to rewrite the denominator, $p(i-1,0) + p(i-1,2) = 1 - p(i-1,1) = 1 - p(i,2)$, and one obtains Eq. (3.6).

A similar argument can be used to compute the joint probability $p((i,2) \wedge (i+1,0))$, using $p(i+1,0|i,2)$ under the same initial hypothesis

$$p(i+1,0|i,2) \simeq p(i+1,0|(i,0) \vee (i,2)). \qquad (3.40)$$

Using this equation and the normalization condition $p(i+1,0|i,0)p(i,0)+p(i+1,0|i,1)p(i,1)+p(i+1,0|i,2)p(i,2) = p(i+1,0)$ (together with the fact that $p(i+1,0|i,1) = 0$ for obvious geometric reasons), one can show that $p(i+1,0|i,2) \simeq p(i+1,0|i,0)$.

Appendix 3.B   Boundary conditions

We recall the arguments given previously [96, 88, 138] to justify the boundary conditions 3.17.

Left boundary: The left boundary conditions in the continuum limit can be derived from the rate equation. The incoming flux is given by the entrance rate multiplied by the probability of having the first two sites free, which is derived from the normalization condition on site $i = 2$ (given that site $i = 1$ can never contain a trail head):

$$p((1,0) \wedge (2,0)) = 1 - p(2,2) - p(2,1) = 1 - \rho_2 - \rho_3 \qquad (3.41)$$

while the outgoing flux is determined by the usual relation. This yields to:

$$\partial_T \rho_1 \;=\; \alpha(1 - \rho_2 - \rho_3) - \frac{\rho_2(1 - \rho_3 - \rho_4)}{1 - \rho_3} \tag{3.42}$$

In the continuum limit (in first approximation) of the stationary state $\rho_2 = \rho_3 = \rho$ and therefore the equation can be solve for ρ in terms of α to get Eq. (3.17a)

$$\rho(0) = \frac{\alpha}{1 + \alpha} \tag{3.43}$$

This can be seen as if the left density was imposed by the reservoir density to which the system is coupled, which is not ρ, but $\rho/(1 - \rho)$, therefore $\frac{\rho}{\rho_s} = \frac{\rho}{1-\rho} = \alpha$. Note that the current density relation leads for the boundary condition on current too:

$$j(0) = j_\alpha = \frac{\alpha(1 - \alpha)}{1 + \alpha} \; . \tag{3.44}$$

Right boundary: On the right boundary the last two sites are freed at the same time and there is no exclusion on the last site $i = N$, therefore the incoming current on the second last site $i = N - 2$ is the usual one while the outgoing current is given by the occupation of the site $i = N - 1$ (since the last site is empty); consistently with the continuity property, the outgoing current at site $i = N - 2$ is also the gain term for the last site, while the loss term is given by $\beta \rho_N$:

$$\partial_T \rho_{N-1} = \frac{\rho_{N-2}(1 - \rho_{N-1} - \rho_N)}{1 - \rho_{N-1}} - \rho_{N-1} \, , \tag{3.45a}$$

$$\partial_T \rho_N = \rho_{N-1} - \beta \rho_N \; . \tag{3.45b}$$

It is obvious that in the continuum limit the density in the last two sites is different and only a coarse grained quantity like the average density (which is half the coverage density) makes sense: $\rho = (\rho_{N-1} + \rho_N)/2$. One considers this last definition, the stationary state of Eq. (3.45a) with constant incoming current (that gives $\rho(1 - 2\rho)/(1 - \rho) = \rho_{N-1}$) and the stationary state of Eq. (3.45b) (that gives $\rho_{N-1} = \beta \rho_N$), to obtain

$$\frac{\rho(1 - 2\rho)}{1 - \rho} = \rho \frac{2\beta}{1 - \beta} \tag{3.46}$$

which finally gives the right boundary condition:

$$\rho(1) = \frac{1 - \beta}{2} \; . \tag{3.47}$$

The right boundary condition for the current reads:

$$j(1) = j_\beta = \frac{\beta(1 - \beta)}{1 + \beta} \tag{3.48}$$

which has naturally the same form of the left condition because of the effective particle hole symmetry.

Note also that in the HD phase the particles wait a long time before detach giving rise to peculiar correlations: the (coverage) density profile exhibits a sawtooth profile superimposed to the analytical one. By using linear analysis on the discrete map it can be shown that these correlations decay exponentially (but not as fast as the usual boundary layers) to the fix point.

Appendix 3.C   Calculation of the solution Eq. (3.26)

In this appendix we present the detail computation of the solution Eq. (3.26), although it is rather easy to integrate. We are required to solve the first order differential equation:

$$\frac{1}{\Omega_D} \partial_x \left[\frac{\rho(1-2\rho)}{1-\rho} \right] = K \frac{(1-2\rho)^2}{(1-\rho)} - \rho \,. \tag{3.49}$$

This can be rewritten as

$$\partial_x \rho = \frac{\Omega_D(1-\rho)}{2\rho^2 - 4\rho + 1} \left[K(1-2\rho)^2 - \rho(1-\rho) \right] \,, \tag{3.50}$$

which can be integrated by separation of variable, reducing the problem to the computation of the following integral:

$$G(\rho) = \frac{1}{\Omega_D} \int d\rho \frac{1 - 4\rho + 2\rho^2}{(1+4K)(1-\rho)(\rho - \rho_-)(\rho - \rho_+)} = x + const \tag{3.51}$$

upon defining the zeros of the source term (l.h.s. of Eq. 3.49) as:

$$\rho_\pm \equiv \frac{1}{2} \left(1 \pm \frac{1}{\sqrt{1+4K}} \right) \,. \tag{3.52}$$

Equation 3.51 can be now be decomposed as:

$$G(\rho) = \frac{1}{\Omega_D K} \int d\rho \left[\frac{1}{1-\rho} + \frac{A_+}{\rho - \rho_+} + \frac{A_-}{\rho - \rho_-} \right] \tag{3.53}$$

where we have defined the amplitudes

$$A_\pm \equiv \frac{K}{1+4K} \frac{1 - 4\rho_\pm + 2\rho_\pm^2}{(1-\rho_\pm)(\rho_\pm - \rho_\mp)} \,, \tag{3.54}$$

obtained by simply parting the fraction in Eq. 3.51.

Each of the term in Eq. 3.53 is now a simple integral of a logarithm and hence:

$$G(\rho) = \frac{1}{\Omega_D K} \left[\ln(1-\rho) + A_+ \ln(\rho_+ - \rho) + A_- \ln|\rho_- - \rho| \right], , \tag{3.55}$$

which is the function in Eq. 3.26.

Appendix 3.D   Naive MF: where does it fail?

In this appendix we describe the wrong MF approach and its continuum approximation. We will refer to the hydrodynamic equation of the occupation number $n_i^{(1)} \to \rho(x)$ starting from the quantum Hamiltonian (see Ch. 2).

The quantum Hamiltonian for the problem can be easily written if one considers the sites in state "occupied" $((0,1)^t)$ the one with the lead head on it and "empty" $((1,0)^t)$ the one either with no heads or with the trail head of the dimer on it. With this convention the quantum Hamiltonian operator of the model is the sum of the hopping term $\hat{H}_h$, of the attachment-detachment term $\hat{H}_{AD}$ and of the boundaries term $\hat{H}_b$ (which is a special case of the on-off kinetics one):

$$\hat{H} = \hat{H}_h + \hat{H}_{AD} + \hat{H}_b \tag{3.56}$$

where the several parts of the Hamiltonian read

$$\hat{H}_h = \sum_{n=1}^{N-2} \left[\hat{n}_i(1 - \hat{n}_{i+1}) - \hat{s}_i^+ \hat{s}_{i+1}^- \right] (1 - \hat{n}_{i+2}), \tag{3.57}$$

$$\hat{H}_{AD} = \sum_{n=2}^{N-2} \left[\omega_A(1 - \hat{n}_{i-1})(1 - \hat{n}_i - \hat{s}_i^-)(1 - \hat{n}_{i+1}) + \omega_D(\hat{n}_i - \hat{s}_i^+) \right], \tag{3.58}$$

$$\hat{H}_b = \alpha(1 - \hat{n}_1 - \hat{s}_1^-)(1 - \hat{n}_2) + \beta(\hat{n}_{N-1} - \hat{s}_{N-1}^+). \tag{3.59}$$

Using Heisenberg notation and taking the averages one can write the rate equations:

$$\partial_t n_i = n_{i-1}(1 - n_i)(1 - n_{i+1}) - n_i(1 - n_{i+1})(1 - n_{i+2}) +$$
$$+ \omega_A(1 - n_{i-1})(1 - n_i)(1 - n_{i+1}) - \omega_D n_i \tag{3.60}$$

$$\partial_t n_1 = \alpha(1 - n_1)(1 - n_2) - n_1(1 - n_2)(1 - n_3) \tag{3.61}$$

$$\partial_t n_{N-1} = n_{N-2}(1 - n_{N-1})(1 - n_N) - \beta n_{N-1} \tag{3.62}$$

Note that the last site N is always empty and $\partial_t n_N = 0$. Configurations with two adjacent sites occupied are forbidden by the model and the Hamiltonian preserves the number of the accessible configurations: starting from a physically accessible configuration we end up always in a possible configuration. An empty state is a good initial configuration. The possible configurations are therefore less than 2^N (although the Hamiltonian act on space of such dimension).

We start from the rate equation 3.60 without on-off part and use the naive mean field approximation (breaking the hierarchy at the first level: $\langle n_i n_j \rangle = \langle n_i \rangle \langle n_j \rangle$) to get:

$$\partial_t \rho(x) = \rho(x - \epsilon)(1 - \rho(x))(1 - \rho(x + \epsilon)) - \rho(x)(1 - \rho(x + \epsilon))(1 - \rho(x + 2\epsilon)) \tag{3.63}$$

where $\epsilon = 1/N$ is the lattice constant. We apply Taylor expansion to get the continuous description

$$\partial_t \rho = \frac{\epsilon}{2} \partial_x^2 [\rho(1 + \rho - \rho^2)] - \partial_x[\rho(1 - \rho)^2] \tag{3.64}$$

The expression for the current in the continuity equation $\partial_t \rho = -\partial_x j$:

$$j \equiv -\frac{\epsilon}{2}\partial_x[\rho(1+\rho-\rho^2)] + \rho(1-\rho)^2. \qquad (3.65)$$

The current density relation (at zero-th order in ϵ) reads therefore

$$j \equiv \rho(1-2\rho)^2. \qquad (3.66)$$

By taking the derivative, one obtains the maximum at $\rho^* = 1/3$ and $j^* = 4/27$ which are completely different from the exact predictions and from the one of the ad hoc mean field (actually the error is about 20% on the density and 14% on the current).

The on off kinetics is also wrong: from the Hamiltonian 3.58 one expects a rate equation like:

$$\partial_t \rho(x) = \Omega_A(1-\rho)^3 - \Omega_D\rho \qquad (3.67)$$

which leads to the solution of the third degree equation which does not match the MC data. For $K = 2$ for example the error is 23%.

Note that another MF approach could be used: as we said at the end of the previous section the quantum Hamiltonian preserves the system in a sub-manifold of the Hilbert space which contains always physical states; this means that starting from a "good" state (like for example an empty lattice) a Hamiltonian made of:

$$\hat{H}_h = \sum_{n=1}^{N-2} \left[\hat{n}_i - \hat{s}_i^+ \hat{s}_{i+1}^- \right] (1 - \hat{n}_{i+2}), \qquad (3.68)$$

$$\hat{H}_{AD} = \sum_{n=2}^{N-2} \left[\omega_A(1 - \hat{n}_{i-1} - \hat{s}_i^-)(1 - \hat{n}_{i+1}) + \omega_D(\hat{n}_i - \hat{s}_i^+) \right], \qquad (3.69)$$

$$\hat{H}_b = \alpha(1 - \hat{n}_1 - \hat{s}_1^-)(1 - \hat{n}_2) + \beta(\hat{n}_{N-1} - \hat{s}_{N-1}^+) \qquad (3.70)$$

would describe as well the system. The rate equation in the bulk would read therefore:

$$\frac{\mathrm{d}n_i}{\mathrm{d}t} = n_{i-1}(1 - n_{i+1}) - n_i(1 - n_{i+2}) + \omega_A(1 - n_{i-1})(1 - n_{i+1}) - \omega_D n_i. \qquad (3.71)$$

In this case the current density relation would be the same found for the simple TASEP and then $\rho^* = 1/2$; the on-off kinetics, on the other side, would predict the isotherm $\frac{1+2K-\sqrt{1+4K}}{2K}$ which, compare to the exact value and MC simulation, is clearly wrong.

In conclusion, we deduce that the trivial mean field neglects the properties of dimeric particle and fail miserably in any attempt to recover a rate equation from the quantum Hamiltonian.

Appendix 3.E Localization of the shock

The domain wall (DW) localization is the most striking effect of the on-off kinetics on the simple TASEP model. In this appendix we study the dynamics of the simulating a second class particle dynamics and comparing it to analytical calculations in harmonic approximation.

The second class particle is essentially a "ghost" particle, in the sense that its dynamics does not influence but is influenced by the dynamics of the others particles. It hops forward whenever a free site is available and hops back whenever a particle occupies its position. It is statistically the best method to track exactly the position of the domain wall. The "amplitude" of the shock can be defined as the width of the distribution of the second class particle.

The DW dynamics is understood as the motion of a Brownian walker in a harmonic potential. Let p_i be the probability for the DW to be at site i and $w_r(i)$ and $w_l(i)$ the jump rate to the right and to the left. The DW is in the stationary state when

$$w_r(i)p_i = w_l(i+1)p_{i+1} \tag{3.72}$$

This equation can be solved in the continuum limit $y(x) \equiv w_l(x)p(x)$. With this ansatz

$$y'(x) = Ny\left(\frac{w_r(x)}{w_l(x)} - 1\right) + O(1/N^2) \tag{3.73}$$

Therefore the probability is:

$$p(x) = \frac{y(x)}{w_l(x)} \propto \frac{1}{w_l(x)} \int_{x_0}^{x} \left(1 - \frac{w_r(\xi)}{w_l(\xi)}\right) d\xi = \frac{1}{w_l(x)} \exp(-F(x)) \tag{3.74}$$

where F can be replaced, in saddle point approximation around the shock position ($F'(x_s) = 0$), by $F \sim \frac{1}{2}F''(x - x_s)$ and therefore:

$$p(x) \propto \exp\left[-C(x - x_s)^2\right] \tag{3.75}$$

where the amplitude of the DW distribution has been computed from

$$C = \frac{1}{2\sigma^2} = \frac{1}{2}F'' = \frac{N(w_l - w_r)'(x_s)}{2w_r(x_s)} \tag{3.76}$$

The computation of the hopping rates must take into account the fluctuation of particles in the bulk due to LK. We assume that the hopping of the DW happens on a time scale long enough for the system to "rearrange" after a particle leaves or enters the system. With these hypothesis the rates by which the number of particle changes are

$$w_{in} = \alpha(1-\alpha) + \frac{\Omega}{N}\sum_{i=1}^{N}(1 - \rho_i) \tag{3.77}$$

$$w_{out} = \beta(1-\beta) + \frac{\Omega}{N}\sum_{i=1}^{N}\rho_i \tag{3.78}$$

Unfortunately, contrary to the monomer case [83, 69, 62], we cannot perform analytically the sums, and we integrated the functions numerically, comparing the results with the simulations to test the validity of the MF in such a description. In Fig.3.11 the MC data for the width $\sigma(\Omega_D)$ are compared to the numerical ones: discrepancies are due to the harmonic approximation and to the numerical difficulties in measuring the statistical properties of the second class particle. The qualitative picture does not change (also in the case $K = K^*$) compared to the monomer case. Note that the function $\sigma(\Omega_D)$ of the dimers approaches the monomers one for large values of Ω_D. Moreover theory and experiments agree on the fact that the shock localizes (i.e. σ decreases) while increasing Ω_D.
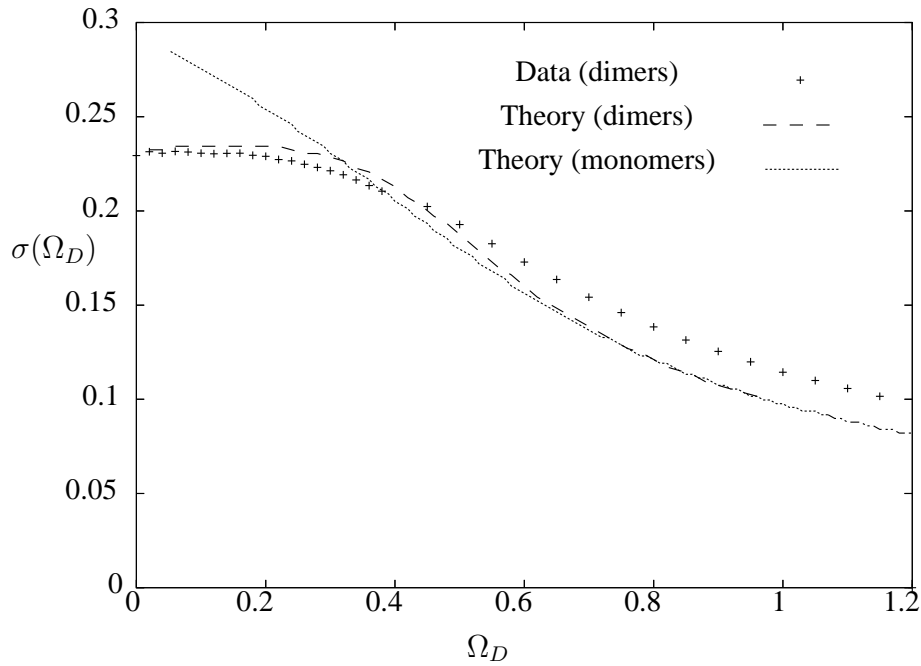
PSfrag replacements

Figure 3.11: Width of the DW vs Ω_D. The graphs shows a comparison between data measured from second class particle (crosses), dimers DW theory (dashed) and monomers DW theory (dotted). A decreasing of the width is visible as Ω_D increases. Parameters: $\alpha = \beta = 0.1$, $K = 2$ and $N = 512$.

Chapter 4

Effect of local inhomogeneities

> Imperfection, rather than perfection,
> in the execution of our assigned or
> elected tasks is more in keeping with
> human nature.
>
> R. Levi Montalcini
> *In praise of imperfection*

Motivated by the presence of structural imperfections of the microtubules that acts as road blocks, we study the influence of an isolated defect on the non-equilibrium steady state of the totally asymmetric exclusion process coupled to Langmuir kinetics (TASEP/LK). We model the defect as a site with a reduced hopping rate. Upon combining mean-field studies with MC simulations we explore the phase behavior in the full parameter range and find the following results. The phase diagram results qualitatively modified as compared to the defect free case, showing new phase coexistence regions. We find it convenient to introduce the concept of a *carrying capacity* as the maximal current that can flow through a given site. This space-dependent quantity is found to depend on the defect parameters, i.e. its position and strength and to essentially determined the phase diagram. For low defect strength its presence is irrelevant for the density and current profile, and the behavior without defect is recovered. Above a certain threshold strength, the density profile shows the influence of the defect on the scale of the system size. The regions where the defect is relevant (called *bottleneck phases*) are identified and studied.

This chapter is organized as follows: in the next section we give a short review of the literature and the motivations for our work. The basic model is introduced in the Section 4.2, together with the general set-up and the effective theory on which we build our analysis. Section 4.3 is devoted to the discussion of our results (phase-diagrams and density profiles). We present our conclusions in Section 4.4.[1]

---

[1]This chapter is almost entirely covered by reference [116].

4.1   Introduction

The idealized systems we have used so far to model the motion of motors along micro-
tubules, does not account for the presence of imperfections or of microtubule associated
proteins on the track. Such defects may slow down the motion of the motor and may reduce
its affinity with the track (and hence its processivity) [37, 99]. It is therefore important
to investigate how robust the picture found so far is upon considering these imperfections.
Here we will concentrate therefore on an isolated defect where the motor motion is slowed
down.

The effect of disorder on the phase behavior has been investigated in a multitude of
equilibrium statistical mechanics [139]. There is by now a good understanding of the
ensuing equilibrium phenomena. In contrast, in non-equilibrium statistical mechanics,
the effect of disorder on dynamics and non-equilibrium steady state is far from being
well understood [140]. Hence exploring the effects of disorder in simple one-dimensional
stochastic many-body models is a worthwhile endeavor.

Being the TASEP one of the simplest one-dimensional non-equilibrium systems, much
effort has been devoted during the last years to the study of its disordered versions (for a
recent review on disorder in non-equilibrium models, see e.g. [140]). There are two natural
ways of including disorder in driven lattice gases: the hopping rates may depend on the
particle attempting to jump (*particle-wise*) or each lattice site may be associated with a
random, quenched, hopping rate (*site-wise*). A third case, where one or various defects are
localized on the lattice (*point-wise*), can be thought as a preliminary study for the site-wise
disorder. In particular, variants of the TASEP with point-wise disorder has been studied in
Refs. [68, 80, 58, 103, 18]. Particle-wise disorder has been considered in Refs. [23, 86, 85])
while site-wise disorder has been investigated in Refs. [149, 82, 43, 60, 39, 42, 70]. As
the TASEP was originally introduced in a biophysical context, it was also recently argued
that studying the TASEP in the presence of clusters of localized bottlenecks is of direct
biological relevance [18].

The lattice-gas model that we consider in this chapter is a nontrivial variant of the
TASEP where the usual dynamics is supplemented with Langmuir kinetics (TASEP/LK).
This model has been presented in Ch. (2). See also Refs. [111, 112, 62]. Here, we consider
what is, arguably, the simplest disordered version of the TASEP/LK model: we assume the
latter to be "perturbed" by the presence of a localized defect, or bottleneck, on the lattice.
As we shall show, already this simple situation, leads to interesting new features which,
remarkably, can be both qualitatively and quantitatively understood within an effective
mean-field theory. Moreover, this work can be considered as a contribution toward the
understanding of the TASEP/LK perturbed by clusters of bottlenecks, which has been
argued to be of biological relevance [109].

4.2 The model and the general set-up

In this section we present the model under investigation. We review the main results of the TASEP with on-off kinetics in the parameter range we are interested in and we give the general set-up used in the following to compute the density profile.

4.2.1 The model

We consider a system of identical particles moving uni-directionally along a finite one-dimensional lattice (with open boundaries) of length L coupled to a reservoir. A localized *bottleneck* (i.e. a defect) is present at site k (with $1 \ll k \ll N$). The N lattice sites are labeled $i = 1, \ldots, N$, so that the lattice spacing is $a = L/N$. The continuum limit will be considered by letting the lattice space vanish when $N \to \infty$ (with $a \xrightarrow[N \to \infty]{} 0$). The reservoir, allowing the attachment/detachment of particles, accounts for a Langmuir kinetics Refs. [111, 112]. A crucial feature of this (and other TASEP-like) model(s) is the excluded volume interaction: double occupancy of any lattice site is prohibited (site exclusion). The (sequential) dynamics of the model under consideration here obeys the following microscopic rules, which are illustrated in Fig. 4.1:

   i. As in the TASEP, if one particle occupies a site $i = 1, \ldots, N - 1$, $i \neq k$, different from the defect, it may hop with unit rate onto the site $i + 1$, provided the latter is empty.

   ii. The motion of each incoming particle at site k (defect) is *slowed down*: the jump to the neighboring empty right site $k + 1$ occurs with rate q (0 < q < 1).

   iii. If one particle occupies a site $i = 2, \ldots, N - 1$, it can detach from the bulk with a rate ω_D

   iv. A particle can attach on an empty site $i = 2, \ldots, N - 1$ with rate ω_A.

   v. At site $i = 1$, a particle enters the lattice with rate α, provided that this first site is empty.

   vi. At $i = N$, a particle leaves the system with rate β.

Alone, the above rules i, v and vi define the TASEP model, while, when they are supplemented with iii and iv, one recovers the TASEP/LK system. Here, the effect of the disorder appears through the rule ii.

In this work we consider the defect as a bottleneck, locally slowing down the stochastic motion of the particles. In this sense, only the case $0 < q < 1$ shall be considered. When $q > 1$, the kinetics of the particles is locally enhanced by the defect and, with respect to the defect free TASEP/LK model, one expects only a variation of the dynamics but not of the static properties. In particular, the phase-diagram for $q > 1$ is the same as in Refs. [111, 112].

For the same reasons as in Refs. [111, 112] (see also Ch. 2, Ch. 3 and Refs. [118, 62]), we shall consider that the attachment and detachment rates scale as

$$\omega_D = \frac{\Omega_D}{N}; \quad \omega_A = \frac{\Omega_A}{N}; \tag{4.1}$$
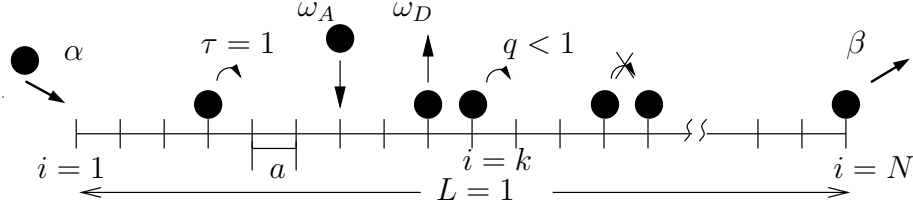

Figure 4.1: Schematic representation of the TASEP with on-off kinetics in the presence of a bottleneck at the site $i = k$. The allowed moves are: forward jump (with rate $q \neq 1$ in $i = k$ and $\tau = 1$ elsewhere), entrance at the left boundary (with rate α) and exit at the right boundary (with rate β), attachment (with rate ω_A), and detachment (with rate ω_D) in the bulk.

To study the phase diagram of TASEP-like systems, one studies the (stationary) local density of particles at site i (acting as "order parameter" in equilibrium models) $\rho_i = \lim_{t\to\infty}\langle \hat{n}_i(t)\rangle$. Here $\hat{n}_i$ denotes the local occupation number operator, with $\hat{n}_i = 1$ ($\hat{n}_i = 0$) when the site i is occupied (empty), and the brackets stands for the average over all the histories. Another crucial quantity for the study of phase transitions in TASEP-like models is the current of particles flowing through the site i. In this steady state, this quantity is $j_i = \lim_{t\to\infty} D_i\langle \hat{n}_i(t)(1 - \hat{n}_i(t))\rangle$, where D_i is the local hopping rate [see Eq.(4.5)].

Following the same steps as in Refs. [111, 112](see also [62] for a recent review) the stationary density is shown to obey:

$$\begin{aligned}
0 &= D_{i-1}\langle \hat{n}_{i-1}(1 - \hat{n}_i)\rangle - D_i\langle \hat{n}_i(1 - \hat{n}_{i+1})\rangle \\
&+ \omega_A\langle 1 - \hat{n}_i\rangle - \omega_D\langle \hat{n}_i\rangle, \quad i = 2,\ldots,N; \tag{4.2} \\
0 &= \alpha\langle 1 - \hat{n}_1\rangle - \langle \hat{n}_1(1 - \hat{n}_2)\rangle; \tag{4.3} \\
0 &= \langle \hat{n}_{N-1}(1 - \hat{n}_N)\rangle - \beta\langle \hat{n}_N\rangle, \tag{4.4}
\end{aligned}$$

where, to account for the defect at site $i = k$, we have:

$$D_i = \begin{cases} 1 & \text{if } i \neq k\,, \\ 0 < q < 1 & \text{if } i = k\,. \end{cases} \tag{4.5}$$

Similarly, one can obtain straightforwardly the equations for the current of the particles. One immediately notices from Eqs. (4.2)-(4.4) that we have to deal with an infinite hierarchy of (coupled) equations (for the density $\langle \hat{n}_i\rangle$ being connected to the two-point correlations $\langle \hat{n}_i\hat{n}_{i\pm1}\rangle$, which then depends on the three-point correlators ...). Obviously,

the same property also holds for the current, which is connected to three-point correlation functions.

Before discussing how to deal with this serious technical difficulty and as a motivation for our analytic approach, let us briefly review the main properties of the TASEP with Langmuir on-off kinetics - hereafter, referred to as TASEP/LK and introduced in Ch. 2.

4.2.2 The TASEP with Langmuir on-off kinetics

The above system, in the absence of defect (i.e. with $q = 1$) reduces to the TASEP/LK model presented in Ch. 2 (see Refs. [111, 112, 62]). Interestingly, the TASEP/LK is characterized by the subtle competition between a simple model of equilibrium (Langmuir kinetics) and the "Ising model" of non-equilibrium statistical mechanics (TASEP). In the presence of attachment/detachment processes, we can no longer rely on the former exact methods [26, 30, 28, 29, 131]. However, building on the experience gained from studying the TASEP, one may expect that a mean-field treatment should also provide an accurate description of this model (the same current-density relationship as in the TASEP holds for the TASEP/LK, as predicted by a MF approach [111, 112]). Considering Eqs. (4.2)-(4.4) with $D_i = 1$, the mean-field analysis simply consists in neglecting any spatial correlations resulting in the following *approximation*:

$$
\begin{align}
\langle \hat{n}_i \hat{n}_{i+1} \rangle &\approx \langle \hat{n}_i \rangle \langle \hat{n}_{i+1} \rangle = \rho_i \rho_{i+1} \,; \tag{4.6} \\
j_i &\approx \langle \hat{n}_i \rangle (1 - \langle \hat{n}_{i+1} \rangle) = \rho_i (1 - \rho_{i+1}) \,. \tag{4.7}
\end{align}
$$

One can assume that the attachment/detachment rates should scale as $\omega_A \sim \omega_D \sim N^{-\theta}$. When $\theta < 1$ the dynamics will be trivially dominated by the Langmuir kinetics, while, as argued in Ref. [69] when $\theta > 1$ one recovers the TASEP behavior. Actually, the only biologically interesting behavior (and the one when analytical results are known), displaying a real interplay and competition between the processes, emerges in the limit where the Langmuir rates scale as in Eqs. (4.1), with $\theta = 1$. Taking the continuum limit with the new spatial variable $0 \leq x = i/N \leq 1$ and Eqs. (4.1), the stationary density $\rho_i \to \rho(x)$ and the current $j_i \to j(x)$ of the TASEP/LK obey, at MF level, the following equations

$$
\begin{align}
(2\rho - 1)\partial_x \rho &- \Omega_D \rho + \Omega_A (1 - \rho) = 0 \,; \tag{4.8} \\
\rho(0) &= \alpha; \quad \rho(1) = 1 - \beta \,; \tag{4.9} \\
j(x) &= \rho(1 - \rho) \,. \tag{4.10}
\end{align}
$$

For further purpose, we introduce the binding constant $K \equiv \Omega_A / \Omega_D$ and discuss the solution of (4.8,4.9) for $\Omega_A = \Omega_D = \Omega$. In this situation, the bulk equation (4.8) admits two possible solutions: either $\rho(x) = 1/2$ (which in this case $K = 1$ correspond to the Langmuir isotherm ρ_I) or a linear profile. Taking into account the boundary conditions (4.9), the solution for the density consists of three pieces which have to be matched properly:

$$
\rho(x) = \begin{cases} \Omega x + \alpha = \rho_\alpha & \text{, left} \\ 1/2 = \rho^* = \rho_I & \text{, middle} \\ 1 - \beta + \Omega(x - 1) = \rho_\beta & \text{, right} \end{cases} \tag{4.11}
$$

As the density in the bulk is non-uniform but linear in the space variable (and piece-wise), also the current $j(x) = \rho(x)[1-\rho(x)]$ displays a spatial dependence. Depending on how the three branches $\rho_{\alpha,I,\beta}$ are matched, various phases and scenarios have to be distinguished. In particular, for $K = 1$ seven phases were identified [111, 112]: in addition to the TASEP phases (LD, HD and MC), four new phases corresponding to the coexistence of low density and maximal current (LD-MC), high density and maximal current (MC-HD), low and high-density (LD-HD) and low-density, high-density with maximal current (LD-MC-HD) emerge from the competition among the TASEP dynamics and the Langmuir kinetics. In the phase LD-HD, there is a discontinuity of the density and only the branches $\rho_{\alpha,\beta}(x)$ are physically available: the low and high density solutions are thus separated by a *domain wall* (*localized* shock).

The case $K \neq 1$ which follows the same lines, but is mathematically more involved, is discussed in detail in Ref. [112]. Let us note that when $K \neq 1$, j^* will be replaced by $j_K^*(x)$, which is now space dependent.

4.2.3 General set-up

After having introduced the TASEP/LK model in the presence of a defect and having reviewed the main properties of the TASEP/LK, we are fully equipped to outline the general ideas devised to study the disordered TASEP/LK system under consideration.

Instead of trying to directly solve the MF version of the equations (4.2-4.5) for the density, as for the TASEP perturbed by the presence of a localized defect [68, 80], we build an *effective* MF theory.

This is obtained by splitting the system at the site k, coinciding with the defect, into two subsystems, called I and II (resp. left and right subsystems), and by identifying the situations where the bottleneck is actually *relevant* (in the sense explained below).

As illustrated in Fig. 4.2 the defect at site k is assumed to be sufficiently far from both boundaries so that we could consider the continuum limit on both subsystems (i.e. $0 < x_d \equiv k/N < 1, \quad N \to \infty$).

The first subsystem, I, is of length kL/N (sites $i = 1, \dots k$ of the original discrete lattice), with particles entering (exiting) the subsystem at the boundary $i = 1$ ($i = k$) with rate α (β_{eff}); while on the second subsystem, II, of length $(1-k/N)L$, particles enter (leave) the system with rate α_{eff} (β) at $i = k+1$ ($i = N$). Except at the sites k and $k+1$, playing the role of "effective boundaries", the motion on both subsystems proceeds according to the TASEP/LK dynamics [111, 112]. To account for the coupling between the subsystems, one considers the current of particles flowing from the site k to $k+1$ and realizes that for the TASEP/LK-like systems *the current is locally conserved along the whole system* (when $N \to \infty$, it is a continuous function; see below). This follows from the definition of the current and Eq.(4.2):

$$j_{i+1} - j_i = \frac{1}{N} \left[\Omega_A - (\Omega_A + \Omega_D)\rho_{i+1} \right] \xrightarrow[N\to\infty]{} 0 \, ; \tag{4.12}$$

this relation formally states that locally the attachment and detachment are irrelevant
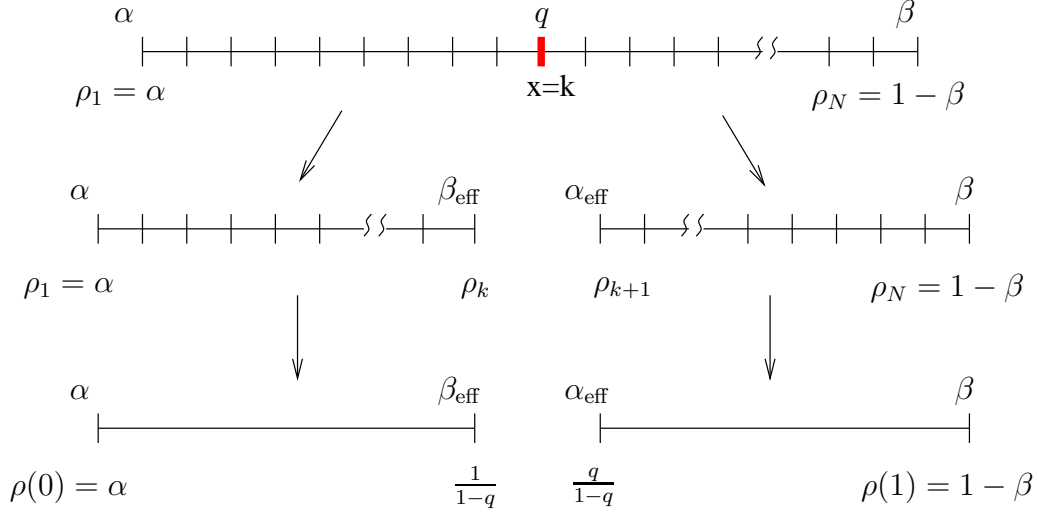
Figure 4.2: Schematic representation of the division in two sub-lattices that allows to apply mean field theory developed earlier to the system with a bottleneck.

(since $\omega_{A,D} = \Omega_{A,D}/N$). In particular, in the vicinity of the defect one has $j_k = j_{k+1}$.

It is necessary to compute the current flowing through the defect. Since locally the current is conserved we resort to the calculations already done for the TASEP with an isolated inhomogeneity and we present them in a form more convenient for our purposes.

At the defect the particle flow is slowed down by a factor q i.e. rescaled by the strength of the defect:

$$j_k = q\rho_k(1 - \rho_{k+1}). \tag{4.13}$$

The fact that the current is conserved in the subsystem I (at the left of the defect) tells us that

$$\rho_{k-1}(1 - \rho_k) = q\rho_k(1 - \rho_{k+1}). \tag{4.14}$$

Assuming the current in subsystem I to be determined by the defect (i.e. assuming the defect to be *relevant*) the density is locally constant $\rho_{k-1} = \rho_k$ which, together with Eq. 4.14 yields to a relation between ρ_k and ρ_{k+1}:

$$1 - \rho_k = q(1 - \rho_{k+1}). \tag{4.15}$$

Similarly on subsystem II the current is conserved:

$$\rho_{k+1}(1 - \rho_{k+2}) = q\rho_k(1 - \rho_{k+1}). \tag{4.16}$$

Again, when the defect is relevant the density in subsystem II is determined by the left effective boundary condition and therefore $\rho_{k+1} = \rho_{k+2}$; this, together with Eq. 4.16 gives:

$$\rho_{k+1} = q\rho_k \, . \tag{4.17}$$

Equations (4.15) and (4.17) define together the value of the density before and after the defect:

$$\rho_k = \frac{1}{1+q} \quad \text{and} \quad \rho_{k+1} = \frac{q}{1+q} \, . \tag{4.18}$$

When the defect is relevant (i.e. when these computations are valid) there is a difference between the densities at its left and right:

$$r \equiv \rho_k - \rho_{k+1} = \frac{1-q}{1+q} \, , \tag{4.19}$$

which clearly reduces to zero when $q = 1$ and the defect turns into a normal site. The quantity r is always positive since, when the defect imposes its current, $\rho_k > \rho_{k+1}$, i.e. locally the density present a discontinuous transition from a high density to a low density profile HD-LD.

Clearly the effective boundary conditions can be related as in simple TASEP/LK to the density as $\rho_{k+1} = \alpha_{\text{eff}}$ and $\rho_k = 1 - \beta_{\text{eff}}$, which gives:

$$\alpha_{\text{eff}} = \beta_{\text{eff}} = \frac{q}{1+q} \, . \tag{4.20}$$

As a consequence of the definition we used, the current *at the defect* reads:

$$j_k = j_{k+1} = \frac{q}{(1+q)^2} \leq j^* = \frac{1}{4} \, , \tag{4.21}$$

which is a concave, increasing function of q that reaches the maximum only when $q = 1$ and there is no longer defect.

These conditions are valid when the defect imposes its current: we will call *relevant* the defect in this situation. If the flux of particles is too low or too high and the defect not strong enough the currents in the two subsystems are defect independent, the effective rates are unimportant and the bottleneck will be said to be *irrelevant*.

As for the TASEP model, the properties of the current will prove to be insightful for understanding the relevance of the defect [80, 136]. Here, like in the TASEP/LK model, the flow of particle displays a spatial dependence. We will call $j_d(x)$ *the current imposed by the defect*; in the vicinity of the defect and the boundaries, the current locally reads $j_d(x_d)$, $j_\alpha(0)$ and $j_\beta(1)$, while, as for the TASEP, the maximal current which can be carried through the bulk (far from the bottleneck) is $j^* = \frac{1}{4}$, which is fixed by exclusion.

Carrying capacity To understand how to connect the currents j_d, j_α, j_β and j^*, we now introduce the concept of the *carrying capacity* of the system, denoted by $\mathcal{C}(x)$. It is defined as the locally (i.e. space-dependent) maximal current that can flow through a site in the bulk of the system (I $\bigcup$ II). In the simple TASEP the carrying capacity is the (constant) maximal current $j^* = 1/4$ and is solely determined by exclusion. In the pure TASEP/LK the carrying capacity is again j^* when $K = 1$ while it becomes a particular space dependent current profile when $K \neq 1$ dependent on the attachment and detachment rates[2]. In the TASEP/LK with one defect $\mathcal{C}(x)$ is a continuous space-dependent function. It is obtained by matching the usual maximal current j^* and the defect imposed current $j_d(x)$: the maximal current in a neighborhood of the defect is given by $j_d(x)$, but if such current reaches the critical value $j^* = 1/4$ in the bulk, then the maximal current remains $1/4$. In the region where the carrying capacity is $1/4$ the defect has no influence and the maximal current is determined by exclusion. Actually if $j_d(x)$ matches j^* the sub-system I behaves as in an a MC-HD phase of the TASEP/LK (or LD-MC in sub-system II). Hence we identify four cases.

If j_d does never reach the value $j^* = \frac{1}{4}$, the carrying capacity of the system is solely determined by the defect:

$$\mathcal{C}(x) = \mathcal{C}_1(x) = j_d(x) \tag{4.22}$$

[as illustrated in Fig. 4.3(a)]. On the other hand, if $j_d = j^*$ for some values $0 < x_2^I < x_d$ and $x_d < x_2^{II} < 1$, the carrying capacity has, close to the boundaries, a flat profile: it coincides with j_d near the defect and then reaches a constant value $\mathcal{C}(x) = \mathcal{C}_2(x) = \frac{1}{4}$ [see Fig. 4.3(b)], thus

$$\mathcal{C}(x) = \mathcal{C}_2(x) = \begin{cases} j_d(x) & , x_2^I < x < x_2^{II} \\ j^* & , \text{else} \end{cases} . \tag{4.23}$$

The concept of a carrying capacity helps to address the issues of the relevance of the defect: in fact if the defect is *irrelevant* the boundaries impose currents such that $j_{\alpha,\beta}(x) < \mathcal{C}(x)$ and the density profile is the same as in the defect free TASEP/LK system. This case corresponds to the situation where the density is sufficiently low (high) and the particles are well separated (or very close to each other): there, we can expect only a local perturbation due to the presence of a bottleneck, traffic effects are the real rate limiting process. When the defect is *relevant* we have to construct the density profile by considering the subsystems I and II coupled via the effective rates α_{eff} and β_{eff} and by identifying, as described in the next section, among the various scenarios emerging from the interplay between the boundary conditions and the defect parameters. One can also mention that, when the defect is closer to one of the boundaries, say the left one, it may happen that only the right

---

[2]Calling $\rho_\beta(x)$ the solution of the density profile for the right boundary, the maximal current that the system can transport reads $\rho_{\beta^*(x)}(1 - \rho_{\beta^*(x)})$ for $K \neq 1$, i.e. the solution for the right boundary when $\beta = \beta^* = 1/2$ (see [112]).

branch of j_d reaches the value $\frac{1}{4}$. In this case [see Fig. 4.3(c)]

$$\mathcal{C}(x) = \mathcal{C}_3(x) = \begin{cases} j_d(x) & , 0 < x < x_2^{II} \\ j^* & , x_2 \leq x < 1 \end{cases}. \tag{4.24}$$

A symmetric reasoning also holds for the right boundary, in which case [see Fig. 4.3(d)]:

$$\mathcal{C}(x) = \mathcal{C}_4(x) = \begin{cases} j^* & , 0 < x < x_2^{I} \\ j_d(x) & , x_2^{I} \leq x < 1 \end{cases} \tag{4.25}$$

When the defect is relevant, we are left with two effective TASEP-LK systems coupled to each other via the effective rates α_{eff} and β_{eff}. These two subsystems shall be studied, following the same lines as for the original TASEP/LK model, by taking the continuum limit $N \to \infty, 0 \leq x = i/N \leq 1$ and introducing $x_d \equiv k/N$ to locate the position of the defect. Thus, in the continuum limit, the right (resp. left) subsystem has a length x_d (resp. $1 - x_d$). The expressions (4.20) for the left and right currents are the same:

$$\lim_{x \downarrow x_d} j_d(x) = \lim_{x \uparrow x_d} j(x) = j(x_d), \tag{4.26}$$

and in the continuum limit

$$j_d(x_d) = q \left[\lim_{x \downarrow x_d} \rho(x) \right] \left[1 - \lim_{x \uparrow x_d} \rho(x) \right] = \frac{q}{(1+q)^2}. \tag{4.27}$$

The density in a neighborhood of the defect is discontinuous and can therefore been written as

$$\lim_{x \downarrow x_d} \rho(x) = \frac{1}{1+q} \qquad \text{and} \qquad \lim_{x \uparrow x_d} \rho(x) = \frac{q}{1+q}. \tag{4.28}$$

A useful property of the TASEP and TASEP/LK models which also holds in the presence of a defect is the particle-hole symmetry [80, 112]: injecting particles to the left boundary can be viewed as a vacancy leaving the lattice. Similarly, a jump of a particle to the right can be interpreted as a hole moving to the left. Also, attachment/detachment of particles in the bulk can be mapped onto the detachment/attachment of vacancies. As a consequence, (expressing all the parameter dependences as subscripts) one has [80, 112]:

$$\rho_{\alpha,\beta,\Omega_A,\Omega_D,q}(x) = 1 - \rho_{\beta,\alpha,\Omega_D,\Omega_A,q}(1-x). \tag{4.29}$$

As the same current-density holds for the TASEP and the TASEP/LK models, the expressions (4.20) are actually the same as those for the simple TASEP [80]. However, because of the subtle interplay between the bulk dynamics and the boundaries (resulting in spatial-dependent current and density), we show hereafter that a single bottleneck drastically affects the phase diagram of the TASEP/LK model and new phases, called *bottleneck-induced*, will appear (when the defect is relevant).
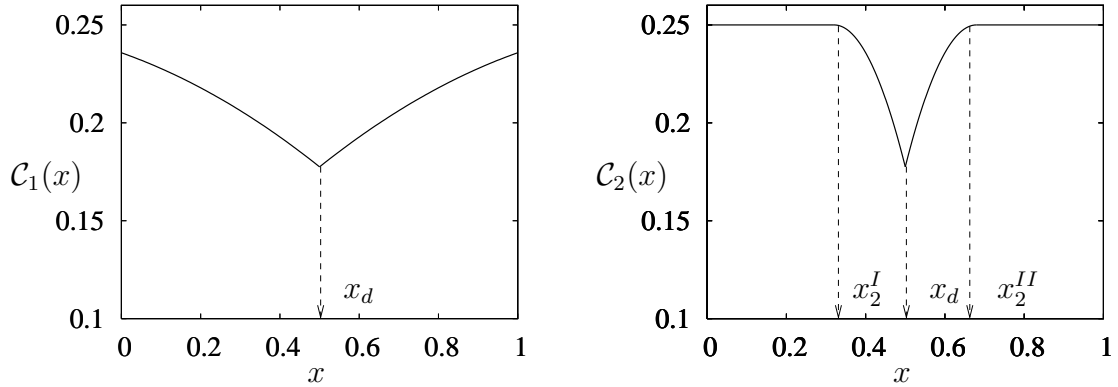
(a) Carrying capacity $\mathcal{C}_1(x)$: the current j_d imposed by the defect is always smaller than $j^* = \frac{1}{4}$.

(b) Carrying capacity $\mathcal{C}_2(x)$: $\mathcal{C}(x)$ reaches a plateau at value $j^* = \frac{1}{4}$ when $j_d(x_2^{I,II}) = j^*$ for $0 < x_2^I < x_d < x_2^{II} < 1$.
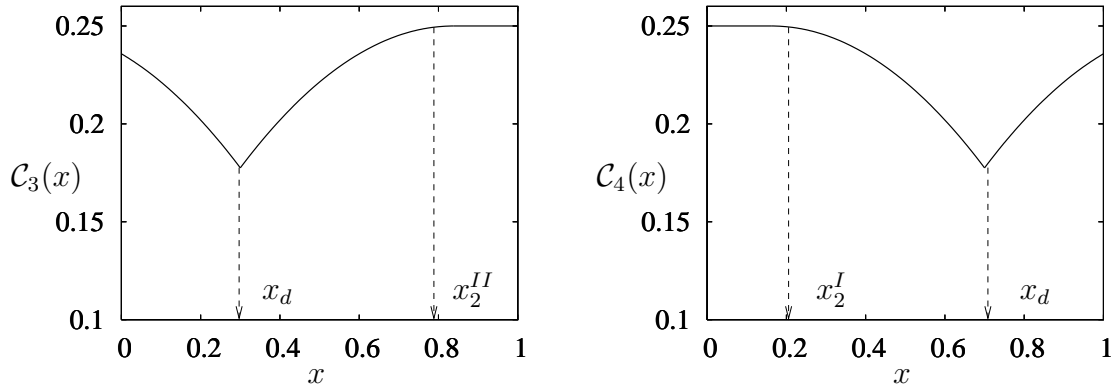
(c) Carrying capacity $\mathcal{C}_3(x)$: $\mathcal{C}(x)$ reaches a plateau at value $j^* = \frac{1}{4}$ when $j_d(x_2^{II}) = j^*$ for $x_d < x_2^{II} < 1$.

(d) Carrying capacity $\mathcal{C}_4(x)$: $\mathcal{C}(x)$ reaches a plateau at value $j^* = \frac{1}{4}$ when $j_d(x_2^I) = j^*$ for $0 < x_2^I < x_d$.

Figure 4.3: The four typical carrying capacity profiles $\mathcal{C}(x)$ displayed by the system (parameters $K = 1$,). Depending on the strength q, on the position x_d of the defect and on the detachment rate Ω_D, the carrying capacity combines in four different ways with the maximal current; each of these profile induces topologically distinct phase diagram.

4.3 Phase-diagram

We are now in position to discuss the phase-diagram of the TASEP/LK model in the presence of a bottleneck of strength $q < 1$ (localized at x_d).

In particular, we shall show that a single defect can perturb the density profile of the TASEP/LK system on a macroscopic scale, being responsible for the emergence of new features: the *bottleneck (sub-)phases* (BP). As discussed in detail below, when the defect is relevant, the BP act either as effective high-density (low-density) coexistence phases on the subsystem I (II) or as an effective maximal current phase, when the defect imposes

the current j_d to the whole system. It is worthwhile mentioning that these new BP have no analogous in the TASEP (or $\ell-$TASEP) model(s) in the presence of a bottleneck: for these systems, it was shown that a defect does not generate new phases: except for the shift of some transition lines, the topology of the phase-diagrams remains the same as for the defect free models [80, 136].

Hereafter, we first discuss in detail the case where $K = 1$, which is mathematically more amenable, and then report, along the same lines, the results for the case $K \neq 1$.

4.3.1   Results and phase-diagrams for the case $K = 1$

In this subsection we solve the equations for the density and the phase diagram. First we give the analytical solution of density profile and than we discuss in detail the phase diagram for two cases of the carrying capacity.

Mathematical preliminaries

In the presence of the defect, within the effective mean-field picture outlined above, one naturally expects the density of the system to be piece-wise and reads

$$\rho(x) = \begin{cases} \rho^I(x), & 0 < x \leq x_d \\ \rho^{II}(x), & x_d < x \leq 1 \end{cases}, \tag{4.30}$$

where $\rho^{I,II}(x)$ are respectively the densities on the subsystems I and II. In the case where attachment and detachment rates are equal, i.e. $\Omega_A = \Omega_D = \Omega$, as in the TASEP/LK model with $K = 1$, these quantities obey the following equation

$$[\partial_x \rho^{I,II} \quad - \quad \Omega](2\rho^{I,II} - 1) = 0, \tag{4.31}$$

supplemented with -both, original (α, β) and effective $(\alpha_{\text{eff}}, \beta_{\text{eff}})$- boundary conditions:

$$\rho^I(0) = \alpha; \quad \rho^I(x_d) = 1 - \beta_{\text{eff}} = \frac{1}{1+q}$$
$$\rho^{II}(1) = 1 - \beta; \quad \rho^{II}(x_d) = \alpha_{\text{eff}} = \frac{q}{1+q}. \tag{4.32}$$

As in the defect free TASEP/LK [111, 112], the possible solutions of these equations on the subsystem I read

$$\rho^I(x) = \begin{cases} \Omega x + \alpha \equiv \rho_\alpha & \text{, left of I} \\ 1/2 \equiv \rho^* & \text{, middle of I} \\ \Omega(x - x_d) + \frac{1}{1+q} \equiv \rho_{\beta_{\text{eff}}} & \text{, right of I,} \end{cases} \tag{4.33}$$

while on the subsystem II, the admissible solutions read

$$\rho^{II}(x) = \begin{cases} \Omega(x - x_d) + \frac{q}{q+1} \equiv \rho_{\alpha_{\text{eff}}} & \text{, left of II} \\ 1/2 = \rho^* & \text{, middle of II} \\ \Omega(x - 1) + 1 - \beta \equiv \rho_\beta & \text{, right of II} \end{cases}. \tag{4.34}$$

To be able to discuss the relevance of the bottleneck and how the six linear pieces of solutions (4.33,4.34) are connected, we need to know the carrying capacity of the system and thus compute the current induced by the defect:

$$j_d = \begin{cases} \rho_{\beta_{\text{eff}}}(1 - \rho_{\beta_{\text{eff}}}), 0 < x \le x_d \\ \rho_{\alpha_{\text{eff}}}(1 - \rho_{\alpha_{\text{eff}}}), x_d \le x < 1 \end{cases} \tag{4.35}$$

and those arising from the left and right boundaries, namely $j_\alpha = \rho_\alpha(1 - \rho_\alpha)$ and $j_\beta = \rho_\beta(1 - \rho_\beta)$. With help of (4.33,4.34), one finds:

$$\begin{align} j_d &= \left(\Omega|x - x_d| + \frac{q}{1+q} \right) \left(\frac{1}{1+q} - \Omega|x_d - x| \right) \tag{4.36} \\ j_\beta &= [\beta + \Omega(1 - x)] [1 - \beta - \Omega(1 - x)] \tag{4.37} \\ j_\alpha &= (\alpha + \Omega x)(1 - \alpha - \Omega x) \tag{4.38} \end{align}$$

Important issues to determine the density profile, in the presence of a relevant defect, are to understand if/when the possible solutions ρ^I and ρ^{II} reach the value $1/2$, corresponding to the maximal current $j^* = 1/4$, and when, on the subsystem I (II), ρ_α and $\rho_{\beta_{\text{eff}}}$ ($\rho_{\alpha_{\text{eff}}}$ and ρ_β) cannot be matched continuously allowing for the presence of a domain wall at position x_w^I (x_w^{II}). These points are addressed by matching the densities and solving the four equations

$$\rho_\alpha(x_1^I) = \rho_{\beta_{\text{eff}}}(x_2^I) = \rho_{\alpha_{\text{eff}}}(x_2^{II}) = \rho_\beta(x_1^{II}) = \rho^* \tag{4.39}$$

to get $x_{1,2}^I$ and $x_{1,2}^{II}$, and

$$\begin{align} 1 - \rho_\alpha^I(x_w^I) &= \rho_{\beta_{\text{eff}}}^I(x_w^I) \tag{4.40} \\ 1 - \rho_{\alpha_{\text{eff}}}^{II}(x_w^{II}) &= \rho_\beta^{II}(x_w^{II}), \tag{4.41} \end{align}$$

to get the two domain walls positions. One thus finds:

$$\begin{align} x_1^I &= \frac{1 - 2\alpha}{\Omega} \tag{4.42} \\ x_2^I &= x_d - \frac{r}{2\Omega} \tag{4.43} \\ x_2^{II} &= x_d + \frac{r}{2\Omega} \tag{4.44} \\ x_1^{II} &= 1 - \frac{1 - 2\beta}{\Omega} \tag{4.45} \\ x_w^I &= \frac{1}{2} \left(x_d + \frac{1}{\Omega} \left\{ \frac{q}{1+q} - \alpha \right\} \right) \tag{4.46} \\ x_w^{II} &= \frac{1}{2} \left(1 + x_d + \frac{1}{\Omega} \left\{ \beta - \frac{q}{1+q} \right\} \right), \tag{4.47} \end{align}$$

where we have introduced $0 < r \equiv \frac{1-q}{1+q} < 1$. We immediately notice that there are two particular values of the defect strength, q_1 and q_2 for which respectively x_2^I and x_2^{II} enters the system. These two values, easily computable from $x_2^I = 0$ and $x_2^{II} = 0$, therefore, help in distinguishing the different current capacities and reads:

$$q_1 \equiv \frac{1 - 2\Omega x_d}{1 + 2\Omega x_d} \quad \text{and} \quad q_2 \equiv \frac{1 - 2\Omega(1 - x_d)}{1 + 2\Omega(1 - x_d)} \tag{4.48}$$

The conditions on the points $x_{1,2}^I$ and $x_{1,2}^{II}$ can be summarized as follows:

  i. $x_2^I > 0$ as long as $q > q_1$ or, equivalently, $\Omega > \frac{r}{2x_d}$;

  ii. $x_2^{II} < 1$ as long as $q > q_2$ or, equivalently, $\Omega > \frac{r}{2(1-x_d)}$;

  iii. $0 < x_1^I < x_d$ as long as $\alpha < \frac{1}{2}$ and $\Omega + 2\alpha > 1$;

  iv. $x_d < x_1^{II} < 1$ for $\beta < \frac{1}{2}$ and $\Omega + 2\beta > 1$.

Similarly, the conditions for having $0 < x_w^I < x_d$ and $x_d < x_w^{II} < 1$ are respectively

$$\frac{q}{1+q} - \Omega x_d < \alpha < \frac{q}{1+q} + \Omega x_d \tag{4.49}$$

and

$$\frac{q}{1+q} - \Omega(1 - x_d) < \beta < \frac{q}{1+q} + \Omega(1 - x_d). \tag{4.50}$$

Note that these identify two special values for each boundary entrance/exit rate:

$$\alpha_1 \equiv \frac{q}{1+q} - \Omega x_d \quad \text{and} \quad \alpha_2 \equiv \frac{q}{1+q} + \Omega x_d \tag{4.51}$$

$$\beta_1 \equiv \frac{q}{1+q} - \Omega(1 - x_d) \quad \text{and} \quad \beta_2 \equiv \frac{q}{1+q} + \Omega(1 - x_d). \tag{4.52}$$

These conditions identify the phase boundaries that will be described in the following.

A study case: $\mathcal{C}_1(x)$

Let us first consider the case where the carrying capacity is entirely determined by the defect, i.e. $\mathcal{C}_1(x) = j_d(x)$. This situation, which is sketched in Fig. (4.3(a)), corresponds to the case where the bottleneck is *efficient* enough to always impose a current $j_d(x) < j^*$, i.e. it arises below a certain strength threshold

$$q < q^* \equiv \min\{q_1, q_2\} \tag{4.53}$$

or equivalently below a threshold value of the detachment rate Ω

$$\Omega < \min\left\{\frac{r}{2x_d}, \frac{r}{2(1 - x_d)}\right\}. \tag{4.54}$$

In the proximity of the defect, this results in the following piecewise density profile:

$$\rho_d(x) = \begin{cases} \rho_{\beta_{\text{eff}}}(x) & \text{, sub-system I (left of } x_d) \\ \rho_{\alpha_{\text{eff}}}(x) & \text{, sub-system II (right of } x_d) \end{cases} \tag{4.55}$$

To determine the density profile and thus the phase diagram, we have to compare the current $j_\alpha(x)$ and $j_\beta(x)$, imposed by the left and right boundaries, with the carrying capacity. To construct the density profile one first needs to determine the current profile of the system. We refer to Fig. 4.4 to first qualitatively illustrate the construction procedure. The current profile depends on the interplay between the carrying capacity and the boundary induced current j_α and j_β. If at least one of the boundary currents lies completely below the carrying capacity the defect is irrelevant (case 1) and its presence is visible only in a spike in the density profile of the simple TASEP/LK (not shown). When the current imposed by the boundary intersects the carrying capacity on the right or on the left the defect becomes relevant and the system can be split into part (case 2). There could also be the case where the current imposed by the boundary overcomes the carrying capacity (case 3); then case the density is the one corresponding to the maximal current i.e. the carrying capacity. Note that when the defect is relevant the sub-system II does not recover the density ρ_I but follows the solution imposed by the defect. Clearly the defect becomes relevant for the left boundary for α larger than a critical value α_1, which is the value for which $j_\alpha(x_d)$ equate $j_d(x_d)$ (or, equivalently, for which $x_w^I < x_d$). Similar line of thoughts hold independently for the sub-lattice II and the right boundary current j_β. Let us see the different cases in details.

Using the results (4.33)-(4.47) and considering the subsystem I, one has to distinguish three cases:

i. When $\alpha < \alpha_1$, j_α never intersects the left branch of $\mathcal{C}_1(x)$ (i.e. $j_\alpha < j_d$ for $0 < x < x_d$). In this case the defect is *irrelevant* and the density profile on the subsystem I is determined by the left boundary, as in the absence of defect: $\rho^I(x) = \rho_\alpha(x)$ (except in the vicinity of the bottleneck, where one has (4.55)]. This situation corresponds to a *low-density* (LD) phase.

ii. When $\alpha_1 < \alpha < \alpha_2$, j_α intersects the left branch of $\mathcal{C}_1(x)$ at x_w^I ($0 < x_w^I < x_d$). This situation is sketched in Fig. 4.5 (left), corresponds to a *relevant* defect and the density reads:

$$\rho^I(x) = \begin{cases} \rho_\alpha(x) & \text{, } 0 < x < x_w^I \\ \rho_{\beta_{\text{eff}}}(x) & \text{, } x_w^I < x \le x_d \end{cases}. \tag{4.56}$$

This situation corresponds to a new (sub-)phase induced by the bottleneck (BP) in which the (effective high) density $\rho_{\beta_{\text{eff}}}$ imposed by the defect coexists with a low-density (sub-)phase ρ_α: as these densities cannot be matched continuously, the interplay between the defect and the left boundary generates a shock (domain wall) localized at x_w^I. This coexistence phase is called LD-BP.
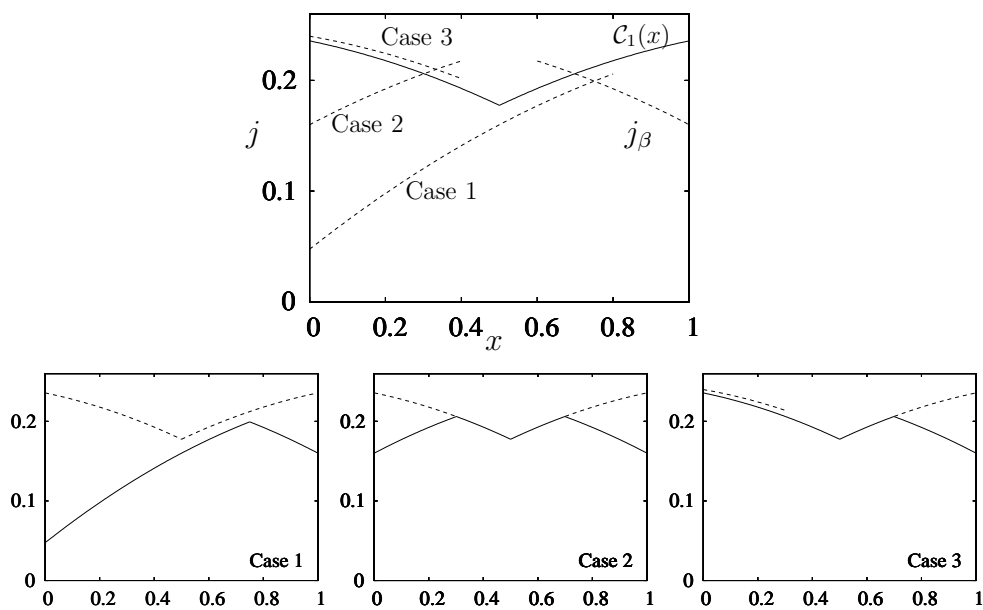
Figure 4.4: Construction of the current profile: the big graph shows how, for the same carrying capacity $\mathcal{C}_1(x)$ (solid line), different cases arise from different boundary-currents (dashed line). Three different profiles are shown in the small graphs (solid line: final current profile, dashed line: defect and boundary current).

iii. When $\alpha > \alpha_2$, j_α is always above the left branch of $\mathcal{C}_1(x)$ (i.e. $j_d < j_\alpha$ for $0 < x < x_d$). In this case, the defect is *relevant* (while the left boundary is irrelevant) and imposes a new maximal current j_d on the subsystem I, which is said to be in a (maximal current) bottleneck phase (BP). In this case the density reads $\rho^I(x) = \rho_{\beta_{\text{eff}}}(x)$.

One proceeds in a similar way for the right subsystem (II). There, when $\beta < \beta_1$, the defect is irrelevant and the density profile is determined by the right boundary, $\rho^{II}(x) = \rho_\beta(x)$. This is a *high-density* (HD) phase. When $\beta_1 < \beta < \beta_2$, the defect is relevant [see Fig. 4.5 (left)] and there is coexistence between a high-density phase and an effective low-density phase generated by the bottleneck (the phase is called BP-HD), this results in a a domain wall at $x_d < x_w^{II} < 1$ and the density reads

$$\rho^{II}(x) = \begin{cases} \rho_{\alpha_{\text{eff}}}(x) & , x_d \le x < x_w^{II} \\ \rho_\beta(x) & , x_w^{II} < x < 1 \end{cases} . \tag{4.57}$$

When $\beta > \beta_2$, the defect dominates and imposes an effective high density phase, called BP, and the density is $\rho^{II}(x) = \rho_{\beta_{\text{eff}}}(x)$.
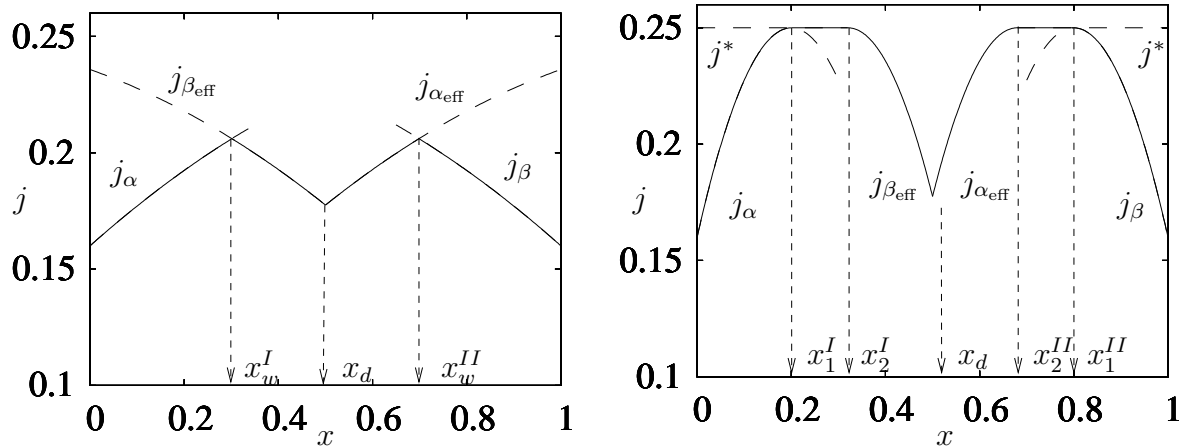

Figure 4.5: Current profiles (solid line) resulting from the matching of the boundary currents and the carrying capacity $\mathcal{C}(x)$ of the system (dashed lines). The left and right picture represent respectively a typical situation where the defect generates the coexistence phase LD-BP-HD (in which localized shock appear at x_w^I and x_w^{II} on both subsystems) and LD-MC-BP-MC-HD (see text).

Considering the global system, we notice that in addition to the phases which were already present in the defect free TASEP/LK system, we obtain four new phases, as summarized in the following table and in the phase diagram 4.6, corresponding to the situations where the defect is actually relevant.

Left↓/Right→	BP-HD	BP
LD-BP	LD-BP-HD	LD-BP
BP	BP-HD	BP

The emergence of these four BP (sub-)phases is the most drastic effect of the bottleneck when $q < q^*$. We have checked the predictions of our MF theory against Monte Carlo numerical simulations (following the Bortz-Kalos-Lebowitz algorithm [15]) and, as shown in Fig. 4.7 and have found a quite good agreement (both qualitative and quantitative) even for relatively small systems: In Fig. 4.7 (case ii), the BP acts as an effective low-density (high-density) phase on (a finite part of) the subsystem I (II), when $0 < x_w^I < x_d$ ($x_d < x_w^{II} < 1$). While, when the defect imposes the current j_d (case iii), the BP corresponds to an effective maximal current phase. The density profiles corresponding to the phase LD-BP-HD is shown in Fig. 4.7(c), where we notice the presence of localized shock (at x_w^I and x_w^{II}) on both subsystems. Figures (4.7(a) and 4.7(d)) corresponds to the phases LD-BP and BP-HD characterized respectively by the presence of a domain wall on the subsystem I (II) at x_w^I (x_w^{II}), while Fig. 4.7(b) illustrates the case where the defect dominates the whole system and imposes the new maximal current BP.

The phase-diagram of Fig. 4.6 shows that the *bottleneck-induced* (sub-)phases (LD-BP-HD, LD-BP, BP-HD and BP) occupy a large part of the phase diagram (shadowed region in Fig. 4.6). Only at the borders of the diagram, corresponding to particularly low/high rates α and/or β, one recovers the same phases as in the defect free TASEP-LK model (there the defect is irrelevant). Remarkably, for $\alpha > \alpha_2$ and $\beta > \beta_2$, i.e. in the right corner of the phase-diagram (darkest shadowed region in Fig. 4.6), the entire system is in a *pure bottleneck phase*: in this situation (case iii) the defect imposes the current $j_d(x)$ as an effective maximal current to the whole system.

For q smaller than the critical strength threshold q^* (see condition in Eq. 4.53), the defect imposes the bottleneck phases in the whole cut $\alpha - \beta$ of the phase diagram. This value can be obtained also setting to zero the values α_1 and β_1 (i.e. finding when the phase boundaries $\alpha = \alpha_1$ and $\beta = \beta_1$ coincide with the axis). The critical strength q^* is therefore the minimum between the value determined from the left and the one from the right [in the symmetric and simplest case $x_d = 1/2$ we obtain $q^* = \Omega_D/(2 - \Omega_D)$].

Flat carrying capacities: the case $\mathcal{C}_2(x)$

We now consider the case where the carrying capacity is, in some section of the lattice, flat, i.e. reaches the value $j^* = \frac{1}{4}$ in the bulk of the system. Here, we shall (mainly) consider the case illustrated in Fig. (4.3(b)), where

$$\mathcal{C}_2(x) = \begin{cases} j_d(x) & , 0 < x_2^I < x < x_2^{II} < 1 \\ \frac{1}{4} & , 0 < x < x_2^I \bigcup x_2^{II} < x < 1 \end{cases}. \tag{4.58}$$

This situation, the richest in terms of new bottleneck phases, arises when $q > \max\{q_1, q_2\}$, which ensures that $0 < x_2^I < x_d$ and $x_d < x_2^{II} < 1$.
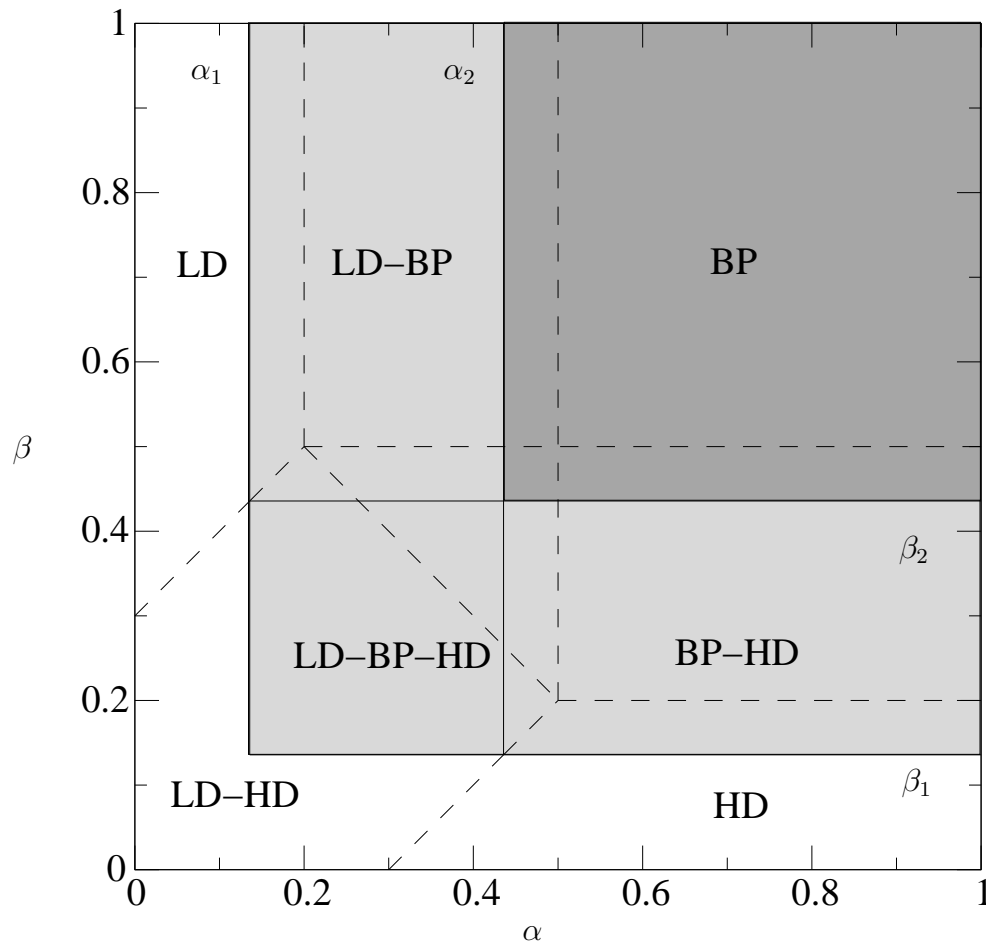
Figure 4.6: Phase diagram for $K = 1$, $\Omega_D = 0.3$, $q = 0.4$ and $x_d = 1/2$, i.e. for the carrying capacity $\mathcal{C}_1(x)$. Continuous lines are the phase boundaries introduced by the defect; dashed lines are the phase boundaries already present in the model without bottleneck. The shadowed region indicates the *bottleneck phases* where the defect is relevant, the darkest one highlights the pure bottleneck phase (for the meaning of the different phases see text).
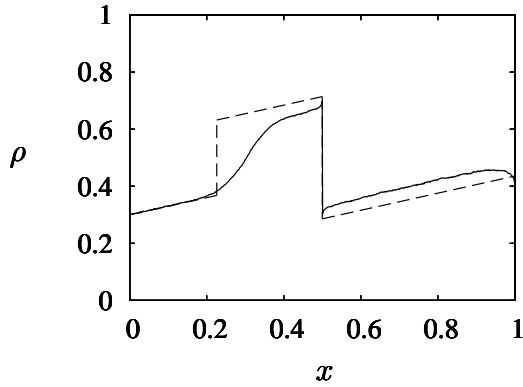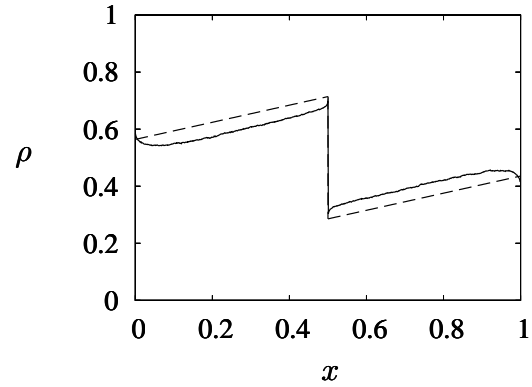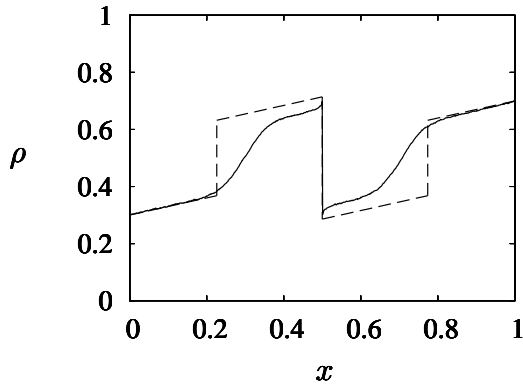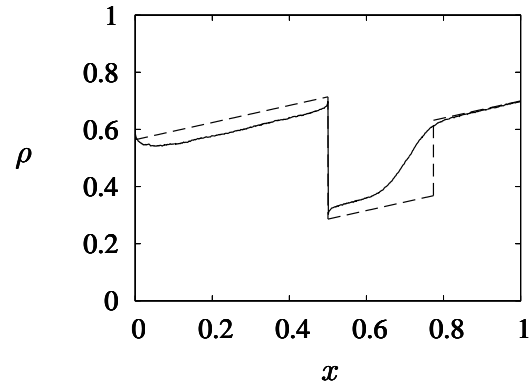
(a) LD-BP phase: $(\alpha, \beta) = (0.3, 0.6)$.

(b) BP phase: $(\alpha, \beta) = (0.6, 0.6)$.

(c) LD-BP-HD phase: $(\alpha, \beta) = (0.3, 0.3)$.

(d) BP-HD phase: $(\alpha, \beta) = (0.6, 0.3)$.

Figure 4.7:   Examples of density profiles in the bottleneck phases. Monte Carlo simulations (continuous line) are compared to analytical mean field predictions (dashed line). The system size is $N = 1024$ and the parameters are $K = 1$, $q = 0.3$, $x_d = 0.5$, $K = 1$, $\Omega_D = 0.3$.

For this carrying capacity, the possibility of having the domain wall at the point $x_2^{I,II}$ implies the existence of two critical values for the entrance/exit rate different from α_2 and β_2:

$$\alpha_2' \equiv \frac{1}{1+q} - \Omega x_d \text{ and } \beta_2' \equiv \frac{1}{1+q} - \Omega(1 - x_d). \tag{4.59}$$

Again, using the results (4.33)-(4.47), to determine the phase diagram one has to distinguish various situations, say on the subsystem I:

i. When $0 < \alpha < \alpha_1$, the left boundary current $j_\alpha < \min(j_d, j^*)$ and is thus always below the carrying capacity $\mathcal{C}_2$. In this case, the defect is *irrelevant*, $\rho^I(x) = \rho_\alpha(x)$ and the subsystem I is in a LD phase.

Left↓/Right→	BP-HD	BP-MC-HD	BP-MC
LD-BP	LD-BP-HD[7]	LD-BP-MC-HD[4]	LD-BP-MC[1]
LD-MC-BP	LD-MC-BP-HD[8]	LD-MC-BP-MC-HD[5]	LD-MC-BP-MC[2]
MC-BP	MC-BP-HD[9]	MC-BP-MC-HD[6]	MC-BP-MC[3]

Table 4.1: Bottleneck phases for the case $\mathcal{C}(x) = \mathcal{C}_2(x)$. For each phase, the label (1-9) refers to a given region of the (shadowed part) of the phase-diagram represented in Fig. 4.9.

ii. When $alpha_1 < \alpha < \alpha'_2$, the left boundary current j_α never reaches the maximal value j^*, but intersects the left branch of $j_d(x)$ at $0 < x^I_w < x_d$. In this case, the defect is *relevant* and the (left) density profile is

$$\rho^I(x) = \begin{cases} \rho_\alpha(x) & , 0 < x < x^I_w \\ \rho_{\beta_{\text{eff}}} & , x^I_w \leq x < x_d \end{cases}. \tag{4.60}$$

This situation corresponds to a LD-BP phase, where the BP acts as an effective high-density sub-phase imposed by the defect. As a consequence, a shock forms in the subsystem I and there is a domain-wall localized at x^I_w.

iii. When $\alpha'_2 < \alpha < \frac{1}{2}$, the left boundary current j_α reaches the maximal value j^* at x^I_1. In this case, the defect is *relevant* and the (left) density profile is

$$\rho^I(x) = \begin{cases} \rho_\alpha(x) & , 0 < x < x^I_1 \\ \rho^* & , x^I_1 \leq x < x^I_2 \\ \rho_{\beta_{\text{eff}}} & , x^I_2 \leq x < x_d \end{cases}. \tag{4.61}$$

This situation corresponds to a LD-MC-BP phase, where the BP acts as an effective high-density sub-phase imposed by the defect followed by a MC sub-phase (where the density is constant: $\rho^I(x) = \rho^*$) and LD phase imposed by the left boundary.

iv. When $\alpha > \frac{1}{2}$, the left boundary current $j_\alpha > \max(j_d, j^*)$ and is thus always above the carrying capacity $\mathcal{C}_2$. As a consequence, the defect is *relevant* and the current in I follows the carrying capacity and the (left) density reads

$$\rho^I(x) = \begin{cases} \rho^* & , 0 < x < x^I_2 \\ \rho_{\beta_{\text{eff}}} & , x^I_2 \leq x < x_d \end{cases}. \tag{4.62}$$

This situation corresponds to a MC-BP phase.

For each case (ii-iv) where the defect is relevant, we can symmetrically have as many bottleneck-induced profiles on the subsystem II. These are obtained as above: when appropriate, the right HD boundary phase replaces the left LD phase, $\rho^I_{\beta_{\text{eff}}}$ is replaced with $\rho^{II}_{\alpha_{\text{eff}}}$, etc. We therefore find nine new bottleneck phases induced by the (relevant) presence

of the defect, as summarized in Tab. (4.1).

We now discuss in some more details the most interesting situation, arising when the currents $j_\alpha(x_1^I)$ and $j_\beta(x_1^{II})$ reach the maximal value $j^* = \frac{1}{4}$ on both subsystems I and II. This can happen provided that $\alpha < \frac{1}{2}, \beta < \frac{1}{2}$ and $\beta + 2\Omega > 1$, which ensures $0 < x_1^I < x_d$ and $x_d < x_1^{II} < 1$. The density profile is therefore six-fold:

$$
\rho(x) = \begin{cases}
\rho_\alpha & , 0 < x < x_1^I \\
\rho^* & , x_1^I \le x < x_2^I \\
\rho_{\beta_{\text{eff}}} & , x_2^I \le x < x_d \\
\rho_{\alpha_{\text{eff}}} & , x_d \le x < x_2^{II} \\
\rho^* & , x_2^{II} \le x < x_1^{II} \\
\rho_\beta & , x_1^{II} \le x < 1
\end{cases}
\tag{4.63}
$$

This case, denoted LD-MC-BP-MC-HD, is illustrated in Fig. 4.8 (left) and corresponds to the coexistence of a low-density (LD) sub-phase (on I), two maximal current (MC) sub-phases (one in both subsystems) and effective high/low density bottleneck-induced sub-phases (both called BP) on the subsystems I/II and a high density phase (on II).

We have also checked the our MF predictions against Monte Carlo numerical simulations and, as illustrated in Fig. 4.8 and, again, have found both qualitative and quantitative agreement (even for relatively small systems).

The above discussion provides all the information to determine the phase-diagram corresponding to a system with a flat carrying capacity $\mathcal{C}_2(x)$ [i.e. when $q > \max\{q_1, q_2\}$]. The phase diagram, shown in Fig. 4.9, displays twelve phases, three of them (LD, HD and LD-HD) are the same as in the TASEP/LK model and are found at the borders of the diagram [for small (large) value of the rate α (β)], when the defect is irrelevant. The nine bottleneck phases appear in the core of the phase diagram (shadowed region in Fig. 4.9), for intermediate values of α and β. Here, we no longer have a pure BP phase: the genuine BP obtained for the carrying capacity $\mathcal{C}_1(x)$ is now replaced by a MC-BP-MC coexistence phase (right top corner of Fig. 4.9).

To conclude the study of the case $K = 1$, let us mention also the situations where the flat carrying capacity is $\mathcal{C}_3(x)$ or $\mathcal{C}_4(x)$, which is possible when the defect is not in the center of the system: the carrying capacity is $\mathcal{C}_3(x)$ when $q_2 < q < q_1$ and is $\mathcal{C}_4(x)$ when $q < 1 < q < q_2$. In these cases, the phase diagram, directly follows from what we have discussed above. In fact, when $\mathcal{C}(x) = \mathcal{C}_3(x)$, there six new phases induced by the bottleneck. Those are summarized in the following table:

Left↓/Right→	BP-HD	BP-MC-HD	BP-MC
LD-BP	LD-BP-HD	LD-BP-MC-HD	LD-BP-MC
BP	BP-HD	BP-MC-HD	BP-MC

The six bottleneck phases for the case $\mathcal{C}(x) = \mathcal{C}_4(x)$ are obtained in a similar way, as it is clear from the table below:

g replacements

ρ

j
x_d
x_2^I
x_2^{II}
x_1^I
x_1^{II}

j

g replacements

ρ

x_d
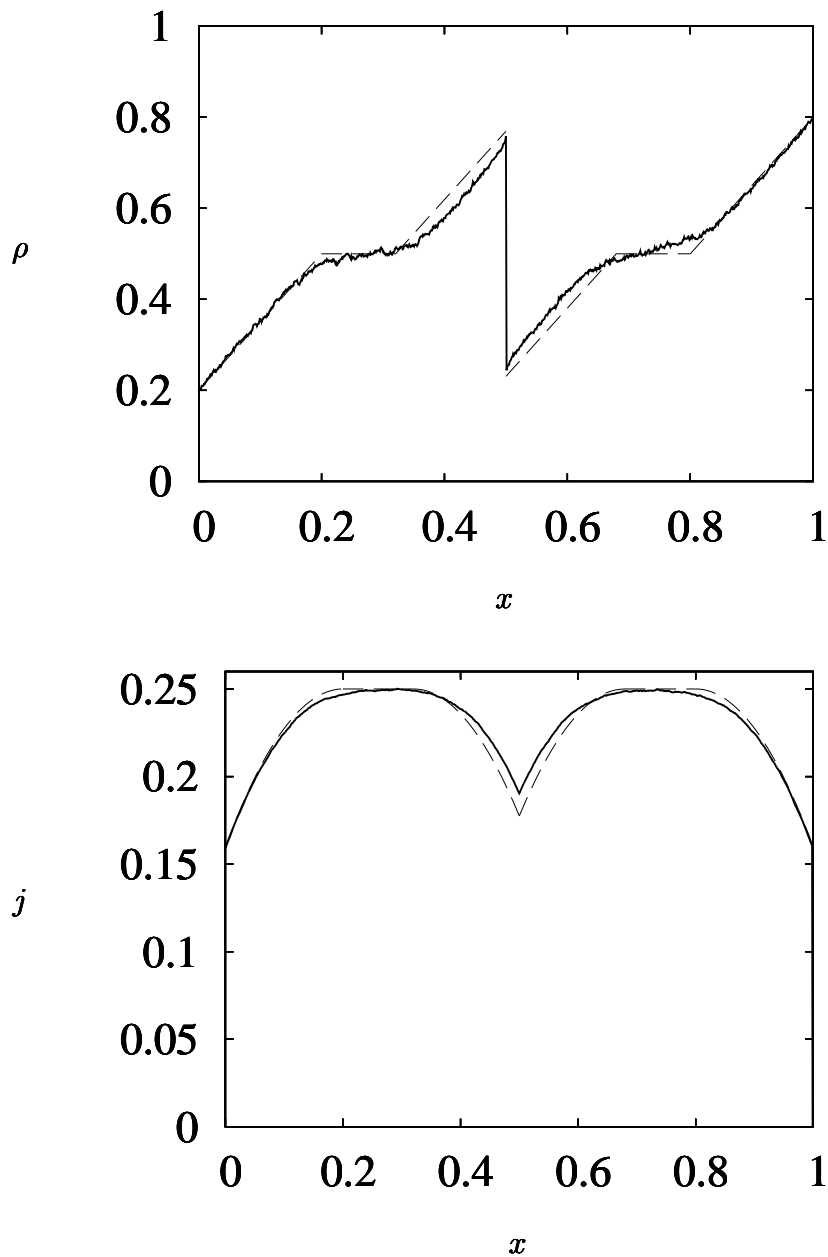x_2^I
x_2^{II}
x_1^I
x_1^{II}

Figure 4.8:   Examples of density profile and current (right) for the system in the LD-MC-BP-MC-HD phase: the defect is relevant and the carrying capacity is $\mathcal{C}_2(x)$. Monte Carlo simulations (continuous line) are compared to analytical mean field predictions (dashed line). The system size is $N = 1024$, $K = 1$, $\Omega = \Omega_D = 1.5$, $(\alpha, \beta) = (0.2.0.2)$ and $x_d = 1/2$: one can clearly distinguish the various phases and note a discontinuity in the density profile in the proximity of the defect.
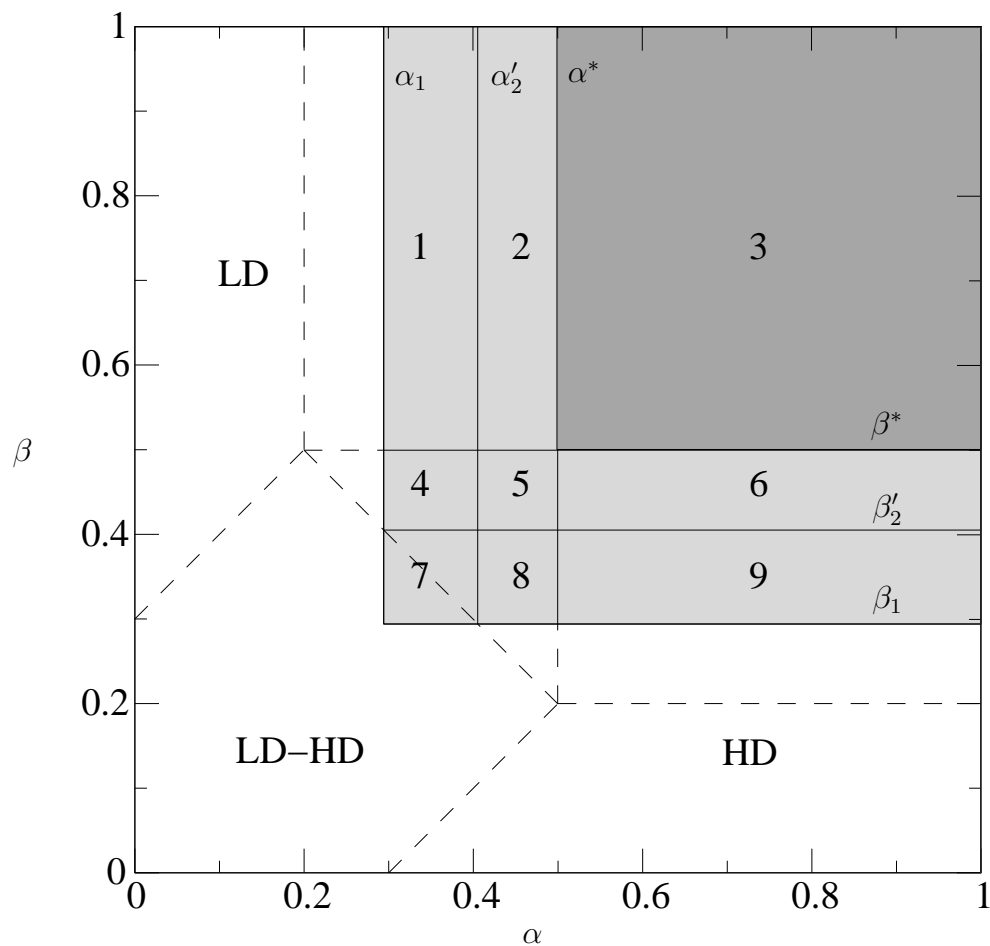
Figure 4.9: Phase-diagram for $K = 1$, $\Omega_D = 0.3$, $x_d = 1/2$ and $q = 0.8$. Continuous lines are the phase boundaries introduced by the defect; dashed lines are the phase boundaries already present in the model without bottleneck. The shadowed region indicates the *bottleneck phases* where the defect is relevant, the darkest one highlights the pure bottleneck phase (for the meaning of the different phases see text and Tab. 4.1).

Left↓/Right→	BP-HD	BP
LD-BP	LD-BP-HD	LD-BP
LD-MC-BP	LD-MC-BP-HD	LD-MC-BP
MC-BP	MC-BP-HD	MC-BP

For both carrying capacities $\mathcal{C}_3(x)$ and $\mathcal{C}_4(x)$, the phase-diagrams are obtained as above.

Topological features

In this subsection we discuss the most important topological features of the phase diagram.

The most relevant property of the phase diagram of the model is the bottleneck phase region. As can be inferred from the graphs a large portion of the phase diagram is dominated by the defect properties. The phase boundaries separating the usual phases from the bottleneck (i.e. $\alpha = \alpha_1$ and $\beta = \beta_1$) are straight lines since they depend only on the detachment rate and on the strength and position of the defect, but not on the entrance exit rates. The transitions between the usual TASEP/LK phases and the bottleneck phases are discontinuous (the density switch discontinuously from ρ_α, i.e. LD to $\rho_{\alpha_{\text{eff}}}$, i.e. LD-MC-BP).

The phase boundaries α_2 (β_2), for $q < q^*$, and α^* (β^*), for $q > q^*$, separate the point where the density profile is totally dominated by the defect from the one where the boundary current still plays a role. Being the position of the domain wall the order parameter, in this case the transition is continuous. A continuous transition is also identified by the boundary α_2' (β_2') since the matching point $x_1^{I,II}$ enters continuously the system.

The interesting transition between the behavior characterized by a carrying capacity $\mathcal{C}_1(x)$ and $\mathcal{C}_2(x)$ can be observe if we plot the cut of the phase diagram in q and α (choosing $\beta > 1/2$), as done in Fig. 4.10. In this graph the line α_1 identifies a first order transition, while α_2, α_2' and $\alpha^* = 1/2$ a continuous transition. The line $\alpha = 1/2 - \Omega_D$ was present in the pure TASEP/LK and marks again a continuous transition. The line $q = q_1$ identifies the continuous transition between the two different carrying capacity, $\mathcal{C}_1(x)$ and $\mathcal{C}_2(x)$. The most relevant points of the phase diagram $\mathcal{P}_1$, $\mathcal{P}_2$, and $\mathcal{Q}$ are shown in the graph. At the point $\mathcal{P}_1$ three continuous transition lines meet: indeed it is a *triple point*. A similar behavior is found at the point $\mathcal{P}_2$ where four phases merge. More interesting is the point $\mathcal{Q}$ where a bifurcation occurs and two continuous transition lines merge with a first order transition α_1: this is a landmark of a *multi-critical point*.

4.3.2 Results and phase-diagrams when $K \neq 1$

The case $K = \Omega_A/\Omega_D \neq 1$ is mathematically more tedious, as for the defect free TASEP/LK model, at MF level (continuum limit), one needs to solve Eqs. (4.8,4.9) which solution implies Lambert functions, which are multivalued functions with two real branches [112]. Here, having split the problem in two subsystems and with the Langmuir isotherm $\rho_I \equiv K/(K+1)$, one has to consider

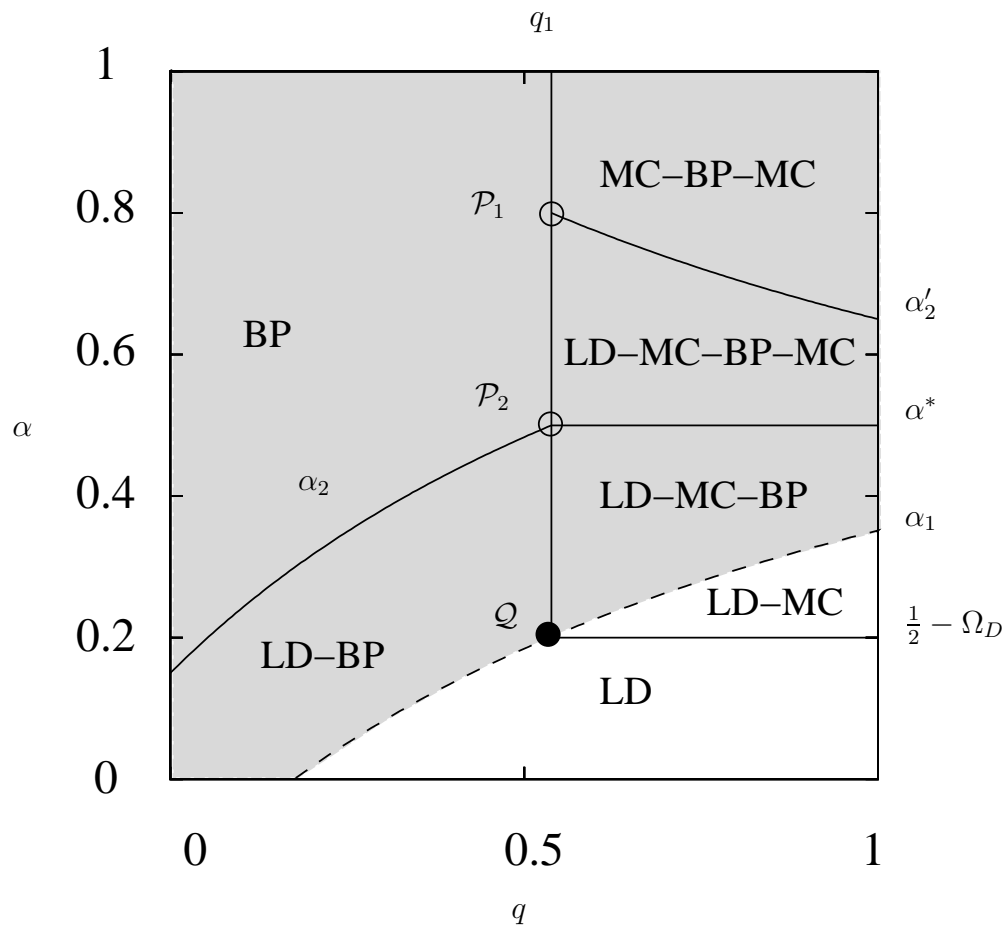$$(2\rho^{I,II} - 1)\partial_x \rho^{I,II}(x) = (K+1)\Omega_D[\rho_I - \rho^{I,II}(x)], \tag{4.64}$$

Figure 4.10: Cut of the phase diagram in q and α (parameters: $K = 1$, $\Omega_D = 0.1$, $x_d = 1/2$ and $q = 0.3$, $\beta > 1/2$). Solid lines identify continuous transitions, while the dashed line a first order transition. The relevant points $\mathcal{P}_{1,2}$ and the multi-critical one $\mathcal{Q}$ are shown in the graph.

again supplemented with the (sub-systems) boundary conditions 4.32 $\rho^I(0) = \alpha;\quad \rho^I(x_d) = \frac{1}{1+q}$ and $\rho^{II}(x_d) = \frac{q}{q+1};\quad \rho^{II}(1) = 1 - \beta$. We refer the readers to Ref. [112] for a detailed mathematical treatment of this kind of equations, and report our results for the phase-diagram and density profile of the TASEP/LK model in the presence of a bottleneck when $\Omega_D \neq \Omega_A$ (i.e. $K \neq 1$). As for the defect free model, one can take advantage of the underlying particle-hole symmetry (4.29) to restrict the discussion to the case $K > 1$ [112]. Except for the mathematical treatment of the MF bulk equation, we follow the same lines as in the case $K = 1$. Again, one has to distinguish the case where the carrying capacity coincides with the current imposed by the defect ($\mathcal{C}(x) = j_d(x)$) from the situation where $\mathcal{C}(x)$ reaches the maximal current value j_K^*. While we $K = 1$ the maximal current available in the bulk was $j^* = 1/4$, here $j_K^*(x) \leq j^*$ is a non-constant space-dependent quantity. When $\mathcal{C}(x) = j_d(x)$, except some topological asymmetries, one essentially recovers the same phase-diagram as in the $K = 1$ situation when the carrying capacity is $\mathcal{C}_1(x)$: as illustrated in Fig. 4.11, the phases are BP, MC-BP, LD-BP and LD-BP-HD. Again, we notice that the core of the phase-diagram is entirely determined by the defect (shadowed region in Fig. 4.11), which is also responsible for a pure BP for sufficiently high rates α and β.

On the other hand, it follows from the analytical solution of the above-mentioned MF equation that the left branch of $j_d(x)$ can never reach the maximal current $j_K^*(x)$ on the subsystem I: because of the functional expression of the solution, the point x_2^I does not lie in subsystem I. Asymmetrically, the point x_2^{II} may lie in subsystem II but the current $j_\beta(x)$ can never reach $j_K^*(x)$, unless $\beta = 1/2$. Essentially, carrying capacities $\mathcal{C}_3(x)$ and $\mathcal{C}_2(x)$ are topologically prohibited (even in the asymmetric case $x_d \neq 1/2$); the carrying capacity $\mathcal{C}_4(x)$ presents, instead of the six phases of the case $K = 1$ (Sec. 4.3.1), only four bottleneck phases.

4.4 Conclusion

This work has been devoted to the study of the effects of a bottleneck (point-wise disorder) on the stationary properties of a biologically inspired microscopic transport model. We have considered a the TASEP coupled the Langmuir kinetics (LK). The role of the bottleneck is to locally slow down any incoming particles.

We have found it convenient to introduce the concept of a *carrying capacity* as the maximal current that can flow through a given site. This s space-dependent quantity is found to depend on the defect parameters, i.e. its position and strength. Within an effective mean-field theory built on splitting the lattice into two subsystems, we have shown that a single bottleneck may determine the carrying capacity, induce new phases and therefore affect the transport properties in the whole systems.

We have shown that a single bottleneck may induce a non-trivial carrying capacity allowing for new phases and therefore affect the transport properties in the whole systems. Many scenarios appear and have been discussed in detail. For each of them, rich phase-diagrams have been obtained and analyzed. In all cases, it was shown that only a small
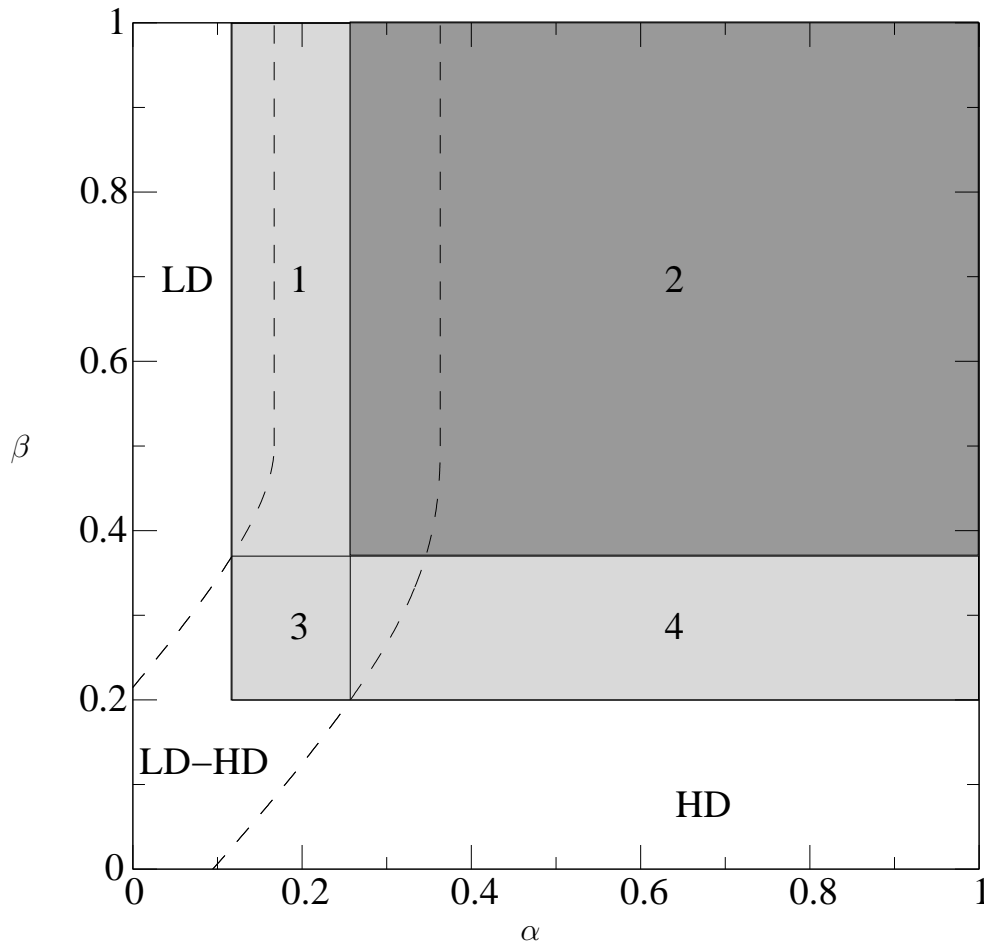
Figure 4.11: Phase diagram for $K = 2$, $\Omega_D = 0.1$, $x_d = 1/2$ and $q = 0.3$. Continuous lines are the phase boundaries introduced by the defect (BP); dashed lines are the phase boundaries already present in the model without bottleneck. The shadowed region indicates the *bottleneck phases* where the defect is relevant, the darkest one highlights the pure bottleneck phase. The numbers stem for the different phases: LD-BP (1), BP (2), LD-BP-HD (3) and BP-MC (4). For the description of the phases see the text and Figs. 4.12 and 4.13.
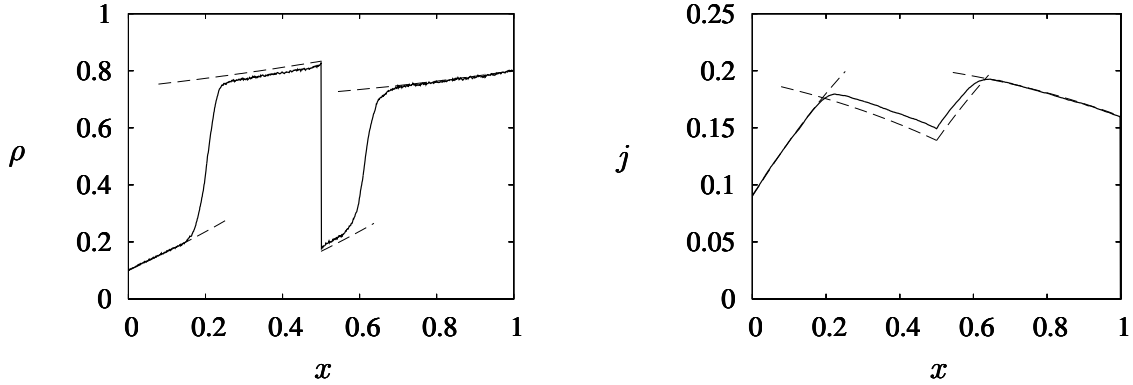
Figure 4.12: Examples of density profile (left) and current (right) showing a case where the defect is relevant ($q = 0.2$) for a system of size $N = 1024$ with rates $\Omega_D = 0.3$, $(\alpha, \beta) = (0.1.0.2)$ and $K = 2$; these parameters identify the phase coexistence LD-BP-HD as explained in the text. Monte Carlo simulations (continuous line) are compared to analytical mean field predictions (dashed line)

part of the latter was not affected by the defect: indeed, the core of the phase-diagram is characterized by *bottleneck induced (sub-)phases*. Depending on the defect strength and position, there are either four, six or nine bottleneck phases. These are characterized by density profiles with localized shocks and kinks in the sub-systems, arising from the matching between the boundary and the defect current. The richness of the phase diagram is even more evident in its $\alpha - q$ cut (Fig. 4.10) where multiple phases merges and a multi-critical point is found. Due to the competition between the TASEP and LK dynamics, the effects of a single bottleneck in the TASEP/LK model are much more dramatic than in the simple TASEP [80], or the so-called $\ell-$TASEP (TASEP for extended objects) [136], where a localized defect was shown to only shift some transitions line in the phase-diagram, but do not affect its topology.

Our results were checked against numerical (Monte-Carlo) simulations, which brings further arguments in favor of the validity of mean-field approaches for studying the TASEP-/LK-like models. The somewhat surprising quantitative validity of this approximate scheme can be traced back to the current-density relationship, which is correctly predicted by the mean-field theory.

We would like to point out that the analysis carried out in this work can be also extended to other variants of the TASEP/LK model. As an example, we mention the case where instead of monomers one could consider the biologically relevant situation depicted in Ch. 3 where dimers (modelling the usual two heads of molecular motors) would move as bound entities according to the ℓ-TASEP and could experience a Langmuir-like on-off kinetics.
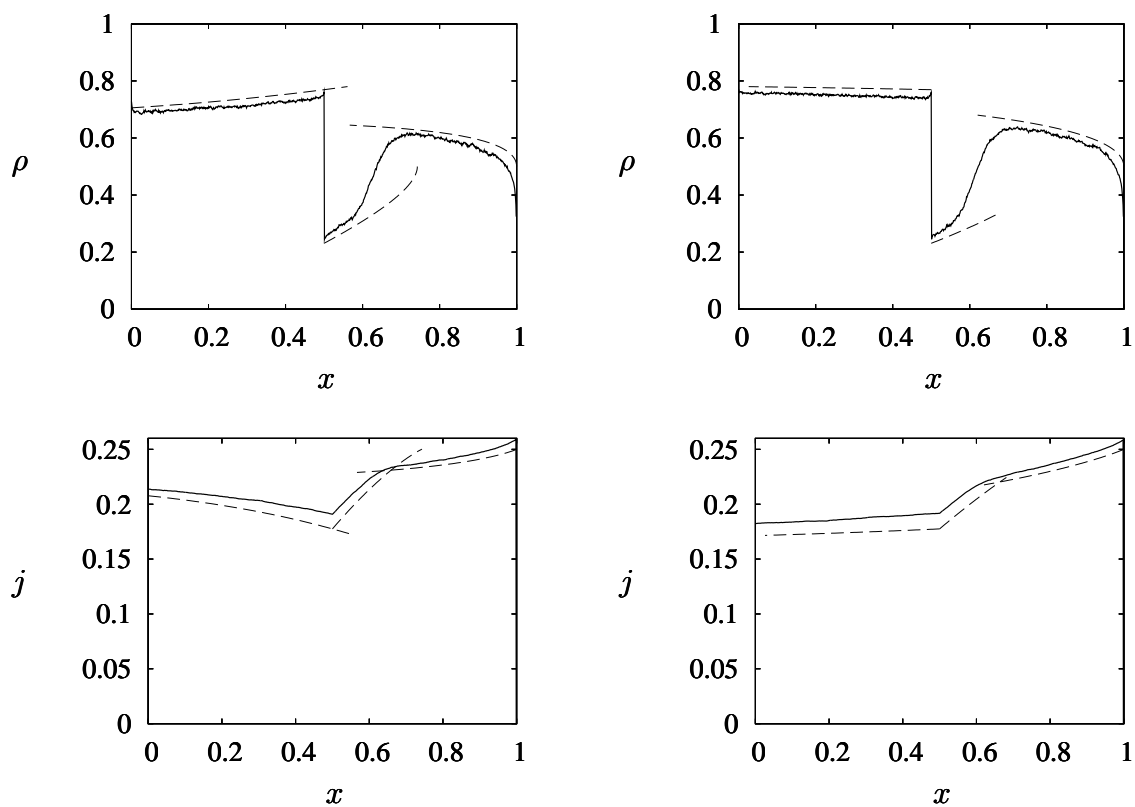
Figure 4.13:   Two examples of density profile and current in the BP-MC phase. Monte Carlo simulations (continuous line) are compared to analytical mean field predictions (dashed line). The system size is $N = 1024$ and the parameters are $q = 0.3$, $K = 2$, $\Omega_D = 0.3$, $\alpha = \beta = 0.8$ (left); and $K = 4$, $\Omega_D = 0.1$, $\alpha = \beta = 0.8$ (right).

Let us remark the intriguing analogy between the behavior of the model we have considered and the transistor. Both systems present a net current between a *source* (left boundary) and a *drain* (right boundary). The defect acts as *gate*, which "regulates" the current at the drain. Interestingly, the gate can be controlled also through the detachment rate, since the carrying capacity depends also on Ω_D.[3] I may be worthwhile to explore this analogy further.

Eventually, we think that this study has clearly shown that the presence of disorder in the TASEP/LK model, even in its simplest form, generally gives rise to quite rich and intriguing features and should motivate further studies of the disordered versions of the TASEP/LK model. In particular, we think that the method outlined in this work could pave the way to study the TASEP/LK models in more 'realistic' and biophysically relevant situations, as in the presence of clusters of competing defects or quenched site-wise randomness.

---

[3]In the biological system that inspired this work the detachment rate can be changed by varying the ATP concentration and therefore the processivity of the motors.

Chapter 5

Dynamics of TASEP

In this chapter we study the dynamics of the totally asymmetric exclusion process with open boundaries by phenomenological theories complemented by extensive Monte-Carlo simulations. Upon combining domain wall theory with a kinetic approach known as Boltzmann-Langevin theory we are able to give a complete qualitative picture of the dynamic correlation function of the process in the low and high density regime and at the corresponding phase boundary. At the coexistence line between high and low density phases we observe a time scale separation between local density fluctuations and collective domain wall motion, which are well accounted for by the Boltzmann-Langevin and domain wall theory, respectively.

In the following section we will discuss the state of the research on the dynamics of TASEP. Then we present the original formulation of Boltzmann Langevin method and we will present how the Boltzmann-Langevin approach can be applied for the TASEP model and calculate the correlation function of the linearized version. Interestingly, it will turn out that the resulting Boltzmann-Langevin equation reduces to the noisy Burgers equation for $\alpha = \beta = 1/2$. In section 5.4 we give a short description of the Monte-Carlo methods used to analyze the correlation functions of the TASEP model. Results obtained from these simulations are compared with the analytical results from the Boltzmann-Langevin and the DW theories in section 5.5. To prove the validity of the method in other systems a short study on the dynamical properties of the TASEP of dimer is presented in section 5.6. Finally, we present a short summary and some outlook. For the reader which is not confident with the concept of scaling exponents and the KPZ universality class we added a short review in the App. 5.B.[1]

5.1 Introduction: dynamics of TASEP

The stationary state (current and density profiles) of the Totally Asymmetric Exclusion process (TASEP) presented in Ch.2 has been studied in great detail over the last years (for recent reviews see e.g. Refs. [25, 132]). Let us recall the main results: in open systems it has

---

[1]This chapter is almost entirely covered by reference [117].

been found by some exact methods [26, 131, 30] that there are three different phases: a high density, a low density and a maximal current phase; compare Fig. 3.1. The coexistence line $\alpha = \beta < 1/2$ marks a discontinuous transition between the high and low density phase, while along the lines $\alpha = 1/2 \leq \beta$ and $\beta = 1/2 \leq \alpha$ the transitions are continuous. There are interesting correlation effects reflected in the shape of the density profiles at the boundaries; only along the disorder line, $\alpha + \beta = 1$, the density profile is flat and there are no spatial correlations.

The dynamic properties of the TASEP model are much less studied. For closed systems exact analytical results [34, 57, 31, 33] have been derived for the largest relaxation time τ. It is found that τ diverges with system size as $\tau \propto L^z$ with a dynamic exponent of $z = 3/2$. For open systems no exact results are available. The spectrum of relaxation times has been studied for small systems using exact enumeration techniques [11, 36]. More recently density matrix renormalization group studies [106] have shown that the largest relaxation times are finite unless $\alpha = \beta = 1/2$, where $\tau \propto L^{3/2}$ as for the periodic system; the results also indicate that $z = 3/2$ in the whole maximal current phase. These studies also confirm the results of a phenomenological approach known as domain wall theory [81, 36]. In this coarse-grained description of the dynamics it is assumed that each particle reservoir at the system's boundary independently fixes a density. The two domains are then joined in the bulk by a phase boundary (domain wall), which performs a random walk due to the randomness of particle flux at the boundaries (see Ch. 2); the domain wall (DW) moves left whenever a particle enters the system and right whenever a particle exits the system. Along the coexistence line the DW theory accounts even for the power spectrum at small frequencies (long time) [144].

DW theory does not describe the dynamics of local density fluctuations. This is evident for periodic systems where the average density profile is flat. In this case it has been shown that the dynamics of the TASEP model maps onto the noisy Burgers equation [92]. It is actually this mapping which allows for the implementation of some exact methods such as the Bethe ansatz [57]. Further progress has also been made upon using mode coupling [150] and renormalization group [49] theories.

Recently a paper by De Gier and Essler [24] compute by Bethe ansatz the relaxation time in any point of the phase diagram (see Sec. 2.2.1, showing the existence of two different critical exponents along the line $\alpha = \beta$: the Edward Wilkinson and the KPZ (see App. 5.B). Their results lead to divide the low and the high density phase in two sub-phases separates by the lines parameterized by

$$\beta_c = \left[1 - \left(\frac{1-\alpha}{\alpha} \right)^{-1/3} \right]^{-1} \text{ for } 0 < \alpha < \frac{1}{2}, \tag{5.1}$$

$$\alpha_c = \left[1 - \left(\frac{1-\beta}{\beta} \right)^{-1/3} \right]^{-1} \text{ for } 0 < \beta < \frac{1}{2}. \tag{5.2}$$

In the HD and LD phase the gap does not depend on the system size in first approximation, but contain correction that scale like L^{-2}. The constant value change within the two sub-

phases. On the coexistence line the gap scale (like in the Edward Wilkinson model) as $E \sim L^{-2}$ (i.e. $z = 2$). While at the critical point $\alpha = \beta = 1/2$ and in the whole MC phase they recover KPZ results with $E \sim L^{-3/2}$ (i.e. $z = 3/2$).

Despite all these remarkable achievements, a complete numerical study of the correlation function has been presented only rather recently and we are going to illustrate the results contained in Ref. [117].

5.2 Boltzmann-Langevin equation in solid state physics

This correspondence between the lattice gas model and the noisy Burgers equation for the periodic case suggests to look for a similar mapping for open systems. In this context, it is useful to recall a successful method in classical and quantum many-body systems, known as Boltzmann-Langevin (BL) equations. This approach, which was first introduced to describe electron transport in the presence of disorder and phonons scattering [78, 79], describes not only the average of the electronic distribution function, but also its fluctuations. Almost contemporary the BL equation was used to compute the fluctuations in hydrodynamic equation of a low-density gas [12]. The applications of this method range from solid state physics to scattering of heavy ions. In the context of electronic transport through nanostructures, this method has recently been widely employed in studies of shot noise (for a review see [13]). It is widely used to study the role fluctuations in heavy ion scattering (triggering the dramatic phenomena of multi-fragmentation of nuclear matter) [141].

The computation of the density correlation functions is achieved by amending the Boltzmann kinetic equation with a Langevin source which takes the stochastic nature of collisions into account. We present here the derivation of the method used in the original reference. Consider a gas of electrons scattered by phonons or/and impurities (e.g. an electron gas in semiconductor) or by molecules (in a weakly ionized plasma). Assume that inter-electronic collisions, generation and recombination of electron are unimportant and consider the scattering system as a thermostat (e.g. the relaxation time of phonons associated with non electronic processes of scattering is small). Note that the system is to be considered driven by an electric field and that the dependence between current and field is not necessarily linear. In this case it is convenient to describe the *transport phenomena* with the classical kinetic (Boltzmann) equation and the *fluctuation phenomena* introducing a Langevin term on the current. The usual Boltzmann equation for an equilibrium electron gas reads

$$\mathcal{L}n(\vec{r}, \vec{p}, t) - S_{\vec{p}}[n] = 0 \tag{5.3}$$

where the *flow term* $\mathcal{L}n$ (with $\mathcal{L}$ the Liouville operator) is equal to the *collision term*

$$S_{\vec{p}}[n] = \sum_{\vec{q}} \left(J_{\vec{q},\vec{p}} - J_{\vec{p},\vec{q}} \right) = J_{\vec{p}}^+ - J_{\vec{p}}^- \tag{5.4}$$

with $J_{\vec{q},\vec{p}} = W_{\vec{q},\vec{p}} n(\vec{r}, \vec{p}, t) \left(1 - n(\vec{r}, \vec{q}, t) \right)$ (where $W_{\vec{q},\vec{p}}$ is the transition rate form state with moment $\vec{q}$ to state with moment $\vec{q}$), which keeps track of the change in particles number due

to collisions. By replacing the number of particles with the sum of a stationary (average number of particle) and a fluctuating part $n_i(t) = \overline{n}_i + \delta n_i(t)$ one can obtain the equation for the fluctuation of the occupation number

$$\mathcal{L}\delta n(\vec{r}, \vec{p}, t) - S_{\vec{p}}[\delta n] = A[\delta \vec{E}, \delta \vec{H}] + \delta J(\vec{q}, \vec{p}, t) \tag{5.5}$$

where the r.h.s. contains the field fluctuation arising from fluctuations in the current and the fluctuations on the current themselves. From this equation via a Fourier transform is possible to get the Green function for the fluctuation on the density and therefore calculate the n-point correlation function for such a quantity.

The advantage of this approach is that the time behavior of the correlation function is a really easy task. The method, though, works well for *dilute systems*: the system cannot be strongly correlated and this is one of the limitation of this approach. A close analogy with the lattice-gas model studied in this chapter arises for the following reason: the requirement of no double occupation of sites has its direct analog in the Pauli principle which forbids double occupation of electronic states.

5.3 Stochastic equations of motion

Let us see how BL equation can be related to the TASEP. At a given time t the microscopic state of the system is characterized in terms of occupation numbers $\{n_i = 0, 1\}$. The dynamics, that we described as a set of rules in the previous section, can be formulated in terms of a *quantum Hamiltonian representation* [35, 56, 114] (for a nice introduction see [132, 126]). In the bulk the corresponding Heisenberg equations for the occupation number operators $n_i(t)$ have the form of a lattice continuity equation

$$\partial_t n_i(t) = J_{i-1}(t) - J_i(t) \tag{5.6a}$$

with the current operator

$$J_i(t) = n_i(t)\left(1 - n_{i+1}(t)\right). \tag{5.6b}$$

The effect of the entrance and exit rates is equivalent to constant particle reservoirs of density α and $1 - \beta$ at auxiliary sites $i = 0$ and $i = N + 1$, respectively.

There are several levels of approximation in dealing with the dynamics of the system. If correlation effects are neglected altogether one arrives at a set of rate equations for the average particle density $\rho_i(t) = \langle n_i(t) \rangle$, which have a form identical to Eq. (5.6) with n_i replaced by ρ_i. To arrive at these equations one has to take the average of Eq. (5.6) and neglect correlations in the spirit of a mean-field or a random phase approximation

$$\langle n_i(t)\, n_{i+1}(t) \rangle \rightarrow \langle n_i(t) \rangle\, \langle n_{i+1}(t) \rangle. \tag{5.7}$$

Then, in the stationary limit the rate equations are equivalent to a nonlinear map

$$\overline{\rho}_i(1 - \overline{\rho}_{i+1}) = J \tag{5.8}$$

with a constant stationary current J. Upon exploiting the properties of this map one can easily reproduce the full phase diagram of the TASEP [97]. Actually, it turns out that the phase diagram [26] obtained in this way is identical to the one obtained from an exact solution of the TASEP in the stationary limit [30, 131]. The density profiles obtained from such a mean-field approach miss correlation effects, especially in the maximal current phase, and the fluctuations of the domain walls.

5.3.1 The Boltzmann-Langevin approach

To go beyond rate equations we follow a line of arguments which leads to what is known as Boltzmann-Langevin (BL) equations in studies of non-equilibrium transport in electron systems [78, 79]. The right hand side of Eq. (5.6a) has a form similar to the *collision integral for impurity scattering* in the Boltzmann equation balancing in-going and out-going currents. In order to account for fluctuation effects around the stationary state, we express both the current and the density as the sum of a deterministic and a fluctuating part

$$n_i \approx \overline{\rho}_i + \delta\rho_i \equiv \rho_i \,, \tag{5.9a}$$
$$J_i \approx \rho_i(1 - \rho_{i+1}) + \delta J_i \,. \tag{5.9b}$$

Since we will use the BL approach only for those regions in the phase diagram where the stationary density is to a good approximation spatially constant we may set $\overline{\rho}_i = \overline{\rho}$. This applies for both the high and low density phase, but not for the phase boundary $\alpha = \beta \leq \frac{1}{2}$, where in addition to density fluctuations on small scales we also have domain wall motion on large scales. The latter modes are obviously not accounted for in the BL formulation. One also has to be cautious in the maximal current phase where boundary layer profiles decay only algebraically as one moves from the boundaries towards the bulk [26].

Upon inserting Eq. (5.9) into the equations of motion, Eq. (5.6), we find a coupled set of Langevin equations for the density fluctuations at each site of the lattice

$$
\begin{aligned}
\partial_t \delta\rho_i(t) &= (1 - \overline{\rho}) \left[\delta\rho_{i-1} - \delta\rho_i \right] - \overline{\rho} \left[\delta\rho_i - \delta\rho_{i+1} \right] \\
&\quad + \delta\rho_i(\delta\rho_{i+1} - \delta\rho_{i-1}) - (\delta J_i - \delta J_{i-1}) \,.
\end{aligned} \tag{5.10}
$$

In order to close these equations we still need to specify the current fluctuations δJ_i. This can be done by exploiting the fact that the occupation numbers are binary variables, which immediately implies that $J_i^2 = J_i$.[2] Hence the variance of the current at a particular site is given by $\mathrm{Var}[J_i] = \langle J_i \rangle (1 - \langle J_i \rangle)$. To be consistent with the approximations already made, we set $\langle J_i \rangle \approx \overline{\rho}(1 - \overline{\rho})$ and finally get

$$\mathrm{Var}[J] = \overline{\rho}(1 - \overline{\rho})(1 - \overline{\rho}(1 - \overline{\rho})) \,. \tag{5.11}$$

---

[2]Note that our derivation *differs* from the argument used in the conventional Boltzmann-Langevin theory. The latter would only yield the low-current approximation $\mathrm{Var}[J_i] = \langle J_i \rangle$.

Our final assumption is that correlations in the current fluctuations are short ranged in space and time such that we can write

$$\langle \delta J_i(t) \delta J_j(t') \rangle = \text{Var}[J] \, \delta_{ij} \, \delta(t - t') \, . \tag{5.12}$$

Note that local current fluctuations are due to the fact that each particle advances randomly at a given rate (set equal to 1), with an exponential distribution of waiting times (in the low density limit).

5.3.2 Gradient expansion

We will now derive a continuous version of the discrete BL equations, Eq. (5.10). To this end we set $x = ia$ and introduce fields $\phi(x,t) = \delta\rho_i(t)$ and $\eta(x,t) = \delta J_i(t)$ for the density and current fluctuations, respectively. Then we get to leading order in a gradient expansion

$$\partial_t \phi(x,t) + (v - 2\phi)\partial_x \phi = \frac{1}{2}\partial_x^2 \phi - \partial_x \eta \, , \tag{5.13}$$

where from now on we measure all length scales in units of the lattice spacing a. Eq. (5.13) has previously been derived along similar lines in Ref. [84]. The noise correlations are given by

$$\langle \eta(x,t)\eta(x',t') \rangle = A\delta(x - x')\delta(t - t') \tag{5.14}$$

with an amplitude $A = \overline{\rho}(1 - \overline{\rho})[1 - \overline{\rho}(1 - \overline{\rho})]$. We have also introduced the collective velocity $v = 1 - 2\overline{\rho}$, which happen to coincide with the expression obtained from the exact non-equilibrium fluctuation-dissipation theorem $v = \partial_\rho J(\rho)$ of an infinite lattice gas [81]. Note that v changes sign at $\overline{\rho} = \frac{1}{2}$ where the stationary current becomes maximal.

The convective nonlinearity $\phi\partial_x\phi$ in Eq. (5.13) can be read as a "shift" in the collective velocity due to fluctuations, which we expect to become important for small v, i.e. close to the phase boundaries between the low and high density phases and the maximal current phase. For densities far away from $\overline{\rho} = 1/2$ we will neglect those nonlinearities. Then, as will be discussed in the next subsection, one can work out all the correlation functions explicitly. These will then be used as a guidance for the discussion of the Monte-Carlo results in section 5.5.

For $\overline{\rho} = \frac{1}{2}$ Eq. (5.13) is identical to the one-dimensional *Burgers equation* [49], which can be mapped onto the Kardar-Parisi-Zhang (KPZ) [74] equation upon introducing a new field h via $\phi = \partial_x h$. The Burgers equation is known to give the following scaling form for the correlation function $C(x,t) = \langle \phi(x,t)\phi(0,0) \rangle$ [49], (see 5.B):

$$C(x,t) = x^{2\chi-2}F(t/x^z) \, . \tag{5.15}$$

Here the roughness exponent χ describes the scaling of the width of the interface, and the dynamic exponent z characterizes the spread in time of disturbances on the surface. In the present case the roughness and the dynamic exponent are known to be [49]

$$\chi = \frac{1}{2}, \quad \text{and} \quad z = \frac{3}{2} \, . \tag{5.16a}$$

This basically means that the system at the critical point relaxes super-diffusively i.e. $C(0,t) \sim t^{-1/z}$ with $z < 2$.

5.3.3 Correlation functions of the linearized Boltzmann-Langevin equation

The linearized Boltzmann-Langevin equation is most conveniently analyzed in Fourier space, where it reads

$$\left[i\omega - ivq + \frac{1}{2}q^2 \right] \phi(q,\omega) = iq\,\eta(q,\omega)\,. \tag{5.17}$$

From this one can immediately infer for the correlation function $C(x - x', t - t') = \langle \phi(x,t)\phi(x',t') \rangle$ in Fourier space

$$C(q,\omega) = \frac{Aq^2}{\left(\omega - vq\right)^2 + \frac{1}{4}q^4}\,, \tag{5.18}$$

and direct space

$$C(x,t) = \frac{A}{\sqrt{2\pi\,|t|}} \exp\left[-\frac{(x - vt)^2}{2|t|} \right]\,. \tag{5.19}$$

Note that $C(x,t)$ is a Gaussian whose center moves with a drift velocity $v = 1 - 2\overline{\rho}$ and which broadens diffusively starting from a δ-function at $t = 0$; height $H(t)$ and width $W(t)$ are given by

$$H(t) = \frac{A}{\sqrt{2\pi|t|}}\,, \tag{5.20}$$

$$W(t) = 2\sqrt{|t|}\,. \tag{5.21}$$

The on-site correlation function decays exponentially for $v \neq 0$,

$$C(0,t) = \frac{A}{\sqrt{2\pi\,|t|}} \exp\left[-\frac{v^2}{2}\,|t| \right]\,. \tag{5.22}$$

For $v = 0$, $C(0,t)$ scales as $t^{-1/2}$ as well as $C(0,\omega)$ like $\omega^{-1/2}$. Note also that the static limit of the correlation function for the linearized theory is

$$\lim_{\omega \to 0} C(q,\omega) = \frac{4A}{4v^2 + q^2} \tag{5.23}$$

which is identical to the correlation function for a Landau theory in a Gaussian approximation usually found in equilibrium thermodynamics [54]. This result suggests that linearized BL theory can be viewed as the analog of the Gaussian approximation for driven lattice gases. The form of Eq. (5.23) implies a correlation length of $1/2v$ which diverges at the critical point $\overline{\rho} = 1/2$.

5.4 Monte-Carlo simulation methods

Of course, linearized Boltzmann-Langevin theory is valid only for very low densities (i.e. low values of α). To go beyond this low density limit and test the range of validity of the linearized BL approach we have performed extensive Monte-Carlo (MC) simulations. To this end we have chosen the random sequential updating algorithm by Bortz, Kalos and Lebowitz (BKL- or n-fold method) [15, 89]. Since it keeps a list of all sites which are possible candidates for a successful update it is (for the present case) faster than conventional methods. Moreover it constitutes a reliable way to simulate *real time* dynamics and achieve an excellent quality in terms of data and computational efficiency in both short and long time regimes.

In a first step one generates a random number $X \in [0, 1)$, that determines which one of the following moves is chosen: a particle entering the system, a particle leaving the system and particle at site i jumping to the right. Then, for a given move a time interval Δt is chosen from an exponential waiting time distribution, where the decay time depends on the size of the list.

In all of our Monte-Carlo runs we started from a configuration generated according to the steady state distribution in order to reduce initial transient effects. After equilibration correlation functions were measured and moving time averages over $O(10^7)$ time windows were performed. Average profiles and correlations do not show any differences between moving time and ensemble average giving explicit proof for ergodicity of the system.

5.5 Dynamic correlation functions

In this section we analyze the correlation function $C(x, t)$ of the density fluctuations $\phi(x, t)$ in space and time. From now on we take $x = 0$ as the central site of the system such that the system is confined to the interval $[-L/2, L/2]$. This is meant to minimize, at least for short times, the influence of the system boundaries. We assume that the system is in a stationary state at the reference time $t = 0$.

As expected from the linearized BL equation, the simulations show that the correlation function starts from a δ-function peaked at the reference site and then moves to the right with velocity v and spreads diffusively as time progresses; for negative times it moves to the left (see Figs. 5.1). Note that our simulations confirm that the peak of the correlation function moves with exactly the collective velocity $v = 1 - 2\overline{\rho}$.

In the following we are going to discuss the form and the time evolution of the correlation function in the α-β plane. Our simulations have been performed mainly along the anti-diagonal $\alpha = 1 - \beta$. This has the advantage that the exact steady state profile is perfectly flat, such that boundary effects are greatly reduced; moreover mean field theory predicts exactly $\overline{\rho} = \alpha$.

Before we enter the discussion let us have a closer look at the characteristic time scales of the system. Correlation functions decay on a scale (see Eq. 5.22)

$$\tau_{\text{relax}} = 2/v^2 \,, \tag{5.24}$$

but at the same time the maximum of the correlation function moves with a velocity v such that it propagates the finite length L of the track in a time

$$\tau_{\text{prop}} = \frac{L/2}{v}.$$
(5.25)

This implies that one can observe the relaxation of the correlation functions only if $\tau_{\text{prop}}/\tau_{\text{relax}} = v\frac{L}{4} \geq 1$, i.e. for rates α and β not too close to the phase boundary to the maximal current phase and of course for large enough systems.

5.5.1   Low density and high density phase

Due to particle-hole symmetry we restrict our discussion to the low density regime. The results for the high density phase are obtained upon simply replacing α by $1 - \beta$.

Figures 5.1 show time series of the correlation function for entrance rates $\alpha = 0.01$ and $\alpha = 0.1$, respectively. In both cases the correlation functions start from a δ-function peak at $t = 0$ which then broadens diffusively with the width scaling as $t^{1/2}$ and the height decreasing as $t^{-1/2}$. Correspondingly the maximum propagates to the right or left with velocity $v = 1 - 2\overline{\rho}$ for $\overline{\rho} < 1/2$ and $\overline{\rho} > 1/2$, respectively (by particle-hole symmetry). As noted above this is an exact result valid for all values of the entrance and exit rates. In Fig. 5.1 we have also shown results for negative time to highlight the symmetry $x \to -x$ and $t \to -t$ which appears in Eq. (5.19).

For low values of α, which corresponds to the low density limit, the results from the linearized BL equations explain the Monte-Carlo results quantitatively. The theory still gives the correct qualitative picture for larger values of α but shows significant quantitative deviations. The actual shapes of the correlation functions have a lower height and are broader than the linearized theory predicts. Nevertheless, the peak height measured in the simulations still shows the $t^{-1/2}$ scaling of the linear theory for values of α not to close to $\alpha = \frac{1}{2}$; see Fig. 5.2.

As can be inferred from Fig. 5.2 the effective exponent describing the peak relaxation slowly crosses over from $1/2$ to $2/3$ upon approaching the critical point $(\alpha, \beta) = (1/2, 1/2)$ along the anti-diagonal of the phase diagram. The exponent $2/3$ is identical to the inverse of the dynamic exponent $1/z$ of the non-linear BL equation (Burgers equation); see Eqs. (5.13) and (5.16).

5.5.2   Coexistence line ($\alpha = \beta < 1/2$)

At the coexistence line the density profile is characterized by a fluctuating domain wall separating a low density from a high density phase. The dynamics of the domain wall can be described as a symmetric random walk with reflecting boundary conditions [81, 132]. In addition to the domain wall motion, a collective mode, there are still stochastic fluctuations of the density in the low and high density wings of the domain wall. Both of these modes should be visible in a measurement of the density-density correlation function.
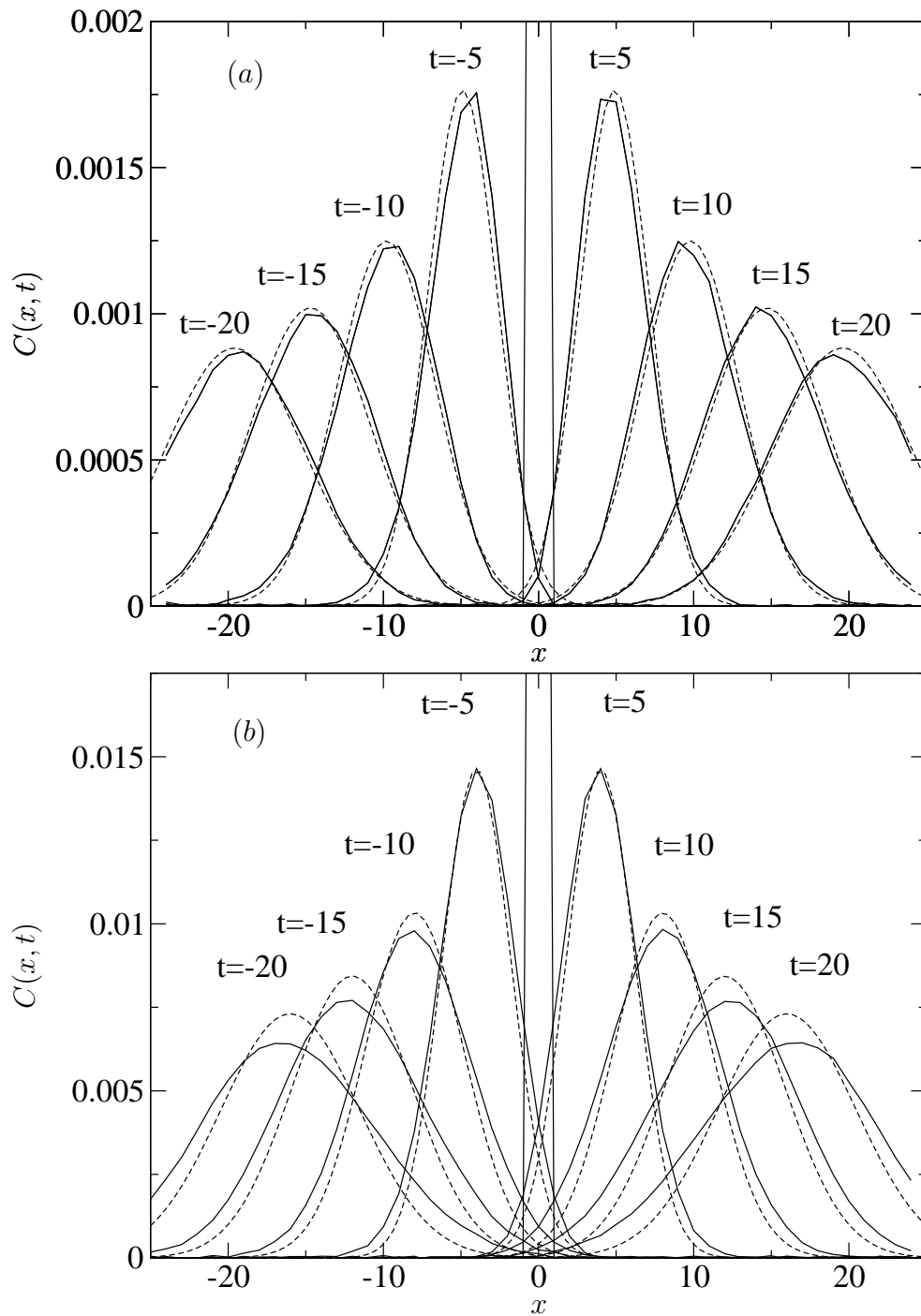
Figure 5.1: Time and space dependent correlation function for a system of 50 sites with rates (a) $\alpha = 0.01$ and $\beta = 0.99$ and (b) $\alpha = 0.1$ and $\beta = 0.9$. Averages are taken over 10 million samples. For the diluted system there is good agreement between the linearized Boltzmann-Langevin theory (dashed line) and the Monte-Carlo simulations (solid line). For denser systems the agreement is only qualitative.
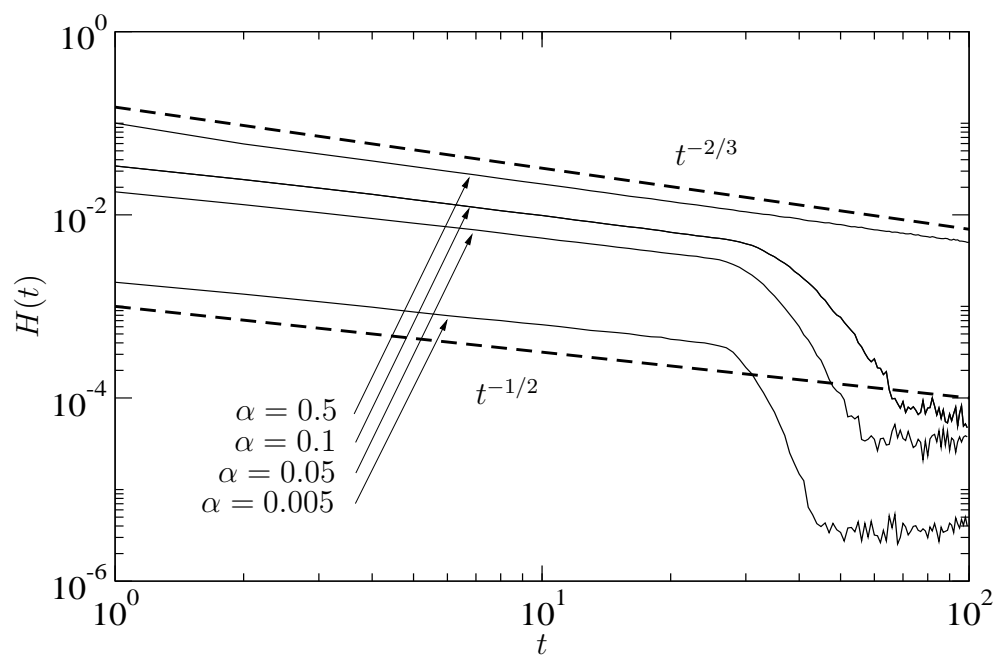
Figure 5.2: Peak height of the correlation function for a system of $N = 50$ sites and a series of entrance rates $\alpha = 0.005$, 0.05, 0.1, 0.5; we have taken $\beta = 1 - \alpha$. Averages of the MC data are taken over 10 millions samples. Upon approaching the critical point $(\alpha, \beta) = (1/2, 1/2)$ the peak height shows a power law behavior with an effective exponent slowly changing from $1/2$ to $2/3$, shown as dashed lines in the graph.
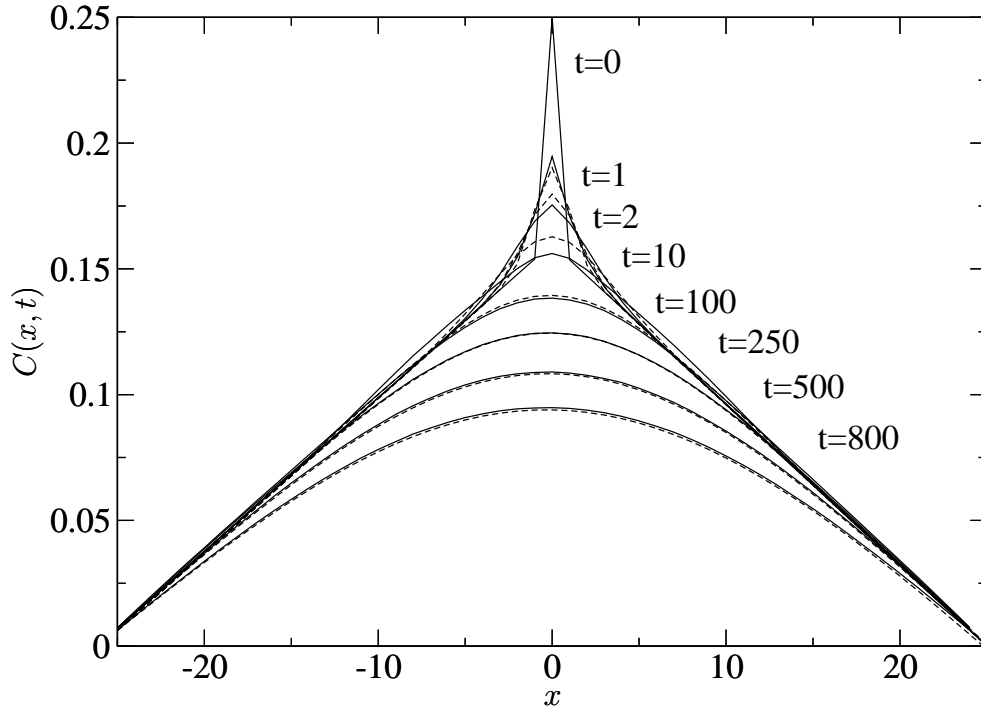
Figure 5.3: Time series of the correlation function $C(x,t)$ versus x for $\alpha = 0.1$ and $\beta = 0.1$; the times are indicated in the graph. The MC data for a system with $N = 50$ sites (solid lines) are compared with a hybrid theory combining local density fluctuations described by the Boltzmann-Langevin equation and the collective domain wall motion (dashed lines). Averages in the MC data are taken over 10 million samples.

Indeed, the profile of the correlation function shows two distinct features; see Fig. 5.3. At $t = 0$ there is a sharp triangle on top of a much broader triangular base. The sharp tip is a result of the local density (BL) fluctuations and can be explained as follows. Consider the correlation function of local density fluctuations $C_{ij}^{\mathrm{BL}}(t) = \langle \phi_i(t)\phi_j(0) \rangle$ on a lattice. Since there are no correlations in the bulk of the system for $t = 0$ it reduces to $C_{ij}^{\mathrm{BL}}(0) = (\langle n_i^2 \rangle - \langle n_i \rangle^2)\delta_{ij}$. Finally, upon using that the occupation numbers are binary variables and the average density in the middle of the system is $\langle n_0 \rangle = \frac{1}{2}$, we obtain $C_{i0}^{\mathrm{BL}} = \frac{1}{4}\delta_{i0}$. The width of the sharp tip is actually a finite size effect resulting from the linear interpolation of the data points. The broader triangular base is explained below in the context of DW theory.

The MC simulations show that the sharp tip quickly relaxes and broadens, whereas the shape of the triangular base evolves on a much larger time scale.

One can rationalize this behavior upon combining results from the DW and BL theory. We start with a discussion of the local density fluctuations. One can derive the short time dynamics for the correlation function from the lattice version of the BL equation, Eq. (5.10), imposing the initial condition $C_{i0}^{\mathrm{BL}}(t = 0) = \frac{1}{4}\delta_{i0}$. As explicitly shown in Appendix 5.A

one finds for the on-site correlation function $C_{00}^{\mathrm{BL}}(t) \sim \frac{1}{4} - \frac{1}{4}|t| + O(t^2)$, while the nearest and next-nearest neighbor correlation functions read as $C_{01}^{\mathrm{BL}}(t) \sim t$ and $C_{02}^{\mathrm{BL}}(t) \sim t^2$. This explains the fast relaxation of the central peak.

In order to understand the broadening of the triangular base we first have to recapitulate some key results of the DW theory [81, 36]. Since one can model the domain wall as a symmetric random walker with reflecting boundary conditions at both ends of the system, the conditional probability of finding the domain wall at site ξ_t at time t given that it was at site ξ_0 at time $t = 0$ reads [133]

$$
\begin{aligned}
P(\xi_t|\xi_0) = & \frac{1}{L} + \frac{2}{L} \sum_{i:\mathrm{even}} e^{-\lambda_i^2 \mathcal{D}t} \cos \lambda_i \xi_t \cos \lambda_i \xi_0 \\
& + \frac{2}{L} \sum_{i:\mathrm{odd}} e^{-\lambda_i^2 \mathcal{D}t} \sin \lambda_i \xi_t \sin \lambda_i \xi_0 ,
\end{aligned}
\tag{5.26}
$$

where $\lambda_i = i\pi/L$ and $\mathcal{D} = \alpha(1-\alpha)/(1-2\alpha)$ is the diffusion constant. Note that this diffusion coefficient is smaller than the one of the BL fluctuations (which is 1), $\mathcal{D} \sim \alpha < 1$, which explains the time-scale separation mentioned above. Averages of an observable $\mathcal{O}$ are understood as integrals over the random variable ξ_t

$$
\langle \mathcal{O}(t,t')\rangle = \int d\xi_t \int d\xi_{t'} P_{\mathrm{st}}(\xi_{t'}) \mathcal{O}(t,t') P(\xi_t|\xi_{t'}) ,
\tag{5.27}
$$

where $P_{\mathrm{st}}(\xi)$ is the stationary probability distribution function. In the present case it is simply a constant, $P_{\mathrm{st}} = 1/L$.

If one approximates the density profile of the domain wall (DW) by a step function, $\psi(x,t) = \alpha + (1-2\alpha)\theta(x - \xi_t)$, the correlation function can easily be calculated as

$$
C^{\mathrm{DW}}(x,x',t-t') = \langle \psi_{\mathrm{d}}(x,t)\psi_{\mathrm{d}}(x',t')\rangle - \langle \psi_{\mathrm{d}}(x,t)\rangle \langle \psi_{\mathrm{d}}(x',t')\rangle =
$$
$$
\frac{2(1-2\alpha)^2}{L^2} \left[\sum_{i:\mathrm{even}} \frac{e^{-\lambda_i^2 \mathcal{D}|t-t'|}}{\lambda_i^2} \cos \lambda_i x \cos \lambda_i x' + \sum_{i:\mathrm{odd}} \frac{e^{-\lambda_i^2 \mathcal{D}|t-t'|}}{\lambda_i^2} \sin \lambda_i x \sin \lambda_i x' \right] .
\tag{5.28}
$$

Here we are mainly interested in the dynamics at time scales $t < L^2/\mathcal{D}$ (so that the system size is large, $L^2 > t\mathcal{D}$, and λ_i is infinitesimal), where the domain wall has not explored the full system yet. Then the sum in Eq. (5.28) can be approximated by an integral, and one finds

$$
\begin{aligned}
C^{\mathrm{DW}}(x,t) = & \frac{1}{2L}(1-2\alpha)^2 \left\{ \left[|x+L|\mathrm{Erf}\left(\frac{|x+L|}{\sqrt{4\mathcal{D}|t|}}\right) - |x|\mathrm{Erf}\left(\frac{|x|}{\sqrt{4\mathcal{D}|t|}}\right) \right] + \right. \\
& \left. + \left(e^{\frac{-(x+L)^2}{4\mathcal{D}|t|}} - e^{\frac{-x^2}{4\mathcal{D}|t|}} \right) \sqrt{\frac{4\mathcal{D}|t|}{\pi}} - \left(x + \frac{L}{2} \right) \right\} .
\end{aligned}
\tag{5.29}
$$

In the limit $t \to 0$ this exactly reduces to the profile of the broad triangular base in Fig.5.3. If one would be allowed to just sum the correlation functions obtained from domain wall

and local density fluctuations, this would fully explain the initial shape of the correlation function. Of course, this is not valid rigorously but seems to be a reasonable approximation. One may argue that the validity of the approximation is due to the time and length scale separation between the local density fluctuations and the collective domain wall motion.

In this spirit we assume that the total density fluctuations Φ can be written as a superposition of local density and domain wall fluctuations, $\Phi(x,t) = \phi(x,t) + \psi(x,t)$, and that these fluctuations are uncorrelated, $\langle \phi\psi \rangle = \langle \phi \rangle \langle \psi \rangle$. Then the full correlation function can be written as a sum

$$C(x,t) = C^{\mathrm{BL}}(x,t) + C^{\mathrm{DW}}(x,t) \tag{5.30}$$

with $C^{\mathrm{DW}}(x,t)$ given by Eq. (5.29) and the local density correlations $C^{\mathrm{BL}}(x,t)$ are obtained either from the continuous or the lattice BL equations depending on the time scale. Note that the density fluctuations on both wings of the domain wall are the same since the average low ($\rho_- = \alpha$) and high ($\rho_+ = 1 - \alpha$) density lead to the same noise amplitude A. Hence we may describe these local density fluctuations by a BL equation with $v = 0$ and $A = \alpha(1-\alpha)(1-\alpha(1-\alpha))$. As can be inferred from Fig. 5.3 the corresponding analytical results compare reasonably well with MC data.

A convenient way for visualizing the various dynamic regimes resulting from domain wall and local density fluctuations is the power spectrum

$$I(\omega) \equiv \frac{1}{T} \left\langle |\Phi(0,\omega)|^2 \right\rangle , \tag{5.31}$$

where T is the total time of integration. It is obvious from Figs. 5.4 and 5.5 that there are three distinct dynamical regimes.

The DW theory, as described above, fully explains the low frequency power law regime $I(\omega) \sim \omega^{-3/2}$. As can easily be shown from specializing Eq. (5.29) to $x = 0$, one finds $I(\omega) \sim L^{-1}\omega^{-3/2}$ [144]. The time window where DW theory is valid ranges from the hopping time $\tau_1 = 1/\mathcal{D}$ to the time needed to travel a distance comparable to the system size $\tau_L \sim L^2/\mathcal{D}$ (note that L is dimensionless). For larger times one expects finite size effects. In frequency space this corresponds to the domain $[\mathcal{D}/L^2, \mathcal{D}]$.

For frequencies larger than $\omega_1 \geq \mathcal{D}$ the dynamics is dominated by local density fluctuations. Those are well described within BL theory. Note that contrary to the fluctuations of the domain wall, these local density fluctuations are independent of the system size; see Figs. 5.4 and 5.5. For time scales larger than the microscopic hopping time of an individual particle (which we have set to 1), one can use the continuum version of the BL theory. Hence for $\omega \leq 1$ one expects $I(\omega) \sim \omega^{-1/2}$ which agrees very well with our MC data; note that when $\alpha = \beta \approx 0$ the distinction is clear (Fig. 5.4) while for $\alpha = \beta \lesssim 1/2$ not only the time scales but also the amplitudes become comparable since $A = \alpha(1-\alpha)(1-\alpha(1-\alpha))$ and $C^{\mathrm{DW}}(0,0) \sim (1-2\alpha)^2/4$ (from Eq. 5.29). Therefore (see Fig. 5.5) the distinction between BL and DW regime becomes clearly visible only at very large time (and large systems). At the critical point the amplitude of the DW correlation is identical to zero (see Eq. 5.28) and therefore the fluctuations are described by BL in its non-linear version.
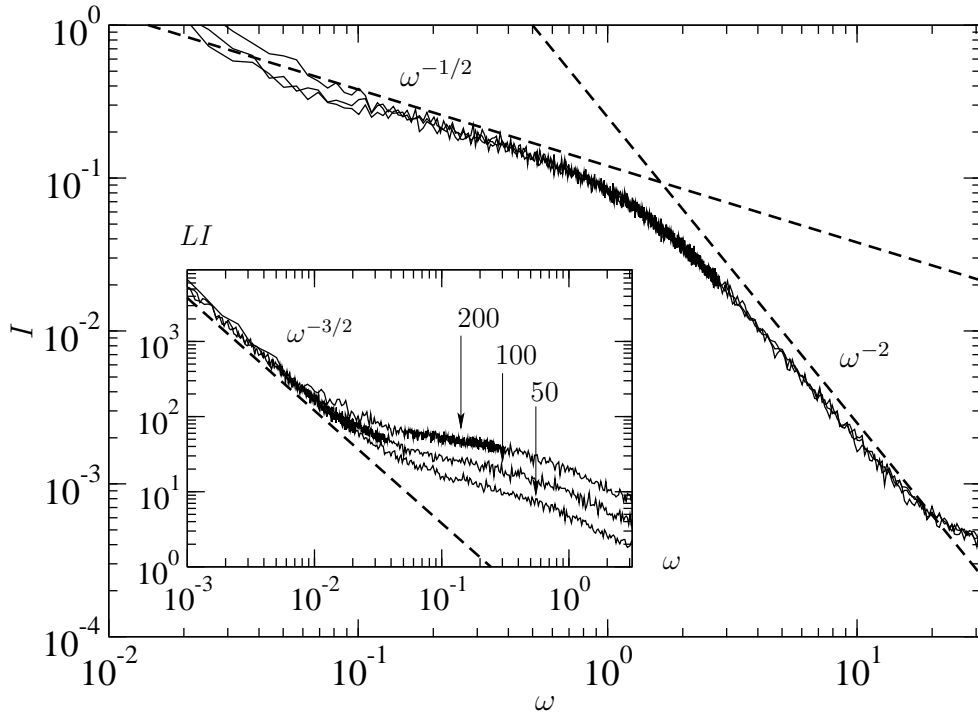
Figure 5.4: Power spectrum for systems of 200, 100 and 50 sites and rates $\alpha = \beta = 0.1$. Averages are taken over 256 samples. The large frequency behavior is dominated by local density fluctuations and well described within a BL theory, while the small frequency regime is dominated by domain wall fluctuations, as a collective mode. The high resolution allows for the identification of a dynamic regime due to the discrete nature of density fluctuations at very short time. **Inset:** rescaled power spectrum showing the long time (small frequency) regime dominated by the DW dynamics.

For larger frequencies one has to account for lattice effects. If one applies the lattice version of the BL theory one finds (see appendix 5.A)

$$C_k(\omega) = \frac{2(1 - \cos(\frac{k\pi}{L}))A}{\omega^2 + \left(1 - \cos(\frac{k\pi}{L})\right)^2} \, . \tag{5.32}$$

In order to obtain the power spectrum $C_k(\omega)$ has to be summed over all modes numbers k. The dominant contribution for large frequencies are due to wave vectors close to the zone boundary, $k = L/2$ resulting in a power spectrum $I(\omega) \sim \omega^{-2}$, which is again well confirmed by our MC data (Figs. 5.4 and 5.5).

5.5.3   Critical Point $\alpha = \beta = 1/2$

For completeness we shortly discuss our results for the correlation function right at the
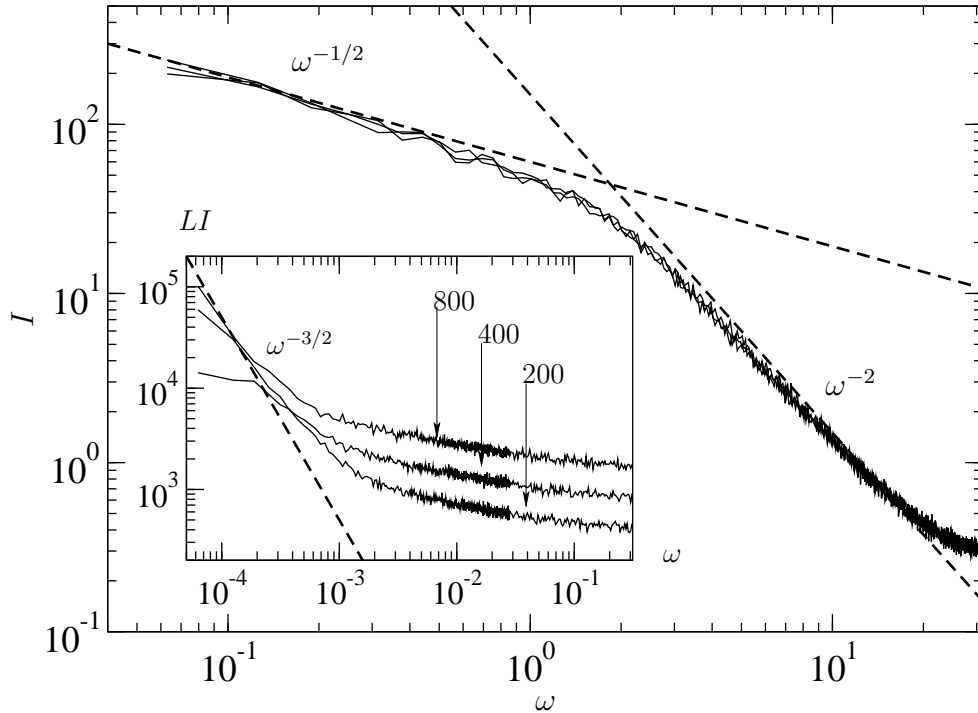
Figure 5.5: Power spectrum for systems of 800, 400 and 200 sites and rates $\alpha = \beta = 0.4$. Averages are taken over 256 samples. The large frequency behavior is dominated by local density fluctuations and well described within a BL theory, while the small frequency regime is dominated by domain wall fluctuations, as a collective mode. **Inset:** rescaled power spectrum showing the long time regime dominated by the DW dynamics. When the time scale of the DW and BL dynamics are comparable the separation between the two dynamics, although still present, is not as sharp as in Fig. 5.4.

critical point ($\alpha = \beta = 1/2$). As can be inferred from Fig. 5.6 the temporal evolution of its shape is qualitatively and quantitatively different from the low and high density phases.

The critical exponents are obtained from a finite size scaling analysis of the height and width of the correlation function. The insets of Figs. 5.7 a and b show Monte-Carlo data for system sizes $N = 10$, $N = 25$ and $N = 50$. These data can be re-plotted upon using the finite size scaling relations for the height and width, respectively,

$$C(x = 0, t) = L^{2\chi - 2} g(t/L^z) = L^{-1} g(t/L^{\frac{3}{2}}) \,, \tag{5.33}$$

$$W(t) = L^{\frac{2\chi + 1}{2}} f(t/L^z) = L f(t/L^{\frac{3}{2}}) \,, \tag{5.34}$$

which will give us numerical values for the critical exponents.

The critical exponents were determined using an algorithm provided by the authors of Ref.[10]. This code computes and minimizes a sum which weights the distance from an interpolating function based on all the given sequences of data. Errors are extracted
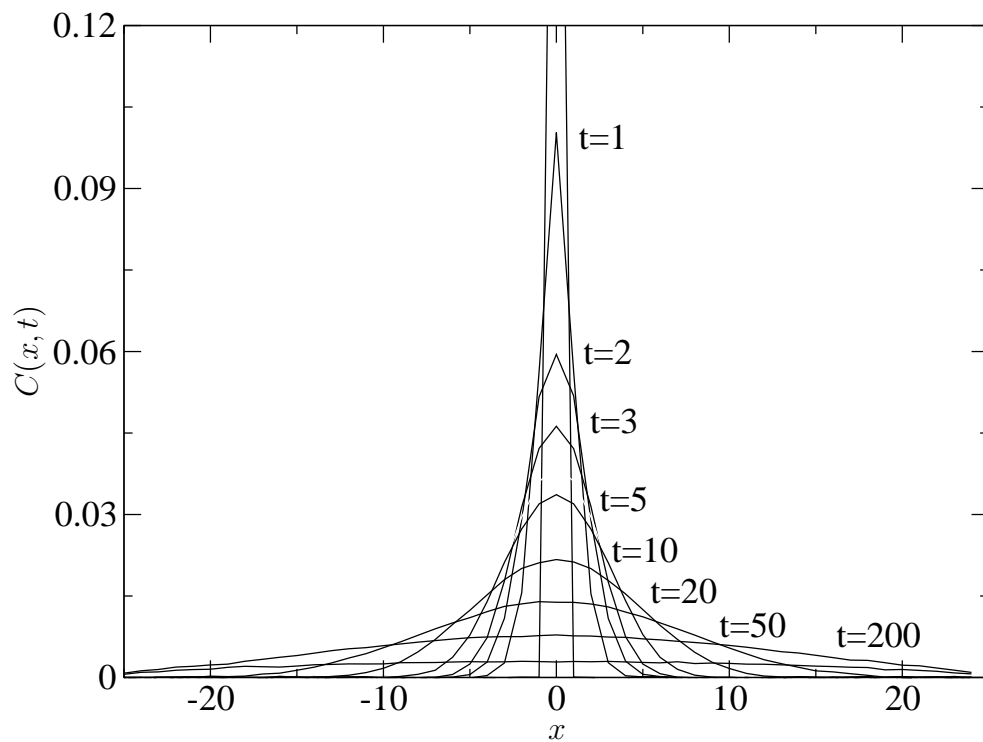
Figure 5.6: Time series of the correlation function $C(x,t)$ versus x at the critical point ($\alpha = 0.5$ and $\beta = 0.5$); the times are indicated in the graph; the system size is $N = 50$. Averages are taken over 10 million samples.
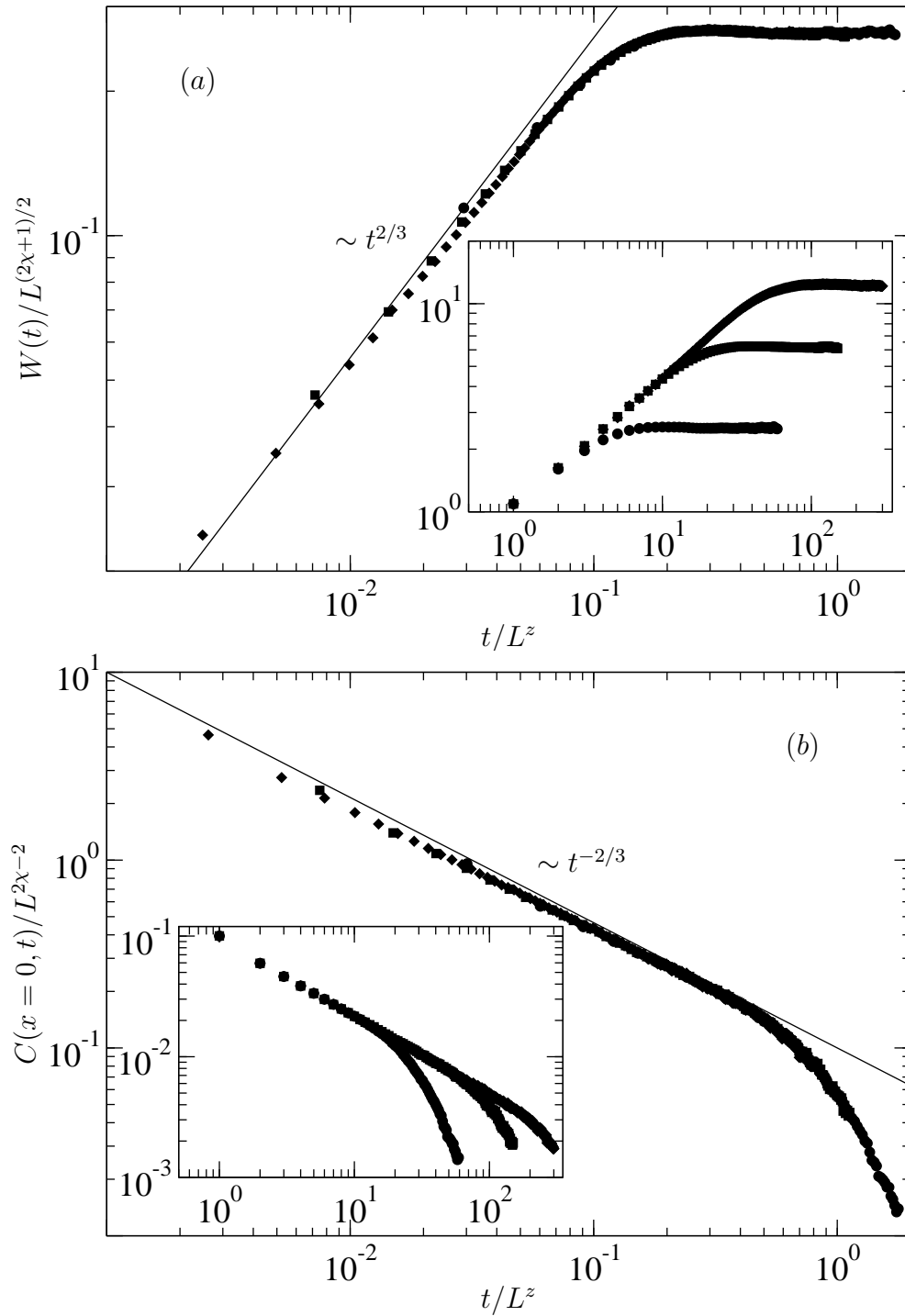
Figure 5.7: (a) Width of the correlation function and (b) autocorrelation. Averages are computed using 10^7 samples at the critical point $\alpha = \beta = 1/2$. The data are rescaled according to Eqs. (5.34) and (5.33) with the exponents presented in the text. Insets show the plots before rescaling.

measuring the width of the minimum of such function (which has been tested to be zero if the values are exact). From this we obtain for the autocorrelation (peak) $2\chi = 0.98 \pm 0.03$ and $z = 1.52 \pm 0.02$, and consistently $2\chi = 0.92 \pm 0.09$ and $z = 1.53 \pm 0.08$ for the width. It constitutes direct numerical evidence for the system belonging to the KPZ universality class ($2\chi = 1$ and $z = 3/2$), as expected from earlier analytical results for periodic systems. Our measurements confirm the numerical results in Ref. [69].

5.6 Boltzmann Langevin method for TASEP of dimers

Basing our calculations on the Ch. 3, we give herafter a first description of the dynamics of the local fluctuations using the Boltzmann Langevin (BL) method in a system of dimers. The result is just a qualitative check that the BL method actually predicts the right dynamics in the critical regime also for the case of extended particles.

Starting from the mean field equation presented in Ch. 3 (Eq. 3.25), we perturbed it via the usual substitution required from BL:

$$n_i \approx \overline{\rho} + \delta\phi \tag{5.35}$$

$$J_i \approx \frac{\rho_i(1 - \overline{\rho}_{i+1} - \overline{\rho}_{i+2})}{1 - \overline{\rho}_{i+1}} + \eta_i \tag{5.36}$$

In this case we have inserted the parameter δ to easily expand $1/(1 - \overline{\rho} - \delta\phi)$ in the following: we are implicitly assuming that the fluctuations (and their derivatives) are small compared to the density. We expand in δ (perturbative parameter) and in ϵ (lattice constant). Finally we subtracts to the result the well known mean field equation 3.25 obtaining an equation for the fluctuations:

$$\partial_t\phi = -\frac{\epsilon}{1 - \overline{\rho}}(v - 2\phi)\partial_x\phi + \frac{\epsilon^2}{2(1 - \overline{\rho})^2}\left[\partial_x^2\phi + \frac{2}{1 - \overline{\rho}}\partial_x(\phi\partial_x\phi)\right] - \partial_x\eta \tag{5.37}$$

where we have introduced the effective velocity $v \equiv 1 - 4\overline{\rho} + 2\overline{\rho}^2$. To complete the picture we need as well the correlations of the current fluctuation $\langle\eta(x,t)\eta(x',t')\rangle = A\delta(x - x')\delta(t - t')$ with $A = \langle j\rangle(1 - \langle j\rangle) =$. If we assume the fluctuations to be smooth the second order non-linear term $(\phi\phi')')$ does not matter (this approximation is indeed rather crude). The linearized BL equation, valid for dilute systems, therefore reads:

$$\partial_t\phi = -\frac{\epsilon v}{1 - \overline{\rho}}v\partial_x\phi + \frac{\epsilon^2}{2(1 - \overline{\rho})^2}\partial_x^2\phi - \partial_x\eta \tag{5.38}$$

By mean of a Fourier transform and the using the fluctuations of the current we find a correlation function, which looks again like a Gaussian which moves with velocity v and spreads with density-dependent diffusion constant $D = 1/(1 - \overline{\rho})$ (while in the simple TASEP it was simply $D = 1$). Note that the velocity is already non-trivial and is different from the one of the single particle (which is from the current-density relation $(1 - 2\rho)/(1 - \rho)$).

At the critical density $\overline{\rho} = \rho^*$ the velocity v is zero. Upon introducing the rescaled lattice constant $a/(1 - \overline{\rho}) = 1$ we obtain the well known noisy Burgers equation:

$$\partial_t \phi - \phi \partial_x \phi = \frac{1}{2} \partial_x^2 \phi - \partial_x \eta \tag{5.39}$$

The model has been analytically proved [3] to belong to the same universality class of the KPZ equation on which the Burgers can be mapped.

As a check of the theory we performed Monte Carlo simulations for systems with flat density profiles and measure the decay of the peak. As presented in Fig. 5.8(a) the maximum move with the velocity predicted by the BL theory, although the agreement is worse than in the case of monomers.

At the same time (see Fig. 5.8(b)) the correlation function relaxes with the diffusive power law $t^{-1/2}$ for $\rho < \rho^*$ and with the sub-diffusive (KPZ) scaling for $\rho \geq \rho^*$, as predicted by the Burgers equations.
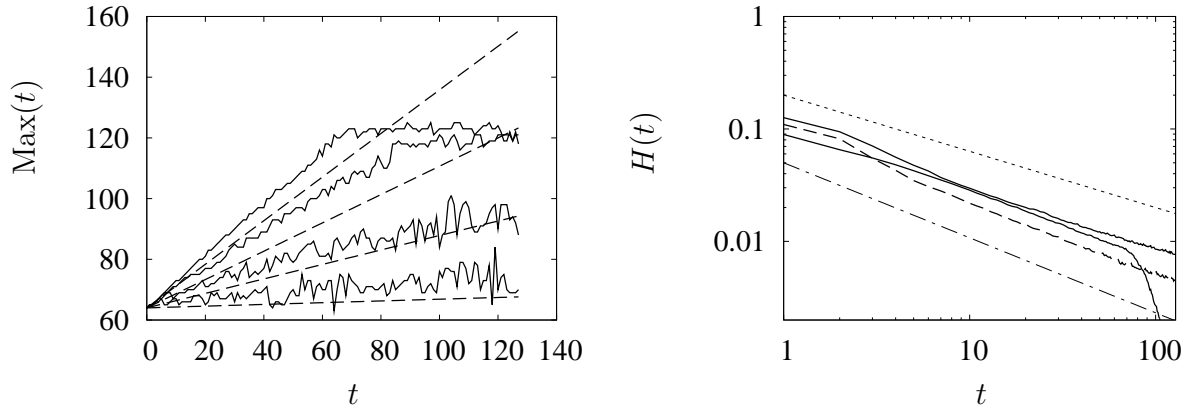
(a) Position of the maximum of the correlation function for different parameters (solid) and comparison with the prediction by BL theory (dashed). Parameters (top to down): $(\alpha, \beta) = (0.1, 0.8182)$, $(0.2, 0.67)$, $(0.3, 0.358)$, $(0.4, 0.43)$ and $N = 128$.

(b) Peak height of the peak of the correlation function for a system of $N = 128$ sites. Simulations (solid, $(\alpha, \beta) = (0.1, 0.8182)$ and $(0.3, 0.358)$, and dashed $(0.4142, 0.4142)$) are compared with the reference power laws $t^{-1/2}$ (dotted) $t^{-2/3}$ (dot-dashed) predicted by BL theory. Compare with Fig. (5.2).

Figure 5.8: Properties of the maximum of the correlation function. The position $Max(t)$ and height $H(t)$ of the peak of the correlation function are compared for different parameters with the theoretical value. As can be seen from the graph the agreement is a bit worse than in the case of monomers but still rather good.

We checked as well the interplay with the domain wall found in the case of monomers in Subsec. 5.5.2 for parameters that allow the formation of a localized domain wall. Studies of the power spectrum (see Fig.5.9) show the three regimes found in the case of monomer: a power law $\omega^{-1/2}$ at short time (large frequencies) due to the discreteness of the lattice, ω^{-2} at intermediate regimes where BL theory is valid, $\omega^{-3/2}$ at long time (small frequencies) that indicates the long time correlations are due to the domain wall motion.
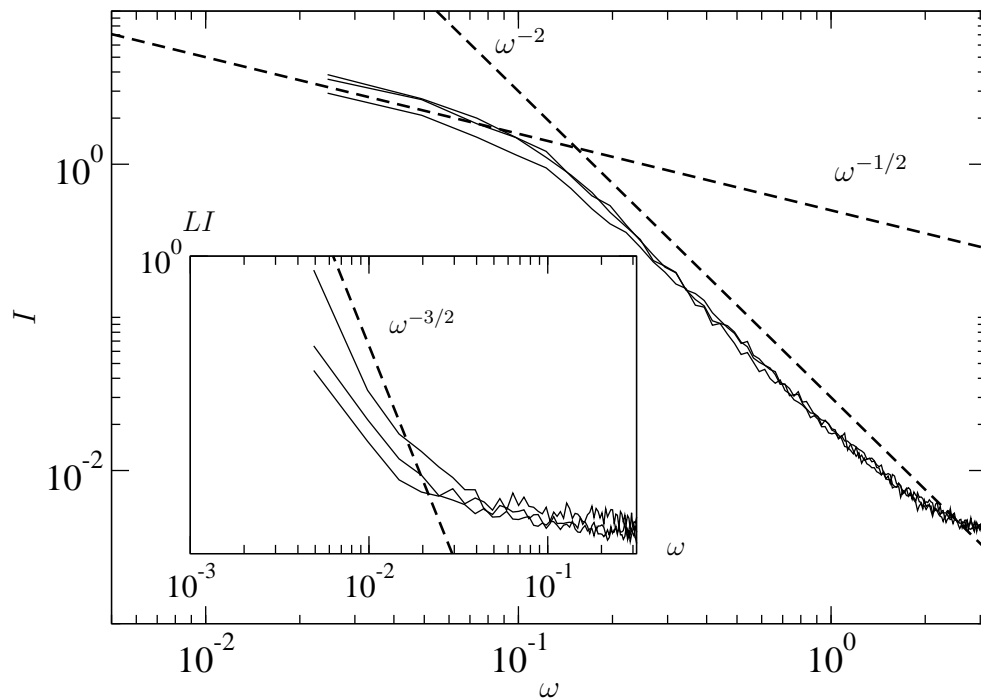
Figure 5.9: Power spectrum for systems of 128, 256 and 512 sites and rates $\alpha = \beta = 0.1$. Averages are taken over 256 samples. The large frequency behavior is dominated by local density fluctuations and well described within a BL theory, while the small frequency regime is dominated by domain wall fluctuations, as a collective mode. The high resolution allows for the identification of a dynamic regime due to the discrete nature of density fluctuations at very short time. **Inset:** rescaled power spectrum showing the long time (small frequency) regime dominated by the DW dynamics.

We take these agreements with the Monte Carlo data as a confirm that the refined mean field introduced in Ch. 3 is indeed correct. Even more puzzling is the fact that the BL method (that has not been so much applied to driven lattice gases) gives indeed the exact critical behavior also in the case of dimers. We hypothesize that the current density (predicted exactly by the refined mean field theory) enters the expansion performed in the BL and the critical behavior emerges from the exclusion (which is reflected in the concavity of $j(\rho)$ and in the effective particle-hole symmetry) and the presence of a maximum in the current density relation.

5.7   Conclusion

In conclusion we have analyzed the dynamics of the TASEP model over the whole parameter range of exit and entrance rate with emphasis on the behavior in the low and high density regime and the corresponding phase boundary. It turns out that most of the dynamics can be nicely explained in terms of the combined effect of local density fluctuations and collective domain wall motion. The dynamics of the domain wall is determined by the stochasticity in the entrance and exit of particles at the system boundaries. Depending on the parameters this yields to a random walk with or without drift towards the boundaries. For the description of the local density fluctuations we have adopted methods from kinetic theories for electronic transport, known as Boltzmann-Langevin approach. Both, the Boltzmann-Langevin and the domain wall approaches are to a large extent phenomenological and hence limited in the range of applicability. Hence we have complemented our studies by extensive Monte-Carlo simulations of the TASEP model using the BKL algorithm which allows us to study the real time dynamics with good accuracy. Our main findings are as follows. For very low densities, the linearized Boltzmann-Langevin theory accounts quantitatively for the shape of the density-density correlations. It becomes less accurate for densities approaching the maximal density of $1/2$ as expected from the approximate nature of the theory. Analogous arguments apply for very high densities by virtue of particle-hole symmetry. For densities close to $1/2$ linearized Boltzmann-Langevin theory is quantitatively wrong but still captures the main features qualitatively. Exactly at the critical point, $\alpha = \beta = 1/2$, the full Boltzmann-Langevin theory is identical to the noisy Burgers equation which is known to be in the same universality class as the TASEP model right at this point.

As summarized by the power spectra in Figs. 5.4 and 5.5 there is a time scale separation between the domain wall motion and the local density fluctuations. For frequencies larger than the hopping time of the domain wall $\mathcal{D}$ it is the local density fluctuations which dominate the spectrum. Upon using the continuous and the discrete version of the linearized Boltzmann-Langevin approach we can fully account for the crossover from $\omega^{-1/2}$ to ω^{-2} in the spectrum. For low frequencies $\omega < \mathcal{D}$ domain wall theory gives a power spectrum of $\omega^{-3/2}$ in agreement with the Monte-Carlo data.

A short study of systems with dimers, based on the refined mean field theory introduced in Ch. 3, confirms that the method, with some adaptations, can be applied to extended

particle and predicts correctly the Burgers equation in the critical regime.

In summary, two rather elementary approaches, domain wall and Boltzmann-Langevin theory, seem to capture most of the observed dynamics of the TASEP model. This suggests that it may be worthwhile to look for more complex systems which also could be described by these simple methods.

Appendix 5.A   Analysis of the BL equation on a discrete lattice

In this appendix we study the time behavior of the correlation function at short times, in the regime where the discreteness of the system plays a major role. We use $\phi_n(t) = \delta\rho_n(t)$ as the discrete equivalent of the field $\phi(x, t)$. We can write an equation of motion for the correlation function multiplying Eq. (5.10) by ϕ_n^0:

$$\frac{\mathrm{d}\langle \phi_n \phi_n^0 \rangle}{\mathrm{d}t} = \langle \phi_{n-1} \phi_n^0 \rangle (1 - \alpha) - \langle \phi_n \phi_n^0 \rangle +$$
$$+ \alpha \langle \phi_{n+1} \phi_n^0 \rangle - \langle \eta_n \phi_n^0 \rangle + \langle \eta_{n-1} \phi_n^0 \rangle \tag{5.40}$$

where $\overline{\rho} = \alpha$ and we neglect the non linear terms. This system of equations involves two point correlation functions for three different lattice sites, but can be written in a closed form (at least for short time regimes) by assuming that:

   i. $\langle \eta_n \phi_n^0 \rangle = 0$ which makes sense being the noise independent on the dynamics itself

   ii. $\langle \phi_{n-2} \phi_n^0 \rangle = 0$ which is reasonable for short time

   iii. $\langle \phi_m^0 \phi_n^0 \rangle = \frac{1}{4}\delta_{mn}$ (this originates the sharp tip in $C(x, t)$)

The central site of the system will be considered the reference site ($n = 0$). Defining $C_i(t) \equiv \langle \phi_{n+i}(t)\phi_n^0 \rangle$ we rewrite Eq. (5.40) as:

$$\frac{\mathrm{d}C_0}{\mathrm{d}t} = (1 - \alpha)C_{-1} - C_0 + \alpha C_{+1} \tag{5.41}$$

multiplying Eq. (5.40 for ϕ_{n-1} and ϕ_{n+1} by analogous reasoning we find a system of linear differential equations:

$$\frac{\mathrm{d}\vec{v}(t)}{\mathrm{d}t} = \hat{M}\vec{v}(t) \tag{5.42}$$

with $\vec{v} = (C_{-1}, C_0, C_{+1})^t$ and $\hat{M} = \begin{bmatrix} -1 & \alpha & 0 \\ 1-\alpha & -1 & \alpha \\ 0 & 1-\alpha & -1 \end{bmatrix}$ For the initial condition $\vec{v}_0 = (0, 1/4, 0)^t$ the solution $\vec{v}(t) = \exp(\hat{M}t)\vec{v}_0$ leads to

$$\begin{aligned} C_0(t) &= \frac{1}{4}e^{-t}\cosh\left(t\sqrt{2\alpha(1-\alpha)}\right) \\ &= \frac{1}{4} - \frac{1}{4}t + \frac{1}{4}(\frac{1}{2} + \alpha - \alpha^2)t^2 + O(t^3) \end{aligned} \tag{5.43}$$

At short time the autocorrelation decays linearly in time from a constant value $(1/4)$, while the other terms grow linearly:

$$
\begin{aligned}
C_{-1}(t) &= \frac{1}{4}\sqrt{\frac{\alpha}{1(1-\alpha)}}e^{-t}\sinh\left(t\sqrt{2\alpha(1-\alpha)}\right)\\
&= \frac{\alpha}{4}t - \frac{\alpha}{4}t^2 + O(t^3) & (5.44)\\
C_{+1}(t) &= C_{+1} = \frac{1}{4}\sqrt{\frac{1-\alpha}{2\alpha}}e^{-t}\sinh\left(t\sqrt{2\alpha(1-\alpha)}\right)\\
&= \frac{(1-\alpha)}{4}t - \frac{1-\alpha}{4}t^2 + O(t^3). & (5.45)
\end{aligned}
$$

Note that even relaxing hypothesis (2), assuming therefore $C_{\pm2} \neq 0$ and dealing with a larger matrix $\hat{M}$, one does not find correction to the leading behavior in time for $C_0(t)$, since correlation functions for more distant sites, as $C_{\pm2}$, scale as $C_{\pm2} \sim t^2$.

In order to look at the behavior in frequency space, we apply the BL scheme in the discrete lattice and extrapolate the regime of the correlation function at large ω. Let us start from the real space-time Boltzmann Langevin Eq. (5.10) and let us introduce the discrete Fourier transform $\phi_k = \sum_{n=-L/2}^{L/2} \phi_n e^{ikn\pi/L}$ where k indicate the mode number. In order to express the linearized BL equation in discrete Fourier space, we multiply Eq. (5.10) by $e^{ikn\pi/L}$ and sum over n. Even though the system is not translational invariant, in this limit the system can be considered as infinite and we do not take care of the boundaries. Performing a Fourier transform in time we get the discrete equivalent of Eq. (5.13):

$$
\left[i(\omega + 2\alpha\sin\frac{k\pi}{L}) + (1 - e^{\frac{ik\pi}{L}})\right]\phi_k(\omega) = \eta_k(\omega)(1 - e^{\frac{ik\pi}{L}}) \tag{5.46}
$$

and find the correlation function

$$
C_k(\omega) = \frac{2A\left(1 - \cos\frac{k\pi}{L}\right)}{\left(\omega - v\sin\frac{k\pi}{L}\right)^2 + \left(1 - \cos\frac{k\pi}{L}\right)^2} \tag{5.47}
$$

where we use the notation $v = 1 - 2\alpha$ and $A = \alpha(1 - \alpha(1 - \alpha))$ as done above.

The dominant contribution for large frequencies are due to wave vectors close to the zone boundary, $k = L/2$ resulting in a power spectrum $I(\omega) \sim \omega^{-2}$, which is again nicely confirmed by our MC data (Figs. 5.4 and 5.5).

The autocorrelation is the sum over all the modes, but the dominant contribution for large frequencies are due to wave vectors close to the zone boundary, $k = L/2$:

$$
C(x = 0, \omega) \simeq \frac{1}{L}\sum_{k=0}^{L-1} \frac{2A\left(1 - \cos\frac{k\pi}{L}\right)}{\omega^2} = 2A\omega^{-2} \tag{5.48}
$$

which (by Wiener-Khinchin theorem) is the power spectrum mentioned in Sec.5.5.2.

Appendix 5.B   KPZ and EW

5.B.1   The models

We have see in chapter 2, Eq. 2.37, that the asymmetric hopping can be mapped to a random sequential adsorption of a particle and hence that the TASEP can be related to model of growth surface in $1+1$ dimension. Anyway it is not trivial is to write a continuum equation of motion able to catch all the features seen in simulations and experiments.

Two model appear to be related to TASEP: the Edward Wilkinson (EW) [38] and the Kardar Parisi Zhang (KPZ) [74]. The first model is basically a diffusive equation that describe the growth simply by penalizing the roughness:

$$\frac{\partial h(\mathbf{x}, \mathbf{t})}{\partial t} = \nu \nabla^2 h\left(\mathbf{x}, \mathbf{t}\right) + \eta(\mathbf{x}, \mathbf{t}) \tag{5.49}$$

where η represent usually a white noise, i.e. a noise with the properties properties:

$$\langle \eta(x, t) \rangle = 0 \tag{5.50a}$$

$$\langle \eta(x, t)\eta(x', t') \rangle = D\delta(x' - x)\delta(t - t'), \tag{5.50b}$$

(although other kind of noises have been studied).

The KPZ equation, in addition to the terms that the previous model proposes, favors the growth perpendicular to the surface (not to the plane), including a nonlinear term (and therefore making the model highly non trivial):

$$\frac{\partial h(\mathbf{x}, \mathbf{t})}{\partial t} = \nu \nabla^2 h\left(\mathbf{x}, \mathbf{t}\right) + \frac{\lambda}{2}\left(\nabla h(\mathbf{x}, \mathbf{t})\right)^2 + \eta(\mathbf{x}, \mathbf{t}) \tag{5.51}$$

This equation can been mapped to two useful forms. Through the so called Cole-Hopf transformation $u(x, t) = \exp[\lambda/2\nu h(x, t)]$ one gets a "simple" diffusion equation in a time-dependent random potential:

$$\frac{\partial u}{\partial t} = \nu \nabla^2 u + (\lambda/2\nu)\eta(x, t)u. \tag{5.52}$$

On the other side, through the transformation $v = -\nabla h$, Eq. 5.51 can be mapped to the noisy Burgers equation:

$$\frac{\partial v}{\partial t} = \nu \nabla^2 v - \lambda v \cdot \nabla v - \nabla \eta(x, t). \tag{5.53}$$

This equation describes the velocity flow of a randomly stirred flux (the noise term), including the usual diffusive term $\nabla^2 v$ and the convective non linear term emerging from the Navier Stokes equation.

5.B.2 Dynamic scaling

It is known that, near a second order critical point, thermodynamic functions obey some generalized homogeneity relations leading to scaling laws. In non equilibrium systems a quantity that is typically measured is the dynamic autocorrelation function: at a critical point there is a characteristic *critical slowing down*, corresponding to a point where the system relaxes fluctuations in an infinite time (the diffusion constant usually vanishes). Relations similar to the one obtained at equilibrium describe the thermodynamic quantities and highlight the critical exponents which identify the universality class of the studied phenomena.

In the growth of surface, one is interested not only in the evolution of the profile $h(\mathbf{x}, \mathbf{t})$ but also in the *width* of the surface defined as:

$$W \equiv \sqrt{\langle h(t) - h(0)^2 \rangle} = \sqrt{C(x, t)}, \tag{5.54}$$

which evolves to a steady state following a power law in time up to a crossover time $t_\times$. Moreover there are dependence of the stationary correlation and on the crossover time on the system size. In the this class of phenomena there are three relevant exponents: χ, ν, and z:

- growth exponent ν, that tells how the stationary profile is reached in time (so it is valid for $t \ll t_\times$

$$W(L, t) \sim t^\chi \tag{5.55}$$

- roughness exponent χ, that indicates how the roughness scale with the system size L at the saturation:

$$W_s(L) \sim L^\nu \tag{5.56}$$

- dynamical exponent z, that specifies how the crossover time scales with the system size:

$$t_\times \sim L^z \tag{5.57}$$

  The value of z has an important practical aspect: it tells how the time the system takes to reach the stationary state scales with the system size and therefore allows to roughly predict the length of simulations and experiments.

In the model for surface growth in $d = 1$, the scaling relation for the correlation $C(x, t)$ reads

$$C(x, t) = x^{2\chi} g(t/x^z) \tag{5.58}$$

In the case of EW model these exponents are $\chi = 1/2$, $\nu = 1/4$ and $z = 2$ but do not correspond to the ones measured that simple ballistic deposition of particles exhibits: this discrepancy motivated therefore some the study where non linear effects becomes important like the KPZ equation. The critical exponents of KPZ where computed through renormalization group techniques both for Eq. (5.51) and Eq. (5.61) and the values identify

the so called Family-Vicsek (or Burgers, or KPZ) universality class $\chi = 1/2$, $\nu = 1/3$ and $z = 3/2$.

The exponents we found can be related to the TASEP one through transformation of the scaling relation 5.58. By Fourier transforming in space and time Eq. 5.58 one gets the correlation function in momentum and frequency:

$$C(k, \omega) = k^{-2\chi-1-z} g(\omega/k^z) \,. \tag{5.59}$$

By integrating the Fourier transform in the mode $1/L < k < \infty$ one gets the autocorrelation function (specialized to $x = 0$) with a cutoff L that gives the finite size scaling:

$$C(x = 0, t) = L^{2\chi} g(t/L^z) \,. \tag{5.60}$$

The KPZ equation relates to the Burgers equation through the transformation $v = -\nabla h$, which yields

$$\frac{\partial v}{\partial t} = \nu \nabla^2 v - \lambda v \cdot \nabla v - \nabla \eta(x, t) \,. \tag{5.61}$$

In this case the scaling form of the correlation function

$$C(x, t) = \langle \tilde{v}(x, t) \tilde{v}(0, 0) \rangle - \langle \tilde{v}(x, t) \rangle \langle \tilde{v}(0, 0) \rangle$$

: are slightly different and can be derived from the previous one by simply substitution:

$$C(x, t) = x^{\chi-z} g(t/x^z) \,. \tag{5.62}$$

By Fourier transforming

$$C(k, \omega) = k^{-\chi-1} g(\omega/k^z) \,. \tag{5.63}$$

The autocorrelation, after an integration and analogously to what done above, reads

$$C(x = 0, t) = L^{\chi-z} g(t/L^z) \,. \tag{5.64}$$

In the special case of KPZ, for which we know the relation $\chi + z = 2$ holds, the last result yields Eq. 5.64. While computing the width of the Gaussian as:

$$W(t) = \int x^2 C(x, t) dx \tag{5.65}$$

and using the Fourier transform to introduce a the cutoff at $x = L$, one get Eq. 5.34.

Chapter 6

Statistical analysis of a tracer particle

Kon ovla so mutavia, kon ovla
ovla kon ascovi
me gava palan ladi
me gava palan bura ot croiuti.
Who is going to tell it?
the ones that remain
I'll follow this migration,
I'll follow this current of wings.

F. de André, *Khorakhané*

The goal of this chapter is to explore the feasibility of single molecule experiments for measuring the density profile in the models we have studied in this thesis. To this end we consider a TASEP with on-off kinetics and simulate the dynamics of tracer particles. It will turn out that a histogram of the tracer position allows to reconstruct the density profile quite accurately, even with a low number of tracer particles.

This chapter is organized as follows. In Sec. 6.1 we explain the motivations from an experimental point of view. In section 6.2 we explain the quantities analyzed in this work. In Sec. 6.3 we present the procedure to reconstruct the density profile from the tracer average velocity and we test the method on some representative set of model parameters. In section 6.4 we present a short summary and some outlook.

6.1 Experimental motivations

A measurement of the density profile can, in principle, be experimentally achieved by using fluorescently labeled motors, e.g. with a green fluorescent protein (GFP), and collecting the emitted light from all the motors. The major drawback of this approach, however, is that the fluorophore often bleaches on a rather short time-scale, affecting (irreversibly) the motion of the motor. The effect of a single "broken" motor could be described in the frame of disordered systems (see Ch. 4). The best suggestion we could think to avoid

this drawback is to perform single molecule imaging experiments. This could be done by labelling a single particle with a fluorescent dye [143] or with a quantum dot [134] (which are more reliable than usual fluorophores since they do not bleach do not influence the motion of the engineered motors). As in any other real experiment, one has to deal with the physical limits of the instruments. Typical TIRF microscopy have a spatial resolution of the order of $\sim 100nm$ (see Ch. 1). This is too low to resolve the distance between two binding sites, which is of the order of $8nm$. The time resolution is of the order of $\sim 200ms$; any information occurring on a time scale smaller than this is lost. Since data are convoluted with the resolution of the instruments, a time-average is already performed by the camera: knowing that the motors move on the scale of $\sim 10ms$, the system is averaged on about 20 time steps. In the following we will convolute our simulated data with the time resolution and take advantage of this time average to study less noisy results.

6.2   Measured quantities

In this section, inspired by the results already known for the TASEP, we discuss those characteristics of the tracer particles which allow for a reconstruction of the density profile.

6.2.1   TASEP results

In the case of the TASEP on a ring, rigorous results are available [100, 87, 31, 44]. Defining the velocity as the limit:

$$v(t) \equiv \lim_{t \to \infty} \frac{\langle x(t) \rangle}{t}, \tag{6.1}$$

the following relation with the bulk density ρ is found

$$\rho = 1 - v. \tag{6.2}$$

This can be understood intuitively since the current is (where the hopping rate is taken to be one) the product of the density with the velocity of the single particle:

$$j = \rho(1 - \rho) = \rho v. \tag{6.3}$$

Another result from the TASEP is that the diffusion constant D, defined as

$$D \equiv \lim_{t \to \infty} \frac{\langle x^2 \rangle - \langle x \rangle^2}{t} \tag{6.4}$$

terms of density simply reads[1] [100, 87, 44]:

$$\rho = 1 - D. \tag{6.5}$$

---

[1]Note that, compared to the simple diffusive case, a factor two is missing in the definition.

The generalization of these properties to extended particles has been worked out in Refs. [45, 129].

An interesting anomalous behavior is observed for the variance of the position of the tracer particle at the critical regime $\rho = 1/2$, where the system becomes sub-diffusive and can be related to the Burgers equation (see Ch. 5):

$$\left\langle x^2 \right\rangle - \left\langle x \right\rangle^2 \sim t^{2/3} \,. \tag{6.6}$$

Inspired by the TASEP results we characterize the motion of the tracer particle by mean of these two quantities that are simply the first two cumulants of a probability density function.

6.2.2 Conditional probability density function

We are interested in are the statistical properties of the tracer particle as described by the conditional probability density function $P(x,t|0,0)$ to find a tracer particle at site x at time t which started at $x = 0$ at $t = 0$. Assuming it is *experimentally* feasible to repeatedly collect the position as a function of time (measured in time unit) for a large number of particles, one may estimate for $P(x,t|0,0)$ by constructing a histogram for the fraction of the total number of particles that reached the site x in time t. A natural choice for the bin size of the histogram in space and time, Δx and Δt, are the expected spatial and temporal resolution in a single molecule experiments.

From the *theoretical* point of view, the model we apply to describe the system is the one-dimensional driven lattice gas introduced in Ch. 5: the TASEP of monomers with on-off kinetics. Since we have seen in Ch. 3, that the TASEP of dimers with attachment and detachment has only quantitative but not qualitative differences to the monomer case (at least in extensive portions of the phase diagram), we confined ourselves to monomers, which are faster to simulate and easier to treat analytically. We simulate these experiments using the same BKL code introduced in the previous chapters, which allows us to track the history of each particle in space and time. From this we construct the "histogram" of the fraction of particle at site x at time t (from the injection in the system at the left end $x = 0$) . The time used for the binning initially is the typical time-step $\Delta t = 1$.

In figure 6.1 the time evolution of $P(x,t|0,0)$ is shown for a set of parameters chosen to allow the formation of a stable domain wall, i.e. $\alpha = \beta = 0.1$, $\Omega_A = \Omega_D = 0.1$ on a systems of $N = 512$ sites. The histogram for the probability density function was deduced from a sample of 2^{14} injected particles.

The probability density function $P(x,t|0,0)$ exhibits a maximum both in space and in time domain which moves with an almost constant velocity (the plots show a snapshot of the dynamics every 20 time units). Figure (6.1(a)) shows a time series for $P(x,t|0,0)$ while Fig. (6.1(b)) shows how $P(x,t|0,0)$ changes in space.

As already motivated in the previous subsection, the most natural quantities to analyze are the first two cumulants of the probability density function. We concentrate therefore on the following quantities, the average and the variance of the position of the tracer particle
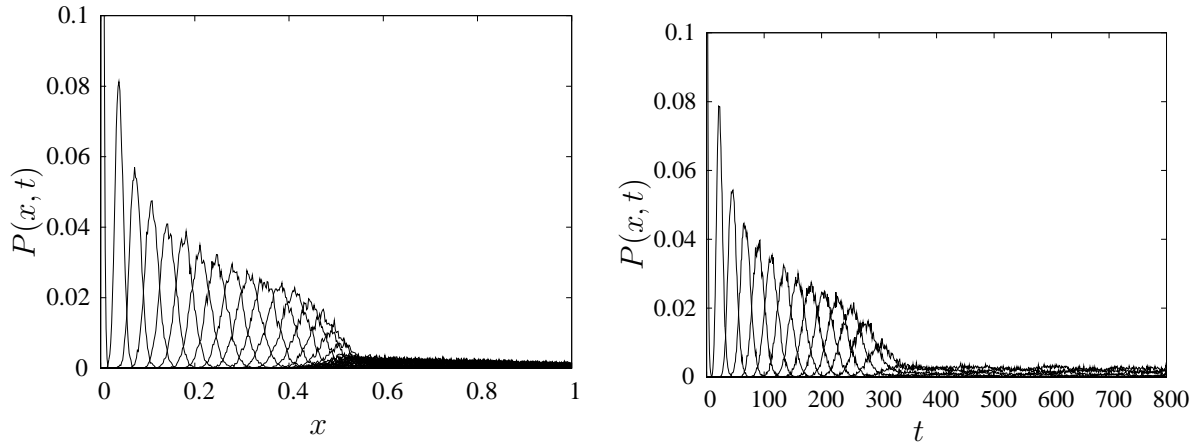
(a) Evolution of $P(x,t)$ plotted in space. Each curve is taken every 20 time units.

(b) Evolution of $P(x,t)$ plotted in time. Each curve is taken every 10 sites.

Figure 6.1: Evolution of the probability distribution function of the tracer particle in time and space, $P(x,t|x(t=0)=0)$. Parameters: $\alpha = \beta = 0.1$, $\Omega_A = \Omega_D = 0.1$, $N = 512$.

as a function of time

$$\langle x(t) \rangle \;\; = \;\; \frac{\sum_x x P(x,t)}{\sum_x P(x,t)} \tag{6.7}$$

$$Var(x(t)) \;\; = \;\; \frac{\sum_x x^2 P(x,t) - \left(\sum_x x P(x,t)\right)^2}{\sum_x P(x,t)} \; . \tag{6.8}$$

Note that a quantity like the maximum of the probability distribution function $X(t) = \text{Max}_x\{P(x,t)\}$ is rather noisy and would not be a good observable. We also measure the average of the distribution in time as a function of space:

$$\langle t(x) \rangle \;\; = \;\; \frac{\sum_t t P(x,t)}{\sum_t P(x,t)} \; . \tag{6.9}$$

Examples of all these quantities are shown in the graphs (6.2(a), (6.2(b)) and 6.2(c)). We discuss hereafter the main features that one can observe from the graphs. The average quantities $\langle x \rangle (t)$ and $\langle t \rangle (x)$ are clearly related (being one the inverse of the other). In Figs. (6.2(a) and (6.2(a)) one can observe two straight regimes, i.e. two velocities. The straight line indicates that the average of the distribution moves with constant velocity. Comparing Fig. 6.2(b) and Fig. 6.2(d) is clear that the kink in the graph $\langle t \rangle (x)$ occurs at the shock position (i.e. $x_w = 0.5$ with these parameters): the particle changes velocity since the density changes from low to high.

Figure (6.2(c)), shows the variance of the position of the tracer particle as a function of the time. After a linear growth in time corresponding to the low density regime (LD in the graph) a sudden jump, occurring at $t \sim 500$ (corresponding to the kink in Fig. 6.2(b)), identifies the position of the shock, where the particle enters the high density phase (HD

(a) Position in time of the average position ($\langle x(t) \rangle$) of the tracer probability distribution function.

(b) Position of the average ($\langle t(x) \rangle$) of the tracer probability distribution function vs space.

(c) Variance of the position versus time

(d) Density profile $\rho(x)$. A shock is localized in the center of the system.
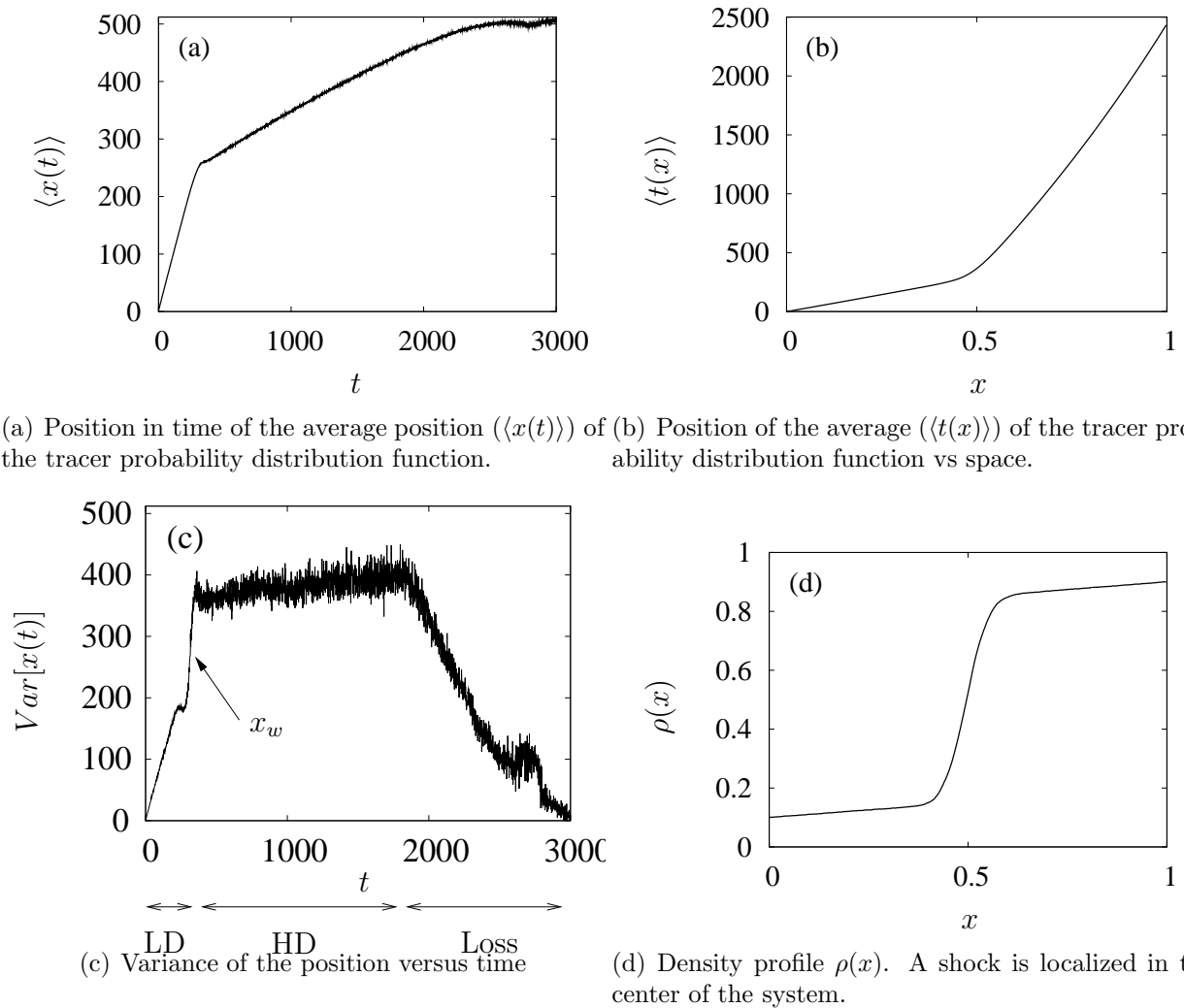
Figure 6.2: (a) Position of average time in space domain compared to (c) the density profile. (b) Average position in time domain compared to (d) Variance of the position of the tracer particle as a function of the time: after the linear diffusive behavior (LD) the tracer diffusion is enhanced by the shock fluctuations (at x_w) and grows slowly in the HD. In the "Loss" part particles are lost from the left boundary. Parameters: $\alpha = \beta = 0.1$, $\Omega_A = \Omega_D = 0.1$, $N = 512$.

in the graph) and from then on the variance remains essentially constant. The decreasing of the variance (*Loss* region in the graph) indicates that the probability density function hits the right boundary and gets localized; this is due essentially because of the loss of particles at the right boundary. This occurs for $t \sim 2000$; from Fig. 6.2(a) it can be seen that at this instant the average $\langle x \rangle (t)$ deviates from the linear regime showing an apparent slowing down of the particle. We argue that the average position is no longer a meaningful observable, since the probability density is highly skewed and the average is effectively shifted to the left.

Note that the probability as defined above is affected by the fact that particles can detach in the bulk before arriving at the right end: this is visible in the fact that the noise of the data progressively increase due to the progressive reduction of the number of particle histories analyzed. We compared the function with the probability distribution function obtained by eliminating from the sample the particles that did not reach the right end of the system: this is a way to measure $P(x, t|0, 0; x(t = max) = 1)$. No difference was observed, corroborating the idea that the two distributions are ideally the same in the limit of large particle number.

6.2.3   Other indicators

As other indicators for the position of the shock, we could also measure the attachment and detachment distribution function (see fig. 6.3). We define the attachment distribution function $P_A(x)$ and $P_D(x)$ as the probability of attaching (detaching) at site x (that becomes now the stochastic variable). To measure these functions we need to collect data also on particles that enter the system in the bulk. The data are collected from the simulations by simply counting the number of particles respectively attaching and detaching at site x and dividing by the total number of particles considered. Figure (6.3) shows interesting correlations (anti-correlations in the case of $P_A(x)$) to the shape of the the density profile and therefore $P_A(x)$ and $P_D(x)$ could be interesting observables to track the shock. The intuitive explanation is that particles attach more likely in the low density profile and detach more likely from the high density profile; consequently they are more likely to travel until the high density phase. Unfortunately these indicators are rather noisy (we remind that the data are collected over 2^{14} injected particles) and therefore will not be used in the following.

6.3   Data analysis

In this section we present the procedure used to convolute the data with an experimental resolution. This procedure will accidentally smooth the curve and this will make possible to extract the average velocity of the tracer particle and hence the density profile. We present some reconstructed profiles and some measurements performed with very low statistics in conditions achievable experimentally: the method suggested here allows for profile reconstruction even with a very low number of particles.
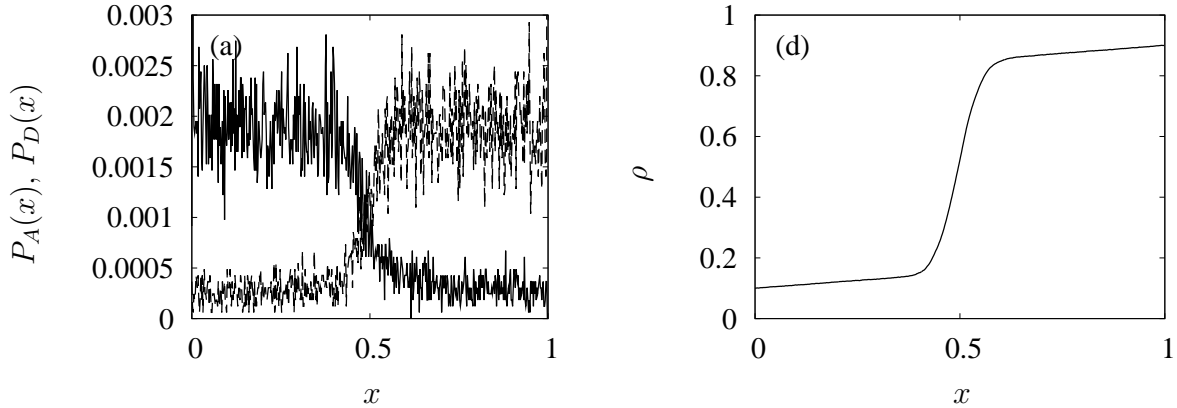
Figure 6.3: (Left) Distribution of attachment $P_A(x)$ and detachment sites $P_D(x)$ compared to the corresponding density profile (right); clearly the majority of the particles attach in the LD phase and the detachment on the HD phase. Parameters: $\alpha = \beta = 0.1$, $\Omega_A = \Omega_D = 0.1$, $N = 512$.

6.3.1 Convolution of the data

We would like to mimic the experimental resolution by binning the data in time. We convolute the data with a resolution function of ~ 50 time step (see Sec. 6.1. Hence every point of the probability density function at each instant is replaced by the time average over a time interval of length $2m$ so that in fact the new probability $P(x, T)$ is drawn from the old one $P(x, t)$ as:

$$\tilde{P}(x, T) = \frac{1}{2m} \sum_{t=T-m}^{T+m} P(x, t) \,, \tag{6.10}$$

with $m = 50$. By reducing the temporal resolution of the instruments one performs an implicit average that eventually improves the data, since the fluctuations on short time scales are averaged out (informations on events occurring at timescale shorter than $2m$ are hence unaccessible). This artefact is visible for the quantities $\langle x \rangle (t)$ and $Var[x(t)]$ in Fig. 6.4.

6.3.2 Density profile reconstruction

After the convolution described above, we want to reconstruct the density profile. Unfortunately, there is no theory for the relation between the density and the tracer properties for the TASEP with Langmuir kinetics. We therefore resort to the following "adiabatic" approximation: we assume the local fluctuations of the density in the bulk due to the on-off kinetics to be relevant only on a long timescale (as in an adiabatic approximation the particles can rearrange quickly after the detachment or the attachment of a particle in the bulk) . In other words, we expect the relations found in the TASEP to be still valid,
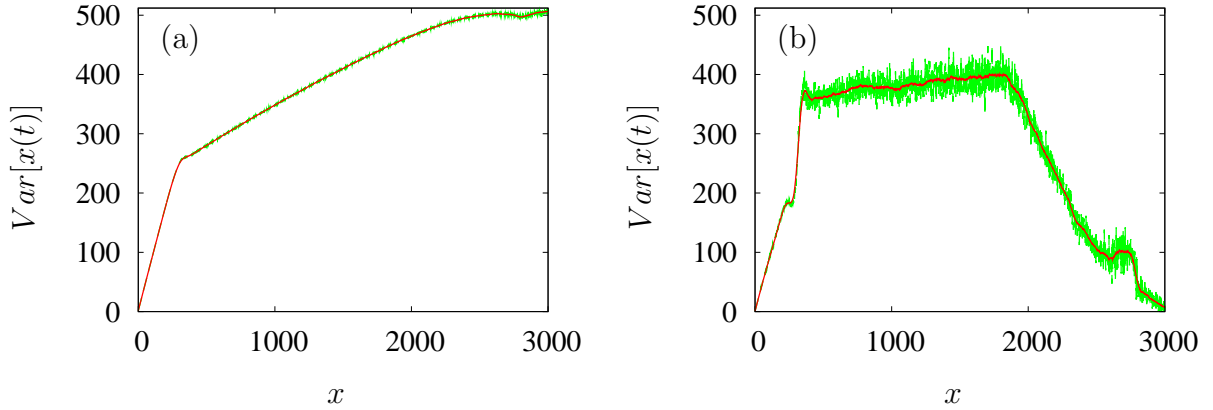
Figure 6.4: Average (a) and variance (b) of the tracer particle position. Light curves represent the original simulated data, solid dark curve represent the data after the convolution with the temporal resolution of the instrument. Accidentally the convoluted date are much less noisy than the original one and allow for differentiation. Parameters: $\alpha = \beta = 0.1$, $\Omega_A = \Omega_D = 0.1$, $N = 512$.

with the complication that ρ is now space dependent. This condition is basically satisfied when the density does not change too abruptly in space and can be considered as locally constant.

We define the velocity as:

$$v(t) \equiv \frac{d \langle x(t) \rangle}{dt} \, . \tag{6.11}$$

This is a time-dependent quantity which may be turned into a local space dependent quantity as follows. The time-dependent average $\langle x \rangle (t)$ can be inverted to express the time as dependent on the space average, i.e. we substitute the time appearing in Eq. 6.11 by $t(\langle x \rangle)$, which is in itself an approximation. The results borrowed form the TASEP state (Eq. 6.2):

$$\rho(x) = 1 - v(x) \, . \tag{6.12}$$

Similarly for the diffusion constant that is defined as

$$D \equiv \frac{\langle x^2 \rangle - \langle x \rangle^2}{t} \, , \tag{6.13}$$

that can be related to the density through:

$$\rho(x) = 1 - D(x) \, . \tag{6.14}$$

Note that in the simple TASEP the randomness parameter, defined as ratio between the variance of the tracer position and its average, is expected to be one (except in the

critical case $\rho = \rho^* = 1/2$). There is no reason why this should be the case in the TASEP with on-off kinetics. We will analyze the deviation form this law induced by the on-off kinetics. We finally turn to investigate the different regimes from the tracer properties, showing that the density profile can be reconstructed from the velocity.

Low density Figure 6.5 shows a comparison between the theoretical prediction, the MC simulation of the density profile and the density profile reconstructed from the tracers dynamics in the LD regime for the TASEP with on-off kinetics (parameters: $\alpha = 0.1$, $\beta = 0.9$, $\Omega_A = \Omega_D = 0.1$, $N = 512$). The agreement between MC simulated density profile and the reconstructed one through 6.12 is showed in Fig. (6.5a), and proved to be really good even for relatively small system size ($N = 512$). A good agreement is also proved in Fig. (6.5c) where the density profile is reconstructed from the diffusion constant obtained through Eq. (6.14). Large deviation from $\rho(x)$ can be observed both in $1 - v(x)$ and $1 - D(x)$ close to the right end of the system where the average position and the average are no more meaningful due to the skewness of the probability distribution function.

Similar considerations can be drawn from Figs. (6.5b,d) showing respectively the time dependence of $\langle x(t) \rangle$ and $Var(x(t))$ and the randomness parameter R: average and variance of the position have the same value and therefore the randomness is approximately one until the distribution, reaching the right end, get more localized: then the variance of the position reduces more rapidly than the average position and consequently the randomness parameter drops to zero.

High density In Fig. (6.6) the parameters are chosen such that the system is in the HD phase (parameters: $\alpha = 9$, $\beta = 0.1$, $\Omega_A = \Omega_D = 0.1$, $N = 512$). The reconstruction can be performed rather accurately through the velocity of the particle (fig. 6.6a). On the other hand the reconstruction from the diffusion constant gives rather poor results Fig. (6.6b). In fact in the time regime one can observe that the mean square displacement grows slower than the average position (Fig. 6.6c): the identity $v = D$ is valid only in the first part where the tracer particle still behaves as a Poisson stepper, but after a transient the system is sub-diffusive: this can be intuitively expected since some fluctuations cannot propagate due to the exclusion and the trapped tracer particle can only move when the next site is free. Consequently the randomness parameter is not one, but decreases progressively (Fig. 6.6d), in agreement with the fact that the variance of the position grows slowlier than the average position.

Maximal current In Fig. (6.7) the MC case is shown (parameters $\alpha = \beta = 0.5$, $\Omega_A = 0.2$, $\Omega_D = 0.1$ and $N = 512$; note $K = 2 \neq 1$). The reconstruction of the density profile works rather well both from the $1 - v$ and from the $1 - D$, although the latter is rather noisy. The randomness (though very noisy) seems to be constant and equal to one up to the instant when the distribution hits the right end. A part from deviation close to the boundary $D \approx v$ and the variance of the position seems to scale with the usual diffusive
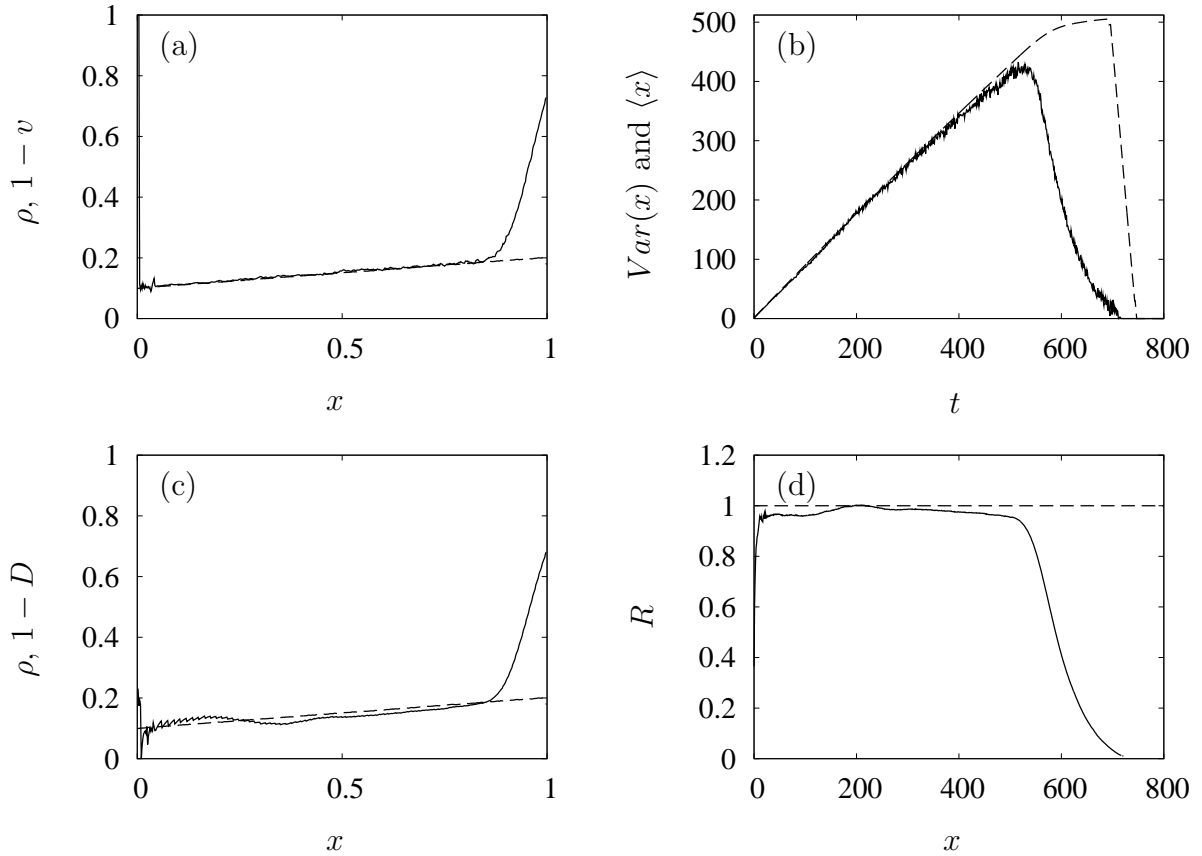
Figure 6.5: Data analysis for the LD regime $\alpha = 0.1$, $\beta = 0.9$, $\Omega_A = \Omega_D = 0.1$, $N = 512$. (a) Reconstructed density profile (solid line) from the relation $\rho = 1 - v$ compared to MC simulations (dashed line). (b) Variance of the position of the tracer (solid) and average position (dashed) of the tracer particle as a function of the time. (c) Reconstructed density profile (solid line) from the the relation $\rho = 1 - D$ compared to MC simulations (dashed line) (d) Randomness parameter (solid) compared to the reference value $R = 1$ (dashed).
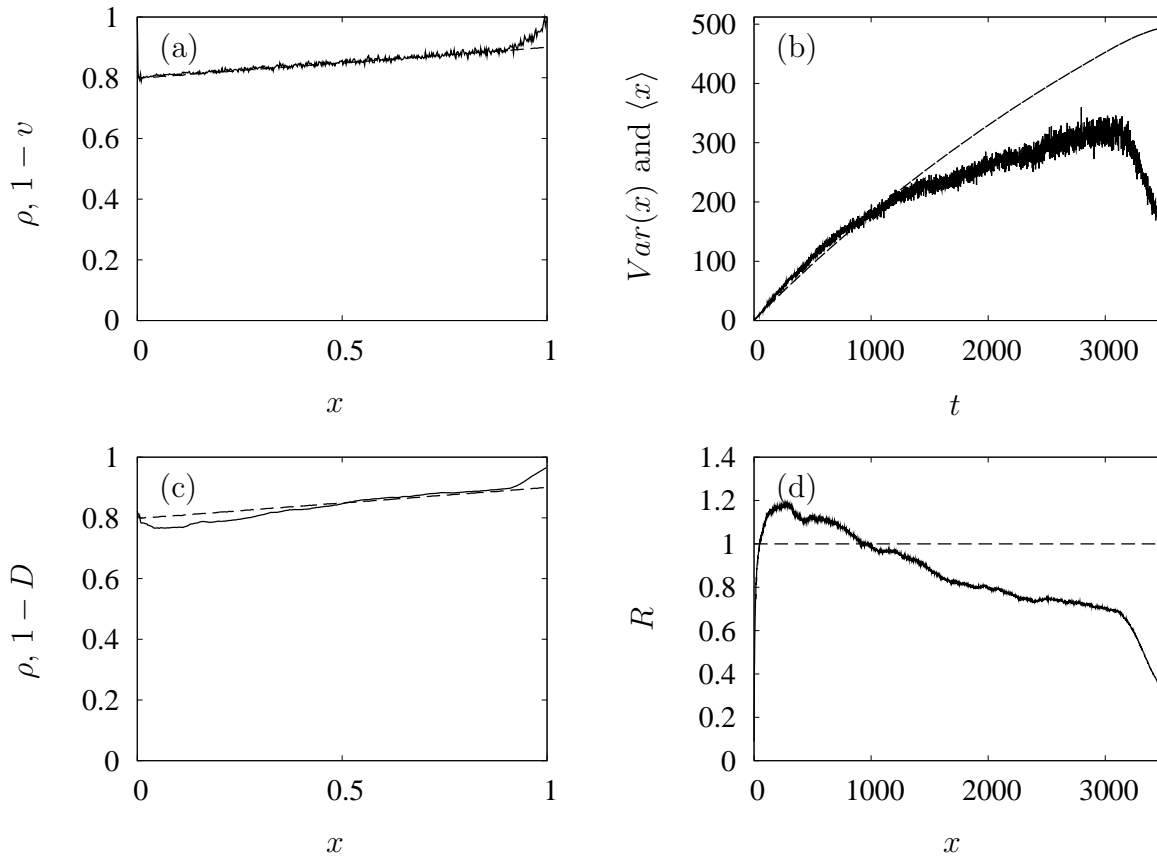
Figure 6.6: Data analysis for the HD regime $\alpha = 0.9$, $\beta = 0.1$, $\Omega_A = \Omega_D = 0.1$, $N = 512$. (a) Reconstructed density profile (solid line) from the relation $\rho = 1 - v$ compared to MC simulations (dashed line). (b) Variance of the position of the tracer (solid) and average position (dashed) of the tracer particle as a function of the time. (c) Reconstructed density profile (solid line) from the the relation $\rho = 1 - D$ compared to MC simulations (dashed line) (d) Randomness parameter (solid) compared to the reference value $R = 1$ (dashed).

behavior: this suggests that the critical scaling found in the simple TASEP $Var(x) \sim t^{2/3}$ (see e.g. Refs. [150, 31]) is somehow lost due to the coupling to the on-off kinetics.
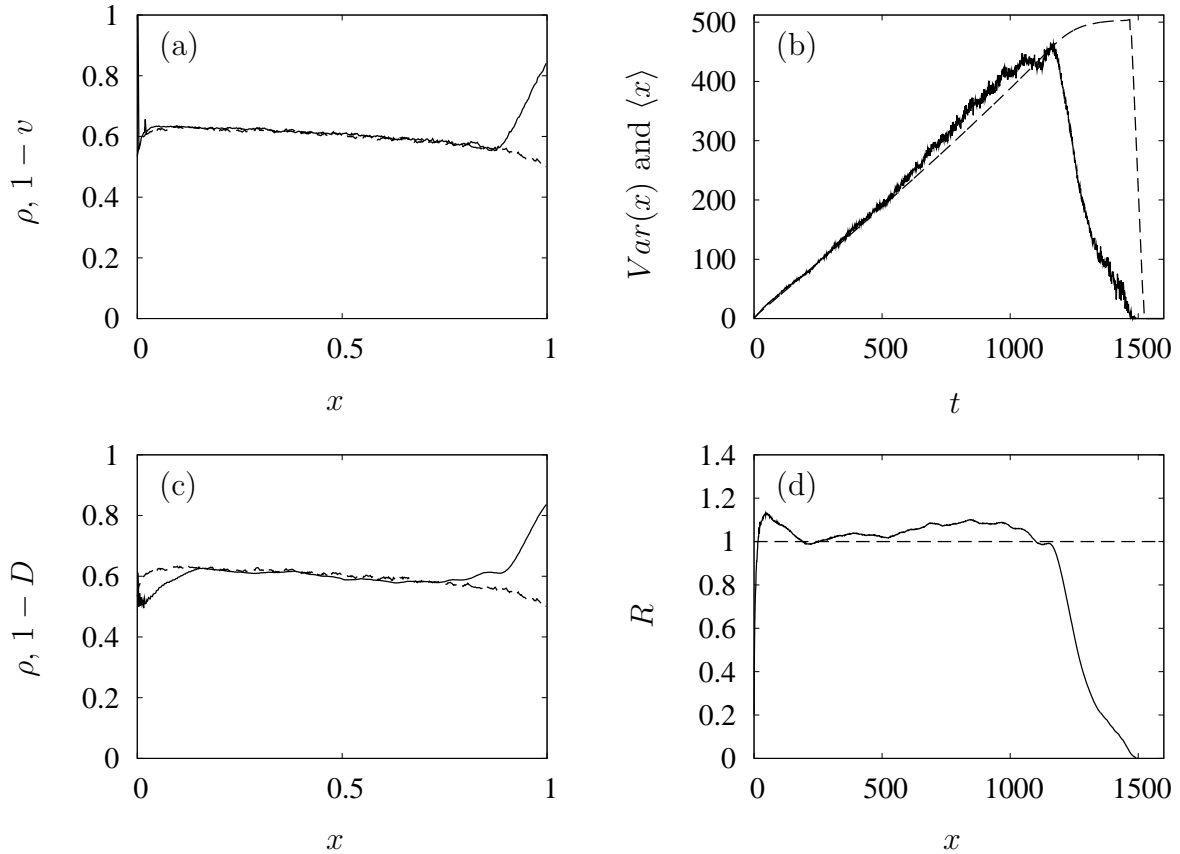

Figure 6.7: Data analysis for the MC regime $\alpha = \beta = 0.5$, $\Omega_A = 0.2$, $\Omega_D = 0.1$, $N = 512$. (a) Reconstructed density profile (solid line) from the relation $\rho = 1 - v$ compared to MC simulations (dashed line). (b) Mean square displacement of the tracer (solid) and average position (dashed) of the tracer particle as a function of the time. (c) Reconstructed density profile (solid line) from the the relation $\rho = 1 - D$ compared to MC simulations (dashed line) (d) Randomness parameter (solid) compared to the reference value $R = 1$ (dashed).

Coexistence LD-HD   The most interesting case is maybe the one shown in Fig. (6.8) where the parameters were chosen such that a domain wall is visible, i.e. the system is in the LD-HD coexistence phase (parameters: $\alpha = \beta = 0.1$, $\Omega_A = \Omega_D = 0.1$ and $N = 512$). By reconstructing the density profile with the velocity, the position of the shock is identified with rather good accuracy: we roughly estimated 0.46 ± 0.05 (value where the velocity is equal to $1/2$) for a system of $N = 512$ sites, versus the $x_w = 0.50 \pm 0.08$ mean field value for the same system-size (the error is $2/\sqrt{N}$, see [112]). The main difference between ρ and $1 - v$ appears in the domain wall region: in fact the domain wall does not show any

symmetry, the density grows from LD on a rather extended region till the HD phase. This is basically the only discrepancy between ρ and $1 - v$ and could be due to the fact that Eq. (6.12) is no longer valid: indeed the shock invalidates the hypothesis that ρ should appear locally continuous.

On the other side the diffusion constant does allow for a good reconstruction only in the LD regime (Fig. 6.8c). From the variance of the position showed in Fig. (6.8b), one can see that after the usual diffusional behavior in the LD phase, the distribution gets basically localized and then is suddenly is allowed to largely diffuse in correspondence of the shock position x_w. The increasing at $x = x_w$, that can be seen also in the randomness Fig. (6.8d) is essentially due to the local fluctuations of the shock that enhance the diffusion (a trace of a first order phase transition). After that, in the HD phase, the particle diffuse very slowly, and the variance of the position remains constant. Finally the tracer get localized at the end (i.e. the mean square displacement decreases), but this is an uninteresting normalization problem due to the exit of particles at the right end of the lattice. From the graphs one can see that once the system enter the high density phase, a sub-diffusive behavior affects the variance which, therefore, does not be scale anymore linearly in time as $\sim Dt$.

In the TASEP with on-off kinetics the equality $v = D$ (i.e. $R = 1$) holds only in the LD and MC phase. Apparently the on-off kinetics break this law: in the HD and LD-HD coexistence there are remarkable deviation from the diffusive law, visible in the plots of the mean square displacement and in the randomness. This phenomenon still call for a complete explanation, but anyway does not affect the validity of the method to track the position of the shock.

6.3.3 Experimentally relevant parameters

In the last part of this section we present some data obtained simulating systems with parameters experimentally testable (the same already presented in chapter 2), i.e. $N = 512$, $\alpha = 0$, $\beta = 1$ (free end) or $\beta = 0$ (blocked end), $\Omega_D = 1$, $K = 1.5$ and $K = 0.5$. Moreover we consider very low statistic, only 128 injected particles, to see whether or not would be possible to identify the different regimes in realistic conditions. As can be seen from Figs. 6.9, in principle it is possible to measure v and extract informations on the density profile from the motion of so few particles.

A general feature of the graphs is the initial noisy reconstructed profile. We argue that this is an artefact due to the convolution procedure, which is not averaging out fluctuations on a sufficiently large interval in the first 50 time steps. A part from this region (confined to the first 10% of the system) and the last part of the lattice, where the loss of particle affect the probability density function as explained in the previous section, the reconstruction works very well for the low density regime (Figs. 6.9a and b). In the high density regime (in particular Figs. 6.9c and d) strong fluctuations can be observed, due to the loss of particles in the bulk reservoir. These fluctuations could be reduced by considering much larger statistic (since the noise scales approximately with the square root of the histories considered).
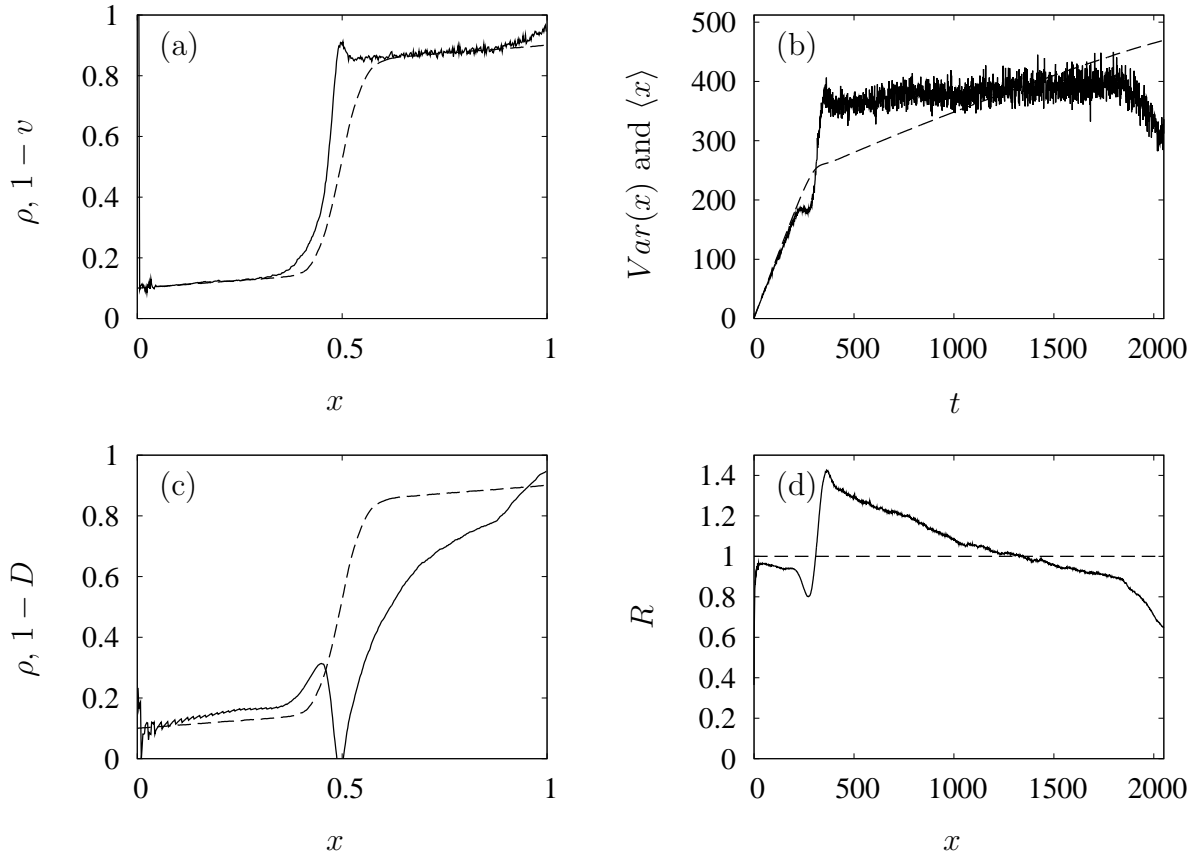
Figure 6.8: Data analysis for the LD-HD regime $\alpha = \beta = 0.1$, $\Omega_A = \Omega_D = 0.1$, $N = 512$. (a) Reconstructed density profile (solid line) from the relation $\rho = 1 - v$ compared to MC simulations (dashed line). (b) Variance of the position of the tracer (solid) and average position (dashed) of the tracer particle as a function of the time. (c) Reconstructed density profile (solid line) from the the relation $\rho = 1 - D$ compared to MC simulations (dashed line) (d) Randomness parameter (solid) compared to the reference value $R = 1$ (dashed).

replacements
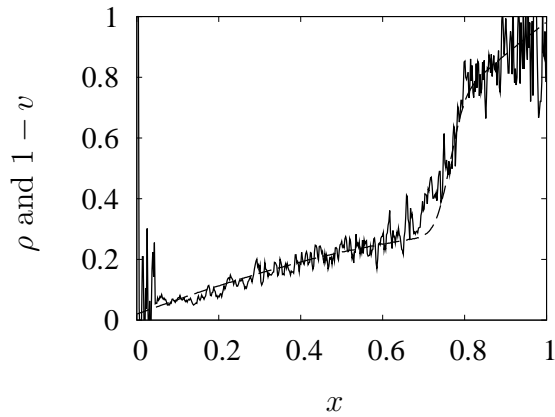
(a) Parameters: blocked end $\alpha = \beta = 0$, $N = 512$, $\Omega_D = 1$, $K = 0.5$
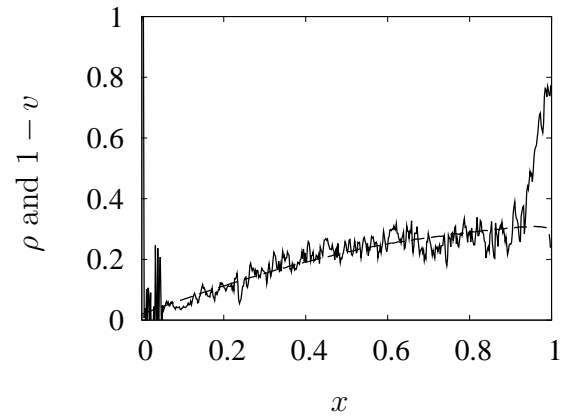
(b) Parameters: open end $\alpha = 0$, $\beta = 1$, $N = 512$, $\Omega_D = 1$, $K = 0.5$

replacements
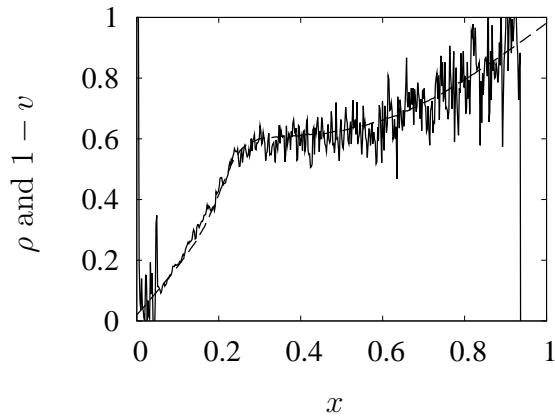
(c) Parameters: blocked end $\alpha = \beta = 0$, $N = 512$, $\Omega_D = 1$, $K = 1.5$
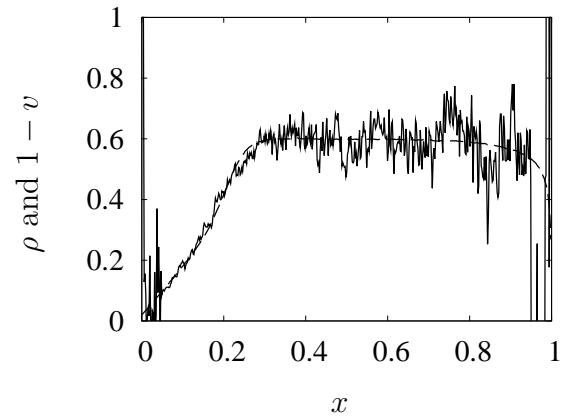
(d) Parameters: open end $\alpha = 0$, $\beta = 1$, $N = 512$, $\Omega_D = 1$, $K = 1.5$

Figure 6.9: Reconstructed density profile (solid line) from the relation $\rho(x) = 1 - v(x)$ compared to MC simulations (dashed line). Physiological conditions are considered. The noise is due to the very low but realistic number of particles (128) considered.

6.4   Conclusion

In this chapter we have proposed an experimental way to reconstruct the density profile in *in vitro* systems. Knowing that single molecule experiments are much easier than observation on systems with many fluorescently labeled motors, we reconstruct the density profile of a TASEP with on-off kinetics from the behavior of a tracer particle.

Assuming it is *experimentally* feasible to repeatedly collect the position of a sufficiently large number of particles as a function of time (measured in time unit), we have constructed a histogram for the fraction of the total number of particles that step x sites in time t from they departure. The quantities we measured on this distribution are essentially the average and the variance of the tracer particle position. From these quantities the velocity v and the diffusion constant D of the particle have been computed. From the velocity we have showed it is possible to reconstruct the density profile using the relation (exact for the simple TASEP) $\rho = 1 - v$ in every region of the phase diagram. Same relations hold for the diffusion constant.

The attempt of reconstructing the density profile from the diffusion constant D (suggested by the fact that in the TASEP $\rho = 1 - D$ fails when the system is too dense (i.e. in the high density and in part of the coexistence phase). This suggests that, while the average position of the particle can be locally described using the well-known TASEP results, the variance of the position exhibits an interesting sub-diffusive behavior when correlations becomes important.

Interestingly enough, in the simulations we did, the statistic does not have to be huge, since the main traffic effect can already be observed with less than one hundred particles. The possibility to measure statistical properties using a single tracer open realistic possibilities of characterize *quantitative* traffic effects and to test the efficiency of the model introduced in our work. In addition, this exploratory study has revealed some interesting features of the tracer dynamics which are worthwhile to explore further on the basis of an analytical theory.

Chapter 7

Conclusions and perspectives

> Nur weil wir fragen und begründen
> können, ist unserer Existenz das
> Schicksal des Forschers in die Hand
> gegeben.
>
> M. Heidegger, *Was ist Metaphysik*

This thesis has been motivated by intracellular transport phenomena, such as kinesins and myosins moving along cytoskeletal filaments or ribosomes along messenger RNA. In both cases molecular motors move uni-directionally along a one-dimensional track. This motion is driven by the free energy released in the chemical hydrolysis reaction of ATP (adenosine-triphosphate). It drives conformational changes of the protein and at the same time switches the affinity to the cytoskeletal filaments. The detailed mechanisms are still a matter of debate and intensive research. They do not concern us here, since we are not interested in the principles governing the chemo-mechanics of individual enzymes, but in the possible cooperativity in the intracellular transport resulting from the interplay between externally driving the system and the interaction between the motors. We are interested in the emergent properties of the system, such as the density and current profiles along the track in the ensuing non-equilibrium steady state.

We have idealized the dynamics in terms of driven lattice gases which model the motors as particles occupying one or more lattice sites whose dynamics is given by a Poisson process, which is the simplest conceivable stochastic process describing directed motion. The track has been represented by a one-dimensional periodic lattice with open boundaries, where particles may enter or leave the system stochastically at some predescribed rates α and β. Interaction between the particles has been restricted to hard core repulsion such that each lattice site can at most be occupied by one particle. As such the system is known as the Totally Asymmetric Simple Exclusion Process (TASEP), which shows a non-trivial phase diagram as a function of the entrance and exit rates. Though describing some key features of intracellular transport this simple model misses several important aspects such as the exchange of particles between molecular track and the cytoplasm, the

extended molecular structure of each motor, and the interaction of motors with microtubule associated proteins which may act as road blocks for intracellular traffic.

The goal of this thesis was to account for some of these additional features and explore their possible relevance for the nature of the non-equilibrium steady state and correlations in the single particle and collective dynamics. To achieve this goal we used both analytical approaches (mean field theories, Langevin equations) and numerical methods (kinetic Monte Carlo simulations).

In the first part of the thesis we build on recent advances in the field, which have been achieved by taking into account particle exchange between the track and bulk solution (Langmuir kinetics). It was found that this violation of current conservation along the track leads to phase coexistence regions in the phase diagram not present in the TASEP. We have extended these studies in two ways: we have studied the effect of the extended nature of the particles and of a defect (bottleneck) on the phase behavior of such systems. The first turns out to give rise to quantitative, the latter even to qualitative changes in the phase behavior.

In addition to the analysis of the properties of the non-equilibrium steady state we have investigated the dynamical properties of a simple TASEP. Using a technique borrowed from solid state physics, the Boltzmann-Langevin method, we have given a complete description of the correlation functions in the whole parameters space. Finally, we have investigated the dynamics of a tracer particle in the TASEP with Langmuir kinetics. The results suggest to use tracer particles as an experimental tool to reconstruct the density profile in the non-equilibrium steady state thus allowing to explore the phase behavior of non-equilibrium systems.

In the following we summarize the main results achieved in our work and the perspectives suggested by each issue.

Dimers.   Molecular motors like kinesins and dyneins are dimeric proteins with two heads which attach specifically to neighboring binding sites on a protofilament of a microtubule. We have generalized previous work in this field to account for the extended nature of the motors and asked what quantitative and qualitative changes occurs in the density profile. We have therefore considered a system of dimers moving in one direction on a one-dimensional track, that can attach to and detach from the bulk (Fig. 7.1); we have asked for the phase behavior in the non-equilibrium steady state in terms of the control parameters (the entrance-exit rates at the boundaries, α and β, and the attachment-detachment rates in the bulk, ω_A and ω_D). The finite processivity of the motors was capture by the *mesoscopic limit* which assumes the global attachment-detachment rates to scale with the system-size: $\Omega_{A,D} = N\omega_{A,D}$; as a byproduct this guarantees competition between boundaries and bulk dynamics and allows us to study the most interesting regimes of the system.

There have been several challenging aspects in this model: (i) it is known that usual mean field approximation do not work in systems of extended particles; (ii) the TASEP of particles of size ℓ (or ℓ-TASEP) is known to have a non-trivial current-density relation
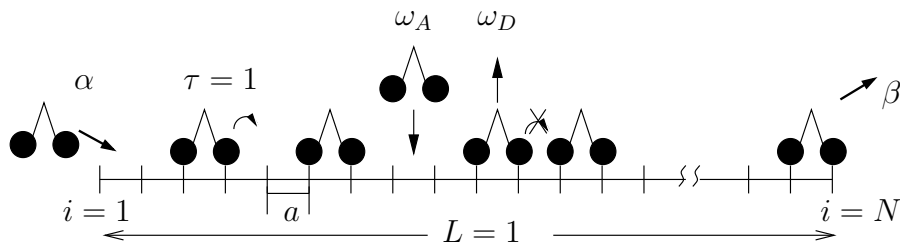
Figure 7.1: Schematic representation of the model with dimers and allowed moves: forward jump (with rate $\tau = 1$), entrance at the left boundary (with rate α), exit at the right boundary (with rate β), attachment (with rate ω_A), and detachment (with rate ω_D) in the bulk.

$j(\rho)$, different from the model with monomers; (iii) even the simple on-off kinetics of dimers exhibits non-trivial dynamics; for example the stationary state is reached from an empty system through a double step relaxation process; (iv) the coupling of an equilibrium process with two intrinsic relaxation regimes (on-off kinetics) to a genuine driven process (the ℓ-TASEP) suggests interesting dynamical phenomena likely to result in new phases and regimes.

We have performed extensive MC simulations and rationalized the results through an analytical theory. In absence of exact solution, the main challenge has been to construct a refined mean field theory, based on probability theory, and to prove the consistency of the approximation for the two competing process (TASEP and the on-off kinetics). We have solved the mean field equation within the mesoscopic limit (i.e. large but bounded systems).

Exploiting the analytical properties of the solution of the mean field equation and the local continuity of the current, we constructed the global density profile. The agreement between the mean field solution and the Monte Carlo simulations is excellent. The solution has also been used to identify the different phases: in addition to the usual phases exhibited by the TASEP (low density, high density, and maximal current) we found several new coexistence regions.

As a consequence of the on-off kinetics, the discontinuous transition along the coexistence line of the TASEP $\alpha = \beta$, splits into two continuous transitions. In the region of the phase diagram enclosed by these phase boundaries, the low and the high density phase are separated by a localized domain wall (shock). Another most striking feature, common to many $1d$ driven lattice gases with on-off kinetics, seems to be the fact that generalized mean field descriptions capture the full details of the phase diagram.

The main effect of extended nature of dimers on the phase behavior of the system is related to the breaking of a symmetry in the problem (particle-hole). This does have quantitative but not qualitative consequences on the density profile and on the phase diagram. The origin of the *robustness* of the picture found for monomers can be traced back to the form of the stationary density profile which depends exclusively on the form of the current-

density relation and of the isotherm of the on-off kinetics. This suggests that the TASEP dynamics washes out the interesting two-step relaxation dynamics that characterizes the on-off kinetics of dimers. The non-trivial outcome is that, in these systems, the diffusion (yet asymmetric) always dominates the large time-scale relaxation.

Further studies on the dynamical correlation functions could point out more subtle differences between the dynamics of dimers and monomers. We conjecture that quite interesting phenomena would arise upon taking into account other interactions between the particles, which suggest to consider alternative current-density relations (with more maxima) or non-trivial on-off isotherm (cooperative on-off kinetics).

PSfrag replacements

Defect. Motivated by the presence of structural imperfections of the track that act as road blocks, in Chapter 4 we have studied the influence of an isolated defect (i.e. point-wise disorder) on the stationary properties of the TASEP of monomers with Langmuir kinetics (LK). The defect has been characterized by a reduced hopping rate $q < 1$ (see Fig. 7.2).
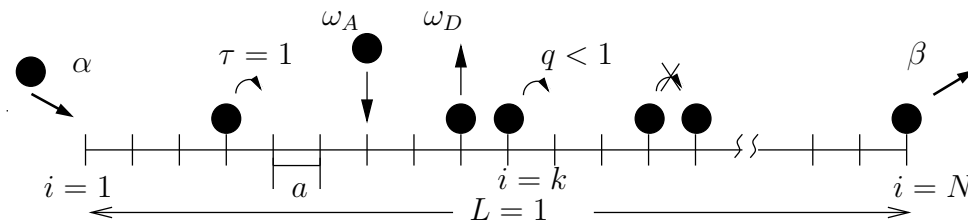

Figure 7.2: Schematic representation of the TASEP with on-off kinetics in the presence of a bottleneck at the site $i = k$. The allowed moves are: forward jump (with rate $q < 1$ in $i = k$ and $\tau = 1$ elsewhere), entrance at the left boundary (with rate α) and exit at the right boundary (with rate β), attachment (with rate ω_A), and detachment (with rate ω_D) in the bulk.

We have found it convenient to introduce the concept of a *carrying capacity* as the maximal current that can flow through a given site. This space-dependent quantity is found to depend on the defect parameters, i.e. its position and strength. Within an effective mean-field theory built on splitting the lattice into two subsystems, we have shown that a single bottleneck may determine the carrying capacity, induce new phases and therefore affect the transport properties in the whole system. Depending on the interplay of the defect-imposed current and the maximal current due to simple exclusion, several carrying capacity profiles occur. For each of them topologically distinct phase diagrams have been obtained and analyzed. In all cases, it was shown that only a small part of the latter was not affected by the defect; in this case the influence of the defect is just a spike in the density profile, that scales out with the system size. Indeed, the core of the phase-diagram is characterized by *bottleneck-induced or defect-dominated (sub-)phases* (see e.g. Fig. 7.3). Depending on the defect strength and position, there are either four, six or nine bottleneck phases. These are characterized by density profiles with localized shocks and kinks in the

sub-systems, arising from the matching between the boundary and the defect current. The richness of the phase diagram is even more evident in its $\alpha - q$ cut where multiple phases merges and a multi-critical point is found. Due to the competition between the TASEP and LK dynamics, the effects of a single bottleneck in the TASEP/LK model are much more dramatic than in the simple TASEP [80], or the so-called $\ell-$TASEP (TASEP for extended objects) [136], where a localized defect was shown to only shift some transitions line in the phase-diagram, but do not affect its topology.
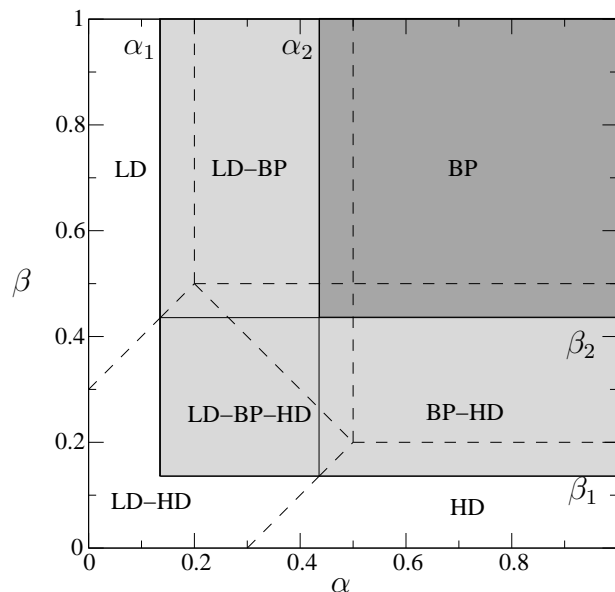

PSfrag replacements

Figure 7.3: Phase diagram for $K = 1$, $\Omega_D = 0.3$, $q = 0.4$ and $x_d = 1/2$. Continuous lines are the phase boundaries introduced by the defect; dashed lines are the phase boundaries already present in the model without bottleneck. The shaded region indicates the *bottleneck phases* where the defect is relevant (for the meaning of the different phases see Ch. 4).

Our results were checked against numerical (Monte-Carlo) simulations, which brings further arguments in favor of the validity of mean-field approaches for studying the TASEP/LK-like models. The somewhat surprising quantitative validity of this approximate scheme can be traced back to the current-density relationship, which is correctly predicted by the mean-field theory.

We would like to point out that the analysis carried out in this work can be also extended to other variants of the TASEP/LK model. As an example, we mention the case where instead of monomers one could consider the biologically relevant situation depicted in Ch. 3 where dimers (modelling the usual two heads of molecular motors) would move as bound entities according to the ℓ-TASEP and could experience a Langmuir-like on-off kinetics.

Eventually, we think that this study has clearly shown that the presence of disorder in the TASEP/LK model, even in its simplest form, generally gives rise to quite rich and intriguing features and should motivate further studies of the disordered versions of the TASEP/LK model. In particular, we think that the method outlined in this work could pave the way to study the TASEP/LK models in more 'realistic' and biophysically relevant situations, as in the presence of clusters of competing defects or quenched site-wise randomness (where the motors are slowed down at several points in the system).

Dynamics. After having analyzed the stationary properties of two TASEP-like models we turned to dynamical properties. This is motivated by the desire of describe the systems beyond mean field, with the hope of catching their critical properties. Unfortunately many driven lattice gases do no have an exact solution, therefore we have developed and tested an approximated method to compute the correlation functions of the TASEP, for which many features are known exactly: chapter 5 is devoted to the analysis of the dynamics of this model over the whole parameter range of exit and entrance rate with emphasis on the behavior in the low and high density regime and the corresponding phase boundary.

It turns out that most of the dynamics can be nicely explained in terms of the combined effect of local density fluctuations and collective domain wall motion. The dynamics of the domain wall is determined by the stochasticity in the entrance and exit of particles at the system boundaries. Depending on the parameters this yields to a random walk with or without drift towards the boundaries. For the description of the local density fluctuations we have adopted methods from kinetic theories for electronic transport, known as Boltzmann-Langevin approach. Both, the Boltzmann-Langevin and the domain wall approaches are to a large extent phenomenological and hence limited in the range of applicability. Our main findings are as follows. For very low densities, the linearized Boltzmann-Langevin theory accounts quantitatively for the shape of the density-density correlations. It becomes less accurate for densities approaching the maximal density of $1/2$ as expected from the approximate nature of the theory. Analogous arguments apply for very high densities by virtue of particle-hole symmetry. For densities close to $1/2$ linearized Boltzmann-Langevin theory is quantitatively wrong but still captures the main features qualitatively. Exactly at the critical point, $\alpha = \beta = 1/2$, the full Boltzmann-Langevin theory is identical to the noisy Burgers equation which is known to be in the same universality class as the TASEP model right at this point.

At the coexistence line $\alpha = \beta$ the density profile can be describe as the result of a Brownian dynamics of a domain wall separating a LD from a HD phase. This dynamical description turned out to be true only on long time-scales. In fact, as summarized by the power spectra in Fig. 7.4, there is a time scale separation between the domain wall motion and the local density fluctuations. For frequencies larger than the hopping time of the domain wall $\mathcal{D}$, it is the local density fluctuations which dominate the spectrum. Upon using both continuous and discrete version of the linearized Boltzmann-Langevin approach we can fully account for the crossover from $\omega^{-1/2}$ to ω^{-2} in the spectrum. For low frequencies $\omega < \mathcal{D}$ the domain wall theory gives a power spectrum of $\omega^{-3/2}$ in agreement
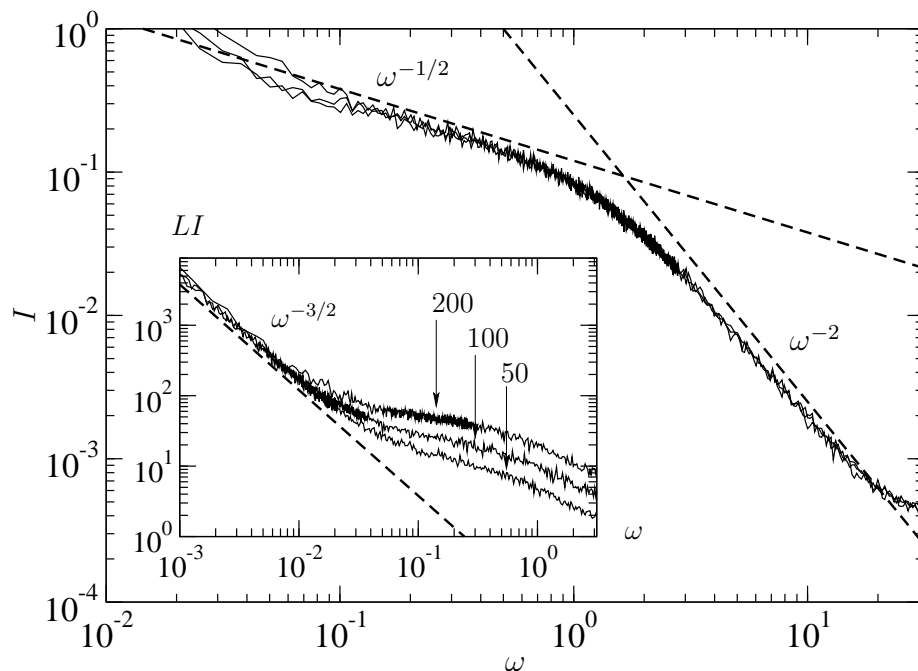
Figure 7.4: Power spectrum for systems of 200, 100 and 50 sites and rates $\alpha = \beta = 0.1$. Averages are taken over 256 samples. The large frequency behavior is dominated by local density fluctuations and well described within a Boltzmann-Langevin theory, while the small frequency regime is dominated by domain wall fluctuations, as a collective mode. The high resolution allows for the identification of a dynamic regime due to the discrete nature of density fluctuations at very short time. **Inset:** rescaled power spectrum showing the long time (small frequency) regime dominated by the domain wall dynamics.

with the Monte-Carlo data.

A preliminary study of systems with dimers, based on the refined mean field theory introduced in Ch. 3, confirms that the method, with some adaptations, can be applied to extended particles and correctly predicts the Burgers equation in the critical regime.

In summary, two rather elementary approaches, domain wall and Boltzmann-Langevin theory, seem to capture most of the observed dynamics of the TASEP model, both in the case of monomer and in the one of extended particles. Studies on the dynamics of the TASEP with on-off kinetics could highlight some new aspects missing in the simple TASEP.

Tracer. The density profile in the non-equilibrium steady state can in principle be measured experimentally by using fluorescently labeled motors and collecting the emitted light from all the motors [143, 65]. Unfortunately this method is not reliable, since the fluorophores often bleach on rather short time-scale, affecting (irreversibly) the motion of the motor. In the final chapter we have proposed an experimental method to track the

presence of a shock and to reconstruct any density profile in *in vitro* systems by analyzing the statistical properties of a tracer particle in a TASEP with on-off (Langmuir) kinetics (TASEP/LK).

Assuming it is *experimentally* feasible to repeatedly collect the position of a sufficiently large number of particles as a function of time, we have constructed histograms for the fraction of the total number of particles that step x sites in time t from they departure. The quantities we extracted from this distribution are essentially the average and the variance of the position of the particle. From these quantities the average velocity v and the diffusion constant D of the particle have been computed. From the velocity we have shown that it is possible to reconstruct the density profile using the relation (exact for the simple TASEP) $\rho(x) = 1 - v(x)$ in every region of the phase diagram. The same relation hold for the diffusion constant.

The attempt of reconstructing the density profile from the diffusion constant D (suggested by the fact that in the TASEP $\rho = 1 - D$) fails when the system is too dense (high density and part of coexistence phase). This suggests that, if the average position of the particle can be locally described with the TASEP feature, the variance of the position exhibits an interesting sub-diffusive behavior when correlations becomes important. From a mathematical point of view this aspect still calls for a theory of the fluctuations in this kind of systems.

Interestingly enough, in the simulations we did, the statistics does not have to be huge, since the main traffic effect can already be observed with less than one hundred particles. The possibility to measure statistical properties using a single tracer opens realistic possibilities of characterize *quantitative* traffic effects and to test the efficiency of the model introduced in our work. In addition, this exploratory study has revealed some interesting features of the tracer dynamics which are worthwhile to explore further on the basis of an analytical theory.

Future perspectives. The various aspects treated in this thesis do not cover all the problems of $1d$ driven lattice gases coupled to a bulk reservoir. The availability of approximate (and rather simple) methods used in this work to treat these models encourages future developments along two main research lines.

The *biological* relevance of the system stimulates the creation of more detailed models: for example the role of the several microfilaments in the microtubule (multi-lane systems), the system in confined geometry (see Refs. [95, 76, 77]) and the role of finite processivity in collective transport [16] are still to be clarified. Mitotic processes like the formation of spindles, seem to require the presence of many motors to pull two microtubules one to the other; this system has been the object of many studies [107] but exclusion and formation of jams have not been considered yet.

From a more *physical* perspective one could investigate the fluctuations in case of attachment and detachment, or the effect of more complex interactions between the particles, both on the TASEP process, where they give non trivial current-density relations, and on the on-off kinetics, where interesting spatial correlations arise. On a different line, disorder

does not only influence the motion of the motors but also their processivity, i.e. different coupling to the bulk reservoir could inspire new class of models. Mapping to other systems, as growth processes or elastic fluctuating lines (directed polymers in random media and vortices in High-T_c superconductors), opens possible new perspectives.

In conclusion, we have highlighted how the modelling of the biological systems that originally inspired this work, still far from reality, is in its very early stage; nevertheless it has motivated a number of variations of the TASEP that deserve the attention of the non-equilibrium statistical mechanics community. We hope to have revealed some interesting aspects of a field of growing interest and to have convincingly argued that the interplay between statistical mechanics and cell biology continues to be surprisingly fruitful for both subjects. Never like in this case the motto [50] quoted several times in the last years has been so appropriate:

Ask not what physics can do for biology,
ask what biology can do for physics.

Bibliography

[1] E. Adam, L. Billard, and F. Lançon. Class of Monte Carlo algorithms for dynamic problems leads to an adaptive method. *Phys. Rev. E*, 59:1212, 1999.

[2] B. Alberts, A. Johnson, J. Lewis, M. Raff, K. Roberts, and P. Walter. *Molecular Biology of the Cell*. Garland Science, New York, NY, USA, 4th edition, 2002.

[3] F.C. Alcaraz and R.Z. Bariev. Exact solution of the asymmetric exclusion model with particles of arbitrary size. *Phys. Rev. E*, 60:79–88, 1999.

[4] E. D. Andjel, M. Bramson, and T. M. Liggett. Shocks in the asymmetric exclusion process. *Prob. Theory Rel. Fields*, 78:231, 1988.

[5] M. Aridor and L.A. Hannan. Traffic jam: a compendium of human diseases that affect intracellular transport processes. *Traffic*, 1:836–851, 2000.

[6] R. D. Astumian. Thermodynamics and kinetics of a brownian motor. *Science*, 276:917–922, 1997.

[7] R. D. Astumian and M. Bier. Fluctuation driven ratchets: molecular motors. *Phys. Rev. Lett.*, 72:11, 1994.

[8] G.D. Bachand, S.B. Rivera, A.K. Boal, J. Gaudioso, J. Liu, and B.C. Bunker. Assembly and transport of nanocrystal CdSe quantum dot nanocomposites using microtubules and kinesin motor proteins. *Nanoletters*, 4(5):817–821, 2004.

[9] J.M. Berg, J.L. Tymoczko, L. Stryer, and N.D. Clarke. *Biochemistry*. W.H. Freeman and Company, New York, NY, USA, fifth edition, 2002.

[10] S.M. Bhattacharjee and F. Seno. A measure of data collapse for scaling. *J. Phys. A*, 34:6375–6380, 2001.

[11] U. Bilstein and B. Wehefritz. Spectra of non-hermitian quantum spin chains describing boundary induced phase transitions. *J. Phys. A*, 30:4925–4938, 1997.

[12] M. Bixon and R. Zwanzig. Boltmann-Langevin equation and hydrodynamic fluctuations. *Phys. Rev. E*, 187:267–272, 1969.

[13] Y. Blanter and M. Büttiker. Shot noise in conductor. *Phys. Rep.*, 336(1-2):1–166, 2000.

[14] R.A. Blythe and M.R. Evans. The Lee-Yang theory of equilibrium and non-equilibrium phase transition. *Braz. Journ. Phys.*, 33:464, 2003.

[15] A.B. Bortz, M.H. Kalos, and J.L. Lebowitz. A new algorithm for Monte Carlo simulation of Ising spin systems. *J.Comput.Phys.*, 17:10, 1975.

[16] O. Campás, Y. Kafri, K.B. Zeldovich, J. Casademunt, and J.-F. Joanny. Collective dynamics of molecular motors pulling on fluid membranes. `arXiv:q-bio.SC/0512018`, 2005.

[17] J. Cardy. Field theory and non-equilibrium statistical mechanics. Troisieme cycle de la physique en Suisse Romande, 1998.

[18] T. Chou and G. Lakatos. Clustered bottleneck in mRNA translation and protein synthesis. *Phys. Rev. Lett.*, 93:19, 2004.

[19] D. Chowdhury, L. Santen, and A. Schadschneider. Statistical physics of vehicular traffic and some related systems. *Phys. Rep.*, 329:199, 2000.

[20] D. Chowdhury, A. Schadschneider, and K. Nishinari. Physics of transport and traffic phenomena in biology: from molecular motors and cells to organisms. *arxiv:physics/0509025*, 2005.

[21] European Commission (Energy & Transport), White Paper European transport policy for 2010: time to decide, 2001.

[22] S. Courty, C. Luccardini, Y. Bellaiche, G. Cappello, and M. Dahan. Velocity and processivity of individual kinesins in living cells determined by single quantum dot imaging. Submitted to Nature Materials, 2006.

[23] Z. Cshaók and T. Vicsek. Traffic models with disorder. *J. Phys. A*, 27:L591, 1994.

[24] J. de Gier and F.H.L. Essler. Bethe ansatz solution of the asymmetric exclusion process with open boundaries. *Phys. Rev. Lett.*, 95:240601, 2005.

[25] B. Derrida. An exactly soluble non-equilibrium system: The asymmetic simple exclusion process. *Phys.Rep.*, 301(1-3):65–83, 1998.

[26] B. Derrida, E. Domany, and D. Mukamel. An exact solution of one-dimensional asymmetric exclusion model with open boundary. *J. Stat. Phys.*, 69:667–687, 1992.

[27] B. Derrida and M. R. Evans. The asymmetric exclusion model: exact results through a matrix approach. In V. Privman, editor, *Nonequilibrium statistical mechanics in one dimension.* Cambridge University Press, Cambridge, UK, 1997.

[28] B. Derrida and M.R. Evans. Exact correlation functions in an asymmetric exclusion model with open boundaries. *J.Phys.I France*, 3:311–322, 1993.

[29] B. Derrida and M.R. Evans. Bethe ansatz solution for a defect particle in the asymmetric exclusion process. *J. Phys. A*, 32:4833–4850, 1999.

[30] B. Derrida, M.R. Evans, V. Hakim, and V. Pasquier. Exact solution of a 1D asymmetric exclusion model using a matrix formulation. *J. Phys. A*, 26:1493–1517, 1993.

[31] B. Derrida, M.R. Evans, and D. Mukamel. Exact diffusion constant for one dimensional asymmetric exclusion models. *J. Phys. A*, 26:4911–4918, 1993.

[32] B. Derrida, S.A. Janowsky, J.L. Lebowitz, and E.R. Speer. Exact solution of the total asymmetric simple exclusion process: shock profiles. *J. Stat. Phys.*, 73:813–842, 1993.

[33] B. Derrida, J.L. Lebowitz, and E.R. Speer. Free energy functional for nonequilibrium systems: an exactly solvable case. *Phys. Rev. Lett.*, 87:150601, 2001.

[34] D. Dhar. An exactly solved model for interfacial growth. *Phase Transition*, 9(1):51, 1987.

[35] M. Doi. Second quantization representation for classical many-particle system. *J. Phys. A*, 9:1465–1477, 1976.

[36] M. Dudziński and G.M. Schütz. Relaxation spectrum of the asymmetric exclusion process with open boundaries. *J. Phys. A*, 33:8351–8363, 2000.

[37] A. Ebneth, R. Godemann, K. Stamer, S. Illenberger, B. Trinczek, E.-M. Mandelkow, and E. Mandelkow. Overexpression of tau protein inhibits kinesin dipendent trafficking of vescicles, mitochondria, and endoplasmic reticulum: implication for Alzheimer's disease. *J. Cell. Bio.*, 143(3):777–794, 1998.

[38] S.F. Edwards and D.R. Wilkinson. The surface statistics of a granular aggregate. *Proc. R. Soc. London, Ser. A*, 381(1780):17–31, 1982.

[39] C. Enaud and B. Derrida. Sample-dependent phase transition in disordered exclusion models. *Europhys. Lett.*, 66(1):83–89, 2004.

[40] V.A. Engelhardt and M. Lyubimova. Myosin and adenosinetriphosphatase. *Nature*, 144:668–670, 39.

[41] J.W. Evans. Random and cooperative sequential adsorption. *Rev. Mod. Phys.*, 65(4):1281–1330, 1993.

[42] M. E. Evans, T. Hanney, and Y. Kafri. Disorder and non-conservation in a driven diffusive system. *Phys. Rev. E*, 70:066124, 2004.

[43] M.R. Evans. Exact steady state of disordered hopping particle model with parallel and ordered sequential updating. *J. Phys. A*, 30:5669–5685, 1997.

[44] P.A. Ferrari and L.G. Fontes. Poissonian approximation for the tagged particle in asymmetric simple exclusion. *J. Appl. Prob.*, 33:411–419, 1997.

[45] A.A. Ferreira and F.C. Alcaraz. Anomalous tag diffusion in the asymmetric exclusion model with particles of arbitrary sizes. *Phys. Rev. E*, 65:052102, 2002.

[46] R.P. Feynman, R.B. Leighton, and M. Sands. *The Feynman lectures of physics*, volume 1. Addison-Wesley publishing company, Menlo Park, CA, USA, 1963.

[47] M.E. Fisher and A.B. Kolomeisky. The force exerted by a molecular motor. *Proc. Natl. Acad. Sci. USA*, 96:6597–6602, 1999.

[48] P.J. Flory. Intramolecular reaction of substituted vinyl polymers. *J.Am.Chem.Soc.*, 61:1518–1521, 1939.

[49] D. Forster, D. R. Nelson, and M. J. Stephen. Large-distance and long-time properties of a randomly stirred fluid. *Phys. Rev. A*, 16:732, 1977.

[50] H. Frauenfelder, P.G. Wolynes, and R.H. Austin. Biological physics. *Rev. Mod. Phys.*, 71(2):419–430, 1999.

[51] E. Frey and A. Vilfan. Anomalous relaxation kinetics of biological lattice-ligand binding models. *Chemical Physics*, 284:287–310, 2002.

[52] C.W. Gardiner. *Handbook of stochastic methods.* Springer-Verlag, 1985.

[53] D.T. Gillespie. Exact stochastic simulation of coupled chemical reactions. *J. Phys. Chem.*, 81(25):2340–2361, 1977.

[54] N. Goldenfeld. *Lecture on phase transition and the renormalization group.* Frontiers of physics. Westview Press, Boulder, CO, USA, 1992.

[55] L.S.B. Goldstein. Kinesin molecular motors: transport pathways, receptors and human diseases. *PNAS*, 98(13):6999–7003, 2001.

[56] P. Grassberger and M. Scheunert. Fock-space methods for identical classical objects. *Fortschritte der Physik*, 28:547, 1980.

[57] L.H. Gwa and H. Spohn. Bethe solution fo the dynamical-scaling exponent of the noisy Burgers equation. *Phys. Rev. A*, 46(2):844–854, 1992.

[58] M. Ha, J. Timonen, and M. de Nijs. Queuing transition in the asymmetric simple exclusion process. *Phys. Rev. E*, 68:056122, 2003.

[59] J.S. Hager, J. Krug, V. Popkov, and G.M. Schütz. Minimal current phase and universal boundary layers in driven diffusive systems. *Phys. Rev. E*, 63:056110, 2001.

[60] R.J. Harris and R.B. Stinchcombe. Disordered asymmetric simple exclusion process: mean-field treatment. *Phys. Rev. E*, 70:016108, 2004.

[61] H. Hinsch. Competition of driven and diffusive motion in two-lane lattice gas models. Master's thesis, Freie Universität Berlin, 2005.

[62] H. Hinsch, R. Kouyos, and E. Frey. From intracellular traffic to a novel class of driven lattice gas models. In A. Schadschneider, T. Pöschel, R. Kühne, M. Schreckenberg, and D.E. Wolf, editors, *Traffic and Granular Flow '05*, Berlin, 2006. Springer.

[63] L. Van Hove. Sur l'intégrale de configuration pour les systèmes de particules á une dimension. *Physica*, 16(2):137–143, 1950.

[64] J. Howard. *Mechanics of motor proteins and the cytoskeleton*, chapter 13. Sinauer Associates, Inc., Sunderland, MA, USA, 2001.

[65] J. Howard. *Mechanics opf motor proteins and he cytoskeleton*. Sinauer Associates, Inc., Sunderland, MA, USA, 2001.

[66] Urban mobility study 2005, 2005.

[67] H. E. Huxley. The double array of filaments in cross-striated muscle. *J. Biophys. Biochem. Cytol.*, 3:631–648, 1957.

[68] S.A. Janowsky and J.L. Lebowitz. Finite-size effects and shock fluctuations in the asymmetric simple-exclusion process. *Phys. Rev. A*, 45:618–625, 1992.

[69] R. Juhász and L. Santen. Dynamics of an exclusion process with creation and annihilation. *J. Phys. A*, 37:3933–3944, 2004.

[70] R. Juhász, L. Santen, and F. Iglói. Partially asymmetric exclusion process with quenched disorder. *Phys. Rev. Lett.*, 94:010601, 2005.

[71] F. Jülicher, A. Ajdari, and J. Prost. Modelling molecular motors. *Rev. Mod. Phys.*, 69(4):1269–1281, 2001.

[72] F. Jülicher and J. Prost. Spontaneous oscillations of collective molecular motors. *Phys. Rev. Lett.*, 78(23):4510–4513, 1997.

[73] N.G. Van Kampen. *Stochastic process in physics and chemistry*. North Holland publishing company, 1981.

[74] M. Kardar, G. Parisi, and Y.C. Zhang. Dynamic scaling of growing interfaces. *Phys. Rev. Lett.*, 56(9):889–892, 1986.

[75] S. Klumpp. *Movements of molecular motors: diffusion and directed walks.* PhD thesis, Universität Potsdam, 2003.

[76] S. Klumpp and R. Lipowsky. Phase transition in systems with two species of molecular motors. *Europhys. Lett.*, 66(1):90–96, 2004.

[77] S. Klumpp, T. M. Nieuwenhuizen, and R. Lipowsky. Self-organized density patterns of molecular motors in arrays of cytoskeletal filaments. *Biophys. J.*, 88:3118–3132, 2005.

[78] M. Kogan and A. Ya. Shul'man. Theory and fluctuations in a non-equilibrium electron gas. *Sov.Phys.JETP*, 29:3, 1969.

[79] Sh. Kogan. *Electronic Noise and Fluctuations in Solids.* Cambridge University Press, New York, NY, USA, 1996.

[80] A. B. Kolomeisky. Asymmetric simple exclusion model with local inhomogeneity. *J. Phys. A*, 31:1152–1164, 1998.

[81] A.B. Kolomeisky, G.M. Schütz, E.B. Kolomeisky, and J.P. Straley. Phase diagram of one-dimensional driven lattice gases with open boundaries. *J. Phys. A*, 31:6911–6919, 1998.

[82] K.M. Kolwankar and A. Punnoose. Disordered totally asymmetric simple exclusion process: exact results. *Phys. Rev. E*, 61(3/4):2453–2456, 2000.

[83] R. Kouyos. Disorder and phase-separation in the total asymmetric exclusion process. Master's thesis, Hahn-Meitner Institut, Berlin, 2004.

[84] J. Krug. Boundary-induced phase transitions in driven diffusive systems. *Phys. Rev. Lett.*, 67(14):1882–1885, 1991.

[85] J. Krug. Phase separation in disordered exclusion models. *Braz. J. Phys.*, 30(1):97–104, 2000.

[86] J. Krug and P.A. Ferrari. Phase transitions in driven diffusive systems with random rates. *J. Phys. A*, 29:L465, 1994.

[87] R. Kutner and H. van Beijeren. Influence of a uniform driving force on tracer diffusion in a one-dimensional hard-core lattice gas. *J. Stat. Phys.*, 39(3/4):317–325, 1985.

[88] G. Lakatos and T. Chou. Totally asymmetric exclusion processes with particle of arbitrary size. *J. Phys. A*, 36:2027–2041, 2003.

[89] D.P. Landau and K. Binder. *Monte Carlo simulations in statistical physics.* Cambridge University Press, Cambridge, UK, 2000.

[90] G. Lattanzi. *Statistical physics approach to protein motors.* PhD thesis, SISSA, 2001.

[91] G. Lattanzi and A. Maritan. Force dependence of the michaelis constant in a two-state ratchets model for molecular motors. *Phys. Rev. Lett.*, 86:1134–1137, 2001.

[92] J. L. Lebowitz, E. Presutti, and H. Spohn. Microscopic models of hydrodynamic behavior. *J. Stat. Phys.*, 51(5-6):841–862, 1988.

[93] T. D. Lee and C. N. Yang. Statistical theory of equation of state and phase transition I. Lattice gas and Ising model. *Phys. Rev. E*, 87(3):410–419, 1952.

[94] S. Leibler and D.A. Huse. Porters versus rowers: a unified stochastic model of motor proteins. *J. Cell. Bio.*, 121(6):1357–1368, 1993.

[95] R. Lipowsky, S. Klumpp, and T.M. Nieuwenhuizen. Random walk of cytoskeletal motors in open and closed compartments. *Phys. Rev. Lett.*, 87:108101, 2001.

[96] C.T. MacDonald and J.H. Gibbs. Concerning the kinetics of polypeptide synthesis on polyribosomes. *Biopolymers*, 7:707–725, 1969.

[97] C.T. MacDonald, J.H. Gibbs, and A.C. Pipkin. Kinetics of biopolymerization on nucleic acid templates. *Biopolymers*, 6:1–25, 1968.

[98] M. O. Magnasco. Forced thermal ratchets. *Phys. Rev. Lett.*, 71(10):1477–1481, 1993.

[99] E. Mandelkow and E.-M. Mandelkow. Kinesin motors and disease. *Trends in Cell Biol.*, 12:585–591, 2002.

[100] A. De Masi and P.A. Ferrari. Self-diffusion in one-dimensional lattice gas in the presence of an external field. *J. Stat. Phys.*, 38(3/4):603–613, 1985.

[101] D. Mattis and M.L. Glasser. The uses of quantum field theory in diffusion-limited reactions. *Rev. Mod. Phys.*, 70(3):979–1001, 1998.

[102] J.D. McGhee and P.H. von Hippel. Theoretical aspects af DNA-protein interaction: co-operative and non-co-operative binding of large ligands to a one-dimensional homogeneous lattice. *J. Mol. Biol.*, 86:469–489, 1974.

[103] N. Mirin and A.B. Kolomeisky. Effect of detachments on asymmetric simple exclusion processes. *J. Stat. Phys.*, 110(3-6):811–823, 2003.

[104] D. Mukamel. Phase transition in nonequilibrium systems. In M. E. Cates and M. R. Evans, editors, *Soft and fragile matter: nonequilibrium dynamics, metastability and flow*, page 205. Institute of Physics Publishing, Bristol, UK, 2000.

[105] J.D. Murray. *Mathematical biology I.* Springer, New York, NY, USA, 2nd edition, 1993.

[106] Z. Nagy, C. Appert, and L. Santen. Relaxation times in the ASEP model using a DMRG method. *J. Stat. Phys.*, 109:623–639, 2002.

[107] F.J. Nédélec, T. Surrey, A.C. Maggs, and S. Leibler. Self-organization of microtubules and motors. *Nature*, 389:305–308, 1997.

[108] P. Nelson. *Biological physics: energy, information, life.* W.H. Freeman and Company, New York, NY, USA, 2003.

[109] K. Nishinari, Y. Okada, A. Schadschneider, and D. Chowdhury. Intra-cellular transport of single-headed molecular motors KIF1A. *Phys. Rev. Lett.*, 95:118101, 2005.

[110] A. Parmeggiani. *Rendement énergétique et stochasticité des moteurs moléculaires.* PhD thesis, Université de Paris VII, 2000.

[111] A. Parmeggiani, T. Franosch, and E. Frey. Phase coexistence in driven one dimensional transport. *Phys. Rev. Lett.*, 90:086601, 2003.

[112] A. Parmeggiani, T. Franosch, and E. Frey. The totally asymmetric simple exclusion process with Langmuir kinetics. *Phys. Rev. E*, 70:046101, 2004.

[113] A. Parmeggiani, F. Jülicher, A. Ajdari, and J. Prost. Energy transduction of isothermal ratchets: generic aspects and specific examples close to and far from equilibrium. *Phys. Rev. E*, 60:2127–2140, 1999.

[114] L. Peliti. Path integral approach to birth-death process on a lattice. *J. Phys. (Paris)*, 46:1469, 1985.

[115] P. Pierobon, T. Franosch, and E. Frey. Driven lattice gas of dimers coupled to a bulk reservoir. Accepted for publication in Phys. Rev. E, e-print: cond-mat/0603385, 2006.

[116] P. Pierobon, M. Mobilia, R. Kouyos, and E. Frey. Bottleneck-induced transitions in a minimal model for intracellular transport. *Phys. Rev. E*, 74:036109, 2006.

[117] P. Pierobon, A. Parmeggiani, F. von Oppen, and E. Frey. Dynamic correlation function and Boltzmann Langevin approach for driven one dimensional lattice gas. *Phys. Rev. E*, 72:036123, 2005.

[118] V. Popkov, A. Rákos, R.D. Willmann, A.B. Kolomeisky, and G.M. Schütz. Localization of shocks in driven diffusive systems without particle number conservation. *Phys. Rev. E*, 67:066117, 2003.

[119] V. Popkov and G.M. Schütz. Steady-state selection in driven diffusive systems with open boundaries. *Europhys. Lett.*, 48(3):257, 1999.

[120] V. Privman, editor. *Nonequilibrium Statistical Mechanics in One Dimension.* Cambridge University Press, 1997.

[121] V. Privman and P. Nielaba. Diffusional relaxation in dimer deposition. *Europhys. Lett.*, 18(8):673–678, 1992.

[122] E. Pronina and A. Kolomeisky. Theoretical investigation of totally asymmetric exclusion process on lattices with junction. *J. Stat. Mech.*, page P07010, 2005.

[123] T. Reichenbach, T. Franosch, and E. Frey. Exclusion process with internal states. *Phys. Rev. Lett.*, 97:050603, 2006.

[124] P. Reimann. Brownian motors: noisy transport far from equilibrium. *Phys.Rep.*, 361:57–265, 2001.

[125] F. Ritort. Work fluctuations and transient violations of the second law: perspective in theory and experiments. *Séminaire Poincaré*, 2:63–87, 2003.

[126] J. E. Santos. *Non-equilibrium dynamics of reaction diffusion processes*. PhD thesis, University of Oxford, 1997.

[127] J.E. Santos, T. Franosch, A. Parmeggiani, and E. Frey. Renewal processes and fluctuation analysis of molecular motor stepping. *Phys. Biol.*, 2:207–222, 2005.

[128] B. Schmittmann and R.K.P. Zia. *Statistical mechanics of driven diffusive systems*, volume 17 of *Phase Transition and Critical Phenomena*. Academic Press, London, UK, 1995.

[129] G. Schönherr and G.M. Schütz. Exclusion process of particles of arbitrary extension: hydrodynamic limit and algebraic properties. *J. Phys. A*, 37:8215–8231, 2004.

[130] G. Schütz. Time-dependent correlation functions in a one-dimensional asymmetric exclusion process. *Phys. Rev. E*, 47(6):4265–4277, 1993.

[131] G. Schütz and E. Domany. Phase transition in an exactly soluble one-dimensional exclusion process. *J. Stat. Phys.*, 72:277–296, 1993.

[132] G.M. Schütz. *Exactly solvable models in many-body systems*, volume 19 of *Phase Transition and Critical Phenomena*. Academic Press, London, 2001.

[133] M. Schwarz and D. Poland. Random walk with two interacting walkers. *J. Chem. Phys.*, 63(1):557–568, 1975.

[134] A. Seitz and T. Surrey. Processive movements of single kinesins on crowded microtubules visualized using quantum dots. *The EMBO Journal*, 25(2):267–77, 2006.

[135] L. B. Shaw. *Analysis of a driven one-dimensional lattice gas model for protein synthesis and comparison to experimental data*. PhD thesis, Cornell University, 2004.

[136] L.B. Shaw, A.B. Kolomeisky, and K.H. Lee. Local inhomogeneity in asymmetric simple exclusion process with extended objects. *J. Phys. A*, 37:2105–2113, 2004.

[137] L.B. Shaw, J.P. Sethna, and K.H. Lee. Mean field approaches to the totally asymmetric exclusion process with quenched disorder and large particles. *Phys. Rev. E*, 70:021901, 2004.

[138] L.B. Shaw, R.K.P. Zia, and K.H. Lee. Totally asymmetric exclusion process with extended objects: A model for protein synthesis. *Phys. Rev. E*, 68:021910, 2003.

[139] R.B. Stinchcombe. *Dilute magnetism*, volume 7 of *Phase Transition and Critical Phenomena*. Academic Press, New York, NY, USA, 1983.

[140] R.B. Stinchcombe. Disorder in non-equilibrium models. *J. Phys.: Condens. Matter*, 14:1473–1487, 2002.

[141] E. Suraud, S. Ayik, M. Belkacem, and J. Stryjewski. Applications of Boltzmann-Langevin equation to nuclear collisions. *Nuclear Physics A*, 542:141, 1992.

[142] K. Svoboda, P.P. Mitra, and S.M. Block. Fluctuations analysis of motor protein movement and single enzyme kinetics. *Proc. Natl. Acad. Sci. USA*, 91:11782–11786, 1994.

[143] K. Svoboda, C.F. Schmidt, B.J. Schnapp, and S.M. Block. Direct observation of kinesin stepping by optical trapping interferometry. *Nature*, 365:721–727, 1993.

[144] S. Takesue, T. Mitsudo, and H. Hayakawa. Power-law behavior in the power spectrum induced by Brownian motion of a domain wall. *Phys. Rev. E*, 68:015103(R), 2003.

[145] U.C. Täuber. Critical dynamics. `http://www.phys.vt.edu/ tauber/utaeuber.html`, 2005. Unpublished lecture notes.

[146] U.C Täuber, M. Howard, and P. Vollmayr-Lee. Application of field-theoretic renormalization group methods to reaction-diffusion problems. *J. Phys. A*, 38:R79–R131, 2005.

[147] C.J. Thompson. *Classical equilibrium statistical mechanics*. Oxford University Press, New York, NY, USA, 1988.

[148] L. Tonks. The complete equation of state of one, two and three-dimensional gases of hard elastic spheres. *Phys. Rev.*, 50:955–963, 1936.

[149] G. Tripahty and M. Barma. Steady state and dynamics of driven diffusive systems with quenched disorder. *Phys. Rev. Lett.*, 78:3039–3042, 1997.

[150] H. van Beijeren, R. Kutner, and H. Spohn. Excess noise for driven diffusive systems. *Phys. Rev. Lett.*, 58(18):2026, 1985.

[151] K. Visscher and M.J. Schnitzer S.M. Block. Single kinesin molecules studied with a molecular force clamp. *Nature*, 400:184–189, 1999.

[152] D.M. Warshaw, G.G. Kennedy, S.S. Work, E.B. Krementsova, S. Beck, and K.M. Trybus. Differential labeling of myosin V heads with quantum dots allows direct visualization of hand-over-hand processivity. *Biophys. J.*, 88:L30–L32, 2005.

[153] http://www.rpi.edu/dept/bcbp/molbiochem/MBWeb/mb2/part1/kinesin.htm.

[154] http://www.stanford.edu/group/blocklab/kinesin.html.

[155] http://www.www.carolguze.com/text/.

[156] C. N. Yang and T. D. Lee. Statistical theory of equation of state and phase transition I. Theory of condensation. *Phys. Rev. E*, 87(3):404–409, 1952.

Acknowledgements

Paolo, you have to believe!

Erwin Frey

(private communication)

I am deeply grateful to my supervisor Prof. E. Frey for having suggested the topic of this thesis and for his constant scientific and moral guidance, support and help. I am in debt with Prof. F. von Oppen whose ideas were crucial for a part of the work. A special thank goes to the coauthors of the paper based on Chapter 3 and Chapter 4 Dr. T. Franosch and Dr. M. Mobilia, for their invaluable help. In the first part of the work and Chapter 5 I had important support and encouragements from Dr. A. Parmeggiani.

I profited from useful (and sometimes endless!) discussions with Dr. G. Lattanzi, Dr. J. Santos, Prof. K. Kroy, Dr. P. Benetatos, R. Kouyos, H. Hinsch, F. Wagner, F. Höfling, Dr. R. Thul. I profited also from the visit of the guests at the Hahn-Meitner Institut (Berlin) and the Ludwig-Maximilians-Universität (Munich): in particular I would like to thank Prof. D. Nelson, Prof. R. Zia, Prof. U. Täuber, Dr. G. Cappello, Dr. Y. Kafri, Dr. T. Liverpool, Dr. A. J. Dalmaroni, Dr. T. Schilling, O. Campas.

I acknowledge the financial support of the Hahn-Meitner Institut (HMI, Berlin) during these three years.

<div align="center">*   *   *</div>

The process of writing a thesis is mostly a personal, human, involving life-experience, in particular when this experience is lived abroad. In this second part of the acknowledgments I want to thank in a special (and informal) way the people that contributed to my personal growth in these three years! in a word friends, colleagues or just acquaintances that came across my life and somehow left a sign. Some of them (but not all!) appeared in the previous section!

Let me start with *Erwin*. I have already acknowledge his scientific help. Here I want to thank him for his endless patience and constant (successful) effort to create a fruitful and lively environment first in Berlin and then in Munich. For constantly teaching, with his broad spectrum of interests, that a good scientist should be first of all a good fellow!

I am grateful to *Thomas "Froschon" Fico-Supremo*, the Master of the mesoscopic limit, that contributed a lot to this work (he thinks he has written almost everything, but he

knows is not true!). Luckily, despite his vicinity in these three years I think I am relatively normal, which is in itself a miracle;-)! All in all he is a nice guy, I just wonder who will be his target now that he will not have any Italian around!

Again a great thank to *Mauro* that not only made possible Ch.4 but above all supported me morally in the worse time (and prepared for the future ones)!

To *Andrea*, who taught me the art of "spippolare" (i.e. computer simulations), the equivalence research=suffer and various pearls of wisdom in "bolognese".

A special thank goes to *Gianluca (aka Latitanzi, Talibanzi, Tulipanzi, Tarallanzi)* and to *Mario* for their enthusiasm and friendship. For being reference points humanly and scientifically. For having shared with me their (Talibanzic and Salizzonic) philosophies of life and to some extents, moulded me as man and researcher. Two friendships that will never be forgotten.

To the people and colleagues at the HMI for the nice environment, the fruitful discussions and, of course, for the fun: *Sylvia, Quincy, Andemar* and the red wallet (b.t.w. I changed it one year ago!), *Martin, Kajetan, Benedikt, Maximilian* that helped me with the german bureaucracy at the very beginning of this adventure, *Alexander, Klaus* for having dreamed of me (God!), *Oskar, Sebastian, Felix, Panayotis, Tobias, Rüdiger, Azam, Andreja, Amit and Abhik*, and the heroic sub-groups of the "Thursday DVD night".

To *Jaime*, for his love for Italy, his speeches on geopolitics, science (and of science fiction), life, saudade, and "gnocche" (that he brought to Berlin)! Thanks to *Andrea* and *Sofia*:-)!

To *Claus and Antje*, that enhance my fatherly instinct (not yet over the threshold!) allowing me to dandle their *Cederic*! one of the strongest moment of the time here!

To *Frederik*, who, since my first day was much more than a simple office mate, more than a system administrator, and more than my personal Linux and LATEXguru! I hope to have paid him back by introducing Valentina to him! (ok probably I still owe him a couple of beer!). Thanks to *Valentina*, for being so "radical-chic", and for her sweet effort to give me a more relaxed attitude, for dropping in the office with a smile than often changed the day (I know it was for Frederik, but it was important!).

To *Sven*, whose fate (or torture) is to share the office with Italians! for the great time we had during his endless Diplomarbeit and his help in moving, preparing talks, making parties! To *Sebastian*, musical, physical, cultural and sometimes spiritual guide! I would thank *Andrea*, but he might turn jealous!;-)

To *Hauke* for having shared the great adventure of a travel Berlin-Munich and helped me with the moving, the proofreading of these acknowledgement...and all the rest! And to all the other that helped me in this transition, especially *Mark* and *Riccardo*.

To *Katrin*, my Tandempartnerin in Berlin, reference point in the capital, party-mate, concert-mate, BBQ-on-the-roof-mate, and more: her sight on the city is what I really miss of Berlin!

To the "Berlin intellectual circle": *The D'Alfonsos (Lorenzo, Giulia, Sofia), Gianluca, Alessandro, Micol, Mario, Gianluca, Luca, Gabriele, Sandro ("my lawyer")*, with whom I shared parties, dinner, nights in Berlin, comfortable travels on a military van, and The Cake at the radio! in particular thanks to *Silvia* (l'amica-filosofa) for having explained

Heidegger at 4 a.m. on the U1[1]

To *Anna*, finally someone that speaks more than I do. For our endless chats in swimming pool, our nights queing for the MoMA, our kebabs and our lives. And to *Omar*, her worthy boyfriend.

My life in Berlin was surrounded by lovely and special persons that made me love the city, turned me a bit into a "Ossie" and taught me German (in fact I am writing in English!). Es war eine super Zeit mit euch! Danke *Emu, Karo (and Miron), Anne, Anke, Moppi, Mandy, Ricke, Tobias*, und allen Freunden der WG in Weichselstr.26, F'hain - Berlin!

All the Munich friends: *Katrin and Gregor* (the Pakka will not be famous, but we had great fun!), *Bea and all the "romans", Valentina, Albane, Marina*, my Tandempartnerin in München *Pavlina, Stefano, Ekaterina, Pierre-Aime*, all the Italians of München: *Marino, Pasquale, Sabine, Elisadipisa, Sebastian, Anatol, Clarissa, Konstanze, Veronic(k)a*, and many others. A special thank to the *"zwei Königinen" Katharina & Valentina*: a sort of new eyes to look at the world and the strongest motivation to finish, they know why;-)!

Thanks to my flatmates in Munich, *Helene, Axel, Kris, Mustafa, Aysegül* and all the people hanging around the WG in Giselastr.3! For the great atmosphere they could create in so little time and for their constant support.

To *Tobias* (not only for the abstract in german!) and to all the group in Munich *Uli, Richard* and his parties;-), *Karen, Georg, Nico, Wolfram, Thomas, Steffi, Jan-Timm*. A special acknowledge to the proofreading work of *Marta*: I will pay you back in three year! just catch me, ok? For the moral support to Marta, thanks to *Alvaro*!

To *Francesco, Ni Yan and their daughter Angela* (I am sure this is the first thesis where her name appears!). For the strong friendship and the strong life-experience we are enjoying! you know:"La vita la vivi o la scrivi" (Pirandello), there will be time for our book, do not worry, now it is time for something else!

To *Zobbe*, our man in Paris, because he saw all the flat I have lived in! and because our emigrants lives are anyway entangled!

To the great *Mattia* (and *Giulia* as well), since our fates seem to be somehow similar and related! And I thank him for having unintentionally suggested in his thesis the last acknowledge (see below).

To *Sergio*, a "dandy hero", our man in London. More than that: a friend and "researcher" that influenced very much my life.

Thanks to the friend that visited me in Berlin (*Francesco M., Francesco D.L, Ni, Zobbe, Pucci, Moira*, and many others). Thanks to the friends that have always considered me one of them. Even when it was difficult to communicate, even if only half an hour per month they were always ready to welcome me: *Matteo S.(-uman and -tievano), Rita, Adelaide, Anna, Luca & Laura, Filippo, Moira, Ilaria, Elisa*, and many others.

The friends that got married during this three years and "force" me to go back to Italy or somewhere else: *Davide & Chiara, Fabio & Maria, Roberta & Michele, Antonio & Ambra, Luca & Laura*.

---

[1]The citation in the conclusion is its suggestion and the result of that night!

This work would have not be possible without the constant support and love of one special person, *Daria*, whom I warmly thank for having given me so much in these three years. I hope, and believe, that there will be one day the right moment and the right place to give her back so much. I also thank her family for the support and love.

Ai *miei genitori*, che non so davvero come ringraziare. Che non hanno mai smesso di accompagnare in aeroporto e in stazione "il loro bambino", "il tedesco" o "l'emigrante". Che mi hanno sempre abbracciato da lontano...si saranno pentiti di avermi fatto cosí, ma in fin dei conti si sono divertiti anche loro! A *Fabio* perché sta diventando una bella persona, perché piú cresce e piú mi sento suo fratello e perché un po' mi dispiace averlo costretto a fare il figlio unico questi tre anni!

Alla mia famiglia estesa, fatta di *zii, cugini/e e nonni* (questi ultimi che tanto hanno pianto e pregato ad ogni mio viaggio, ok è un dottorato, neanche andassi in guerra!)

Last but not least "To *myself*, for once..."

Finally a special thank to the thousands of people I met on the way these years. I probably forgot someone. Maybe if *you* are reading these pages your name deserves to be here too:.........................!

This work had been typeset by Paolo Pierobon using LATEX.

CURRICULUM VITAE
Paolo Pierobon

Affiliation: Arnold Sommerfeld Center
Working address: Theresienstr.37, D-80333 München, Germany
Home address: Giselastr.3, D-80802 München, Germany
Other contact address: via Monte Civetta 6, 31044 Montebelluna (TV), Italy
Telephone: +49 2180 4558 or +49 0179 9155507
E-mail: `paolo.pierobon@physik.lmu.de`

Date of Birth: 1st February 1978
Nationality: Italian
Marital Status: Single

Education

- December 2002 - February 2006, *PhD student in Prof.Dr.E.Frey's group.* Statistical and biological physics.

- 1997 - 2002, *Degree in Physics. Final mark 110/110.* Università degli studi di Padova (Italy).

- 1991 - 1997, *Diploma di Maturità scientifica. Final mark 60/60.* Liceo Scientifico Statale Primo Levi, Montebelluna (Italy). High school with scientific studies.

Experiences abroad

- March 2005 to May 2006: graduate student at the Arnold Sommerfeld Center, München, Germany.

- December 2002 - March 2005: graduate student at the Hahn-Meitner Institut, Berlin, Germany.

- 18/4/2002-18/5/2002: Guest student at Kavli Institute for Theoretical Physics, S.ta Barbara California, Affiliate to the program *Dynamics of Complex and Macromolecular Fluids.*

- October 2001 - April 2002: Erasmus exchange program during diploma thesis with Dr. T. Liverpool. *Imperial College*, London.

Employment and other activities

- 12/2002 - 12/2005, *Hahn-Meitner Institut, Berlin:* PhD student. Teaching assistant for the course of Statistical mechanics. Help in the supervision of diploma thesis.

- 2/1999 - 2/2000, *Natural History Museum, Montebelluna:* Guide and demonstrator for mathematics and physics exhibitions

- 9/1997 - 6/2001, Private tutoring of mathematics and physics to high school and undergraduate students.

Skills

- *Languages:* Italian (mother tongue), English (fluent), German (good), French (conversational).

- *Computer Skills:* programming knowledge in C/C++ and related numerical libraries. Competent with Latex, Mathematica, Maple, and with the main office and graphic applications both under Linux and Windows. Basic knowledge of shell programming (Bash and Perl).

Publications

i. *Dynamic correlation function and Boltzmann Langevin approach for a 1d driven lattice gas*, P. Pierobon, A. Parmeggiani, F. von Oppen and E. Frey, Phys. Rev. E 72, 036123,

ii. *Introduction to Nonextensive Statistical Mechanics and Thermodynamics*, C. Tsallis, F. Baldovin, R. Cerbino, and P. Pierobon, Proceedings of the 1953-2003 Jubilee ”Enrico Fermi” International Summer School of Physics. Available on `http://arxiv/abs/cond-mat/0309093`.

iii. *Driven lattice gas of dimers coupled to a bulk reservoir*, P. Pierobon, T. Franosch and E. Frey. Accepted for publication in Phys. Rev. E. Available on `http://arxiv/abs/cond-mat/0603385`.

iv. *Bottleneck-induced transitions in a minimal model for intracellular transport*, P. Pierobon, M. Mobilia, R. Kouyos and E. Frey, Phys. Rev. E 74, 031906